UDRI

UNIVERSITY
of DAYTON
RESEARCH
INSTITUTE

NAV AIR

Report

CORROSION-FATIGUE ASSESSMENT PROGRAM – FINAL REPORT

· ·

March 2008

Wally Hoppe
William Braisted
Jennifer Pierce
Garry Abfalter

1. REPORT DATE **MAR 2008**	2. REPORT TYPE	3. DATES COVERED **00-00-2008 to 00-00-2008**

4. TITLE AND SUBTITLE **Corrosion-Fatigue Assessment Program**	5a. CONTRACT NUMBER
	5b. GRANT NUMBER
	5c. PROGRAM ELEMENT NUMBER
6. AUTHOR(S)	5d. PROJECT NUMBER
	5e. TASK NUMBER
	5f. WORK UNIT NUMBER

7. PERFORMING ORGANIZATION NAME(S) AND ADDRESS(ES) **University of Dayton Research Institute,Structural Integrity Division,300 College Park,Dayton,OH, 45469-012**	8. PERFORMING ORGANIZATION REPORT NUMBER

9. SPONSORING/MONITORING AGENCY NAME(S) AND ADDRESS(ES)	10. SPONSOR/MONITOR'S ACRONYM(S)
	11. SPONSOR/MONITOR'S REPORT NUMBER(S)

12. DISTRIBUTION/AVAILABILITY STATEMENT
Approved for public release; distribution unlimited

13. SUPPLEMENTARY NOTES

14. ABSTRACT

15. SUBJECT TERMS

16. SECURITY CLASSIFICATION OF:			17. LIMITATION OF ABSTRACT	18. NUMBER OF PAGES	19a. NAME OF RESPONSIBLE PERSON
a. REPORT **unclassified**	b. ABSTRACT **unclassified**	c. THIS PAGE **unclassified**	**Same as Report (SAR)**	**245**	

CORROSION-FATIGUE ASSESSMENT PROGRAM – FINAL REPORT

Contract No.: N00014-06-C-0643

March 31, 2008

FINAL REPORT

Prepared for:

Dr. Paul Hoffman
Government Technical Program Manager
Naval Air Warfare Center – Aircraft Division
Code 4.3.3.1
48110 Shaw Rd., Unit 5
Patuxent River, MD 20670-1906

Prepared by:

Wally Hoppe, Principle Investigator
UNIVERSITY OF DAYTON RESEARCH INSTITUTE
Structural Integrity Division
300 College Park
Dayton, OH 45469-0120

Table of Contents

List of Figures

List of Tables

Foreword

This report describes the technical work accomplished during the period from 25 September 2006 through 31 March 2008 for the Naval Air Warfare Center – Aircraft Division under Contract Number N00014-06-C-0643. Engineering Software Research and Development, Inc. (ESRD), and The Boeing Company were the major subcontractors on the program. Dr. Paul Hoffman was the Contract Monitor.

Mr. Wally Hoppe of the UDRI Structural Integrity Division was the Principal Investigator for the contractual effort. Mr. Robert Andrews (until 30 June 2007) and Mr. Michael Bouchard (after 1 July 2007), Division Heads of the Structural Integrity Division, served as overall Program Managers. Ms. Ollie L. Scott and Gloria Hardy provided program management services. The following UDRI employees contributed to the major accomplishments on this contract: Dr. Bill Braisted, Mr. Garry Abfalter, Ms. Jennifer Pierce, Mr. Brian Frock, Mr. Bob Olding, and Dr. Ray Ko. Andrea Snell provided editorial and formatting services. Additional contributors included: Mr. Dave Rusk of NAVAIR; Dr. Barna Szabo, Dr. Ricardo Actis and Mr. Brent Lancaster of ESRD; and, Dr. Krishnan K. Sankaran, Dr. Herb Smith, Jr., and Mr. Bert Neal of Boeing.

Section 1
Executive Summary

In June 2003, UDRI was placed on contract, as prime, to lead in an effort to study the effect that corrosion has on the fatigue life of high-strength steels on Navy applications. In September 2005, UDRI was placed under contract to AES to continue the effort begun by the earlier program. In September 2006, UDRI was placed under contract to continue the efforts from the two previous contracts. The Navy High-Strength Steel Corrosion-Fatigue Assessment Program was designed to ensure reliability and supportability of current and emerging Naval aircraft by providing requisite engineering support to evaluate issues relevant to corrosion-fatigue of airframe components. The purpose of these contracts was to develop tools that can be used to specify the maintenance options for corroded components and to provide a sound engineering basis for selecting the best fleet maintenance options. Essentially, the program was to provide quantifiably justified maintenance criteria for environmentally induced damage (i.e., corrosion) in high-strength steels.

The overall objectives of these programs included the following outcomes:

- A corrosion severity classification scheme (i.e,. cosmetic, mild, and severe) tied to component reliability or reduction in fatigue life,
- Corrosion metrics associated with these corrosion classifications,
- Nondestructive inspection (NDI) methods, requirements, and procedures for measuring corrosion severity via these corrosion metrics, and
- Component disposition tools and procedures to make engineering disposition decisions based on detailed corrosion profiles and validated life prediction assessment models.

The plan to meet these overall objectives consisted of the following activities:

- Determining the effect of corrosion on fatigue life of high-strength steels through corrosion-fatigue experiments supported by other baseline tests,
- Developing corrosion metrics based on surface profiles, correlating metrics to life reduction, and using these results to develop corrosion classification criteria,
- Investigating and developing NDI methods and procedures to determine corrosion severity via correlations of NDI to corrosion metrics, and

- Developing physics-based analysis methods to determine effective stress concentration factors for corrosion, correlating the analysis predictions to corrosion-fatigue tests, and validating on component tests.

These research tasks are part of a multi-year, multi-contract program. The first contract was initially funded in June 2003 for one year, followed by a second year of funding and extensions to August 2006. The second contract was awarded in September 2005 for one year and was extended to September 2007. The third and final contract was awarded in September 2006 and extended to 31 March 2008. The entire effort lasted four years and ten months. The University of Dayton Research Institute was prime on the first contract, with Engineering Software Research and Development (ESRD), Inc. and The Boeing Company as subcontractors. UDRI was a subcontractor to AES on the second contract, with ESRD, Boeing, and Computational Mechanics, Inc. as second-tier subcontractors under UDRI. UDRI was, again, the prime contractor on the third contract to ONR, with ESRD and The Boeing Company as subcontractors.

This document reports activities under the third of these three contracts supporting the overall objectives of the program. The third program contract significantly overlapped the timeframe of the second and focused on:

- Preparation for corrosion-fatigue tests and baseline material tests on Aermet 100,
- AF1410 tests on specimens with micro-machined features,
- AF1410 shank tests,
- Validation tests on cadmium-plated AF1410 corrosion-fatigue specimens,
- Calibration of the equivalent stress riser model
- Development of a grid model for life prediction,
- A Nondestructive Evaluation study to correlate grid surface roughness statistics determined from nondestructive evaluation methods to that determined from the white light interference microscopy measurements, and
- Verification and validation of the equivalent stress riser model, which included preparation and testing of cadmium-plated corrosion-fatigue specimens, along with equivalent stress riser model life predictions based on corrosion profile measurements.

Section 2
Introduction

2.0 Background

Navy carrier-based aircraft employ high-strength steel in many components including landing gear and arrestment shanks. The service life of these components are generally defined by fatigue caused by load cycles. However, aircraft must operate in coastal environments that result in corrosion-assisted fatigue of airframe components. The effect of corrosion on component fatigue life has not been quantified. This problem is most acute for high-strength steel, such that it is important to determine how to quantify remaining life considering both cycle-dependent and time-dependent damage mechanisms. A quantifiable metric must be established to estimate remaining life due to the presence of corrosion.

2.1 Purpose and Goals

The Navy High-Strength Steel Corrosion-Fatigue Assessment and the following programs were designed to ensure reliability and supportability of current and emerging Naval aircraft by providing requisite engineering support to evaluate issues relevant to corrosion-fatigue of airframe components. The purpose was to develop tools that can be used to specify the maintenance options for corroded components and to provide a sound engineering basis for selecting the best fleet maintenance options. Essentially, the program was to provide quantifiably justified maintenance criteria for environmentally induced damage (i.e., corrosion) in high-strength steels.

The overall objectives of this program included the following outcomes:

- A corrosion severity classification scheme (i.e., cosmetic, mild, and severe) tied to component reliability or reduction in fatigue life,
- Corrosion metrics associated with these corrosion classifications,
- Nondestructive inspection (NDI) methods, requirements, and procedures for measuring corrosion severity via these corrosion metrics, and
- Component disposition tools and procedures to make engineering disposition decisions based on detailed corrosion profiles and validated life prediction assessment models.

The plan to meet these overall objectives consisted of the following activities:

- Determining the effect of corrosion on fatigue life of high-strength steels through corrosion-fatigue experiments supported by other baseline tests,

- Developing corrosion metrics based on surface profiles, correlating metrics to life reduction, and using these results to develop corrosion classification criteria,

- Investigating and developing NDI methods and procedures to determine corrosion severity via correlations of NDI to corrosion metrics, and

- Developing notch-based analysis methods to determine effective stress concentration factors for corrosion, correlating the analysis predictions to corrosion-fatigue tests, and validating on component tests.

2.2   Relationship to Other Contracts/Programs

These research tasks are part of a multi-year, multi-contract program. The first contract was initially funded in June 2003 for one year, followed by a second year of funding and extensions to August 2006. The second contract was awarded in September 2005 for one year and was extended to September 2007. The third and final contract was awarded in September 2006 for one year and extended to March 2008. The entire effort lasted four years and ten months. The University of Dayton Research Institute was prime on the first contract, with Engineering Software Research and Development (ESRD), Inc. and The Boeing Company as subcontractors. UDRI was a subcontractor to AES on the second contract, with ESRD, Boeing, and Computational Mechanics, Inc. as second-tier subcontractors under UDRI. UDRI was, again, the prime contractor on the third contract to ONR, with ESRD and The Boeing Company as subcontractors. The ESRD Final Report for the third contract is included in this report in Appendix A. The Boeing Final Report for the third contract is found in Appendix B. While these subcontractors have played important roles in this program, specific references to their final reports are not necessarily made in this report. Details of their activities are found in the respective final reports.

2.3   Summary of Accomplishments

This document reports activities under the third of these three contracts supporting the overall objectives of the program. Specific activities during this timeframe have made use of the tools and methods developed during the first and second contracts and reported in the final reports of those

programs [1] and [2]. Activities of the third contract focused primarily on additional tests and characterization of corrosion-fatigue experiments, as well as developing methods to calibrate the equivalent stress riser model developed on the earlier contracts, development of a grid model that can make use of nondestructive evaluation data for corrosion-severity classification, and verification and validation.

During the first contract, NAVAIR, UDRI, and its team members designed, manufactured, and subsequently fatigue tested 54 AF1410 corrosion-fatigue test specimens. Each specimen had been prepared according to a test matrix that included growing corrosion according to a UDRI-developed protocol for various exposure times: zero, 3, 6, and 12 hours, respectively, using the electrochemical method developed for this purpose. Subsequent to growing corrosion in circular patches, the specimens were cleaned in a Turco solution to remove the corrosion products without further altering the specimen surface. After this, the specimens were ultrasonically inspected. Later specimens were also eddy current inspected. The final step prior to fatigue testing provided high-resolution surface profiles of the corroded surface via a white light interference microscopic system. The test matrix also stipulated load conditions covering a range of loads of interest. During test, marker bands were introduced on any fracture surface by varying the R value of the load in a predetermined manner. In addition, some specimens were monitored by penetrent inspections to identify crack initiation sites. As of the end of the first contract, all AF1410 specimens in the first set had been fatigued until failure. Several specimens had been subject to additional investigation to attempt preliminary validation of models being developed as described below. Results of these tests in terms of peak stress versus cycles to crack initiation were reported in the final report.

Also, during the first contract, a significant effort was put forth to develop corrosion-fatigue models. Initial efforts were directed at implementation of finite element analysis (FEA) methods to calculate stress concentration due to the corrosion based on detailed profiles of the corrosion surface. This approach was discovered to be intractable, in that the FEA mesh required to capture the fine details of the corrosion surface made computation so excessively long, as to be impossible. Further efforts to simplify the surface profile produced unreliable FEA results, given that the simplifications that were designed to reduce computation time required more manageable meshes, which were then not representative of the actual surface profile. Similarly, efforts to simplify the corrosion details by assuming simpler geometric profiles, such as rounded cones, produced stress concentrations that were overly dependent on small changes in the assumed shape of the corrosion feature.

In parallel with these efforts, a study was being conducted to develop so-called global/ local models, which attempted to provide the requisite detail at a local level, while using less detail at the global level. Unfortunately, these approaches were also unsuccessful.

In a related study, a pit metric was developed that could estimate the stress concentration of a semi-ellipsoidal pit with a simple formula based on the dimensions of the principal axes of the pit and accounting for load direction. This simple formula was used in further developments later in the program.

When faced with the intractable nature of the FEA methods to the problem of calculating the stress concentration of a corroded surface, UDRI took an innovative tact to the problem by decomposing the surface into two-dimensional spatial frequency components. The stress concentration for each component was then estimated and the net effect of all components was determined by an inverse Fourier Transform. The theoretical basis for this admittedly approximate method to determine stress concentration is documented in the final report of the first contract on this program. Also included in that report are results of case studies performed to compare this so-called elasticity approach to FEA results for special cases. These studies defined practical limits for the applicability of the elasticity solution, which happen to be realistic for the levels of corrosion of interest on this program. That is, the levels of corrosion seen in the specimens tested on this program fall well within the region that should produce small errors in the estimation of stress concentration. There is, to be sure, a residual concern over this approach, or any approach, that is limited by the resolution of the surface profile. However, there is hope, as will be seen later, that the extremely small features that would produce large stress concentrations might be mitigated by a notch size effect.

Near the end of the first contract, the elasticity approach to estimation of stress concentration was tested by comparing the location of crack initiation sites on corroded specimens with the high-stress regions found from the elasticity solution applied to the profiles generated by the white light interference microscopic system on the same surfaces. The results on these preliminary checks were exceptionally promising and indicated that, while not all high-stress points cracked, all cracks did initiate in high-stress regions and very near the peak stress in that local area. Additional validation of this model would have to wait until the second contract.

An issue arose during the development and execution of the first set of AF1410 corrosion-fatigue tests (Set A specimens). The associated specimens had been grit blasted and were suspected to have a resultant residual stress. After X-ray diffraction measurements confirmed this suspicion, a decision was made to manufacture a second set of AF1410 specimens. The manufacture of these specimens was started during the first contract.

It was also of interest to extend the methods being developed to other high-strength steels, such as 300M. However, previously conducted tests on a USAF program suggested that 300M would be extremely sensitive to corrosion attack, possibly due to the introduction of inter-granular corrosion. A decision was made to test only nine 300M corrosion-fatigue specimens to confirm the results of the USAF study. Creation of these specimens was started on the first contract on the Navy Corrosion-Fatigue program.

Aermet 100 was also selected for study. Specimen manufacture and tests on this material were primarily the focus of the third contract.

A nondestructive evaluation (NDE) investigation was also conducted on the first contact. After studying several methods to address the problem, it was concluded that the most promising NDE method is ultrasound. Subsequently, a series of ultrasonic measurements were made of various corroded surfaces. Included in these experiments were angle beam and normal incidence pulse-echo techniques using amplitude, time-of-flight, and frequency domain techniques. Normal incidence time-of-flight and Fourier phase slope methods seemed the most promising of the techniques.

As it has turned out, the second program contract significantly overlapped the timeframe of the first. Activities on the second contract focused on completion of AF1410 Set A tests, completion of AF1410 Set B tests, extending the modeling effort to reliability models for life prediction, development of corrosion metrics, preparation of 300M and Aermet 100 specimens (including preliminary tests on these materials), and the development of an implementation scheme.

To finish the analysis of the AF1410 Set A corrosion-fatigue tests, each fracture surface on the specimens was compared to the corrosion profile on the adjacent surface to identify the corrosion feature that initiated the crack. Dimensional measurements were taken of each corrosion feature and used to estimate stress concentration factors. Simple life predictions based on these estimates were compared to actual life measured in the fatigue tests.

Baseline and corrosion-fatigue tests were conducted on a second batch of AF1410 (Set B) specimens. The corrosion-fatigue specimens were designed to exclude the grit blasting. They also had smoother surfaces than Set A. As a result of both of these facts, the test matrix included lighter corrosion exposure levels: zero, 1.5, 3, and 6 hours, respectively. As was true of the first set, this set was prepared in the same way, including ultrasonic and eddy current, as well as white light interference measurements of the surface profile. After fatigue testing, each specimen was examined to microscopically ascertain the number of cycles to crack initiation and to measure the dimensions of the critical feature that initiated the crack.

A small number of 300M corrosion-fatigue specimens were manufactured for the purpose of verifying the results of the earlier USAF study showing that 300M could tolerate very little corrosion without losing the majority of its fatigue life. Other associated tests were conducted in anticipation of these fatigue tests. Unfortunately, once fatigue testing was initiated and as fracture surfaces were examined, it became apparent that the batch of 300M that was used for these specimens, including earlier NAVAIR strain-life specimens, was contaminated with titanium inclusions. This contamination renders all test specimens and previous test results of little value. At this point, these activities on 300M were terminated.

In the interest of extending the methods developed on this program to other materials, quantities of Aermet 100 were purchased and the manufacture of test specimens was initiated.

A major objective of this program was to develop modeling techniques to predict the effect that corrosion-induced surface roughness has on fatigue life. As mentioned above, an elasticity approach had been developed on the first contract to estimate the stress concentration due to corrosion. On the second contract, the results of this method were compared to the stress concentration calculated on pits using FEA and the UDRI pit metric. It was found that, while the elasticity approach could identify spots of high stress, it did not always find stress concentrations in precise agreement with FEA.

In addition to this finding, attempts to make life predictions directly from the stress concentration map from the elasticity model were unsuccessful. In particular, UDRI attempted to make life predictions based on the stress concentration maps by treating each pixel in the map as having a certain probability of failure that was based on extensions of Weibull's formalism, ac-

counting for area effects in the same way Weibull accounted for specimen length. The probability of failure of each pixel was calculated using the stress concentration, the stress-strain curve, a fit to the Coffin-Mason relationship for strain-life data, Morrow's factor, and an extension of the Weibull formalism to account for pixel size. A statistical manipulation then produced the probability of failure (to crack initiation in this case) for all pixels in the corrosion patch. Preliminary trials were encouraging, but additional test cases revealed that the method was not always conservative in its predictions.

Subsequent to the above discoveries, NAVAIR developed the Equivalent Stress Riser (ESR) model, which models the life – not of pixels, but of individual pit-like features in the corrosion identified by the elasticity model [3]. The stress concentration for each feature is estimated using the UDRI pit metric, as improved by ESRD's extension to account for differences between FEA results and the pit metric and to account for orientation of the pit with respect to the load direction. In the ESR model, the probability of failure is calculated from strain-life data and a Peterson notch sensitivity factor, which moderates the effect of the stress riser by a factor dependent on the size of the notch. In particular, notches with smaller root radii are hypothesized to have smaller effects on life than notches with the same stress concentration, but larger root radii. The cumulative effect of all features is handled probabilistically. A set of algorithms was developed on the program to search through the stress concentration map to find regions of interest (ROIs) with high stress concentration. An ellipsoid is fit to each ROI and the root radii are estimated. Tests of the ESR model on the corrosion-fatigue specimens have shown a consistent conservativeness in the life predictions. The question of how to deal with this conservativeness was a topic for the third contract.

In parallel with efforts to develop life prediction models, a study of various statistical metrics for corrosion severity was conducted. In particular, standard and novel roughness statistics were calculated and compared to corrosion-fatigue test results to investigate the effectiveness of each candidate metric as a measure of both corrosion severity and effect on fatigue life. Standard roughness metrics included R_a, the mean of the absolute difference between the surface height and the mean surface height, and R_q, the standard deviation of the surface height (or more accurately, the root-mean-square of the surface height). Variations on these metrics included scaling the metric by the applied load and constructs involving the stress concentration values. While

some of these novel metrics showed improved correlations to reduction in fatigue life, the improvements were marginal. R_q and R_a seem to provide the most robust metrics for surface roughness; however, there remains a need to account for the local applied load. In addition, studies were carried out to understand the effect of spatial resolution on the metric values and on correlation to reduction in fatigue life. This work anticipates the ultimate implementation of low-resolution NDE methods to screen components and categorize corrosion severity. Down-sampled and filtered white light surface height profiles were used to calculate surface roughness metrics, which were then compared to the same metrics determined from full-resolution surface height profiles.

Finally, during the second contract on the Navy Corrosion-Fatigue Assessment Program, an implementation strategy was developed. This scheme is described by a flow chart starting with a visual inspection of the component on-board an aircraft carrier. If corrosion is observed, it is cleaned and an inspection performed. The relatively low resolution of this inspection prohibits a detailed application of the equivalent stress riser model; however, the inspection can be used to calculate corrosion metrics, such as R_a or R_q, and then to classify the corrosion as cosmetic, mild, or severe. If the corrosion is cosmetic, it will have no significant impact on component life and the component can be cleaned and coated (to prevent corrosion) and returned to service. If the corrosion is deemed to be severe, then the component is removed from service; the reduction in fatigue life is too great to allow the component to remain in service. If the corrosion is mild, then a replica is made of the corrosion, which is then sent to the depot for a high-resolution surface height mapping and subsequent analysis. At this point, the Equivalent Stress Riser model is applied in order to make a disposition decision concerning the component.

Just as there was much overlap in schedule between the first and second contracts on this program, there has been much overlap between the second and third. During the third contract, the program focused on AF1410 arrestment shank life predictions and fatigue tests, continued preparation of Aermet 100 tests (some of which were started), investigations into methods to calibrate the ESR model, development of a grid method of corrosion classification and life prediction, and verification and validation of the various models developed on the program. Verification and validation included both a series of tests on AF1410 micro-machined fatigue test specimens and manufacture and blind tests of cadmium-plated AF1410 corrosion-fatigue test specimens, with associated life predictions from the ESR model.

Earlier in the program, replicas were made of the inside surface of three real AF1410 arrestment shanks that had been taken out of service. Each shank was found to have corrosion on this inner surface. A fixture was manufactured that would allow the curved replicas of the inner shank surface to be scanned with the white light interference microscope to map the surface profile for study on the program. Due to the curvature of the replicas, only very narrow strips of the surface profiles could be captured without repositioning the replica. While the fixture simplified this process, each replica required weeks of scanning on the white light interference microscope to construct an accurate and complete profile of the surface height variations. Therefore, only selected portions of the replicas were scanned. In the meantime, the shanks were fatigue tested to failure. Results of the life predictions and tests are found in an accompanying report [4].

As mentioned above, Aermet 100 test specimen manufacture continued on the third contract. A set of 74 corrosion-fatigue specimens was fabricated and polishing begun. Other specimens for baseline material tests were also made, including strain-life specimens. The baseline and strain-life tests were begun on this program, but these tests and the corrosion-fatigue tests will need to be completed on a subsequent program. Details of the specimens and tests completed on this program are discussed in the appropriate sections in this report and an ancillary report [5].

During the previous contract, an equivalent stress riser model was developed. It was discovered that the model gave consistently conservative estimates of life. For this reason, methods were pursued to calibrate the model to produce less-conservative life predictions. One of these attempts is described in this report. The effort was not conclusive and additional study is recommended.

In an effort to establish an implementation scheme that includes an NDE method to classify corrosion, a grid method for life prediction was proposed. In this method, an appropriate surface roughness metric would be determined based on surface height profiles within elements of a grid overlaid on the surface of the specimen or component. During development, these surface height metrics would be determined from white light interference microscope profiles, but in practice, this would need to be determined from NDE methods, such as surface height profiles determined ultrasonically. During this contract, a fit was established between the grid statistics determined from the ultrasonic measurements and those determined from the white light measurements. In practice, the proposed approach would require that grid statistics be found for a

component using the NDE method, from which white light statistics would be calculated using the fit found on this program. The white light statistics would then be used to make a life prediction based on an extension of the equivalent stress riser model to the grid metrics. A corrosion classification could then be made to categorize the corrosion as cosmetic (no impact on life), mild (a moderate impact on life calling for additional analysis with the original equivalent stress riser model), or severe (unacceptable impact on life). The grid model itself is discussed in this report and in an ancillary report referenced herein. The correlation study between NDE and white light measurement of the grid statistics is covered in this report.

An important component of this program has been verification and validation of the life prediction models. Verification refers to steps to confirm that the software code accurately reflects the physics being modeled (code verification) and that the calculations conducted by that code are correct (calculation verification). Validation refers to the steps taken to confirm that the model predictions are experimentally correct. A verification and validation plan was created and considerable work was accomplished on this program. Of particular importance were two sets of validation experiments conducted. A set of fatigue specimens were created with micro-machined features produced in the gauge section of each specimen. The features were designed to have identical stress concentration factors, but of different shapes. The test specimens were all identical in order to have replicate tests that would reveal feature and material effects. The second test was a blind validation experiment on AF1410 cadmium-plated corrosion-fatigue specimens. A small patch was sanded in the center of the gauge section in each plated specimen in order to compromise the cadmium plate (otherwise corrosion would not grow) and then the specimens were exposed to a salt fog containing SO_2 for a set period of time (a different method of growing corrosion than used previously in the corrosion-fatigue tests on this program). Subsequently, the corrosion products were removed, surface height profiles determined, and the specimens fatigue tested until failure. Each fracture surface was examined to ascertain the number of cycles to crack initiation. The surface height profiles were used to make life predictions to compare to the actual, experimentally determined fatigue lives. The results of these tests are included in this report and in the modeling report [4].

This report and the other reports referenced herein give detail to the above accomplishments on this third program contract.

Section 3
Effects of Corrosion Damage on Fatigue Life

3.0   Introduction

A key component of this program has been the creation of a statistically significant database of tests results that could be used to support the creation and validation of models to predict cycles to crack initiation in high-strength steels. As part of the first contract on the program, a set of AF1410 corrosion-fatigue test specimens were manufactured and tested. Supporting material property tests were conducted, including fatigue crack growth rate tests and various others. These results were reported in the final report of the first contract [1]. One challenge encountered on the first tests on AF1410 was that large residual stresses were left in the surface of the corrosion-fatigue test specimens due to the grit-blasting process that was applied to them. Consequently, a second set of AF1410 corrosion-fatigue specimens, without the grit-blasting step, was manufactured as part of the second contract. Additional supporting tests were also accomplished on this second batch of AF1410 specimens as part of the second contract.

With the intent of extending the program to other high-strength steels, a set of 300M steel corrosion-fatigue specimens were prepared under the second contract. Unfortunately, after testing began, it was learned that the batch of 300M used for these specimens was contaminated with titanium inclusions and testing was halted.

Another material was selected for study, Aermet 100, and a set of corrosion-fatigue, baseline material, and strain-life specimens were manufactured. Program priorities caused these tests to be only partially completed; however, a description of these specimens and the associated tests accomplished on the third contract are described in this section.

A set of tests was conducted on AF1410 corrosion-fatigue specimens that had microfeatures machined into them. These tests and results are described in this section and the Boeing final report in Appendix B.

Finally, a set of AF1410 cadmium plate corrosion-fatigue specimens were prepared and tested. These activities are also included in this section.

3.1   300M Testing

The Navy supplied a billet of 300M, approximately 24″ x 48″ x 6″ weighing 1848 lbs., from Metcut Research, Inc. in the normalized and overaged condition. Billet history is as follows:

- Billet, 24″ x 4″ x 6″ (1848 lbs.) received from NAVAIR through Metcut Research approx. 9/15/04.
- Billet hardness measured by Dale Grant. Average hardness: Rc = 23.1 (see Table 3.1).
- Billet cut into smaller pieces by Dayton Forge ~10/04.
- Specimen blanks machined from billet ~8/05.
- Specimen blanks heat treated by Rex Heat Treat – Lansdale, Inc. per Mil-H-6875.
- Heat-treated specimens returned during September 2005.
- AccuGrind Manufacturing Blanchard ground and low-stress ground C-F specimens. Other specimens completed ~1/06.
- Specimen preparation put on hold until 10/06 due to AF1410B test priorities.
- AccuGrind polished C-F gage sections ~11/06.
- First C-F Specimen #622-2 tested at 170 ksi. Specimen fractured after 17,523 cycles.

Test specimen blanks were cut from this billet as described.

Table 3.1. NAVAIR 300M Billet History

Hardness Measurements	
Tester:	Krautkramer Branson MIC 10DL
S/N:	34103-2975
Calibration:	-305
Test by:	D. Grant
Date:	21-Dec-04

Test	AF1410*	300M**
1	47.8	22.2
2	48.9	22.6
3	46.2	25.4
4	47.1	21.1
5	46.4	25.4
6	44.3	22.0
7	45.3	21.6
8	44.5	19.0
9	50.3	24.0
10	46.4	27.9
Mean	**46.7**	**23.1**

Notes:
| * | Long, thin slab |
| ** | Rectangular slab |

3.1.1 Baseline Mechanical Tests

Baseline tests were planned for 300M to determine the hardness, Young's modulus, Poisson's ratio, tensile strength, fracture toughness, and fatigue crack growth rates of the material. The planned test matrix for 300M is shown in Table 3.1.1-1.

Table 3.1.1-1. Planned 300M Test Matrix

Test Type	Load Ratio	Specimen Type	Grain Orientation	Repetitions
Fatigue Crack Growth Rate	0.1	C(T)	T-L	
Fatigue Crack Growth Rate Threshold Region	0.1	C(T)	T-L	2
Fatigue Crack Growth Rate	0.1	C(T)	L-T	3
Fatigue Crack Growth Rate Threshold Region	0.1	C(T)	L-T	2
Fatigue Crack Growth Rate	0.5	C(T)	T-L	3
Fatigue Crack Growth Rate Threshold Region	0.5	C(T)	T-L	2
Fatigue Crack Growth Rate	0.5	C(T)	L-T	3
Fatigue Crack Growth Rate Threshold Region	0.5	C(T)	L-T	2
Fatigue Crack Growth Rate	0.1	M(T)	T-L	1
Fatigue Crack Growth Rate	-1	M(T)	T-L	4
Fatigue Crack Growth Rate	0.1	M(T)	L-T	1
Fatigue Crack Growth Rate	-1	M(T)	L-T	4
Fatigue Crack Growth Rate in NaCl Environment	0.01	C(T)	L-T	2
Fatigue Crack Growth Rate in NaCl Environment	0.01	C(T)	T-L	2
Fracture Toughness	-	C(T)	L-T	6
Modulus Test	-	Flat dogbone	Longitudinal	2
Poisson's Ratio	-	Flat dogbone	Longitudinal	2
Tensile Strength	-	Flat dogbone	Longitudinal	4
Corrosion Fatigue	-	C-F	Longitudinal	60

Specimen coupons for each test specimen were fabricated and heat treated by Rex Heat Treat – Lansdale, Inc. per Mil-H-6875 (the Navy Specification for 300M is GSS 5100) prior to final specimen machining. Based upon a review of a 300M Corrosion-Fatigue Study for the Air Force report [6], NAVAIR decided to suspend baseline mechanical tests for 300M and perform a limited number of corrosion-fatigue tests. Reference 6 describes a study of the corrosion suppression capabilities of different corrosion-preventive compounds (CPCs) used on 300M high-strength steel. The significance of their initial results to the Navy Corrosion-Fatigue study was that the mechanism for corrosion-fatigue interaction and the 300M steel was different than that seen in the AF1410. A relatively small amount of corrosion (one GM9450P corrosion cycle) showed a significant debit in fatigue life. Therefore, to verify the results of the Air Force study on 300M, only 10 corrosion-fatigue tests were planned and are described here.

3.1.2   300M Corrosion-Fatigue Tests

Corrosion-fatigue tests were conducted to assess the effect that corrosion had on the fatigue life of 300M. The test procedures and marker band cycle scheme used previously for AF1410 Set B specimens were employed [1]. Constant-amplitude loading was specified for all 300M corrosion-fatigue plate tests to minimize spectrum effects and provide a direct comparison to constant-amplitude probabilistic strain-life curves. The marker band pattern in Figure 3.1.2-1 and Table 3.1.2-1 is repeated until final specimen fracture.
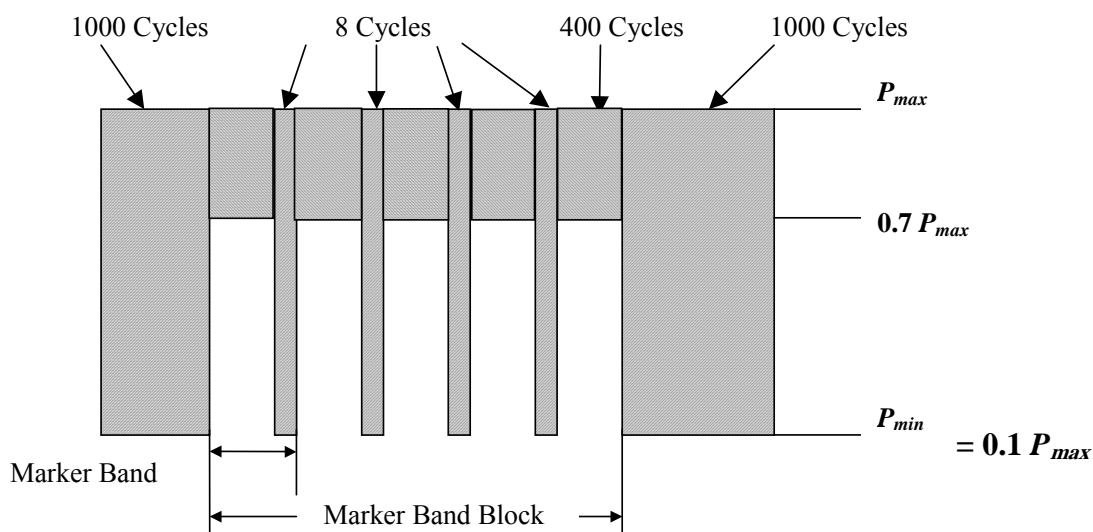
Figure 3.1.2-1. Four-marker band pattern.

Table 3.1.2-1. Marker Band Schedule

Block Number	Constant-Amp. Cycles	Marker Bands at End of Block	Marker Cycles	Total Cycles
1	1000	3	1624	2624
2	1000	5	2440	6064
3	1000	7	3256	10320
4	1000	4	2032	13352
5	1000	6	2848	17200
Repeat Blocks 1 to 5	1000	Restart pattern at 3		

The number of bands in successive marker blocks is ordered non-sequentially to aid in distinguishing between adjacent block marker values on the fracture surface. Quantitative Fractography (QF) was utilized to measure crack depths for estimating the crack initiation life of failed test specimens.

Corrosion-Fatigue Tests – 300M

Corrosion-fatigue (C-F) test specimens were manufactured from a billet of 300M supplied by the Navy. Rough specimen coupons were cut from the billet while in the normalized and overaged condition, in the L-T orientation. Ten C-F coupons 0.75″ x 2.5″ x 16″ of 300M were manufactured by UDRI and heat treated by Rex Heat Treat. All coupons were from the same heat lot (Number 406909) and delivered in a normalized and overaged condition. Following heat treatment, Accu-Grind & Manufacturing Co. machined the 300M coupons into C-F test specimens using low-stress grinding procedures developed for the AF1410B C-F specimens.

Specimen

The 300M C-F test specimens were machined to the same final dimensions as the AF1410B C-F test specimens (shown in Figure 3.1.2-2). The hardness was verified for one specimen and found to be HRc = 55.0.
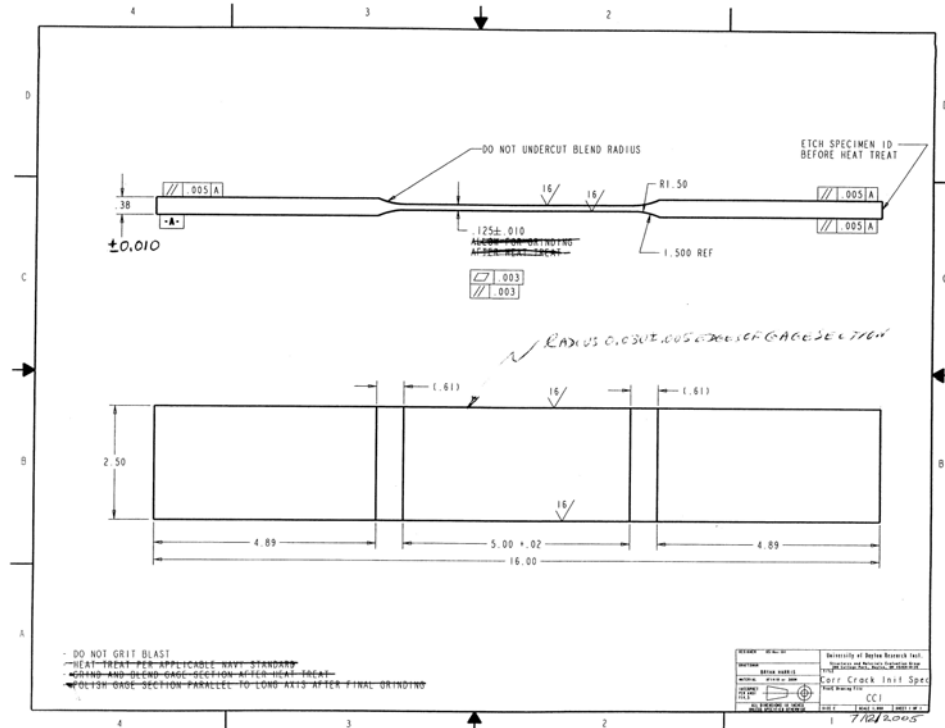
Figure 3.1.2-2. *300M corrosion-fatigue specimen drawing.*

Equipment

Specimens were tested in an MTS closed-loop, servo-hydraulic test machine equipped with a 220 kip actuator and hydraulic grips. The grips were aligned in the test machine using a rectangular bar instrumented with strain gages. Spacers were used to center the test specimens in the grips. An MTS Teststar II controller and PC provided constant-amplitude load control, input of the marker band spectrum, and recorded fatigue data.

Procedures

Each 300M C-F test specimen was mounted and aligned in the hydraulic grips. The controller was programmed for a peak stress of 170 ksi and stress ratio R = 0.1. The C-F specimen was subjected to constant-amplitude axial fatigue loading until failure.

Test Results

Three baseline fatigue tests were planned using bare 300M C-F specimens (no corrosion). C-F baseline specimen 622-2 failed after only 17,523 cycles. The fracture surfaces were cut from the specimens and examined using quantitative fractography. Two cracks were found on the fracture surface of 622-2 that initiated at the surface at very small surface anomalies. Further examination

18

of the fracture surface with SEM revealed that both cracks failed due to Ti-rich inclusions near the surface. A second C-F baseline specimen, 622-4, failed after only 62,491 cycles. SEM examination of this specimen revealed Ti-rich inclusions also. All C-F testing of 300M was halted at the direction of NAVAIR as a result of these findings. See Reference 2 for further details.

3.2   AF1410 Micro-Machined Specimen Study

3.2.1   Micro-Machined Specimen Testing

ESRD proposed a study to determine the effect of microscale surface features on the locations of sites of crack initiation from the point of view of patterns of simple, tightly regimented geometric features. The study was conducted as outlined in ESRD's final report included in Reference [2].

Specimen

Micro-machined test specimen blanks were cut from the grip end tabs of previously tested AF1410B corrosion fatigue specimens. Two specimen blanks, 1″ x 4″ were machined from nine tab ends, for a total of 18 specimens. UDRI worked with Accu-Grind & Manufacturing Co. to machine the dogbone specimens per Figure 3.2.1-1. Boeing Corporation machined the micro-machining features into each specimen. The final configuration of the test specimens with the six features is shown in Figure 3.2.1-2. Feature #1 in the image is a horizontal (relative to the vertical load direction) pill shape. Feature #2 is a cone shaped feature. Feature #3 is a horizontal ellipsoid features. Feature #4 is a vertical pill shape. Feature #5 is a second cone. And feature #6 is a vertical ellipsoid.
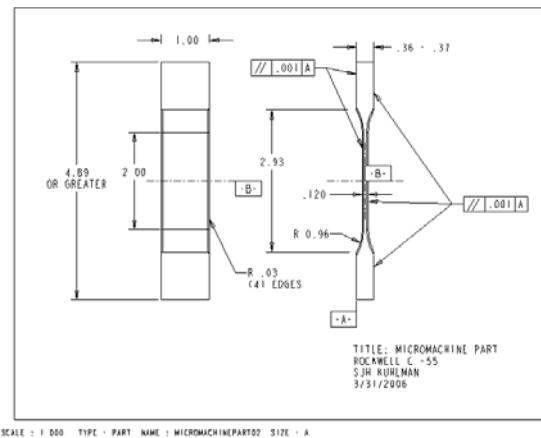
Figure 3.2.1-1. *Micro-machined specimen drawing.*
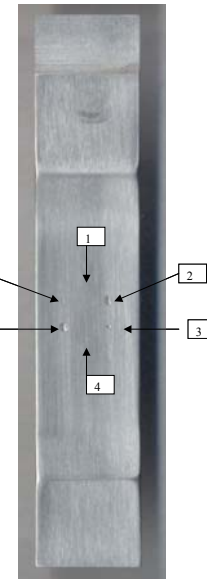
Figure 3.2.1-2. *Typical micro-machined specimen.*

Equipment

An MTS closed-loop, servo-hydraulic test machine equipped with a 50 kip actuator and 50 kip hydraulic grips was used to perform the tests. An MTS 458 controller was used with control signals supplied by a UDRI MATE system. The same marker band spectrum used for the corrosion fatigue specimens was programmed into the MATE system and the grips were aligned in the test machine using a rectangular bar instrumented with strain gages.

Procedures

The residual surface stress in the gage area of three micro-machined test specimens after polishing was determined by Lambda Technologies. Each micro-machined specimen was mounted and aligned in the hydraulic grips. The C-F specimens were subjected to constant amplitude axial fatigue loading. The controller was initially programmed for a peak stress of 170 ksi and a stress ratio R = 0.1. The peak stress had to be increased to produce reasonable duration failures as described below.

Test Results

Lambda Technologies measured the surface residual stress for three micro-machined test specimens shown in Table 3.2.1-1.

Table 3.2.1-1. Surface Residual Stress Measurements

SPECIMEN	RESIDUAL STRESS (ksi)	(MPa)	PEAK WIDTH (deg)
598-11	-118.2 ± 3.7	-815	± 26 3.48
598-14	-101.5 ± 3.3	-700	± 23 3.53
598-15	-107.9 ± 3.6	-744	± 25 3.66

Baseline tests were performed on six bare, polished specimens. At 170 ksi, one specimen did not fail after 3.7 million cycles. The decision was made to increase the peak stress to 180 ksi. This specimen and another ran approximately 4 million cycles before failure. The peak stress was increased to 200 ksi, at which failures occurred within 100,000 cycles. The decision was made to test the micro-machined specimens at a peak stress of 200ksi to ensure early failures. A total of 10 micro-machined AF1410 specimens were tested to failure as shown in Table 3.2.1-2. Tested specimens were provided to the IMMC Group for inspection of the fracture surfaces.

Table 3.2.1-2. Micro-Machined Test Matrix

AF1410 Micro-machined Specimen Test Matrix										
STL ID No.	Width	Thickness	X-Sect. Area	Corrosion Type	Fatigue Start Date	Fatigue End Date	Stress (ksi)	Cycles to Failure	End Pts Recorded	Notes
598-11	1.01633	0.12115	0.12313	Baseline	3/1/2007	3/1/2007	200	90,441	180,882	4
598-14	1.01650	0.12137	0.12337	Baseline	2/28/2007	2/28/2007	200	55,148	110,296	
598-16	1.01633	0.12080	0.12277	Baseline			170	278,218	556,436	2
598-18	1.01633	0.12065	0.12262	Baseline	11/13/2006	2/4/2007	170	3,698,000		1
598-18	--	--	--	Baseline	--	2/5/2007	180	258,358		1
598-4	1.01583	0.12055	0.12246	Baseline	2/28/2007	2/28/2007	200	92,900	185,799	
598-6	1.01550	0.12062	0.12249	Baseline	2/6/2007	2/21/2007	180	4,522,917		
598-15	1.01617	0.12130	0.12326	Baseline						5
598-17				Baseline						5
598-1	1.01633	0.12118	0.12316	Micro-machined	3/2/2007	3/2/2007	200	11,109	22,219	
598-10	1.01650	0.12072	0.12271	Micro-machined	3/6/2007	3/6/2007	200	8,416	16,832	
598-12	1.01650	0.12082	0.12281	Micro-machined	3/7/2007	3/7/2007	200	8,726	17,452	
598-13	1.01633	0.12120	0.12318	Micro-machined	3/7/2007	3/7/2007	200	12,697	25,693	
598-2	1.01600	0.12115	0.12309	Micro-machined	3/5/2007	3/5/2007	200	9,279	18,558	
598-3	1.01583	0.12075	0.12266	Micro-machined	3/7/2007	3/7/2007	200	10,351	20,702	
598-5	1.01617	0.12113	0.12309	Micro-machined	3/5/2007	3/5/2007	200	12,433	24,865	
598-7	1.01617	0.12108	0.12304	Micro-machined	2/5/2007	2/5/2007	180	13,735	23,489	3
598-8	1.01600	0.12120	0.12314	Micro-machined	3/6/2007	3/6/2007	200	9,595	19,190	
598-9	1.01567	0.12110	0.12300	Micro-machined	3/6/2007	3/6/2007	200	11,435	22,869	
Notes:										
	1	Specimen tested at 170 ksi with load ramp (microprofiler) 3,698,000 cycles and with sinusoidal function 1,054,045;								
		total cycles at 170 ksi - 4,752, 045; restarted at 180ksi - 258,358 cyles to failure								
	2	Specimen fractured in the grip near transition and original half-hole in tab								
	3	Specimen appears to have failed at large conical feature								
	4	Used for Surface Residual Stress Measurement								
	5	Not Tested								

Typical fatigue results for the micro-machined corrosion-fatigue specimens are as shown in Figure 3.2.1-3.
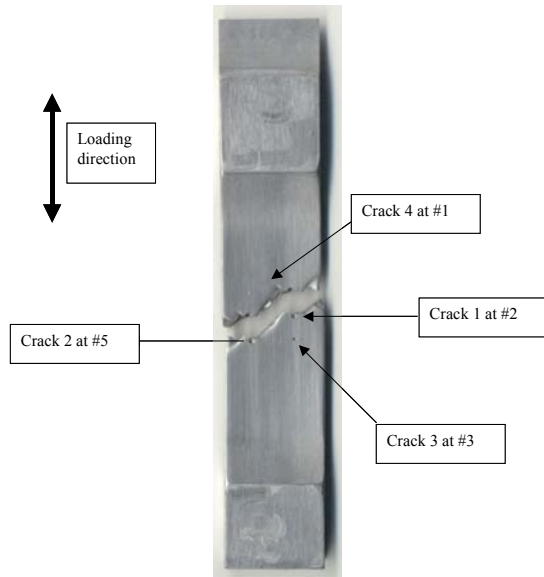
Figure 3.2.1-3. Micro-machine Specimen 598-7 loaded at 180 ksi showing crack initiation sites.

Four cracks were found in this specimen in the largest features that were cone shaped and in the defects whose long dimension ran perpendicular to the loading direction – Cracks 1 and 2 were on the fracture plane, Cracks 3 and 4 were not. The images in Figures 3.2.1-4 through 3.2.1-8 show Cracks 1 and 2 from the fracture plane and Cracks 3 and 4 from the specimen surface.
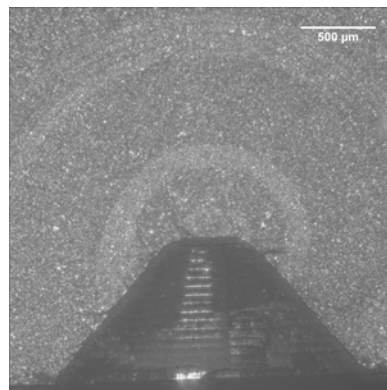
Figure 3.2.1-4. Deep-focus image of Specimen 598-7 – Crack 1 at Feature #2.
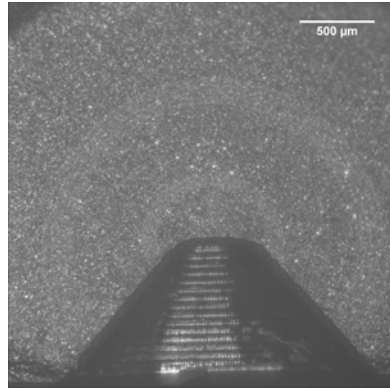
Figure 3.2.1-5. *Deep-focus image of Specimen 598-7 – Crack 2 at Feature #5.*
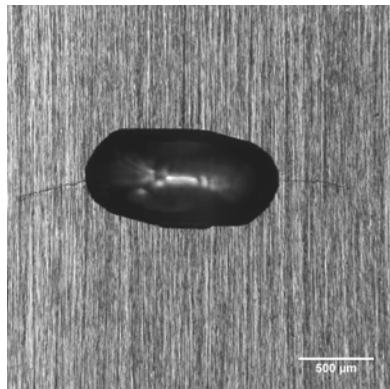
Figure 3.2.1-6. *Deep-focus image of Specimen 598-7 – Crack 3 at Feature #3.*
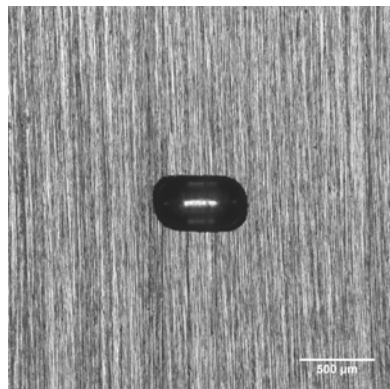
Figure 3.2.1-7. *Deep-focus image of Specimen 598-7 – Crack 4 at Feature #1.*

The fourth crack is deep within Feature #1 and did not grow all the way out to the surface.
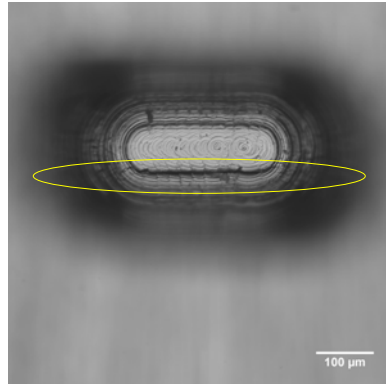
Figure 3.2.1-8. Magnification of deep-focus image of Specimen 598-7 – Crack 4 at Feature #1.

No cracks were found in the features whose long dimension ran parallel to the loading direction (see Figures 3.2.1-9 and 3.2.1-10).
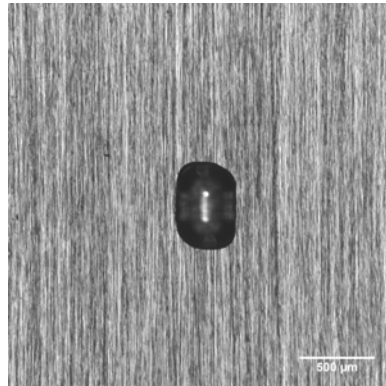
Figure 3.2.1-9. Deep-focus image of Specimen 598-7 – Feature #4.
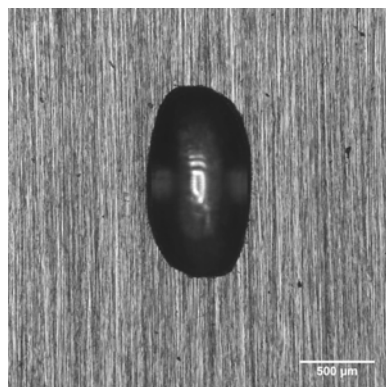
Figure 3.2.1-10. Deep-focus image of Specimen 598-7 − Feature #6.

Additional information about the micro-machine test results can be found in Appendix B.

3.3 AF1410B Cadmium-Plated Corrosion Fatigue Tests

3.3.1 Objective

The objective of this task was to perform an experiment to validate the life-prediction model developed on the program for fatigue of corroded high-strength steel. On the program, experimental and analytical tools were developed to model the effect of corrosion on the fatigue life of AF1410 high-strength steel using laboratory studies. The experimental methods used to develop the model focused on a simple case where bare AF1410 steel specimens with two different surface finishes, grit-blasted and rough-polished, were corroded in the laboratory using an accelerated process developed on the program, and then fatigue tested. The goal of this task was to increase the complexity of the experiment in order to achieve an effect that more closely simulates the service-induced corrosion incurred on fleet arrestment shanks in order to validate the life-prediction model on a more representative test specimen.

3.3.2 Material

For the validation tests, AF1410 fatigue specimens were plated with cadmium (Cd or Cad) and given a chromate conversion coat similar to the fielded arrestment shank components. The material used in this experiment came from the same billet and heat treat lot that is referred to as AF1410 "Set B" or "Batch B". Bare material dogbone specimens were machined to the same geometry and rough polished in the same way as in the experiments used to development the model. The test specimens and extra trial materials were then sent to Southwest United Industries to be low-embrittlement (LE) Cad plated per Boeing Process Specification 13144G, Type II, Class 1. Type II cadmium plating means a supplementary chromate treatment is applied and the Class 1 reference is a minimum thickness requirement of 0.0005″. The specimens were stress-relieved and grit-blasted (in the radius and gage sections) prior to plating, as well as stress relieved to prevent hydrogen embrittlement following the plating process per the specification. Some variation in the color and surface finish was observed in the specimens and some variations in the plating thickness were measured using a magnetic induction device.

3.3.3 Test Methods

Trial Testing

The procedures used to prepare and corrode the validation test specimens were developed by trial testing on small 2″ x 2″ wafers and "dummy" fatigue specimens that were plated in the same way as the actual fatigue test specimens.

For the validation tests, it was decided to mechanically damage, or thin, the plating in a 1-inch diameter area in the center of the gage section to help the corrosion of the steel form in that area and to influence the initiation of corrosion more like that in the fielded component where mechanical damage may also play a role. The small wafers were used to determine the best way to abrade the test area as far as size of grit to use and the amount of removal. A 1-inch circular test area was used in the previous experiments on the program and deemed an appropriately sized and shaped test area for data collection and fatigue testing. X-ray techniques were used to gage the ratio of Fe to Cd during sanding on the wafers and a magnetic induction devise was used to measure residual plating thickness in each case. The wafers were distributed to different facilities for testing using different exposure techniques by UDRI and by Boeing. UDRI exposed wafers using the same technique as during experiments to develop the model described in Reference 1. Boeing exposed the wafers using three different techniques: 1) neutral salt fog, 2) acidic salt fog (salt fog + SO2), and 3) Prohesion (salt fog + humidity and drying cycles). All salt fog exposure techniques used by Boeing followed ASTM G85. More information regarding the corrosion exposure testing performed by Boeing can be found in Appendix B. Once exposed, the wafers were cleaned using Turco alkaline rust remover and their roughness measured using UDRI's NT-8000 optical profilometer. The R_a and R_q results were used to narrow the test conditions to using 180 grit sandpaper for preparation and to expose the specimens using the acidic salt fog technique. The results from the wafers also provided a roughness metric to aim for with the actual fatigue specimens. The results from one of the wafers, which are considered to be desirable for the fatigue test specimens, are shown below in Table 3.3.3-1.

Table 3.3.3-1. Desirable Results from a Trial Test Wafer

	Test	Grit Size	Cd Thickness	Exposure	Time	Area	R_q	R_a
5 corroded	1	180	0.15 mils	SF w/SO2	53.75 hrs.	5.99E+08	9.556307	7.462873
						3.65E+07	4.123146	3.251557

One shortcoming of this trial testing was that the Cd plating thickness on the wafers ended up being thin and not within specification; the plating thickness on the fatigue specimens was considerably thicker and within specification. This fact extended the time of exposure required for the fatigue specimens in the acidic salt fog to get the desirable roughness as seen on the wafers. Therefore, repeating the procedures developed for the wafers on "dummy" fatigue specimens proved to be invaluable and allowed improvements to be implemented on the actual test

specimens. Those that were considered the "dummy" specimens had been fatigue tested to run-out conditions, presumably without damage, during the main experiments on the program.

On the "dummy" specimens, the test area was prepared in the same way as on the wafers. It was expected that the plating outside the 1-inch circular test area would provide for a natural masking over the entire gage section area, as long as the thickness of the plating was adequate. The results of the "dummy" tests showed two important outcomes: 1) small differences in the plating thickness in the test area could extend the required expose time considerably, and 2) there are probably large variations in the plating thickness over the fatigue specimens' gage section, which requires additional protection from corrosion exposure.

Validation Test Specimens

From the lessons learned on the wafers and the "dummy" fatigue specimens, the procedures for preparing and exposing a total of (4) validation test specimens were developed. The validation test specimens were first prepared by UDRI by dry sanding the 1-inch diameter region in the center of the gage section to remove the chromate conversion coating and to damage the cadmium plating. Sanding was performed in the 1-inch region to the same level as done during trial testing using the same confirming x-ray and magnetic induction techniques. Additional sanding was then performed within circular areas that were less than 1-inch in diameter to provide a thickness gradient from the edge of the 1-inch diameter inward, where the very center was thinned all the way down to bare metal. This was to ensure that corrosion would initiate in the center of the gage section.

The specimens were then sent to Boeing where the specimens were further prepared for exposure by masking the entire gage section except for a 1.5-inch diameter circle, which was centered on the 1-inch diameter sanded region. The masking material used was painted on and easily removable. The slightly oversized exposed area (1.5-inch diameter) was to minimize any effects of undercutting at the masked edge by leaving some as-received plating and chromate exposed. The acidic salt fog exposure was performed by Boeing in the same way as the trial testing using ASTM G85-modified techniques for acidic salt fog. A minimum time of exposure was set by trial testing and a visual check for stopping the exposure was defined as corrosion reaching out to the masking diameter. Based on the set criteria, the four specimens were pulled from the test chamber after being exposed for a total of 198 hours when the corrosion extended to the cir-

cular masked edge on each specimen. See Figure 3.3.3-1 for an image showing the specimens after being exposed with the masking still in place.
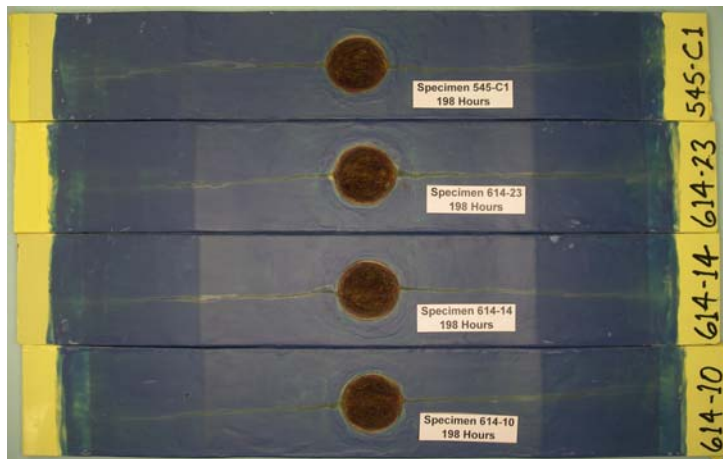
Figure 3.3.3-1. *Cadmium-plated corrosion-fatigue test specimens after exposure with masking still in place.*

Next, the specimens were sent back to UDRI where the masking was stripped and the corrosion by-products cleaned. The same cleaning techniques as used throughout the program were implemented on these specimens. Additional cleaning time was required on these specimens due to the amount of rust formed on the prepared test surface. A residual dark oxide remained on the surfaces of each specimen, even after extensive cleaning. Before and after cleaning images are shown in Figures 3.3.3-2 through 3.3.3-5 for each specimen.

Figure 3.3.3-2. *Cadmium-plated corrosion-fatigue test, Specimen 545-1C pre- and post-cleaning.*
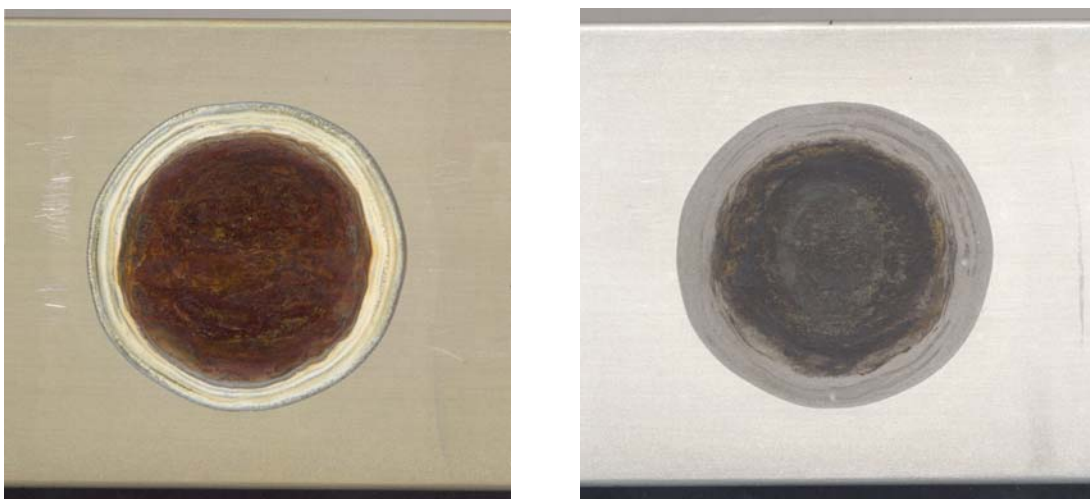
Figure 3.3.3-3. *Cadmium-plated corrosion-fatigue test, Specimen 614-10 pre- and post-cleaning.*
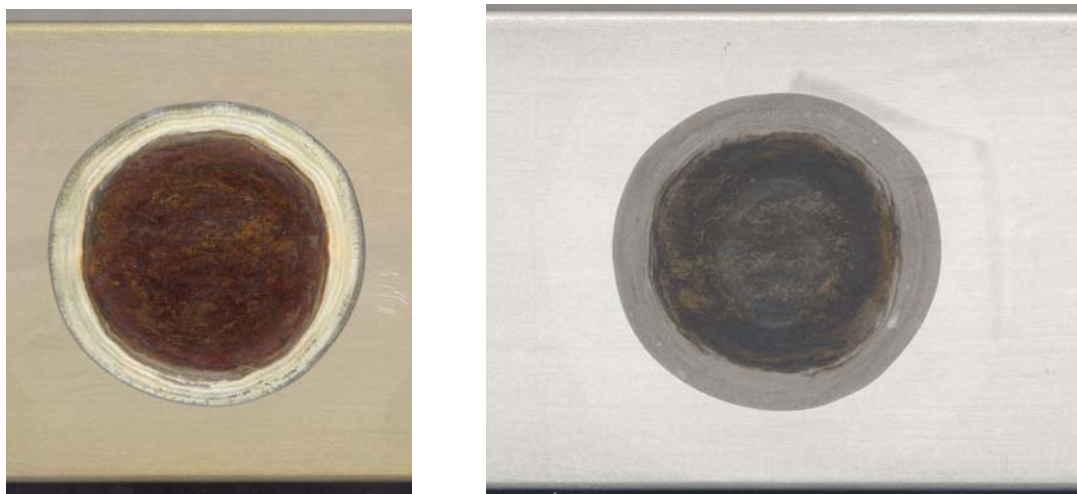
Figure 3.3.3-4. *Cadmium-plated corrosion-fatigue test, Specimen 614-14 pre- and post-cleaning.*
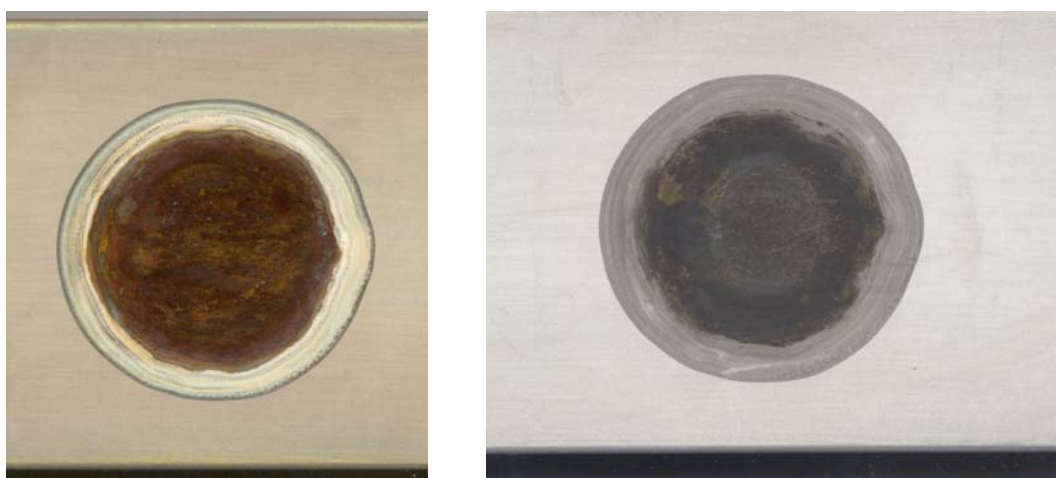
Figure 3.3.3-5. *Cadmium-plated corrosion-fatigue test, Specimen 614-23 pre- and post-cleaning.*

WLI Measured Roughness Statistics

Measurements of the corrosion topography on the corroded validation fatigue specimens were made the same as all others on the program at the University of Dayton Center for Materials Diagnostics using a WYKO NT-8000 optical profilometer. A slightly larger scan area was required to accommodate the slightly oversized corrosion patch left inside the unmasked region on the specimens. The data from the optical profilometer was used to compare roughness statistics and to perform the ROI analysis that feeds the life prediction model being validated. Replicas were also made of each corrosion-fatigue test specimen corrosion patch (no ultrasonic scans were made).

Results shown in Table 3.3.3-2 include the results for salt fog + SO2 exposure of wafers (in black), dummy fatigue specimens (in red), validation fatigue specimens (in blue), and from fielded components at the bottom.

Table 3.3.3-2. Roughness Statistics for the Cadmium-Plated Validation Specimens

	Test	Grit size	Cd thickness	Exposure	Time	Area	Rq	Ra
5 corroded	1	180	0.15 mils	SF w/SO2	53.75 hrs	5.99E+08	9.556307	7.462873
5 non-corroded						3.65E+07	4.123146	3.251557
7 corroded	1	400	0.15 mils	SF w/SO2	53.75 hrs	5.99E+08	3.387376	2.408396
7 non-corroded						3.65E+07	4.086726	2.699124
5 corroded	2	400	0.2 mils	SF w/SO2	62.38	5.99E+08	3.978028	2.978093
5 non-corroded						3.65E+07	4.579924	3.721808
7 corroded	2	180	0.05 mils	SF w/SO2	13.33 hrs	5.99E+08	2.540429	1.971447
7 non-corroded						3.65E+07	2.533804	1.950238
544-7B corroded	3	180	0.11 mils	SF w/SO2	54 hrs	6.94E+08	2.127896	1.491171
544-7B non-corroded						3.69E+07	4.471653	4.040293
545-5C corroded	4	180	0.16 mils	SF w/SO2	144 hrs	6.33E+08	2.618986	1.965789
545-5C non-corroded						1.21E+08	5.842211	4.54937
545-1C corroded	5	180	-0.05 to 0.25 mils	SF w/SO2	198 hrs	6.11E+08	7.781626	6.264256
545-1C non-corroded						7.07E+07	6.83173	5.368288
614-10 corroded	5	180	-0.02 to 0.28 mils	SF w/SO2	198 hrs	6.27E+08	8.487674	6.808064
614-10 non-corroded						7.69E+07	4.212959	3.311019
614-14 corroded	5	180	-0.02 to 0.12 mils	SF w/SO2	198 hrs	6.55E+08	7.315683	5.703609
614-14 non-corroded						9.18E+07	5.065595	4.24396
614-23 corroded	5	180	-0.05 to 0.15 mils	SF w/SO2	198 hrs	6.04E+08	14.77949	12.266828
614-23 non-corroded						8.37E+07	9.90941	8.382012
0735 bottom	1D					4.50E+07	4.167146	2.353748
	2D					4.24E+07	3.450348	2.188325
	3D					3.89E+07	4.314065	2.677822
0099	1					6.24E+06	56.412121	23.62325
	2					4.51E+06	63.031513	31.511585
	3					4.46E+06	60.264525	28.586136

Stress Concentration Calculations and ROI Analysis

White light interference microscopy profiles were processed to find a stress concentration map. The surface height profiles and stress concentration maps were used as input to the ROI analysis described in Reference 2. Thresholds for ROI identification were consistent with AF1410 Set A analysis (stress concentration threshold of 1.3 and area threshold of 36 pixels, or an area of 94 square microns). Tables of ROIs statistics have been provided to NAVAIR for life predictions.

3.3.4   Results

Fatigue Testing

Five of the eleven Cad-plated AF1410B C-F test specimens were fatigue tested as baseline specimens without any corrosion at 170 ksi. Two specimens (544-45C and 547-51D) were trial specimens that had previously been tested without failure. These and the baseline specimens (614-9, -16, and -24) failed in the gage section due to surface anomalies determined to be caused by the grit blasting. The results of the baseline tests are provided in Table 3.3.4-1.

Two Cad-plated C-F specimens (544-7B and 545-5C) were corroded by Boeing for exposure times of 54 and 144 hours, respectively, as trial tests to determine if the corrosion patch was sufficient to generate a fatigue crack. Both specimens had some corrosion in the blend radius on each side. The specimens were tested at 170 ksi and both failed outside of the corrosion patch between the patch and the blend radius. Specimen 544-7B failed due to surface anomalies. Specimen 545-1C failed in a corrosion area near the blend radius. The trial test results are also listed in Table 3.3.4-1.

Four Cad-plated C-F specimens (614-10, 545-1C, 614-14 and 614-23) were corroded for exposure times of 198 hours for validation testing. The gage section on these specimens was masked off, except for the corrosion patch. These specimens were also tested at 170 ksi and the results are also provided in Table 3.3.4-1. Specimen 614-14 failed outside of the corrosion patch, but a crack did initiate inside the corrosion patch. The specimen was cut and broken at this crack for fractography work. All of the other validation specimens failed in the respective corrosion patches. Figure 3.3.4-1 displays photos of the fracture pieces for these four specimens.

Table 3.3.4-1. Results of Cadmium-Plated Corrosion-Fatigue Validation Test

AF1410B Cd Plated C-F Specimen Test Results									
				Exposure	Test	Fatigue	Stress	Cycles to	Fracture
STL #	Width	Thickness	X-Sect Area	Time	Start	End Date	(ksi)	Failure	Area
547-45C	2.4920	0.1180	0.29401	BL-None	10/1/2007	10/2/2007	170	100,018	Crack at the surface
547-51D	2.4945	0.1099	0.27410	BL-None	10/2/2007	10/4/2007	170	161,077	Crack at the surface
544-7B	2.4958	0.1078	0.26905	54 hr	1/10/2008	1/11/2008	170	277,212	Crack at the surface
545-1C	2.4923	0.0773	0.19253	168	3/12/2008	3/13/2008	170	164,438	Thru Corrosion
545-5C	2.4945	0.1117	0.27851	144	2/13/2008	2/14/2008	170	158,963	Crack at the surface
614-9	2.4968	0.1268	0.31668	BL-None	10/9/2007	10/10/2007	170	161,569	Crack at the surface
614-10	2.4953	0.1272	0.31732	168	3/13/2008	3/14/2008	170	143,460	Thru Corrosion
614-14	2.4972	0.1270	0.31714	168	3/14/2008	3/15/2008	170	165,450	Above Corrosion, Crack in Corrosion
614-16	2.4932	0.1273	0.31746	BL-None	10/16/2007	10/17/2007	170	137,620	Crack at the surface
614-23	2.4978	0.1267	0.31639	168	3/17/2008	3/18/2008	170	165,094	Thru Corrosion
614-24	2.4967	0.1282	0.31999	BL-None	10/24/2007	10/25/2007	170	135,129	Crack at the surface
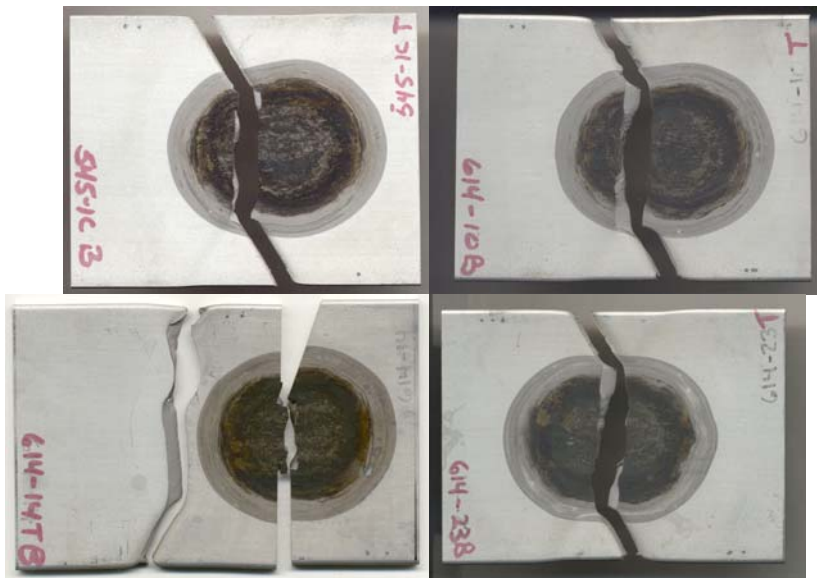
Figure 3.3.4-1. *Fracture pieces of the four validation test specimens with identifiers marked on the specimens.*

Quantitative Fractography and Critical Pit Measurements

Table 3.3.4-2 shows the results of quantitative fractography and critical pit measurements on the cadmium-plated test specimens. The number of cycles to crack initiation is derived from the quantitative fractography measurements and is given in the table. In the case of Specimen 614-14, the first life is for the crack that initiated outside the corrosion patch and the second life is for the crack that initiated inside the corrosion patch. These lives are to be compared to predictions made by NAVAIR for these specimens.

Table 3.3.4-2. Quantitative Fractrography and Critical Pit Measurements

Test Matrix Block	Specimen ID	Facility	Max Stress (ksi)	Main Failure Location	Cycles to Failure	Cycles to a=0.01" crack 1	Cycles to a=0.01" crack 2	Average Dimensions Critical Flaw 1			Average Dimensions Critical Flaw 2		
								H μm	W μm	D μm	H μm	W μm	D μm
Baseline Dummy	547-45C	UDRI	170	surface	100,018	86,480	---			55.4	--	---	---
	547-51D	UDRI	170	corner	161,077	148,504	142,068						
Corrosion Dummy	544-7B*	UDRI	170	surface	277,212	257,547	---	57.2	87.5	33.5	--	---	---
	545-5C*	UDRI	170	at radius	158,963	--	---	---	---	--	--	---	---
	*previously tested to over 1 million cycles												
	614-9	UDRI	170	surface	161,569	144,094	---	---	---	---			
Baseline	614-16	UDRI	170	surface	137,620	117,763	---	105.6	100.6	30.2	--	---	---
	614-24	UDRI	170	surface	135,129	116,894	---	34.5	44.5	30.9			
	614-10	UDRI	170	corrosion	143,460	121,634	---	83.1	112.9	33.6	--	---	---
Corrosion	614-14	UDRI	170	surface/corrosion	165,450	151,403	151,335	---	---	--	65.8	62.3	22.4
	614-23	UDRI	170	corrosion	165,094	148,596	---	50.7	66.7	26.7	--	---	---
Spare	545-1C	UDRI	170	corrosion	164,438	151,029	---	59.7	84.1	26.0	--	---	---
									280.8				
										* this measurement is for the largest overall pit - read commen			

3.4 Aermet100 Testing

The NAVAIR Airframe Technology Team (AIR 4.3.3.5) requested that the testing of AerMet100 be performed per Appendix C, Aermet 100 Test Plan. Due to program priorities, the tasks and test matrix were revised. The reduced AerMet100 Test Plan is shown in Table 3.4-1. Round billets of AerMet100 were obtained for UDRI from Carpenter Steel Company by Aero-space Engineering and Support, Inc. (AES), Ogden, UT. Seven billets 4.125″ in diameter and four billets 7″ in diameter were received from Carpenter. The pedigree, heat treat, and history of the billets have been made available to NAVAIR. AES cut the billets and machined them into the various specimen coupons per UDRI sketches, which were then shipped to UDRI. From there, UDRI rough-machined the specimens and shipped the coupons to Hercules Heat Treat for heat treatment according to Navy Specification PS-15169B. Once heat-treated, the coupons were final-machined by UDRI into the required test specimens.

The revised AerMet100 test matrix in Table 3.4-2 was followed, but not all tests were completed due to program priorities. Baseline material property tests were conducted to establish Young's modulus, Poisson's ratio, tensile strength, fracture toughness, and fatigue crack growth rates of the specimens.

Table 3.4-1. Test Plan for Aermet100 Materials Property Testing

STRESS-STRAIN CURVES & FATIGUE TESTS	
Test Coupon Fabrication	Coupons
Tensile (ASTM E8)	30
Compression (ASTM E9)	30
Strain-Life (ASTM E606)	200
Coupon Tests	Tests
Tensile (ASTM E8)	10
Compression (ASTM E9)	10
Incremental Step (ASTM E606)	10
Strain-Controlled Fatigue (ASTM E606)	90
Load-Controlled Fatigue (ASTM E466)	70

CRACK GROWTH & FRACTURE TOUGHNESS TESTS		
Test Type	R-Ratios	Tests
Crack Growth (+R)	0.1, 0.33, 0.5, 0.8	12
Crack Growth (-R)	-0.33, -1.0	6
Fracture Toughness (K_{Ic})		10

DRAFT STRAIN-LIFE TEST MATRIX		
Test Type	Strain Amplitude (in./in.)	Test Specimens
Low-Cycle Fatigue Tests		
Strain-Controlled	0.020	10
Strain-Controlled	0.015	10
Strain-Controlled	0.012	10
Strain-Controlled	0.010	10
Strain-Controlled	0.009*	15
Strain-Controlled	0.008*	15
Strain-Controlled	0.007*	15
High-Cycle Fatigue Tests		
Load-Controlled	0.006*	15
Load-Controlled	0.0055*	15
Load-Controlled	0.005*	15
Load-Controlled	0.0045*	15
Endurance Limit Tests (1.0×10^7 cycles runout)		
Load-Controlled	TBD*	10

*Initial overstrain for 10 cycles at 1.0% strain amplitude. Periodic overstrain for 2 cycles at 1.0% strain amplitude every 2.5×10^5 cycles.

Table 3.4-2. Revised Test Matrix for Aermet100

Test Type	Load Ratio	Specimen Type	Grain Orientation	Repetitions	Status
Fatigue Crack Growth Rate (E 647)	0.1	C(T)	L-T	5	7
Fatigue Crack Growth Rate Threshold Region	0.1	C(T)	L-T	2	2
Fatigue Crack Growth Rate	0.5	C(T)	L-T	5	5
Fatigue Crack Growth Rate Threshold Region	0.5	C(T)	L-T	2	2
Fatigue Crack Growth Rate	0.1	M(T)	L-T	1	0
Fatigue Crack Growth Rate	-1	M(T)	L-T	4	0
Fatigue Crack Growth Rate in NaCl Environment	0.1	C(T)	L-T	2	0
Fatigue Crack Growth Rate in NaCl Environment	0.5	C(T)	L-T	2	0
Fracture Toughness (E 399)	-	C(T)	L-T	10	10
Modulus Test (E 111)	-	Flat dogbone	Longitudinal	5	5
Poisson's Ratio (E 132)	-	Flat dogbone	Longitudinal	2	2
Tensile Strength (E 8)	-	Flat dogbone	Longitudinal	10	8
Compression (E 9)	-	Cylinder	Longitudinal	10	0
Incremental Step Test (E 606)	-	Uniform Gage Section	Longitudinal	10	0
Strain-Controlled Fatigue (E 606)	-	Uniform Gage Section	Longitudinal	90	7
Load-Controlled Fatigue (E 466)	-	Uniform Gage Section	Longitudinal	70	0
Corrosion Fatigue Endurance	-	C-F	Longitudinal	3	3

3.4.1   Tensile Tests

Heat Treat Tensile Travelers

Specimens

Five round dogbone tensile specimens were machined by UDRI. The gage section was nominally 0.25″ in diameter and 1.25″ long, and the grip section was comprised of 3/8-16 threads. These tensile specimens were heat treated during the same heat treat process as all AerMet100 specimen coupons.

Equipment

Specimens were tested in a 22 kip MTS closed-loop servo-hydraulic test machine with a 22 kip actuator. An MTS 632. 27b-30 mechanical extensometer was calibrated to a Class B2 level and loads were measured with a 22 kip load cell also calibrated to a Class B2 level. A digital data acquisition system was used to record data.

Procedure

Room-temperature tensile tests of the five travelers were performed per ASTM E8 (Tension Testing of Metallic Materials). Specimens were threaded into grips in the machine. The mechan-

ical extensometer was fastened to the specimen using rubber bands. A machine displacement rate of 0.05″/min. was used. Loads were measured with a load cell calibrated to Class A Level. The extensometer was removed prior to fracture.

Results

The elongation, reduction in area, 0.2% yield stress, and ultimate stress results are summarized in Table 3.4.1-1.

Table 3.4.1-1. Tensile Test Data

TENSILE TEST DATA

MATERIAL: **AerMet 100**   Heat Treat: Hercules PS-15169B

DATE: 2/20/07
MACHINE USED: Instron
TEST SPEED in/min: 0.05

ENGINEER: Abfalter/Kuhlman
TECHNICIAN: Woleslagle Don

SPECIMEN NO.	STL-662-1b	STL-662-2	STL-662-3	STL-662-4	STL-662-5	AVG	MMPDS S-Basis
TEST TEMPERATURE	72	72	72	72	72		
GAGE LENGTH ORIG. (IN)	1.005	1.003	1.004	1.006	1.005		
GAGE LENGTH FINAL (IN)	1.157	1.158	1.151	1.158	1.149		
ELONG. (IN)	0.151	0.155	0.146	0.152	0.144		
ELONG. %	**15.1**	**15.4**	**14.6**	**15.1**	**14.4**	**14.9**	10.0
ORIG. WIDTH OR DIA. (IN)	0.2487	0.2485	0.2499	0.2488	0.2509		
ORIG. THICKNESS (IN.)							
FINAL WIDTH OR DIA.(IN)	0.1610	0.1590	0.1600	0.1580	0.1620		
FINAL THICKNESS (IN.)							
AREA ORIGINAL (SQ. IN.)	0.0486	0.0485	0.0490	0.0486	0.0494		
AREA FINAL (SQ. IN.)	0.0204	0.0199	0.0201	0.0196	0.0206		
REDUCT. OF AREA	0.0282	0.0286	0.0289	0.0290	0.0288		
REDUCT. OF AREA %	58.0	59.0	59.0	59.7	58.3	**58.8**	50.0
LBS @.2% OFFSET	12790	12630	12890	12650	12690	**12730.0**	
YIELD STRENGTH (KSI)	263.17	260.41	263.06	260.29	256.88	**260.8**	245.0
ULT. LOAD (LBS)	14256	14069	14326	14246	14283		
ULT. STRENGTH (KSI)	293.33	290.08	292.37	293.13	289.13	**291.6**	290.0
Hardness						TBD	52-55
MODULUS MSI							28.0

ASTM E8 Tensile Tests for Modulus, Poisson's Ratio, Yield and Ultimate Strength

Modulus Tests

Specimens

Fifteen ASTM E8 flat dogbone specimens approximately 8″ long were machined from heat-treated coupons by UDRI. The gage section was nominally 3.75″ long and the rectangular gage area was nominally 0.5″ x 0.375″.

Equipment

Specimens were tested in a 60 kip Instron Model #4486 electromechanical test machine. An MTS 632.27b-30 mechanical extensometer with a 2″ gage length was calibrated to a Class B2 level. Loads were measured with a 60 kip load cell calibrated to a Class A level. A digital data acquisition system and Vishay P-500 Strain gage readout box were used to record data. Four Micro-Measurements CEA-06-125UW-350 strain gages were applied axially to the specimens at the midpoint of the gage length as shown in Figures 3.4.1-1 to 3.4.1-3. An MTS 650.03 mechanical extensometer was calibrated to a Class A level. The results of the extensometer calibration can be found in Appendix D.
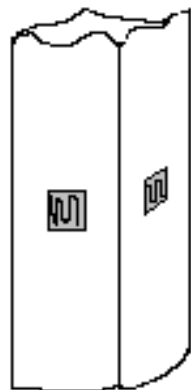
Gages Back to Back

Figure 3.4.1-1. Modulus strain gage locations.
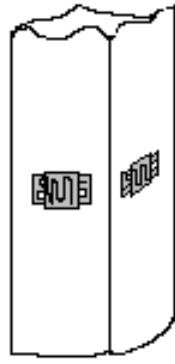
Gages Back to Back

Figure 3.4.1-2. Poisson's ratio strain gage locations.
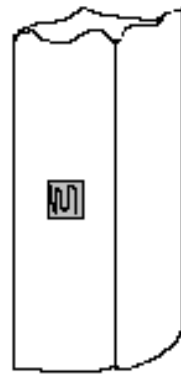
Gages Back to Back

Figure 3.4.1-3. Tensile strain gage locations.

Procedure

Room temperature modulus tests were performed per ASTM E111 (Standard Test Method for Young's Modulus, Tangent Modulus, and Chord Modulus). Specimens were mounted in the grips of the machine. The strain gages were zeroed and a shunt calibration performed. The mechanical extensometer was fastened to the specimen using rubber bands. The load was raised by increments of 500 lbs using manual control and the load and strain measurements were recorded at each increment. The load was increased until the maximum strain gage reading was 0.0025″/in strain and then lowered back to zero. The loading and unloading process was repeated two more times. The specimen was rotated between loading sequences and the mechanical extensometer was moved to help detect bending.

Results

Results from the three modulus loading sequences for the five specimens can be found in Table 3.4.1-2. Plots of the modulus tests can be found in Figures 3.4.1.-4 to 3.4.1-18.

Table 3.4.1-2. Aermet100 Modulus Data

Specimen ID	STL 677-11	STL 677-12	STL 677-13	STL 677-14	STL 677-15
Test 1	29.3	28.1	27.9	29.0	28.9
Test 2	29.1	29.1	28.6	28.7	29.0
Test 3	27.6	28.3	28.6	28.9	28.7
Average	28.7	28.5	28.4	28.9	28.9
Std. Dev.	0.93	0.53	0.40	0.15	0.15

Modulus Test Aermet100 STL677-11 Run 1

Legend:
- Extensometer
- Gages 1&3
- Gages 2&4
- Linear (Extensometer)
- Linear (Gages 1&3)
- Linear (Gages 2&4)

$y = 313,359x - 1,076$
$R^2 = 1$

$y = 282,476x + 126$
$R^2 = 1$

$y = 282,874x + 140$
$R^2 = 1$
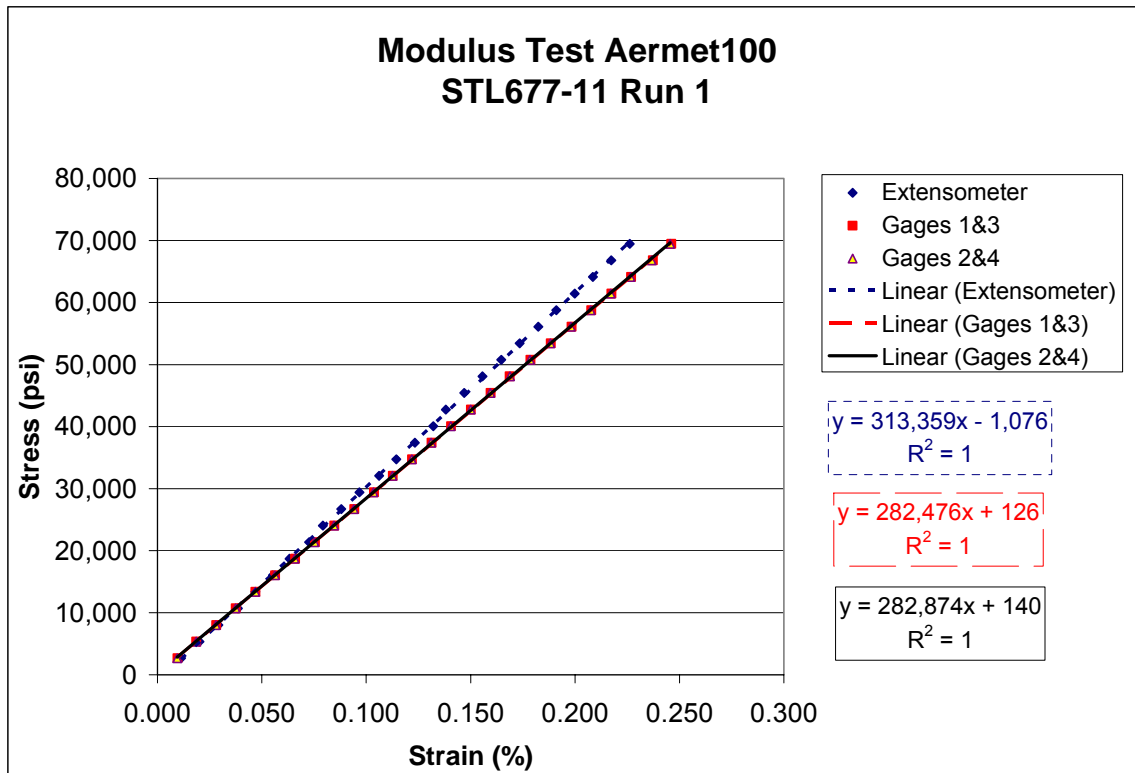
Figure 3.4.1-4. *Aermet100 flat dogbone, Specimen STL667-11, Test 1.*
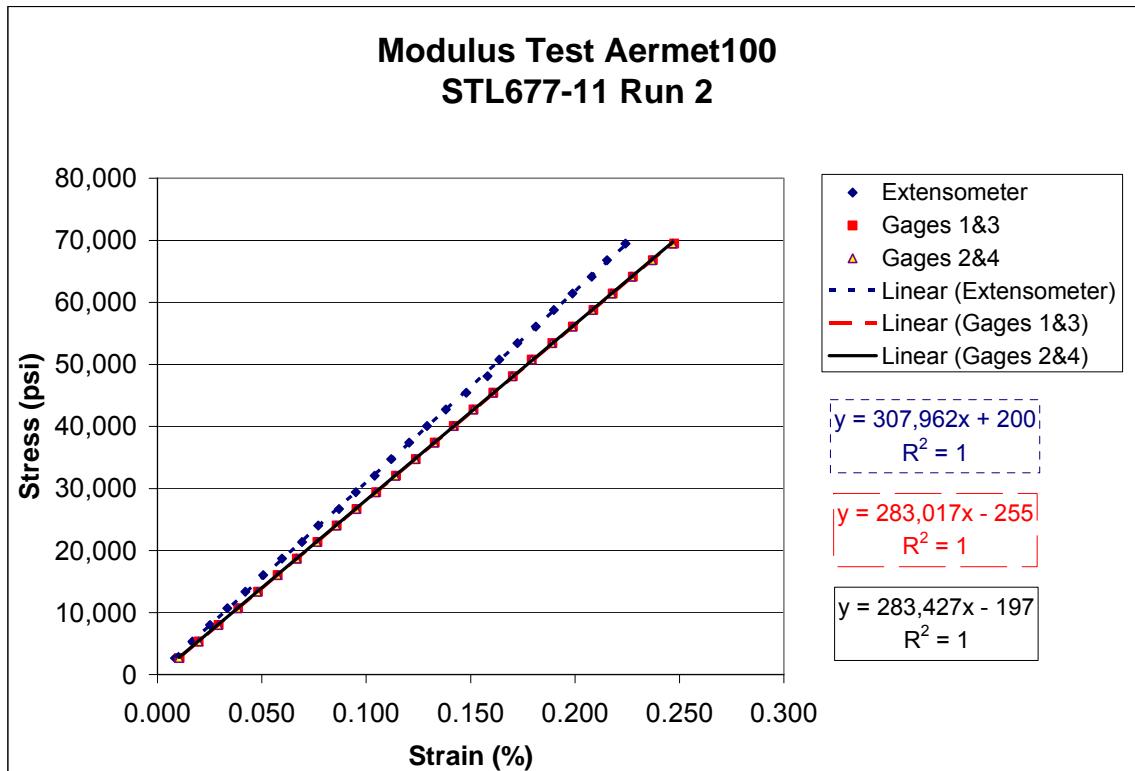
Figure 3.4.1-5. *Aermet100 flat dogbone, Specimen STL667-11, Test 2.*
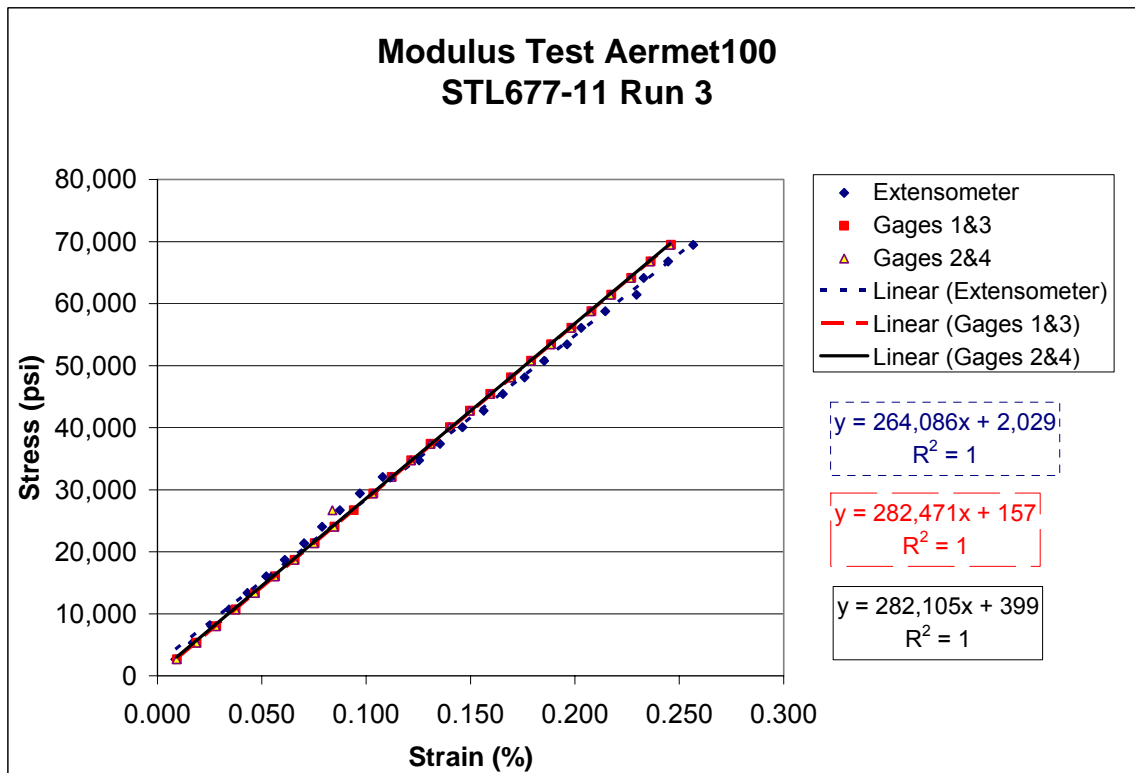
Figure 3.4.1-6. *Aermet100 flat dogbone, Specimen STL667-11, Test 3.*
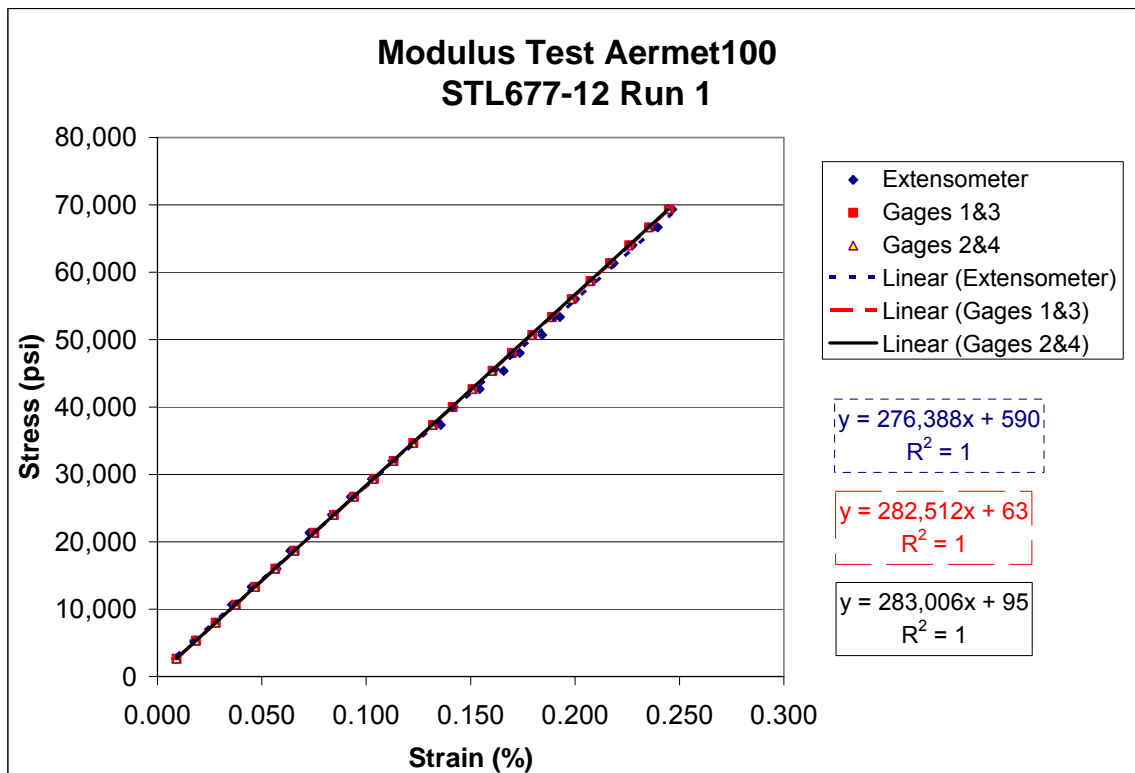
Figure 3.4.1-7. *Aermet100 flat dogbone, Specimen STL667-12, Test 1.*
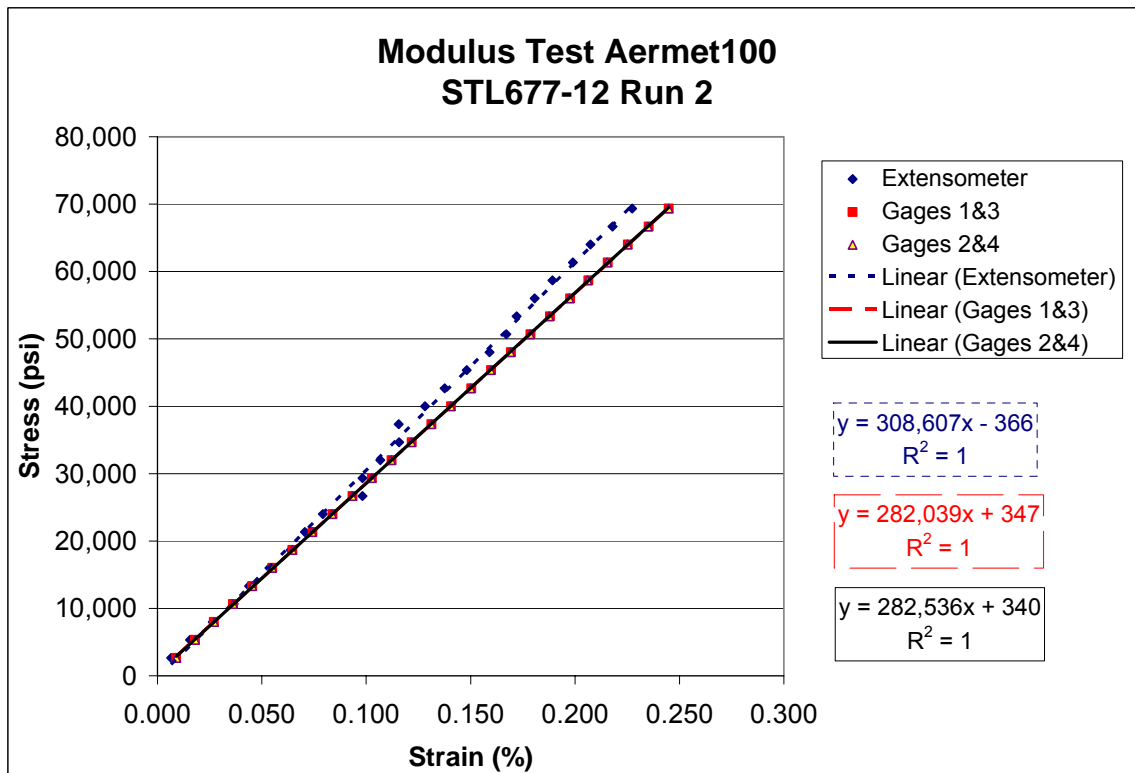
Figure 3.4.1-8. *Aermet100 flat dogbone, Specimen STL667-12, Test 2.*

41
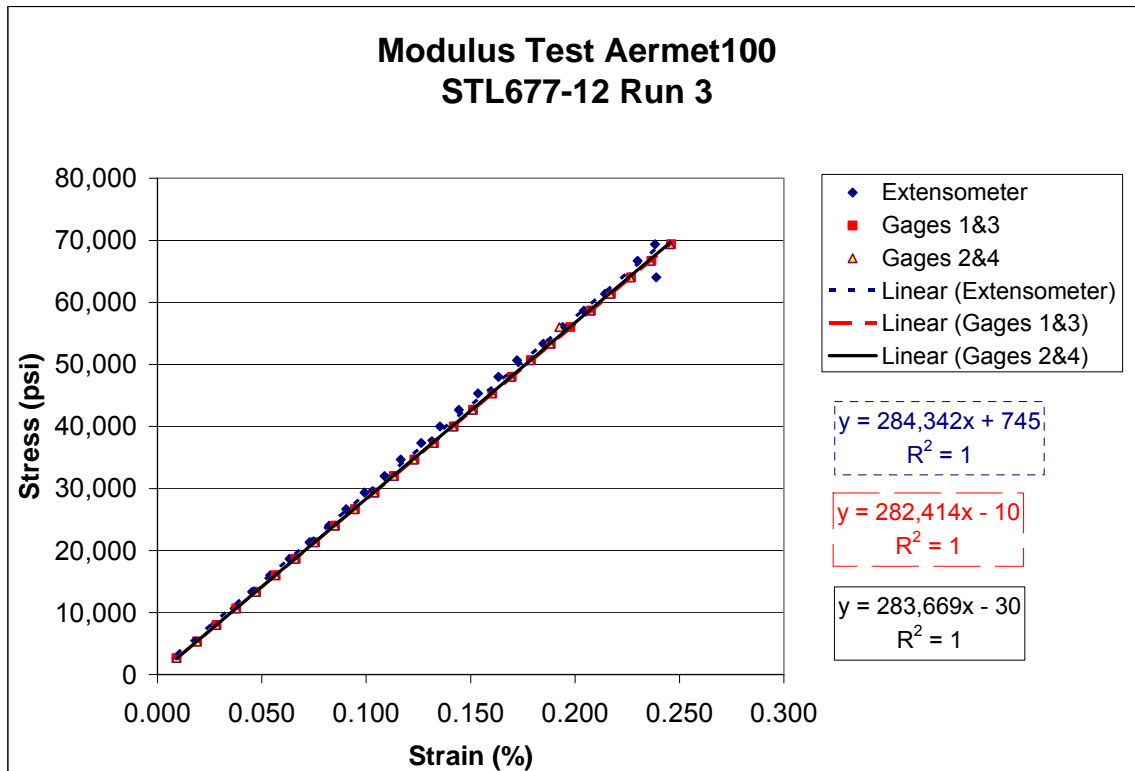
Figure 3.4.1-9. *Aermet100 flat dogbone, Specimen STL667-12, Test 3.*
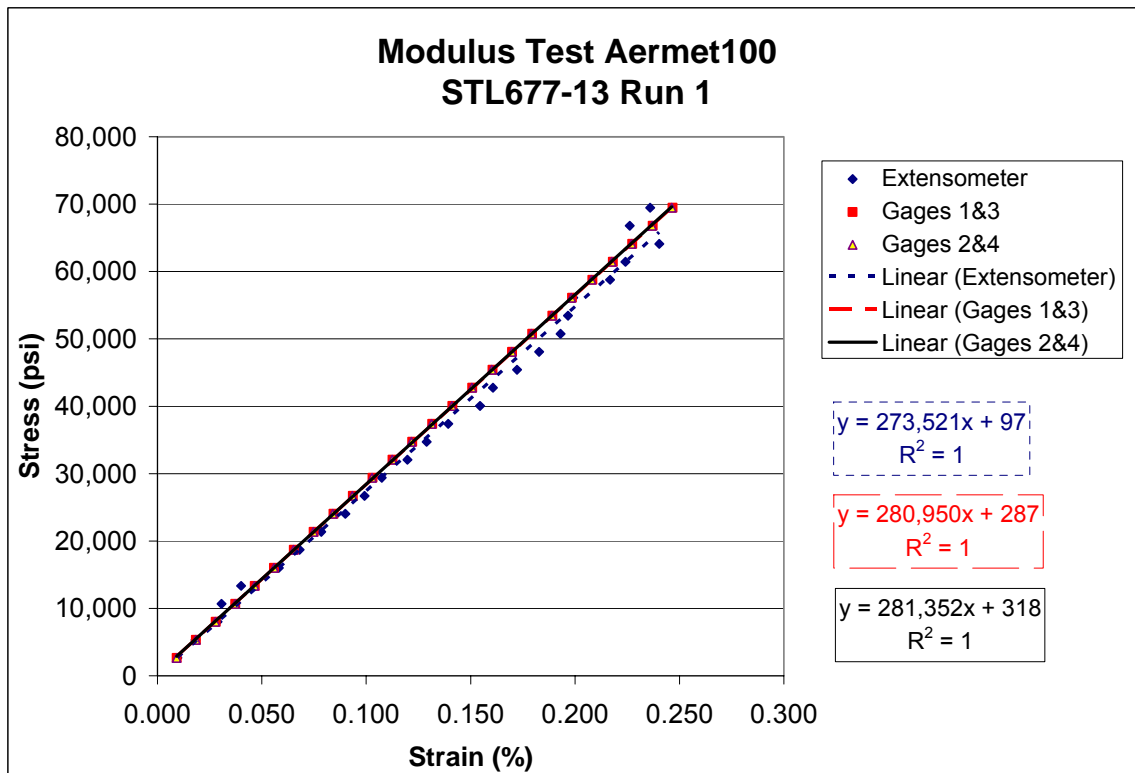
Figure 3.4.1-10. *Aermet100 flat dogbone, Specimen STL667-13, Test 1.*
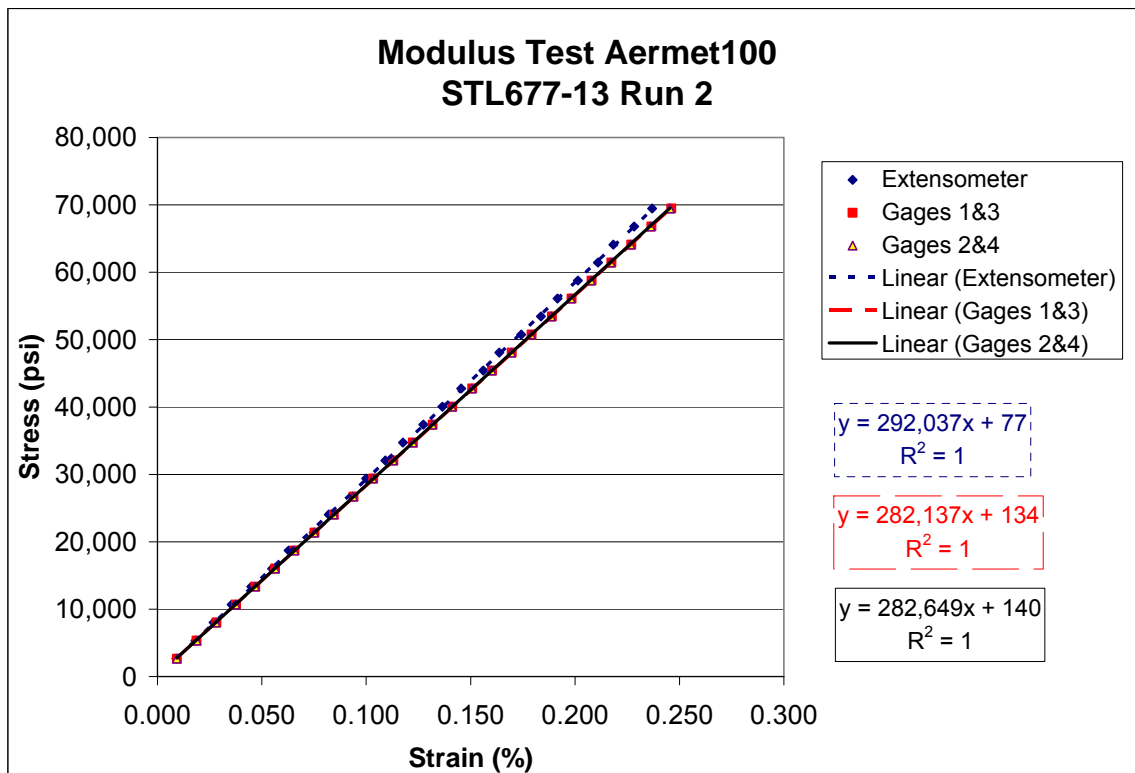
Figure 3.4.1-11. *Aermet100 flat dogbone, Specimen STL667-13, Test 2.*
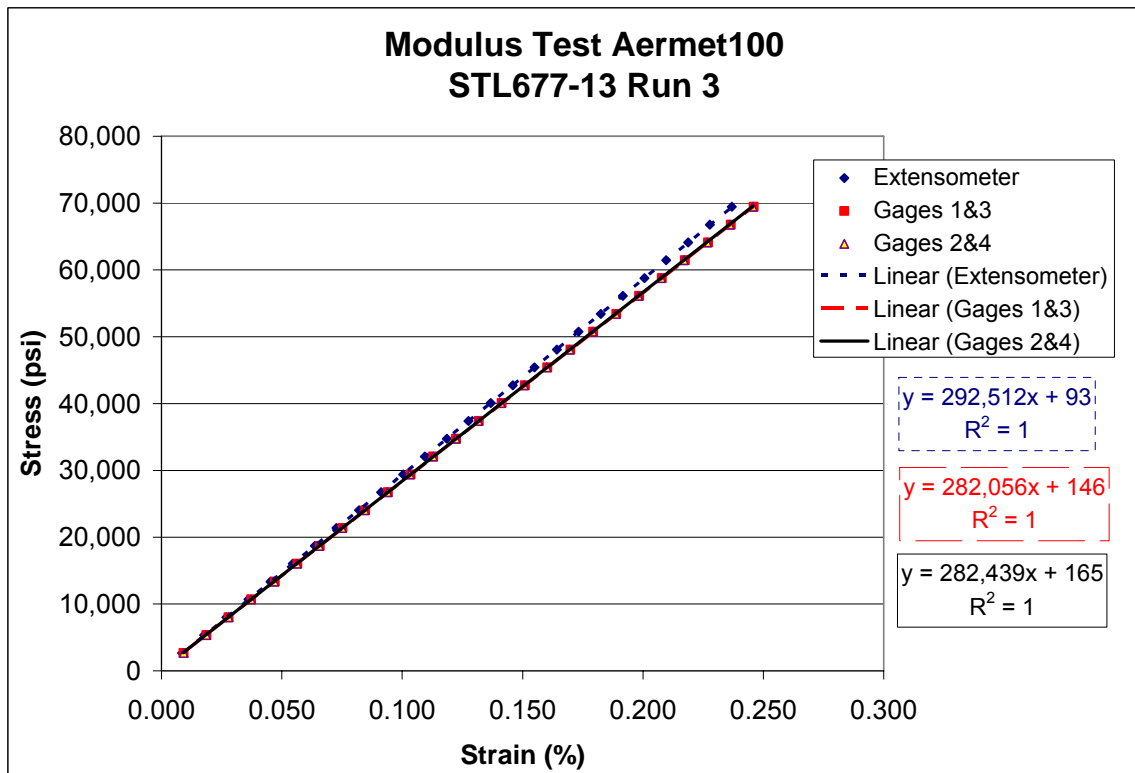
Figure 3.4.1-12. *Aermet100 flat dogbone, Specimen STL667-13, Test 3.*

43
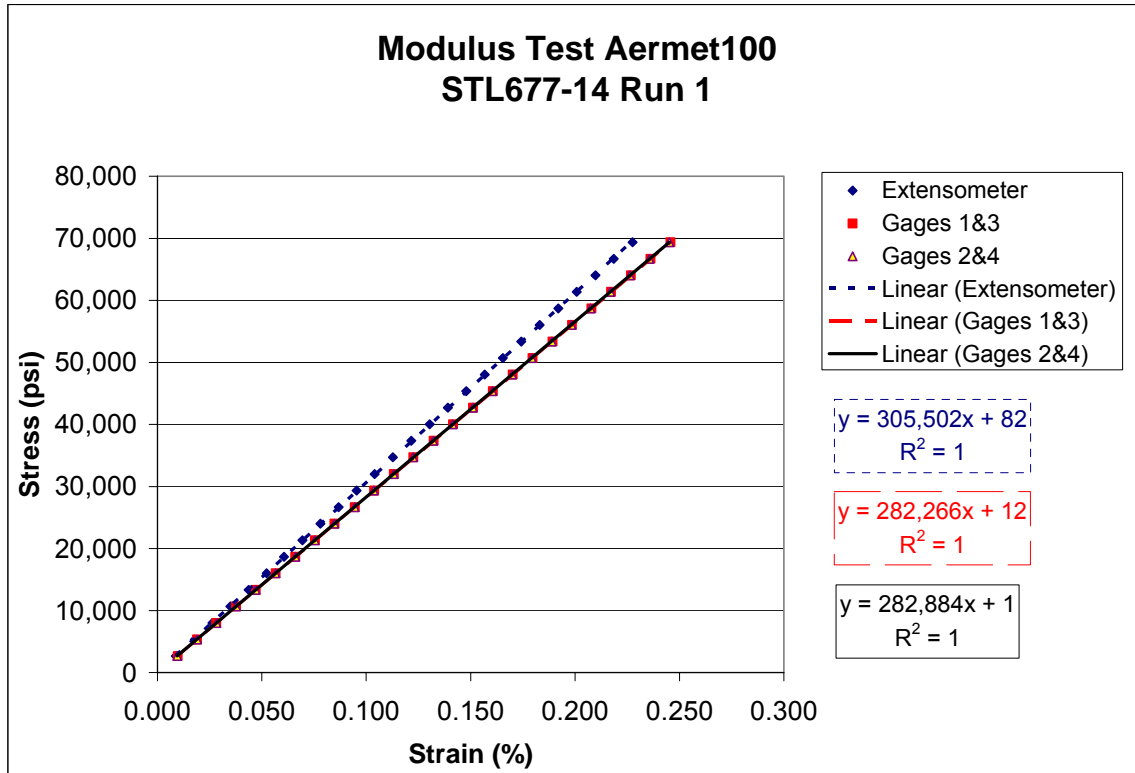
Figure 3.4.1-13. *Aermet100 flat dogbone, Specimen STL667-14, Test 1.*
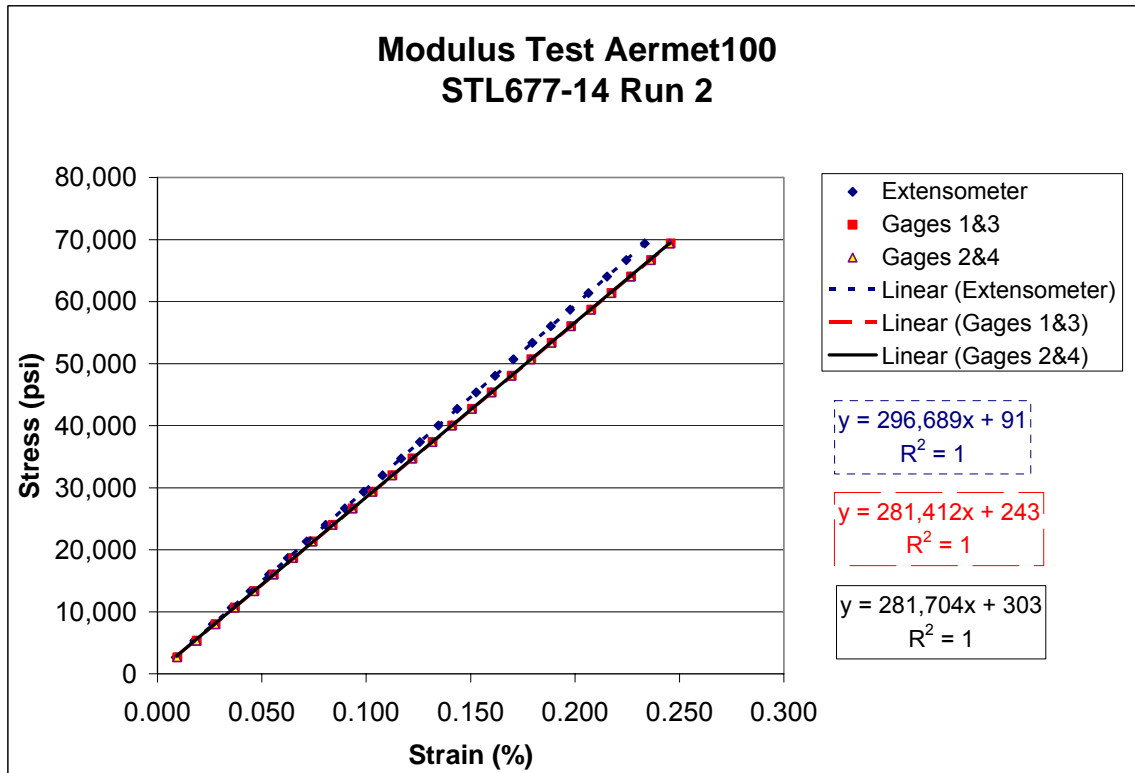
Figure 3.4.1-14. *Aermet100 flat dogbone, Specimen STL667-14, Test 2.*

44
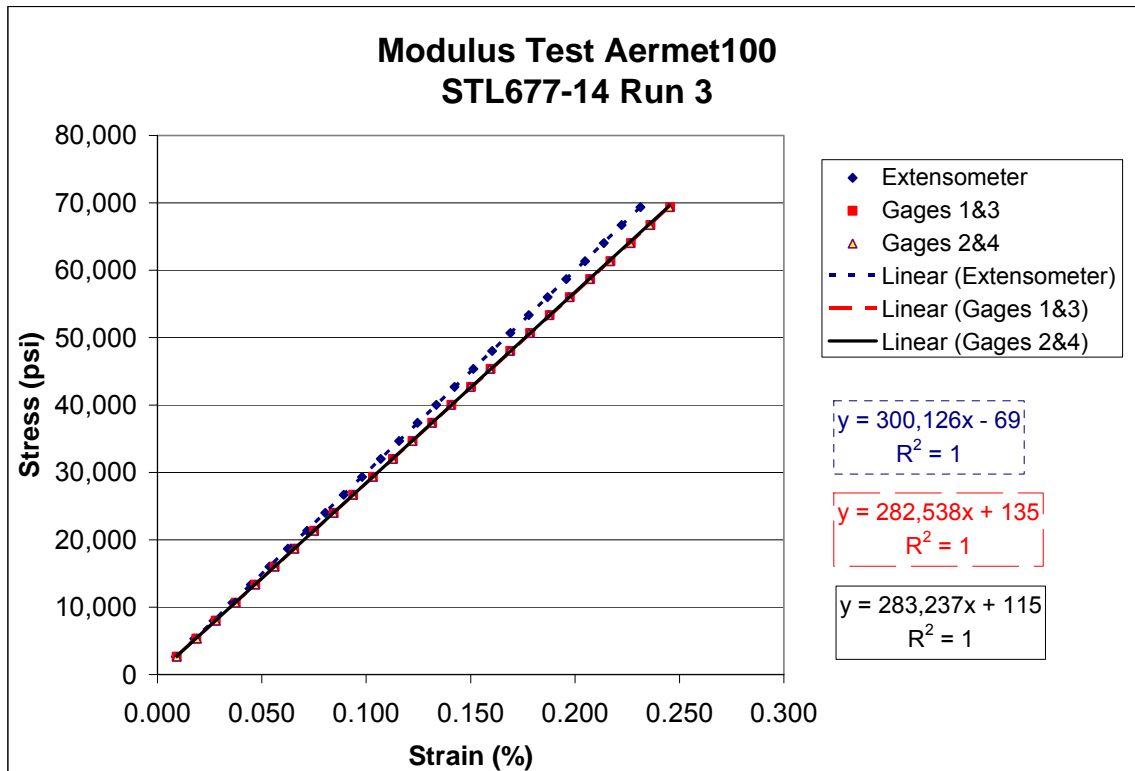
Figure 3.4.1-15. *Aermet100 flat dogbone, Specimen STL667-14, Test 3.*
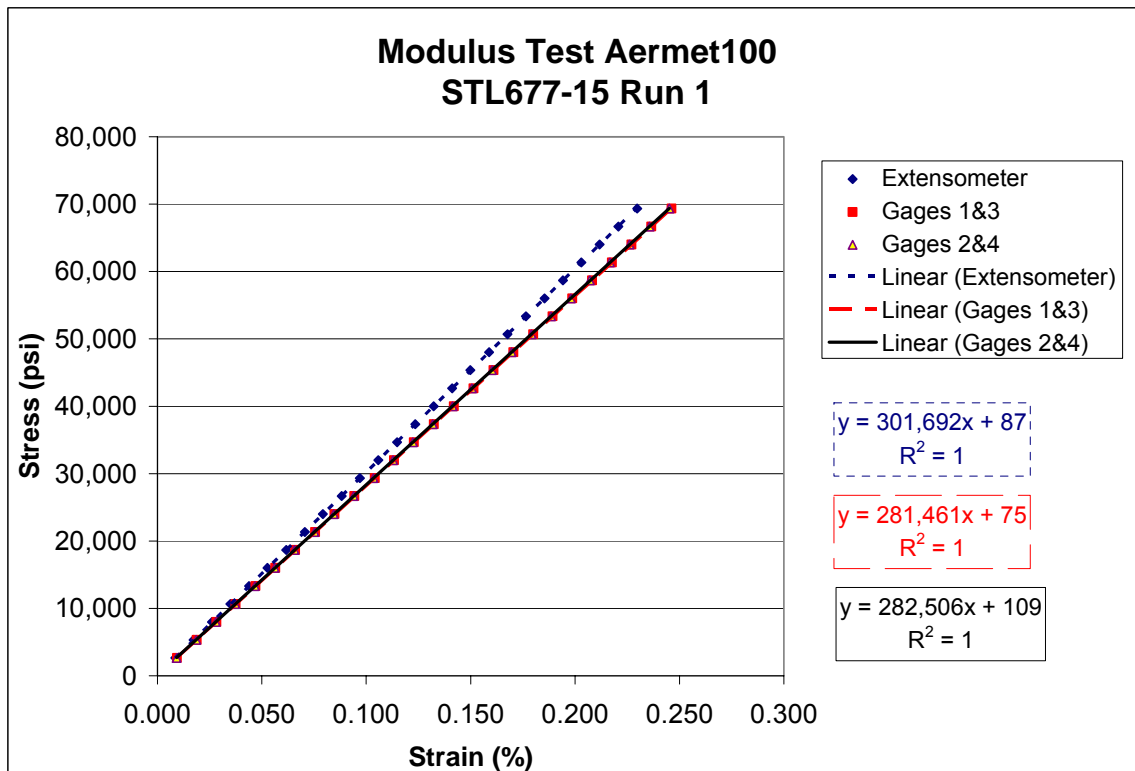
Figure 3.4.1-16. *Aermet100 flat dogbone, Specimen STL667-15, Test 1.*
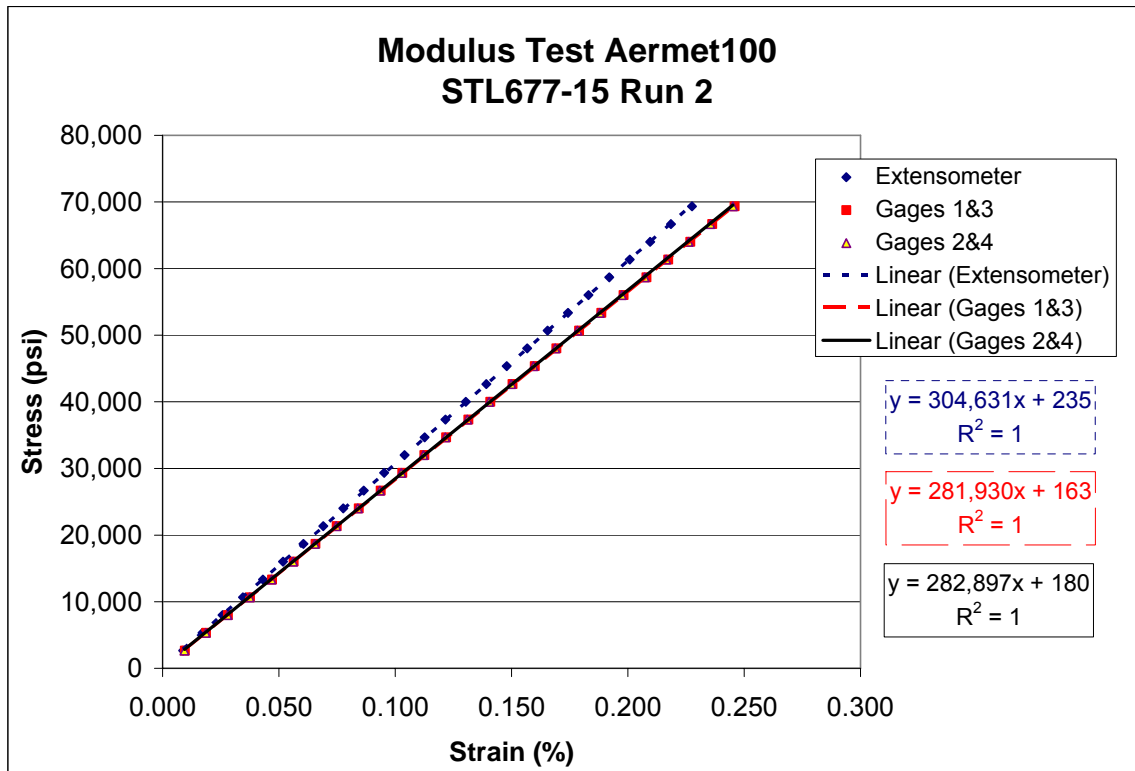
Figure 3.4.1-17. *Aermet100 flat dogbone, Specimen STL667-15, Test 2.*
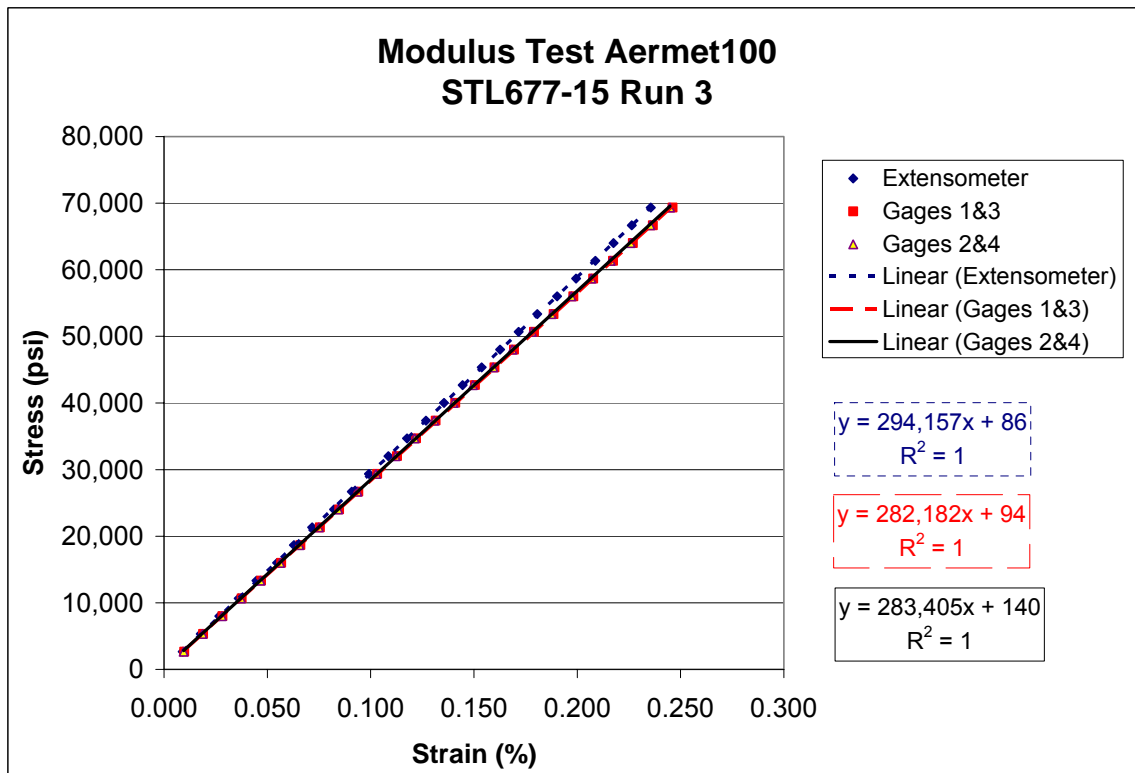
Figure 3.4.1-18. *Aermet100 flat dogbone, Specimen STL667-15, Test 3.*

<u>Poisson's Ratio Testing</u>

Specimen

Two of the same flat dogbone tensile specimens were used for both Poisson's ratio and modulus testing.

Equipment

The same 60 kip Instron test machine, load cell, data acquisition system, and extensometer were used for Poisson's ratio and modulus testing. Four Micro-Measurement CEA-06-062WT-350 strain gages were applied to the specimens at the mid-point as shown in Figures 3.4.1-2 and 3.4.1-19. These gages were T-type, which means they could measure longitudinal and transverse strain simultaneously.
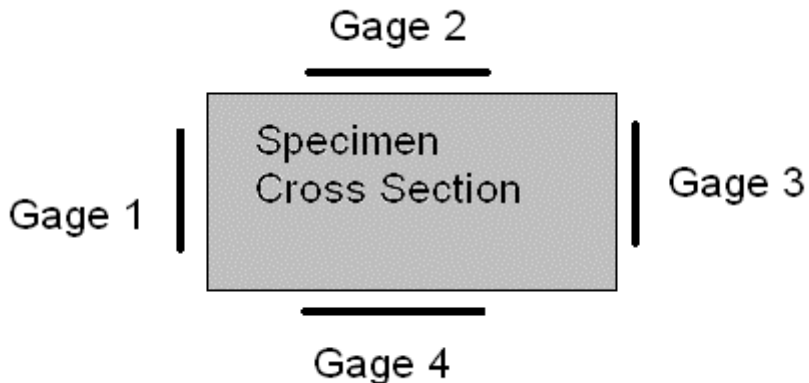
Figure 3.4.1-19. *Diagram of strain gage layout for Poisson's ratio tests.*

Procedure

Poisson's ratio tests were performed in accordance with ASTM E132 (Standard Test Method for Poisson's Ratio at Room Temperature). Specimens were mounted into grips in the machine, the strain gages zeroed, and a shunt calibration performed. The load was raised by increments of 500 lbs using a hand control and the load and strain measurements were recorded at each increment. The load was increased until the maximum strain gage reading was 0.025″/in strain and then lowered back to zero. The loading and unloading process was repeated one to two more times.

Results

Results from the three Poisson loading sequences for both specimens can be found in Table 3.4.1-3. Plots of the Poisson's Ratio tests are shown in Figures 3.4.1-20 to 3.4.1-25.

Table 3.4.1-3. Results of Poisson's Ratio Tests

	Poisson's Ratio	
	STL677-9	STL677-10
Test 1	0.2904	0.28835
Test 2	0.2916	0.28835
Test 3	0.2877	0.28845
Average	0.290	0.288

Poisson's Ratio Aermet100 STL677-9 Run1

Gages 1&3
Gages 2&4
Linear (Gages 1&3)
Linear (Gages 2&4)

$y = -0.2895x - 0.0002$
$R^2 = 0.9999$

$y = -0.2913x - 4E-05$
$R^2 = 0.9995$
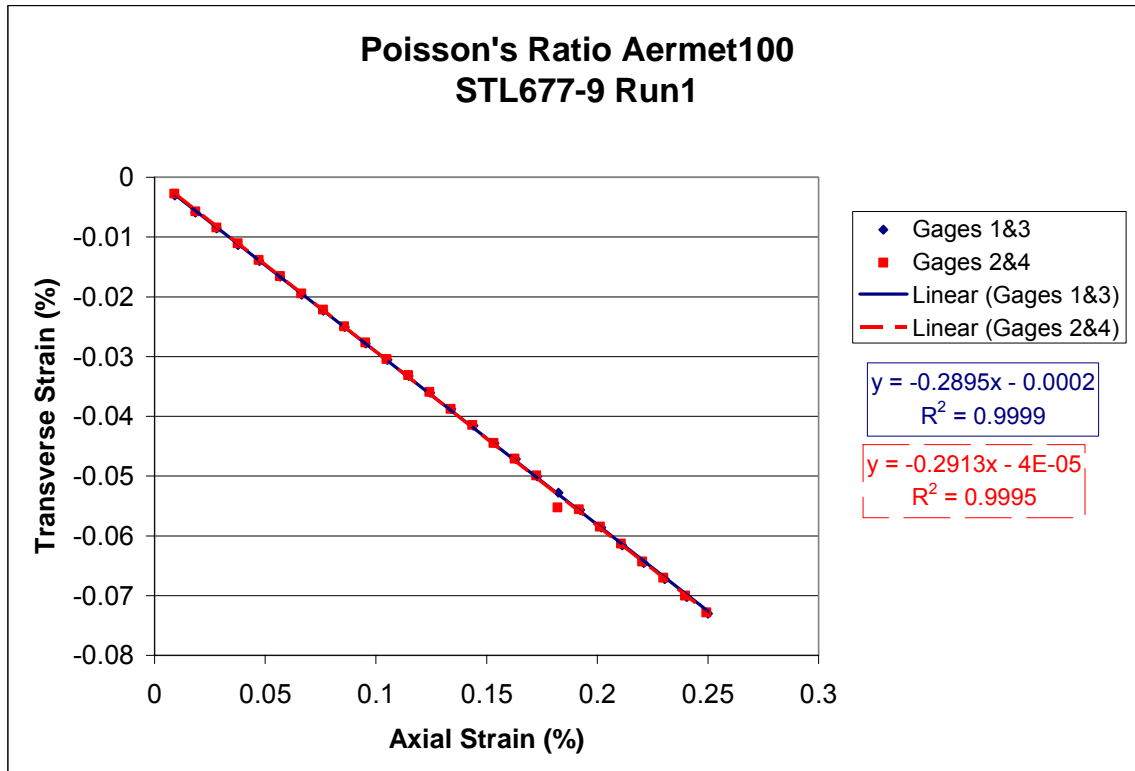
Figure 3.4.1-20. Aermet100 flat dogbone, Specimen STL677-9, Test 1.
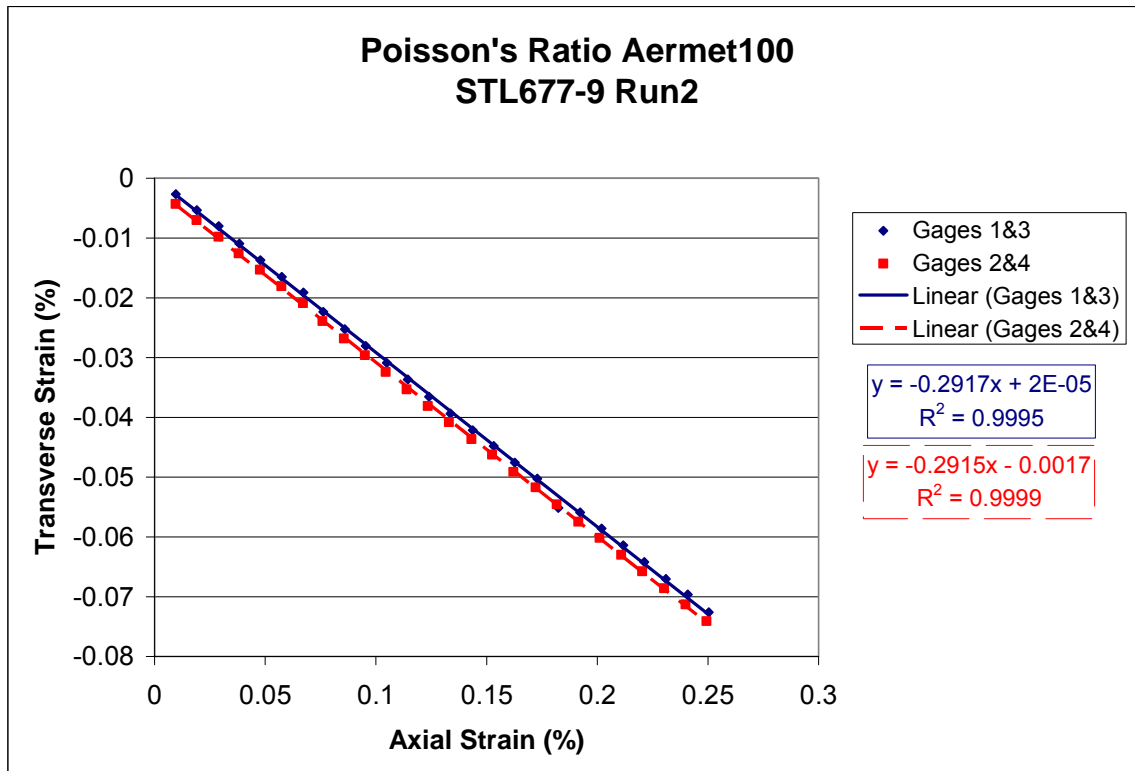
Figure 3.4.1-21. *Aermet100 flat dogbone, Specimen STL677-9, Test 2.*
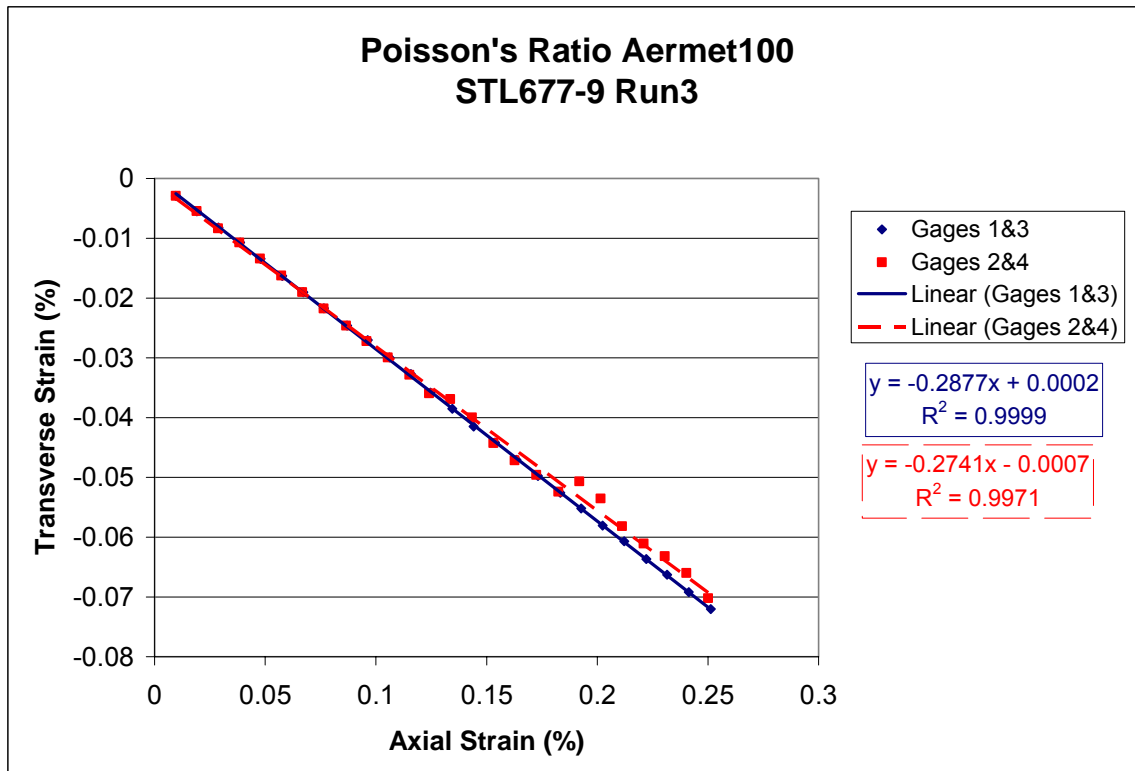
Figure 3.4.1.-22. *Aermet100 flat dogbone, Specimen STL677-9, Test 3.*
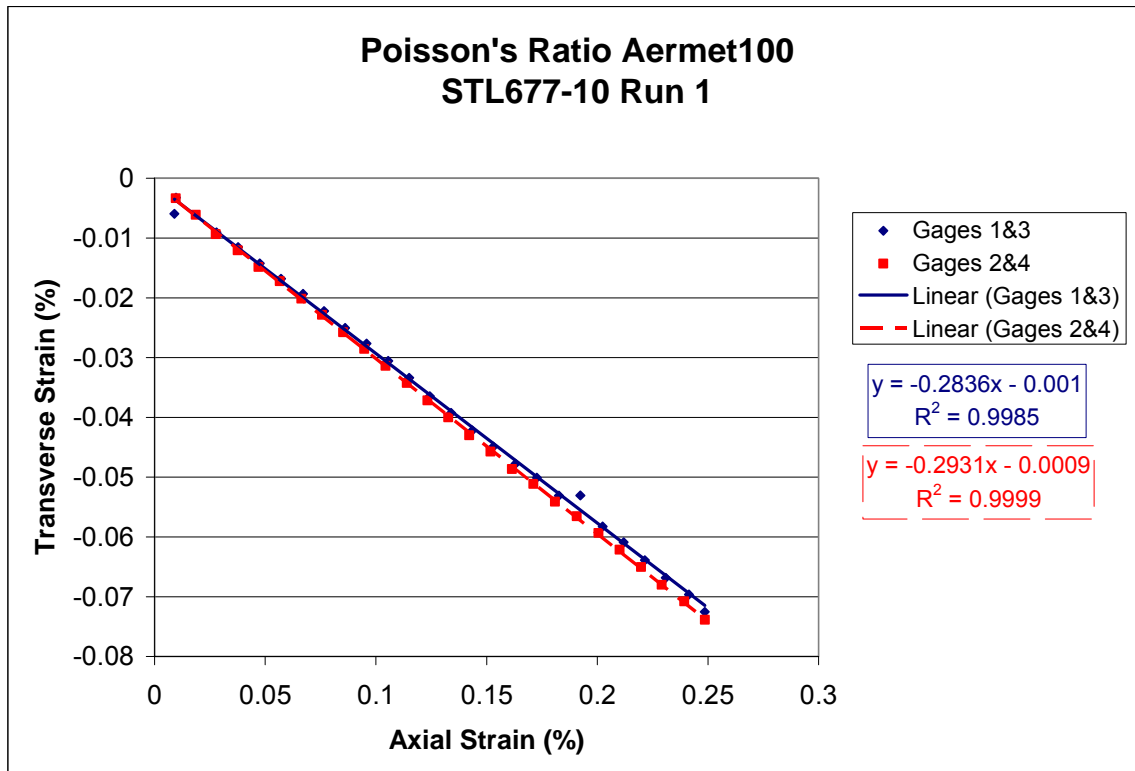
***Figure 3.4.1-23.*** *Aermet100 flat Ddogbone, Specimen STL677-10, Test 1.*
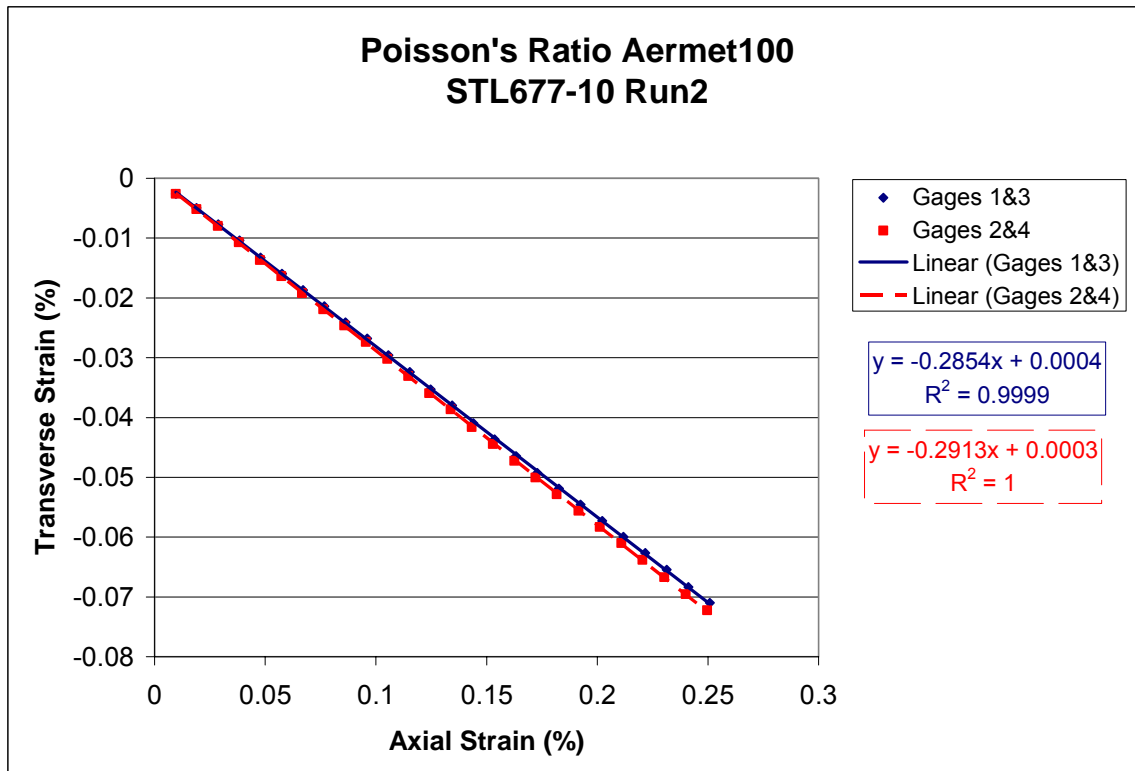
Figure 3.4.1-24. *Aermet100 flat dogbone, Specimen STL677-10, Test 2.*
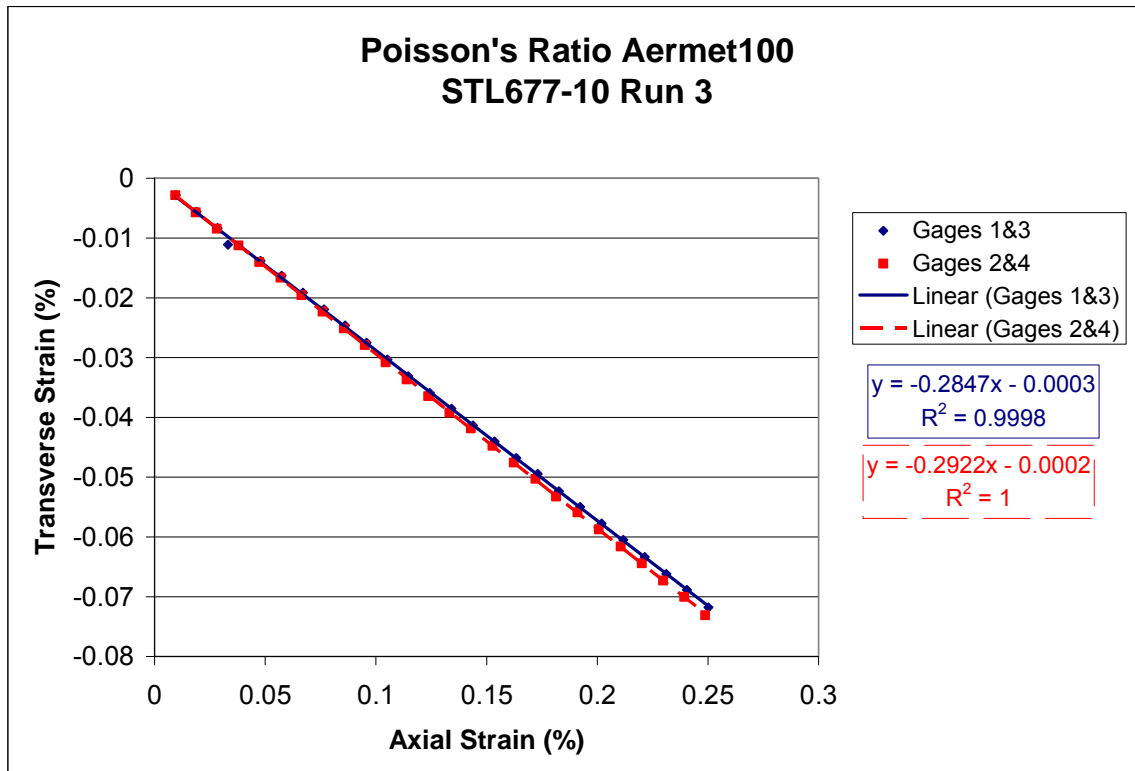
Figure 3.4.1-25. *Aermet100 flat dogbone, Specimen STL677-10, Test 3.*

<u>Yield and Ultimate Tensile Tests</u>

Specimen

The same tensile specimens used for the modulus and Poisson's Ratio tests were tested to fracture to determine the yield and ultimate strength.

Equipment

The same test machine and load cell were used. The MTS Model #632.27B-30 extensometer with a 1″ gage length was calibrated to a Class B2 level.

Procedure

Tensile tests were performed in accordance with ASTM E8 (Standard Test Methods for Tension Testing of Metallic Materials) and ASTM E646 (Standard Test Method for Tensile Strain-Hardening Exponents [n-Values] of Metallic Sheet Materials). Specimens STL677-7, 8, and 9 were reduced in cross sectional area prior to the tensile test.

The tensile test results for each test are provided in Table 3.4.1-4. Plots of stress versus strain curves are shown in Figures 3.4.1-26 and 3.4.1-27. The stress versus strain curve for each specimen has a little bump, or discontinuity, at 2% strain. This bump is a result of switching strain rates in order to obtain data for the calculation of the strain-hardening exponent.

Table 3.4.1-4. ASTM E8 Tensile Test Results

ASTM E8 Tensile Test Results			
	Ultimate Tensile Strength (psi)	Yield Strength (psi)	% Elongation
STL677-1	288,000	254,000	invalid
STL677-2	298,000	261,000	9.70
STL677-3	297,000	251,000	9.65
STL677-4	239,000	249,000	9.71
STL677-5	297,208	258,000	9.67
STL677-7	291,000	260,000	9.65
STL677-8	290,000	255,000	9.71
STL677-9	290,000	266,000	9.64
STL677-11	298,000	280,000	9.67
STL677-12	299,000	271,000	9.65
STL677-13	275,000	253,000	9.69
STL677-14	300,000	261,000	9.65
Average	288,517	259,917	9.67
Standard Deviation	17095	8918	0.03
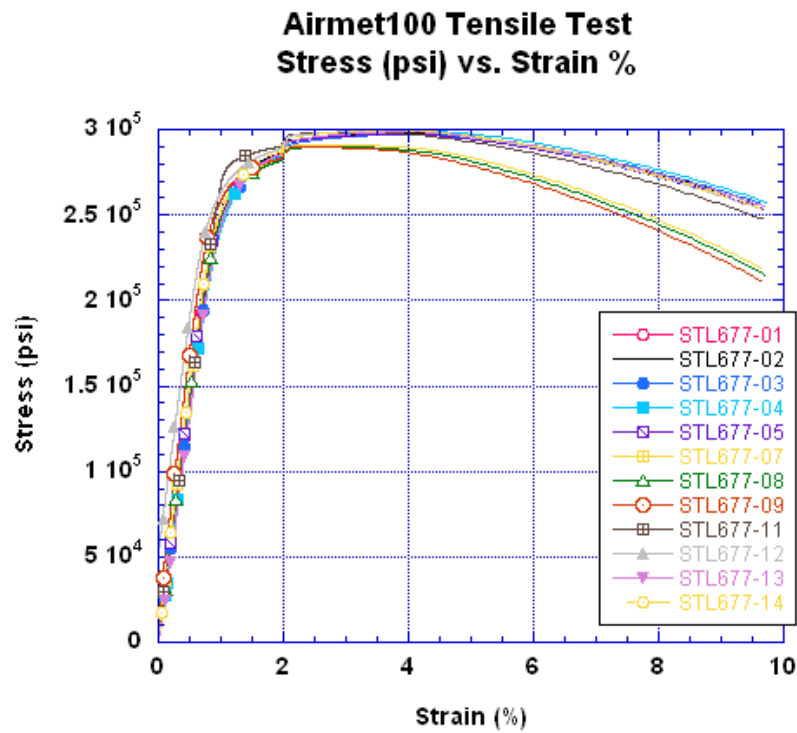
Figure 3.4.1-26. *Stress versus strain curves for Aermet100 steel.*
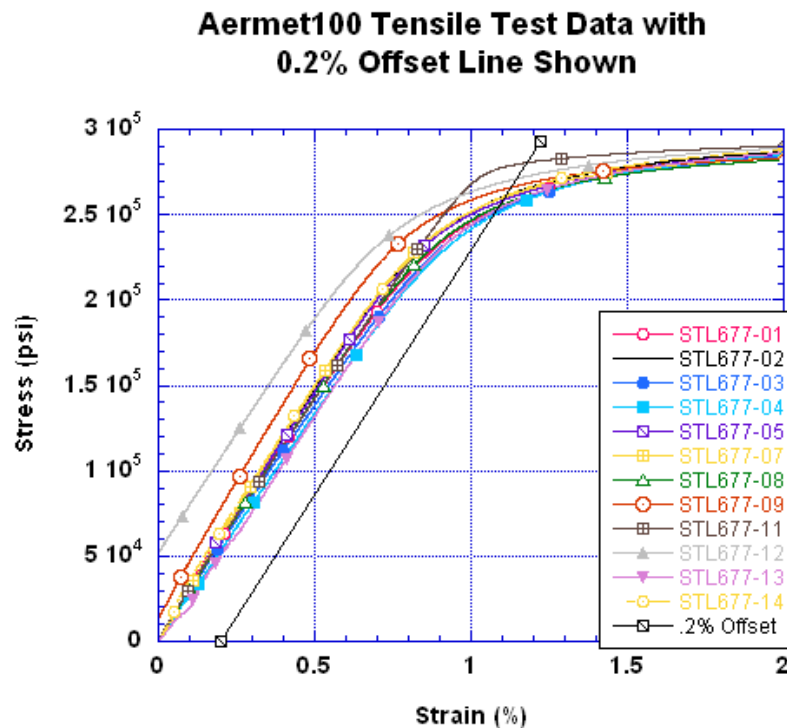
Figure 3.4.1-27. *Elastic region of the stress versus strain curves for Aermet100 steel.*

53

3.4.2. Fracture Toughness Tests

Specimen

Compact tension, C(T), specimens were fabricated in the long-transverse, L-T, orientation from the billet of AerMet100. Specimen coupons were heat-treated at Hercules Heat Treat and then finish-machined by UDRI. Specimens had a width, W, of 2″and thickness, B, of 1″ in accordance with ASTM E399 Standard Test Method for Plane-Strain Fracture Toughness of Metallic Materials.

Equipment

Tests were performed in a MTS closed-loop, servo-hydraulic test machine equipped with a 22 kip actuator. A strain gage displacement transducer was used to measure the crack-opening displacement (COD) during tests. Loads were measured using a calibrated load cell.

Procedure

Ten fracture toughness tests were performed in ambient laboratory air in accordance with ASTM E399. Specimens were first fatigue pre-cracked. Load and COD were sampled and digitally recorded during the test. Data were analyzed in accordance with ASTM E399 using Excel spreadsheets and plots.

Results

A summary of fracture toughness test results can be found in Table 3.4.2-1. All tests met the validity criteria listed by ASTM E399; the K_{IC} values determined were in the published range for AerMet100. The average fracture toughness found for this material was 128.54 ksi√(in).

Table 3.4.2-1. Fracture Toughness Results

FRACTURE TOUGHNESS DATA SHEET FOR CT GEOMETRY

MATERIAL: Aermet100
FORM:
DATE: May 2007

ENGINEER: Sarah Kuhlman
TECHNICIAN: Ron Glett
FATIGUE MACHINE: MTS # 7
TENSILE MACHINE: MTS # 7

Specimen Number	STl-678-1	STl-678-2	STl-678-3	STl-678-4	STl-678-5	STl-678-6	STl-678-7	STl-678-8	STl-678-9	STl-678-10
Orientation										
Test temperature/RH °F./%	74/54	74/54	74/54	74/54	74/54	74/54	74/54	74/54	74/54	74/54
Machined notch (in)	0.7155	0.714	0.7148	0.7153	0.71675	0.7185	0.71675	0.72175	0.71525	0.7175
Y.S. (ksi)	240	240	240	240	240	240	240	240	240	240
Modulus (msi)	29	29	29	29	29	29	29	29	29	29
K-max (final precrack)		57.12	58.03	57.13	57.12	57.9	57.75	57.26	57.34	57.52
P-final precrack (lbs)	3000	9200	9200	9200	9200	9200	9200	9200	9200	9200
Number of fatigue cycles	156882	12828	13188	13272	13140	13144	13004	12892	13096	12976
B (in)	1.00100	1.00150	1.00100	1.00100	1.00100	1.00100	1.00100	1.00050	1.00100	1.00100
E1 (in)	1.75900	1.75150	1.75200	1.75850	1.75925	1.76000	1.75800	1.75900	1.75225	1.75200
E2 (in)	2.26175	2.25575	2.25450	2.26175	2.26150	2.26225	2.26050	2.26150	2.25475	2.25425
W (in)	2.01038	2.00363	2.00325	2.01013	2.01038	2.01113	2.00925	2.01025	2.00350	2.00313
L1 (in)	0.98200	0.98400	0.96250	0.97800	0.97900	0.97400	0.97650	0.97400	0.96700	0.94900
L2 (in)	0.97300	0.96900	0.95850	0.96450	0.96200	0.96750	0.96650	0.96800	0.96250	0.94450
L3 (in)	0.98300	0.97550	0.96850	0.97400	0.97350	0.97050	0.97250	0.97250	0.96450	0.94750
ST1 (in)	1.51700	1.52050	1.52450	1.51650	1.51250	1.51650	1.51650	1.52350	1.51900	1.50450
ST2 (in)	1.51300	1.53800	1.51650	1.52200	1.52250	1.52100	1.52450	1.52150	1.52200	1.50450
a1 (in)	1.02838	1.01963	1.04075	1.03213	1.03138	1.03713	1.03275	1.03625	1.03650	1.05413
a2 (in)	1.03738	1.03463	1.04475	1.04563	1.04838	1.04363	1.04275	1.04100	1.04100	1.05863
a3 (in)	1.02738	1.02813	1.03475	1.03613	1.03688	1.04063	1.03675	1.03525	1.03900	1.05563
a avg (in)	1.03104	1.02746	1.04008	1.03796	1.03888	1.04046	1.03742	1.03792	1.03883	1.05613
a ST1 (in)	1.00100	0.99750	0.99500	1.00150	1.00600	1.00250	1.00200	0.99750	1.00000	0.99800
a ST2 (in)	1.00500	0.98000	1.00300	0.99600	0.99600	0.99800	0.99400	0.99950	0.99700	0.99800
P max (lbs)	18660	18180	17230	17860	17770	18150	18020	17670	17950	17270
P (Q) lbs	18660	18180	17230	17860	17770	18150	18020	17670	17950	17270
K (Q) (ksi√in)	**132.19**	**128.92**	**124.77**	**127.95**	**127.45**	**130.40**	**129.10**	**126.62**	**129.69**	**128.36**
Rsc	0.8182	0.7993	0.7803	0.7958	0.7931	0.8119	0.8031	0.7874	0.8103	0.8116
K-max (final precrack)/K(Q)<0.6	VALID	VALID	VALID	VALID	VALID	VALID	VALID	VALID	VALID	VALID
Pmax/P(Q) < [1.1]	VALID	VALID	VALID	VALID	VALID	VALID	VALID	VALID	VALID	VALID
P final fatigue (lbs)/P(Q) < [0.6]	VALID	VALID	VALID	VALID	VALID	VALID	VALID	VALID	VALID	VALID
a & B > 2.5(KQ/Y.S.)^2	VALID	VALID	VALID	VALID	VALID	VALID	VALID	VALID	VALID	VALID
w-a > 2.5(KQ/Y.S.)^2	VALID	VALID	VALID	VALID	VALID	VALID	VALID	VALID	VALID	VALID
a(ave.)(15%) > a(avg.)- a(ST1)	VALID	VALID	VALID	VALID	VALID	VALID	VALID	VALID	VALID	VALID
a(avg.) (15%) > a(avg.)- a(ST2)	VALID	VALID	VALID	VALID	VALID	VALID	VALID	VALID	VALID	VALID
a1-a2 < a(avg.)(10%)	VALID	VALID	VALID	VALID	VALID	VALID	VALID	VALID	VALID	VALID
a2-a3 < a(avg.)(10%)	VALID	VALID	VALID	VALID	VALID	VALID	VALID	VALID	VALID	VALID
a3-a1 < a(avg.)(10%)	VALID	VALID	VALID	VALID	VALID	VALID	VALID	VALID	VALID	VALID
[0.45 to 0.55] = a / W	VALID	VALID	VALID	VALID	VALID	VALID	VALID	VALID	VALID	VALID
ST1 a = .050 or .025W	VALID	VALID	VALID	VALID	VALID	VALID	VALID	VALID	VALID	VALID
ST2 a = .050 or .025W	VALID	VALID	VALID	VALID	VALID	VALID	VALID	VALID	VALID	VALID
Type of Fracture	fraction oblique	fraction oblique	fraction oblique	fraction oblique	fraction oblique	fraction oblique	fraction oblique	fraction oblique	fraction oblique	fraction oblique
Valid Test ?	**VALID**	**VALID**	**VALID**	**VALID**	**VALID**	**VALID**	**VALID**	**VALID**	**VALID**	**VALID**
						JE/UDRI/05/07				
returns the lesser of a or B:	1.001	1.0015	1.001	1.001	1.001	1.001	1.001	1.0005	1.001	1.001
returns W-a	0.979	0.976	0.963	0.972	0.972	0.971	0.972	0.972	0.965	0.947
returns .050 or .025W for a-ST1	0.050	0.050	0.050	0.050	0.050	0.050	0.050	0.050	0.050	0.050
returns .050 or .025W for a-ST2	0.050	0.050	0.050	0.050	0.050	0.050	0.050	0.050	0.050	0.050
PQ/Pmax check	1	1	1	1	1	1	1	1	1	1
precrack-Kmax/KQ check	1	1	1	1	1	1	1	1	1	1
a,B >2.5(k/ys)^2	1	1	1	1	1	1	1	1	1	1
W - a >2.5(k/ys)^2	1	1	1	1	1	1	1	1	1	1
a ST1to Lavg check:	1	1	1	1	1	1	1	1	1	1
a ST2 to Lavg check:	1	1	1	1	1	1	1	1	1	1
a1-a2 check:	1	1	1	1	1	1	1	1	1	1
a2-a3 check:	1	1	1	1	1	1	1	1	1	1
a3-a1 check:	1	1	1	1	1	1	1	1	1	1
.45<a<.55 check:	1	1	1	1	1	1	1	1	1	1
a ST1 to greater of (.050 or .025W)	1	1	1	1	1	1	1	1	1	1
a ST2 to greater of (.050 or .025W)	1	1	1	1	1	1	1	1	1	1
sum of checks (12=valid)	12	12	12	12	12	12	12	12	12	12

3.4.3 Fatigue Crack Growth Rate Tests

Specimens

A total of 30 C(T) specimens were machined. As seen in Figure 3.4.3-1, they had a nominal width, W, of 2″ and thickness, B, of 0.20″ and were used primarily for tests with positive load ratios. Center-cracked, M(T), specimens, as seen in Figure 3.4.3-2, had a nominal width of 3″ and thickness of 0.25″ and were planned for tests with a negative load ratio. Ten M(T) specimens were manufactured; however, none were tested due to higher-priority tests and budget.
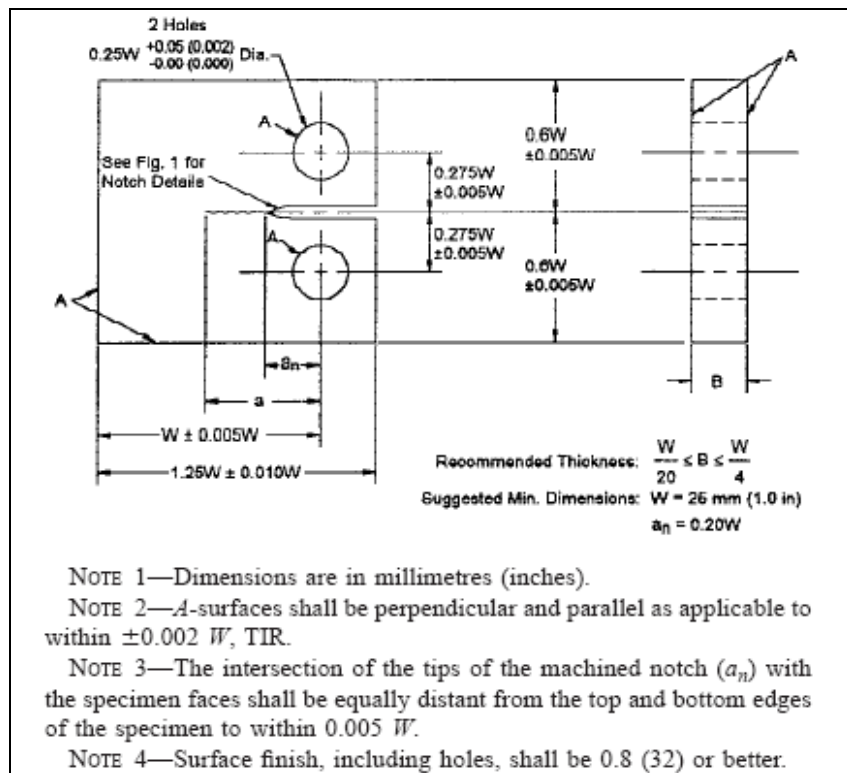
Figure 3.4.3-1. *C(T) specimen.*
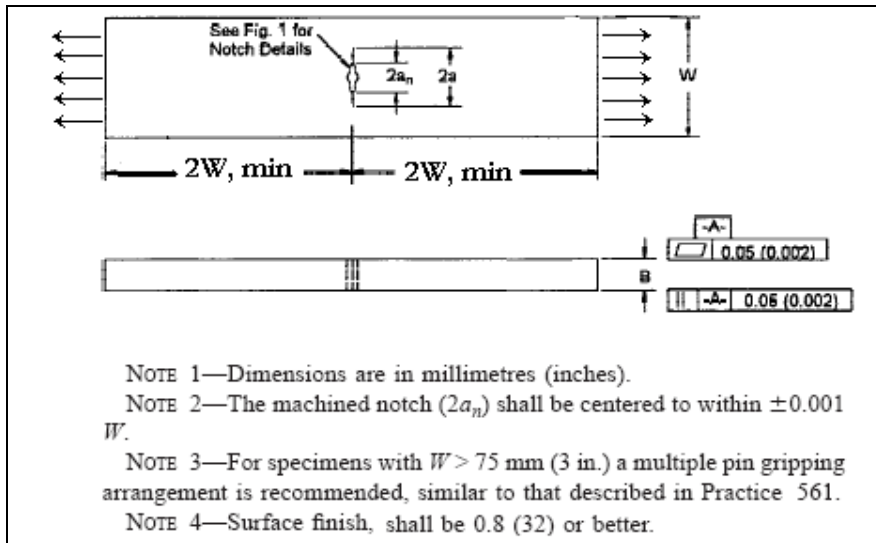
Figure 3.4.3-2. *M(T) specimen.*

Equipment

All tests were conducted on MTS closed-loop, servo-hydraulic test stations. A PC-based computer system was used for test control and data acquisition. Loads were measured with a load cell and the crack length was measured using the crack opening displacement method outlined in ASTM E647. A strain gage displacement transducer was used to measure the crack-opening displacement (COD) during tests. Clevises and pins were used to load the C(T) specimens.

Procedure

All tests were conducted in accordance with ASTM E647-00, Standard Test Method for Measurement of Fatigue Crack Growth Rates. Pre-cracking and tests were done in a laboratory-air environment (72°F, 40 to 50% relative humidity). Pre-cracking and threshold tests were conducted using the decreasing delta K procedure method described in ASTM E647. Some threshold tests were pre-cracked using a few compression cycles. Otherwise, tests were performed using the constant-force-amplitude procedure after pre-crack or initial threshold tests.

Data reduction was performed using either the secant method or the seven-point incremental polynomial method to calculate the crack growth rate.

57

Results

A summary of the fatigue crack growth rate testing can be found in Table 3.4.3-1, along with summary plots in Figures 3.4.3-3 through 3.4.3-9. The slight differences in fatigue crack growth rates between duplicates are relatively insignificant and can be explained by specimen-to-specimen variability.

Table 3.4.3-1. Aermet100 Fatigue Crack Growth Rate Results

Test Type	Load Ratio	Specimen Type	Repetition	Specimen ID	Date Completed	Final Optical Length (in)	Failure Load (lbs)
Fatigue Crack Growth Rate	0.1	C(T)	1	678-45	5/14/2007	1.700	556.5
Fatigue Crack Growth Rate	0.1	C(T)	2	678-44	5/18/2007	1.652	717
Fatigue Crack Growth Rate	0.1	C(T)	3	678-43	5/25/2007	1.681	244
Fatigue Crack Growth Rate	0.1	C(T)	4	678-39	6/20/2007	1.872	481
Fatigue Crack Growth Rate	0.1	C(T)	5	678-38	6/22/2007	1.820	Fractured
Fatigue Crack Growth Rate Threshold Region	0.1	C(T)	1	678-35	7/16/2007	0.511	-
Fatigue Crack Growth Rate Threshold Region	0.1	C(T)	2	678-31	8/30/2007	0.945	-
Fatigue Crack Growth Rate	0.5	C(T)	1	676.42	6/4/2007	1.698	331
Fatigue Crack Growth Rate	0.5	C(T)	2	678-41	6/15/2007	1.7034/1.706	518
Fatigue Crack Growth Rate	0.5	C(T)	3	678-40	6/19/2007	1.665	695
Fatigue Crack Growth Rate	0.5	C(T)	4	678-37	6/25/2007	1.679	607
Fatigue Crack Growth Rate	0.5	C(T)	5	678-36	6/30/2007	1.655	882
Fatigue Crack Growth Rate Threshold Region	0.5	C(T)	1	678-30b	8/22/2007	1.091	-
Fatigue Crack Growth Rate Threshold Region	0.5	C(T)	2	678-33a	8/3/2007	0.0867	-
Fatigue Crack Growth Rate	0.1	M(T)	1				
Fatigue Crack Growth Rate	-1	M(T)	1				
Fatigue Crack Growth Rate	-1	M(T)	2				
Fatigue Crack Growth Rate	-1	M(T)	3				
Fatigue Crack Growth Rate	-1	M(T)	4				
Fatigue Crack Growth Rate in NaCl Environment	0.1	C(T)	1				
Fatigue Crack Growth Rate in NaCl Environment	0.1	C(T)	2				
Fatigue Crack Growth Rate in NaCl Environment	0.5	C(T)	1				
Fatigue Crack Growth Rate in NaCl Environment	0.5	C(T)	2				
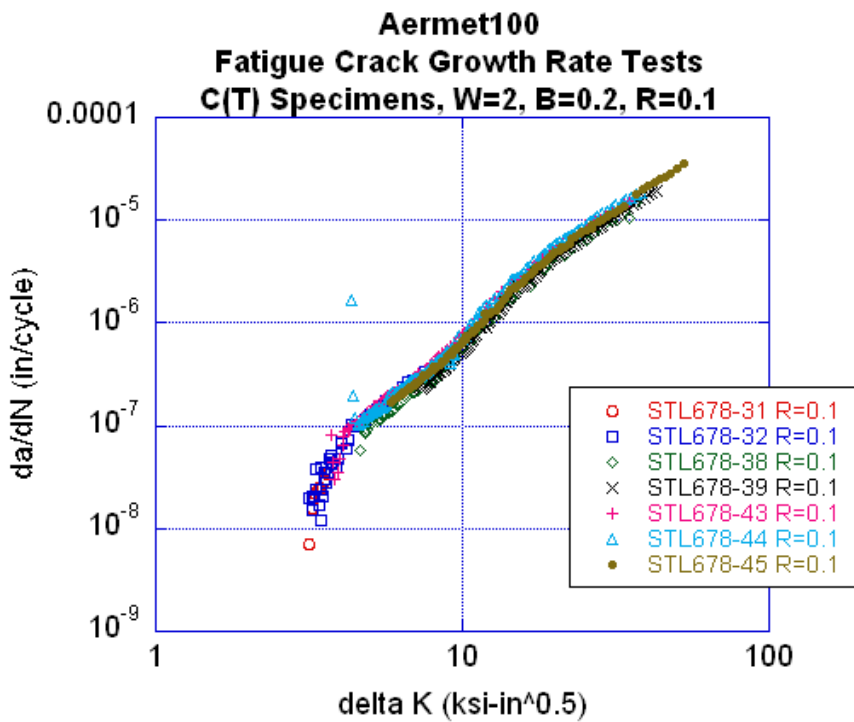
Figure 3.4.3-3. *FCGR data at R = 0.1 with threshold.*
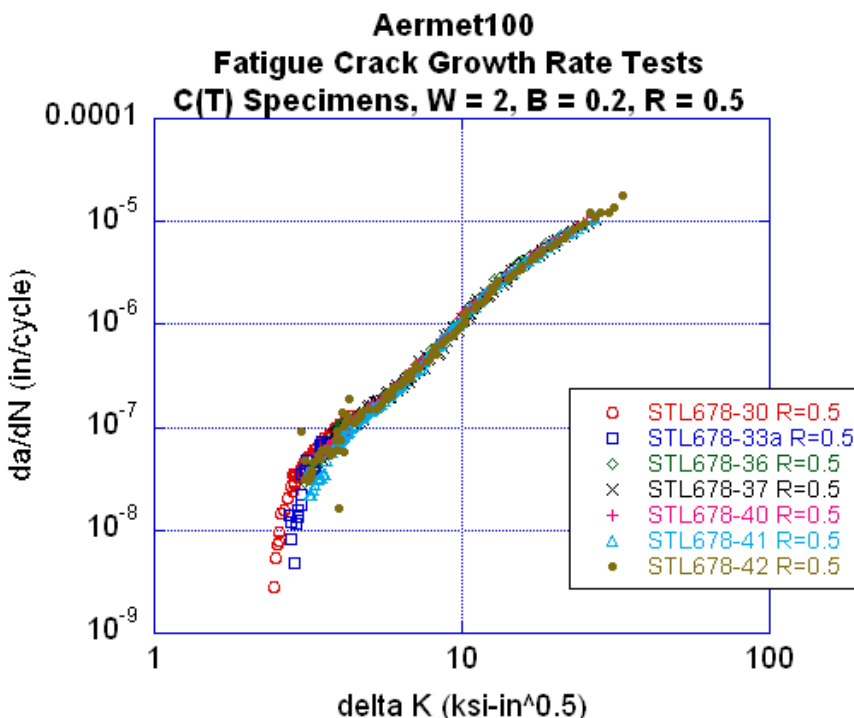
Figure 3.4.3-4. *FCGR data at R = 0.5 with threshold.*
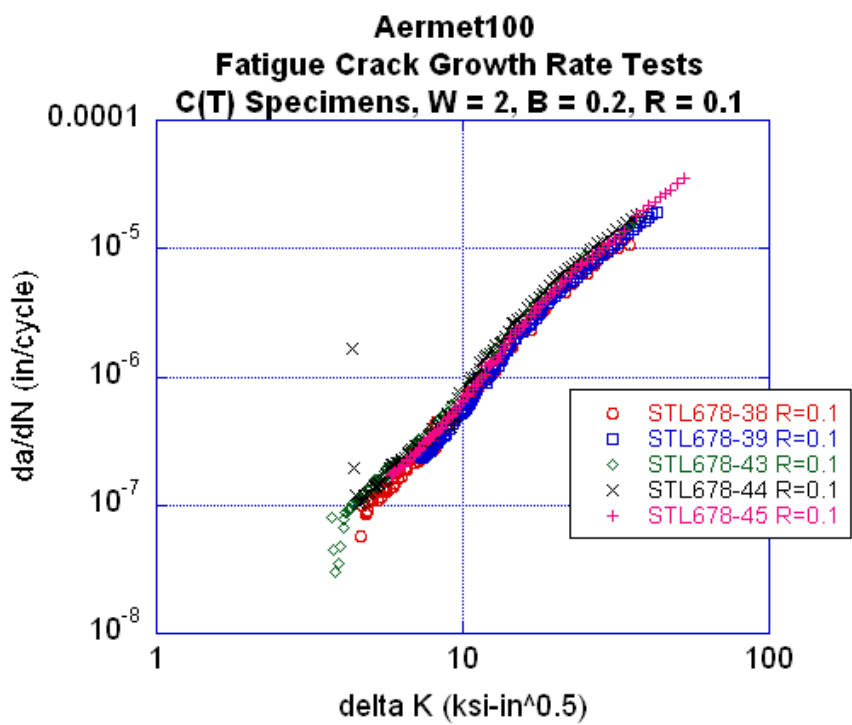
Figure 3.4.3-5. *FCGR data at R = 0.1.*
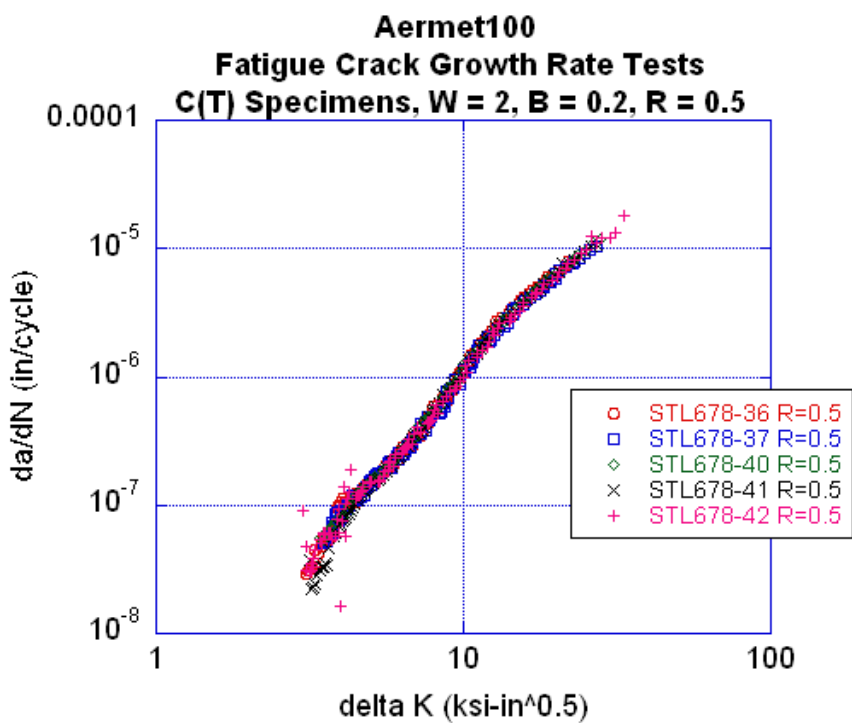
Figure 3.4.3-6. *FCGR data at R = 0.5.*
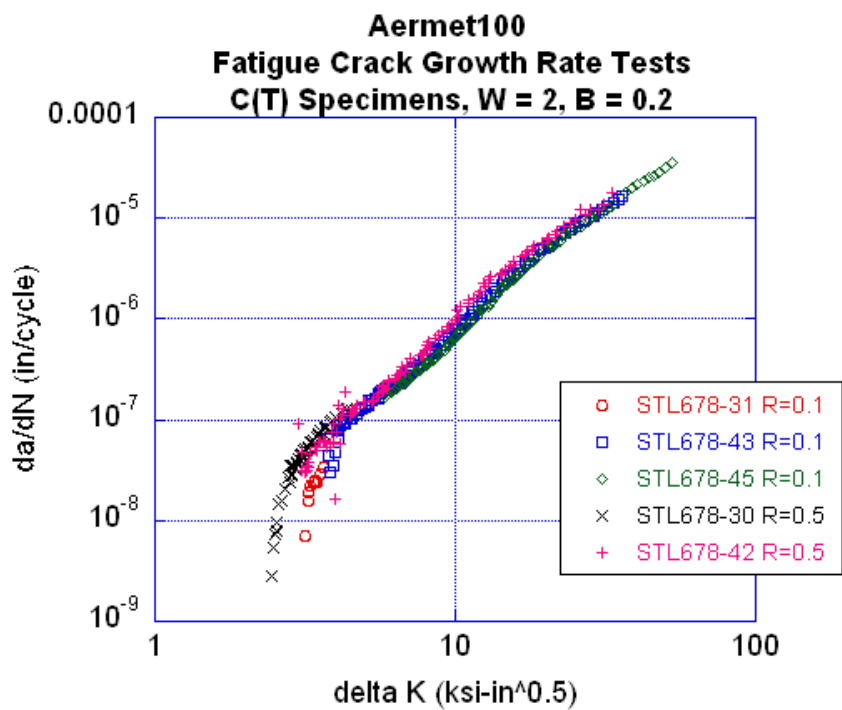
Figure 3.4.3-7. *FCGR summary plot.*
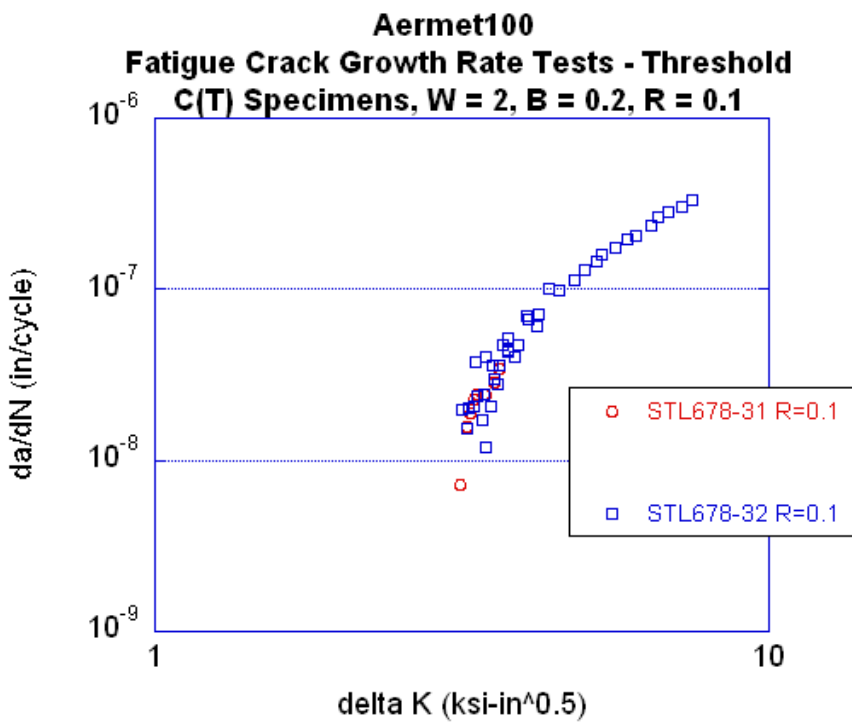
Figure 3.4.3-8. *FCGR threshold data at R = 0.1.*
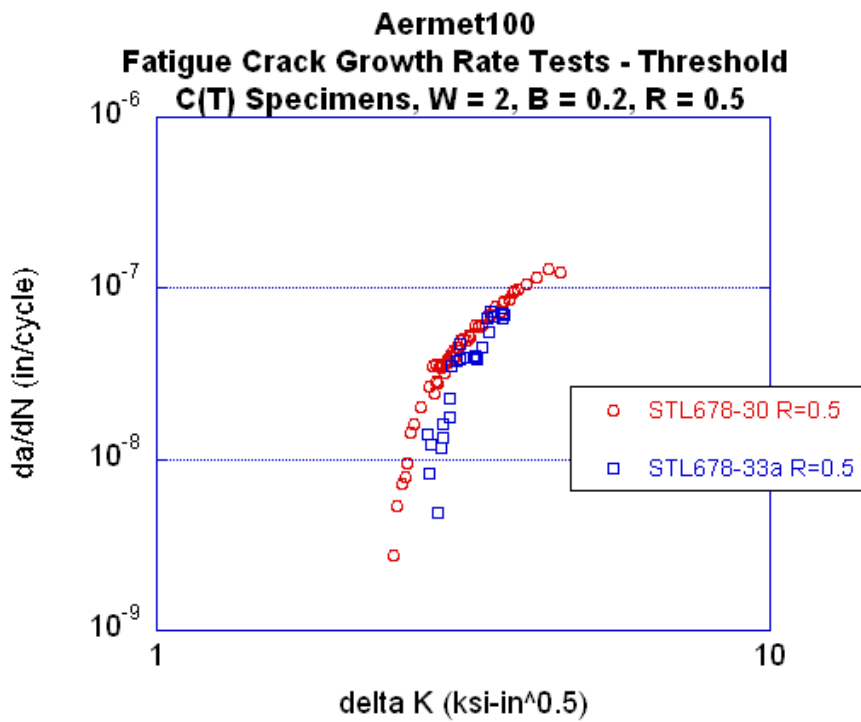
Figure 3.4.3-9. *FCGR threshold data at R= 0.5.*

3.4.4   Strain Life Testing

Strain life testing was planned that originally included incremental step testing (ASTM E606), strain-controlled fatigue (ASTM E606), and load-controlled fatigue with overstrain (ASTM E466). The test matrix was reduced to that shown in Table 3.4-1 due to program priorities. UDRI subcontracted the strain life specimen manufacture and testing to Metcut Research, Inc. due to equipment and time conflicts. A total of 179 E606 specimens with a 0.75″ gage length x 0.375″ diameter were manufactured. Metcut also fabricated and tested three ASTM E8 tensile specimens from the same lot of material used for the E606 specimens. Tensile results are shown in Table 3.4.4-1. Metcut completed 39 low-cycle, strain-controlled tests at four strain amplitudes prior to UDRI issuing a stop-work order due to program funding changes. The strain life test results are shown in Appendix E. The remaining untested specimens were returned to UDRI.

Table 3.4.4-1. Metcut Strain-Life Tensile Test Results
(extracted from Metcut Laboratory Report, Project 0741-85143-2, dated June 18, 2007)

Material Identification: AerMet 100
Drawing Number: 4013195-603
Nominal Gage Dimensions: 0.25 in. dia. x 1.36 in. egl.
Testing Specification: ASTM E-8(04)
Extensometer Gage Length (in.): 1.0 in.
Strain Rate through 0.2% yield: 0.005 in./in./min.
Head Rate thence to failure: 0.05 in./min.
Test Temperature (°F): 70

Metcut Test Number	Specimen Identification	U.T.S. (ksi)	0.2% Y.S. (ksi)	Elong. (%)(a)	R.A. (%)
T-167008	16-11	293	263	12	67
T-167009	21-4	283	256	12	69
T-167010	23-7	289	259	11	67

Notes: (a) Value based on overall length measurements

3.5   Corrosion-Fatigue Tests

Corrosion-fatigue tests were conducted to assess the effect that corrosion had on the fatigue life of AerMet100. Constant-amplitude fatigue tests were performed incorporating the same marker band spectrum as for AF1410B C-F specimens.

Specimens

A total of 74 corrosion-fatigue (C-F) specimen coupons (3.0″ x 17″ x 0.75″) were rough-cut from the billets of the AerMet100 by AES, while in the normalized and overaged condition, in the L-T orientation. UDRI sent the C-F coupons to Hercules Heat Treat along with the other specimen coupons for heat treatment and contracted with AccuGrind Manufacturing Co., Inc. for final machining and transverse low-stress grinding per UDRI specifications and drawing (Figure 3.5-1).

Following low-stress grinding, UDRI hand-polished the gage section of each specimen in accordance with the procedures in Appendix F.

Three baseline bare AerMet100 C-F specimens underwent the same chemical cleaning process used for the AF1410B C-F specimens. Prior to fatigue testing, aluminum tabs were bonded with M-Bond 200 adhesive to the tabs of the test specimens to protect the faces of the hydraulic wedge grips.

1. L = Overall as received length
2. Grinding of the blank shall be done without significant heating of the blank
3. Gage section and radii between tabs can be low stress ground across the width to within 0.025" of final thickness
4. Low stress grind final 0.01" in direction parallel to long axis of specimen on (4) surfaces in between the tabs, see specification "Metallic Test Specimen Preparation, Low Stress", Attachment 1
5. Final metal removal should be parallel to long axis of specimen per ASTM E466, see Attachment 2
6. Machining marks visible at 20x that are not parallel to long axis of specimen within 10 degrees are NOT acceptable per ASTM E466, see Attachment 2
7. Grinding flaws visible at 20x are not permitted on the surfaces between the tabs
8. All corner edges (radius 0.030") in the gage section and radii must be ground or polished parallel to the long axis
9. No random scratches shall be visible in the gage section upon completion. The gage section shall be protected from scratches

Figure 3.5-1. Corrosion-fatigue specimen drawing.

64

Equipment

Specimens were tested in an MTS closed-loop, servo-hydraulic test machine equipped with a 220 kip actuator and hydraulic grips. The grips were aligned in the test machine using a rectangular bar instrumented with strain gages and spacers were used to center the test specimens in the grips. An MTS Teststar II controller and PC provided constant amplitude load control, input of the marker band spectrum, and recorded fatigue data.

Procedures

Each AerMet100 C-F test specimen was mounted and aligned in the hydraulic grips with the controller programmed for a peak stress of 160 ksi and stress ratio R = 0.1. Each C-F specimen was subjected to constant-amplitude, axial fatigue loading and the same marker band spectrum used previously until failure. Endurance fatigue tests were performed on the first baseline bare AerMet100 C-F specimen starting at a peak stress level of 160 ksi. After 1 million cycles, the peak stress level was increased to 165 ksi, at which the baseline C-F specimens failed within a reasonable number of cycles. Another two baseline bare AerMet100 specimens were tested to failure. Testing of AerMet100 C-F specimens was suspended due to funding limitations. The remaining C-F specimens were preserved by coating with oil and placed in separate plastic tubes for storage.

Test Results

The results of the three AerMet100 baseline C-F tests are shown in Table 3.5-1.

Table 3.5-1. Preliminary Corrosion-Fatigue Test Results for Aermet100

AerMet100 Corrosion-Fatigue Specimen Results									
Specimen No.		Forging		Width	Thickness		Fatigue	Stress	Cycles to
STL #	Suffix	Section	Grind Status	(in)	(in)	Used for	End Date	(ksi)	Failure
680 -	1A	34B	Transverse	2.5330	0.1263	Endurance	4/27/2007	160	1,083,238
680 -	1A	34B				Endurance	4/27/2007	165	144,668
680 -	2A	33B	Transverse	2.5313	0.1240	Endurance	5/13/2007	165	334,465
680 -	3A	32B	Transverse	2.4918	0.1335	Endurance	6/16/2007	165	159,844

Section 4

Model Development

4.0 Introduction

One of the primary goals on the program was to develop models to predict the effect that corrosion has on the fatigue life of high-strength steels. The equivalent stress riser (ESR) model was created on the previous contracts during this program. As documented in Reference 2, this model is consistently conservative. During the third contract, efforts were directed towards calibrating the model so as to remove some, if not all, of this conservativeness. In addition, a grid model was proposed to allow predictions of life based on NDE inspection results.

4.1 ESR Model Calibration

An extreme value approach to calibration of the ESR model was proposed. If just one C-F specimen is considered – the ith specimen – then each ROI (labeled by the index j) will have a probability defined by the model, a probability density function (pdf), and a cumulative distribution function (cdf). These pdf's and cdf's represent the parent population from which the k_f's for each ROI are sampled. Starting with the NAVAIR notch sensitivity equation, let the cdf for a given ROI, j, for a given specimen, i, (describing the model) be given by:

$$F(kf_i, kt_{i,j}, r_{i,j} : \alpha, \sigma) = F(\log(kf_i - 1) \,|\, \log(kt_{i,j} - 1) - \log(1 + (\alpha / r_{i,j})^2), \sigma)$$

where k_{fi} is the specimen k_f value, then this cdf applies for all ROIs, including the critical ROI as individual samples from the population. However, the cdf for the entire sample needs to be known. The cdf for the extreme value for this specimen is the product of the cdfs for all ROIs on this specimen. Letting G and g be the cdf and pdf for the extreme value for this population of ROIs for specimen i, then:

$$G(kf_i : \alpha, \sigma) = \prod_j F_j(kf_i, kt_{i,j}, r_{i,j} : \alpha, \sigma)$$

To get the pdf for the extreme value for this set of ROIs, this equation is differentiated with respect to k_f:

$$g(kf_i : \alpha, \sigma) = \frac{dG(kf_i : \alpha, \sigma)}{dkf_i}$$

66

To construct a likelihood function, the product of the pdfs over all specimens needs to be optimized. Since the log function retains the maximum, a likelihood function as the log of the product can be constructed, which is the same as the sum of logs:

$$L = \sum_i \log(g(kf_i : \alpha, \sigma))$$

L must then be optimized for the model parameters.

This function can be expanded and simplified. Since g is the derivative of a product, the product rule can be used:

$$g(kf_i : \alpha, \sigma) = \frac{dG(kf_i : \alpha, \sigma)}{dkf_i} = \sum_k \left(f(kf_i, kt_{i,k}, r_{i,k} : \alpha, \sigma) * \prod_{j \neq k} F(kf_i, kt_{i,j}, r_{i,j} : \alpha, \sigma) \right)$$

$$= \sum_k \left(\frac{f(kf_i, kt_{i,k}, r_{i,k} : \alpha, \sigma)}{F(kf_i, kt_{i,k}, r_{i,k} : \alpha, \sigma)} * \prod_j F(kf_i, kt_{i,j}, r_{i,j} : \alpha, \sigma) \right)$$

$$= \prod_j F(kf_i, kt_{i,j}, r_{i,j} : \alpha, \sigma) * \sum_k \left(\frac{f(kf_i, kt_{i,k}, r_{i,k} : \alpha, \sigma)}{F(kf_i, kt_{i,k}, r_{i,k} : \alpha, \sigma)} \right)$$

Since g is now a product of two factors, the log of these factors is the sum of the logs:

$$L = \sum_i \log(g(kf_i : \alpha, \sigma)) = \sum_i \log \left(\prod_j F(kf_i, kt_{i,j}, r_{i,j} : \alpha, \sigma) * \sum_k \left(\frac{f(kf_i, kt_{i,k}, r_{i,k} : \alpha, \sigma)}{F(kf_i, kt_{i,k}, r_{i,k} : \alpha, \sigma)} \right) \right)$$

$$= \sum_i \left(\log \prod_j F(kf_i, kt_{i,j}, r_{i,j} : \alpha, \sigma) + \log \left(\sum_k \left(\frac{f(kf_i, kt_{i,k}, r_{i,k} : \alpha, \sigma)}{F(kf_i, kt_{i,k}, r_{i,k} : \alpha, \sigma)} \right) \right) \right)$$

$$= \sum_i \sum_j \log(F(kf_i, kt_{i,j}, r_{i,j} : \alpha, \sigma)) + \sum_i \log \left(\sum_k \left(\frac{f(kf_i, kt_{i,k}, r_{i,k} : \alpha, \sigma)}{F(kf_i, kt_{i,k}, r_{i,k} : \alpha, \sigma)} \right) \right)$$

This expression does not include any products and should be relatively easy to carry out. It should be noted that there are factors that might be missing in this expression related to the derivative of the cdf, F, to get the pdf, f. For instance, if the model assumes a normal distribution, then the mean is given by:

$$\mu_{i,j} = \log(kt_{i,j} - 1) - \log(1 + \alpha / r_{i,j})$$

or

$$\mu_{i,j} = \log(kt_{i,j} - 1) - \log(1 + (\alpha / r_{i,j})^2)$$

depending on the form of the model. And the standard deviation is given by σ. Then the expression above must include a factor of:

$$\frac{1}{(kf_i-1)\sigma}$$

in the second term, inside the inner summation to account for the derivative of the argument of the cdf:

$$L = \sum_i \sum_j \log\left(\Phi((\log(kf_i - 1) - \mu_{i,j})/\sigma)\right) + \sum_i \log\left(\sum_k \left(\frac{\phi((\log(kf_i-1)-\mu_{i,k})/\sigma)}{\Phi((\log(kf_i-1)-\mu_{i,k})/\sigma)} * \frac{1}{(kf_i - 1)\sigma}\right)\right)$$

Note that the second term in the above expression uses the index k instead of j. Since the two terms are completely independent, k can be changed to j without loss of generality. The index k was used to make a distinction between the index being differentiated and the rest of the j-1 factors in the product.

This expression for the likelihood function does not distinguish between the critical ROI and the rest of the ROIs. This formalism also does not including censored ROIs in a formal way. The reason is that the set of ROIs, including the critical ROI, is considered one set of samples from the population of such sets with the given set of ROIs for that specimen. The extreme value formulation automatically includes all of the ROIs in the determination of the probabilities for that specimen. The critical ROI then is not anything special. All that is needed to know is that all of the ROIs (including the critical ROI) had a k_f that was less than the k_f value found for this specimen.

To test this proposed approach, the model was calibrated on a subset of AF1410 Set A corrosion-fatigue test specimens (14, 20, 36, 58, 59, 62, 21, 29, 12, 37, and 41). The model parameters were found to be as follows: α = 0.547 mm and σ = 0.566 (unitless) for the assumed Peterson model[1]:

  ln(kf-1) = ln(kt-1)-ln(1+α/r) + δ

where δ has a zero mean and standard deviation of σ. Predictions were then made for other AF1410 Set A corrosion-fatigue test specimens (42, 5, 6, 51, and 62). Figures 4.1-1 through 4.1-5 show the results of these predictions where the vertical line indicates the actual fatigue life found in the experiment.

---

[1] Note that the description above assumes a slightly different model in which α/r is squared. In the test cases, a Peterson model was used since it gave better results.
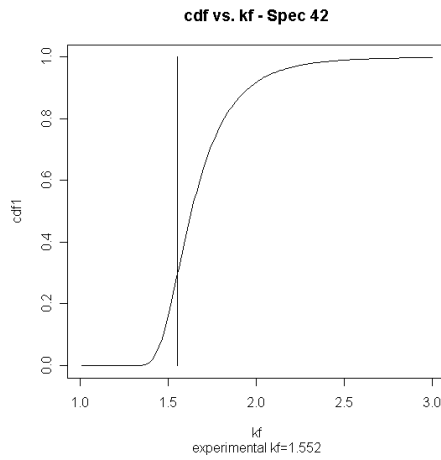
Figure 4.1-1. *Calibrated ESR model prediction and plate critical k_f for AF1410 Set A Specimen 42.*
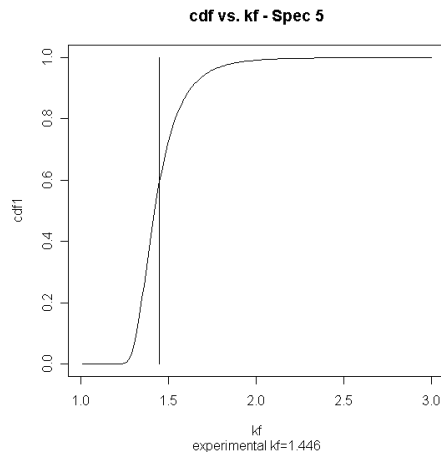
Figure 4.1-2. *Calibrated ESR model prediction and plate critical k_f for AF1410 Set A Specimen 5.*
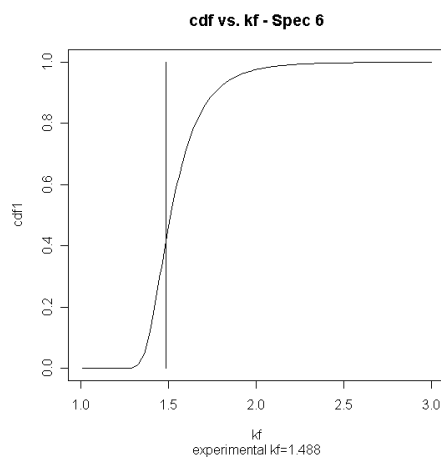
Figure 4.1-3. *Calibrated ESR model prediction and plate critical k_f for AF1410 Set A Specimen 6.*

69
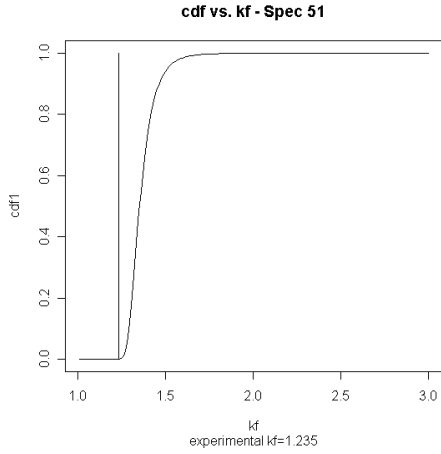
Figure 4.1-4. *Calibrated ESR model prediction and plate critical k_f*
for AF1410 Set A Specimen 51.
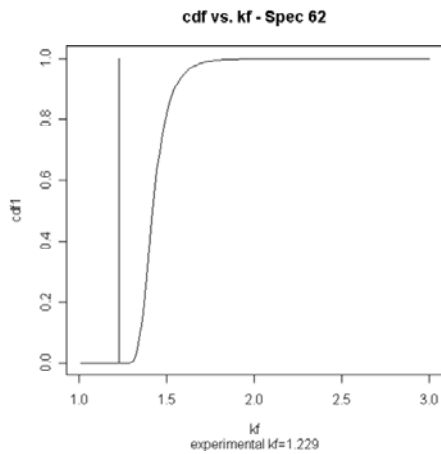
Figure 4.1-5. *Calibrated ESR model prediction and plate critical k_f*
for AF1410 Set A Specimen 52.

As can be seen from these plots, this method of calibration has promise. All but one of the test cases predicted a life within the transition of the probability plot. Only Specimen 52 was overly conservative.

4.2   Grid Model

In the implementation scheme presented in Reference 2, there was a requirement to make a decision on the severity of corrosion based on the results of an NDE inspection. In general, NDE inspections do not have spatial resolution as good as the white light interference microscope. In fact, the resolution of NDE systems are significantly poorer than the white light interference microscope used to develop the ESR model. As a result, conventional NDE systems that are

70

available to the inspector in the field or onboard an aircraft carrier are not able to resolve individual features causing crack initiation. Consequently, there is a need to establish other metrics for corrosion severity.

On the first two contracts, various surface roughness metrics and variations on these metrics were studied. It was determined that standard surface roughness metrics, such as R_a and R_q, provide a correlation to life, but ultimately, these metrics must also account for the local applied stress. The grid model was proposed to do just this. A square grid is superimposed over the surface of the component. Each grid element is 1 mm by 1 mm for the purposes of this program, although other grid sizes were studied. Within each grid, a local mean surface height is determined and then removed, and then R_a and R_q are determined. These grid surface height statistics extracted from WLI scans of corroded areas can then be compared to similar results from NDE inspections using the same grid. This comparison is reviewed in section 5 below.

In order to further develop the grid model, it was necessary to determine the critical grid elements in which the crack initiated. This was done for both AF1410 Set A and Set B corrosion-fatigue specimens. Figures 4.2-1 and 4.2-2 display the k_{fc} for each plate in Set A and Set B, respectively, versus the critical R_a value for that plate, taken from the WLI image grid element in which the crack initiated. Both plots show a trend line. While these trend lines are not the same, it is clear that k_{fc} correlates well with the critical R_a determined from the grid analysis.
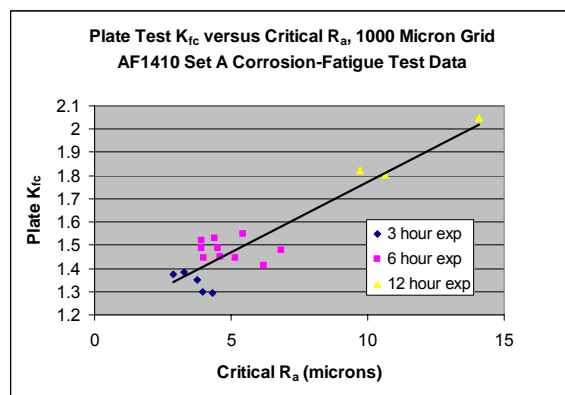
Figure 4.2-1. *Plate test k_{fc} versus critical R_a for a 1000-micron grid for AF1410 Set A corrosion-fatigue test data.*
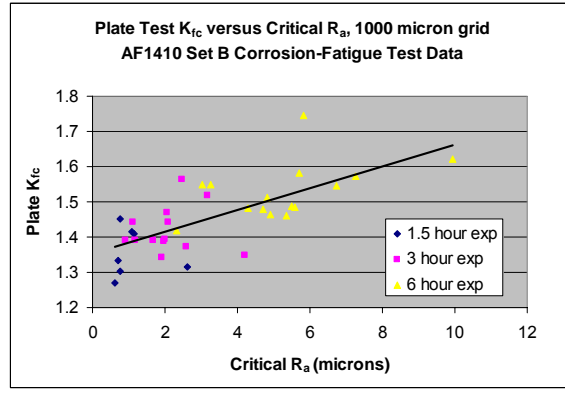
Figure 4.2-2. *Plate test k_{fc} versus critical R_a for a 1000-micron grid for AF1410 Set B corrosion-fatigue test data.*

Tables 4.2-1 and 4.2-2 show the Critical Grid analysis results for the AF1410 Set A and Set B data, respectively.

Table 4.2-1. Results of Critical Grid Analysis for AF1410 Set A Corrosion-Fatigue Test Data

			Grid Averages					
			1000 μm resolution					
	Plate	Plate	Critical	Critical	Max.	Max.	Critical %	Critical %
Specimen	R_a	R_q	R_a	R_q	R_a	R_q	R_a	R_q
15	3.127	4.21	3.952	5.346	6.421	7.547	94.7	96.3
21	2.919	4.426	2.883	4.16	5.043	6.595	51.3	34.7
29	2.972	3.992	3.267	4.243	5.591	9.32	89.4	87
36	2.739	3.976	4.335	5.446	5.734	7.072	99.3	98.6
62	3.128	4.2	3.753	4.775	5.188	6.345	96.4	95.1
5	3.158	4.16	3.982	5.184	6.681	8.052	90.7	91.5
6	3.55	4.7	3.937	5.031	9.352	10.975	83.1	82.2
12	3.786	4.96	6.196	8.001	7.895	9.256	99.2	99.6
14	3.234	4.634	6.853	8.34	7.629	8.739	99.9	99.9
20	3.291	4.394	5.433	7.632	8.593	10.004	96.2	99
37	3.478	4.716	4.395	5.756	6.735	8.156	90.8	91.6
41	3.4558	4.5752	5.179	6.648	7.814	9.272	96	96.9
42	3.34	4.513	3.921	5.256	8.057	9.248	81.6	84
58	3.506	4.647	4.505	5.92	7.631	9.479	91.4	93.2
59	3.263	4.363	4.612	5.784	8.682	10.104	91.8	91.5
35	5.027	6.951	9.726	13.318	14.281	16.867	97.9	99.2
38	5.229	7.427	14.084	18.678	16.927	18.894	99.8	99.9
46	5.298	7.313	10.642	13.862	13.104	16.039	99	99.5

Table 4.2-2. Results of Critical Grid Analysis for AF1410 Set B Corrosion-Fatigue Test Data

	Grid Averages					
	1000 μm resolution					
	Critical	Critical	Max.	Max.	Critical %	Critical %
Specimen	R_a	R_q	R_a	R_q	R_a	R_q
544-9C	0.7596	1.1317	2.4748	2.7567	81.85	85.96
545-3D	0.70833	0.8898	2.4512	2.6517	82.74	82.74
547-26A	1.1363	1.4454	2.3425	2.7214	93.813	94.706
545-2A	1.0809	1.3613	2.9291	3.2363	92.088	92.326
547-50B	0.6036	0.729	2.3565	2.807	77.037	76.026
614-7	0.777	0.9912	2.336	2.676	83.58	84.355
614-11	2.615	3.104	2.615	3.104	100	100
545-6A	2.6023	3.1209	3.8607	4.3702	97.501	97.799
545-10D	2.4693	2.9693	4.1044	4.7087	97.1446	97.323
547-22C	2.0445	2.5128	4.9589	5.638	88.5782	88.5187
547-37B	1.1277	1.4415	3.6911	4.3506	72.9328	73.1707
547-9M	2.003	2.3508	4.7804	5.2958	93.039	91.85
547-5A	1.6863	2.3408	4.238	4.825	88.994	92.088
547-23B	3.1676	3.892	4.7697	5.5815	98.3343	98.6318
544-5C	2.1	2.7601	3.7924	4.3123	96.2522	97.739
614-4	0.914	1.3364	3.9442	4.7583	69.066	71.9215
614-12	1.167	1.6192	4.1603	5.5801	75.1338	77.1565
614-21	4.2024	4.7469	5.4091	6.2483	99.6431	99.5836
614-1	1.9684	2.4015	4.358	4.882	91.85	91.9096
614-15	1.912	2.297	3.4067	3.9665	95.1814	94.7055
544-8C	5.7124	7.1536	8.4398	9.119	99.0482	99.4051
544-10C	3.039	3.586	7.538	8.418	85.127	83.34
547-6A	4.2875	5.389	8.503	9.42	93.634	94.884
547-20B	4.692	5.429	8.4564	9.556	97.32	96.6
547-36B	7.2576	8.3671	8.6128	9.6417	99.762	99.762
544-3B	5.8199	7.103	10.522	12.2359	97.323	97.323
547-16B	3.2621	4.3229	7.864	9.6029	88.3998	91.076
547-2C	5.3591	6.2932	10.2866	11.5859	98.5128	98.0369
547-31B	4.9242	5.6289	8.6817	9.6783	97.8584	97.3825
614-3	2.3209	2.9939	8.4912	9.3304	77.2754	77.1565
614-8	5.579	6.6038	8.5887	10.162	97.1446	97.323
614-13	6.7249	8.5335	9.631	10.47	98.69	99.52
614-5	4.8292	5.8754	8.796	10.153	94.8245	95.4194
614-6	9.9308	10.9466	11.883	13.5319	99.4646	99.3456
614-19	5.5015	6.3388	8.9858	10.0879	96.9661	96.7281

Grid statistics can be used in a roughness metric model, just as ROI statistics are used in the ESR model, to generate a histogram of k_{fc} values. Roughness metric life predictions from the grid model will use the k_{fc} histogram and a modified version of the ESR algorithms. This method assumes that notch locations are correlated with corrosion and that there is a single notch in each metric grid block with the average critical notch k_{fc} value. A limited number of life predictions were made with this grid, or roughness metric, model. Table 4.2-3 shows predictions for three

AF1410 Set A corrosion-fatigue specimens based on the grid statistics from WLI images and an extension of the ESR model – which relates k_{fc} to grid statistics, rather than relating k_{fc} to the root radius of the ROIs. The preliminary life predictions shown here are consistent with those found from the ESR model on the same specimens.

Table 4.2-3. Comparison of Life Predictions from ESR and Roughness Metric Models

	Test CI Life (cycles)	ESR Pred. Life (50% Prob.)	ESR Pred./Test Life Ratio	Metric Pred. Life (50% Prob.)	Metric Pred./Test Life Ratio
Spec. 62	103,595	42,500	0.410	46,000	0.444
Spec. 58	69,243	31,000	0.448	35,000	0.505
Spec. 59	41,029	20,500	0.500	20,500	0.500

It was found in this study that calculating roughness metric values on a grid gives coarse image representation of a corroded surface; however, the roughness values appear to correlate with levels of crevice corrosion in each grid block. It was also seen that roughness values at critical crack locations are above 90th percentile of all values in most cases. While it is not shown in the data presented here, using grid averages (the mean within each grid) to compute metric values is slightly better than using the image average (a mean derived from the whole image). Furthermore, critical roughness values vs. plate test k_{fc} values show a linear trend with increasing exposure levels. As stated above, preliminary life predictions are consistent with those found from the ESR model. Finally, this method can be adapted to account for stress gradient effects.

There are limitations associated with this method. It assumes that the critical notch locations and severities are correlated with level of corrosion. Test specimens with small amounts of corrosion also show less correlation in critical crack locations; since the corrosion seen in cadmium-plated test specimens might not be as severe as in the corrosion-fatigue test specimens, this could be a problem. Finally, coarse grid spacing gives better metric vs. k_{fc} correlation, but reduces the image resolution.

Section 5
Nondestructive Evaluation

5.0   Introduction

As mentioned in Section 4, the implementation scheme presented in Reference 2 requires making corrosion severity classifications based on the results of NDE inspections. Section 4 has shown how roughness statistics can be used to make life predictions; however, the roughness metrics used in that section were based on the fine resolution obtainable with the white light interference microscope. In this section, a correlation will be established between surface roughness statistics of the corrosion-fatigue specimens derived from ultrasonic inspections and those derived by the white light microscope. This correlation will be demonstrated using statistics determined for 1-mm by 1-mm grid elements.

5.1   Grid Correlation

The following study makes use of AF1410 Set B corrosion-fatigue measurements of surface height profiles using ultrasonic (UT) time-of-flight and white light (WL) interference microscopic profiles. Data from nine specimens were used to calculate roughness values in a grid overlaid on the corrosion patch; each grid element was 1 mm by 1 mm. The specimens included three from each of three different corrosion exposure levels (1.5, 3, and 6 hours) in order to make use of a range of corrosion severities. With each grid, tilt was removed prior to calculation of roughness in the form of the parameter R_q. Figure 5.1-1 shows UT R_q versus WL R_q for the 1.5-hour exposure specimens, Figure 5.1-2 contains the 3-hour exposure plots, and Figure 5.1-3 contains the 6-hour exposure data. Notice the change in scale.

In each figure, the grid data are given by the dark blue diamonds, while a line with a slope of one and a zero intercept is shown in purple. This line represents an ideal correlation between the UT and WL data. Obviously, the data do not fit the ideal correlation line; however, they do show that there is a correlation.

(a)

(b)

(c)
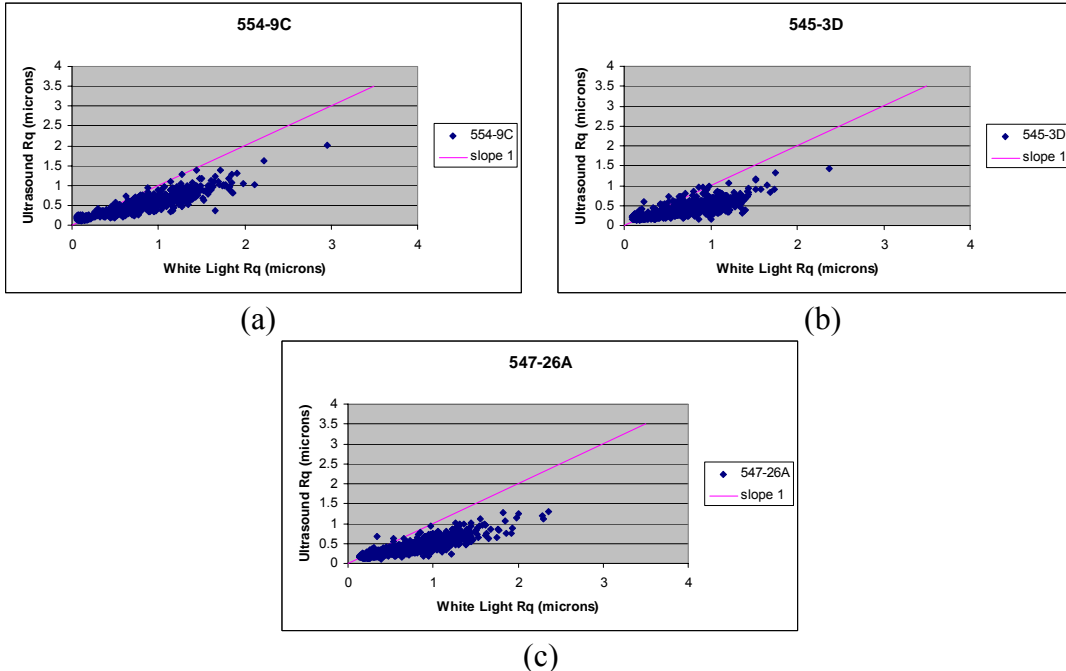
Figure 5.1-1. _Plots R_q for UT versus R_q of WL for 1.5-hour exposure data on AF1410 Set B specimens: (a) 554-9C, (b) 545-3D, and (c) 547-26A._

(a)

(b)

(c)
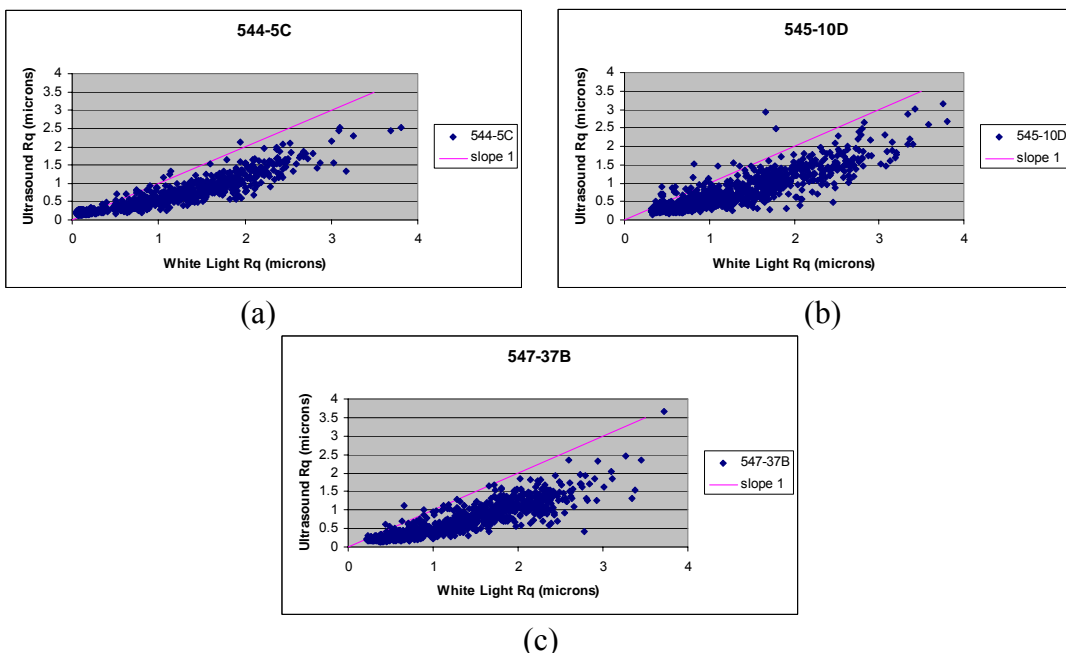
Figure 5.1-2. _Plots R_q for UT versus R_q of WL for 3-hour exposure data on AF1410 Set B specimens: (a) 554-5C, (b) 545-10D, and (c) 547-37B._
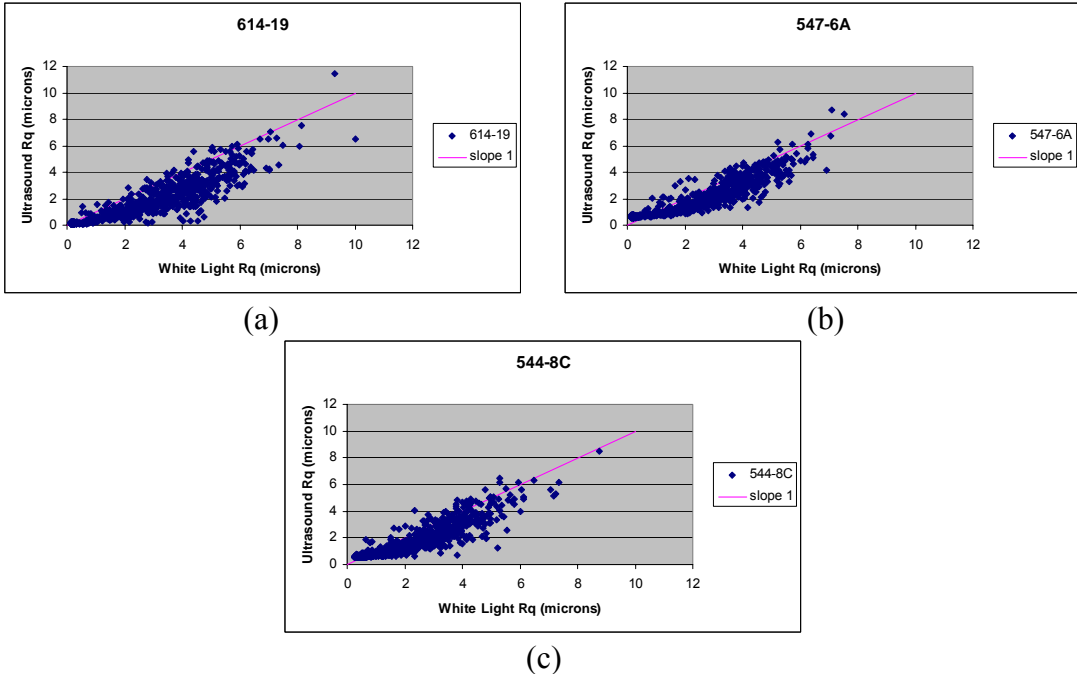
Figure 5.1-3. *Plots R_q for UT versus R_q of WL for 6-hour exposure data on AF1410 Set B specimens: (a) 614-19, (b) 547-6A, and (c) 544-8C.*

There are some interesting observations to note in these plots. First, the trends in the data are not linear, but a leveling off is apparent at small WL R_q values. This is interesting because it suggests that the UT data approaches a minimum nonzero value. Physically, the grid elements with very small WL R_q values represent areas on the corrosion-fatigue specimens without corrosion (outside the corrosion patches). This means that the UT measurements are showing a level of roughness that is really independent of the actual surface roughness in these grid elements. This represents a noise floor in the UT profile measurements. This can be caused by vibration or mechanical dither in the transducer standoff that causes the time-of-flight measurement in the ultrasonic signal to vary randomly at a small level, giving the appearance of a rough surface – even when the surface is actually very flat. This noise could also be of an electronic nature, caused by variations in sampling (digitizing) of the signal in the time domain. In either case, the time-of-flight variations would be expected to be present in all of the UT measurements, but be more noticeable on the smooth, uncorroded regions of the sample. Notice that the noise is different for each set.

The second observation from this data is that the scatter in the UT roughness increases with WL roughness. This points out that, while there is a general correlation, there is still quite a

bit of UT roughness variation from grid element to grid element for the same WL roughness. This suggests that the actual UT response is a complicated phenomenon that is dependent on the actual surface profile in the grid. It might not be possible to do any better than to produce a model of the data that accounts for an assumed random variable representing the effects of the detailed corrosion profile on the UT response.

With these observations in mind, a simple model presents itself. Since R_q is essentially a standard deviation of the surface profile, the limiting value of the UT roughness at small WL roughnesses represents the standard deviation of the time-of-flight variations, or noise. Since variances add together, the simple model would suggest that the measured UT R_q value, UT_m, is given by the following:

$$UT_m = (UT_0^2 + N^2)^{0.5}$$

where UT_0 is the actual UT R_q value that would be measured if the noise were not present and N is the noise, as a standard deviation. N is measured by averaging the UT_m at small WL R_q values. So, the corrected UT roughness value is:

$$UT_0 = (UT_m^2 - N^2)^{0.5}$$

After studying several different models, this simple empirical model seemed best:

$$\ln(UT_m^2 - N^2) = m\ln(WL) + b + \varepsilon$$

The parameter ε is a random variable (normally distributed) with a mean of zero and some standard deviation. In fitting this model to the data, all data points for which UT_m is less than N had to eliminated from the fit to avoid undefined logarithms. In addition, there seemed to be a slope change for points at $\ln(WL)$ equals -1.0; therefore, all points with $\ln(WL)$ less than -1.0 were eliminated. Figure 5.1-4 below shows the data plotted as $\ln(UT_m^2 - N^2)$ versus $\ln(WL)$ for the 1.5-hour exposure data.
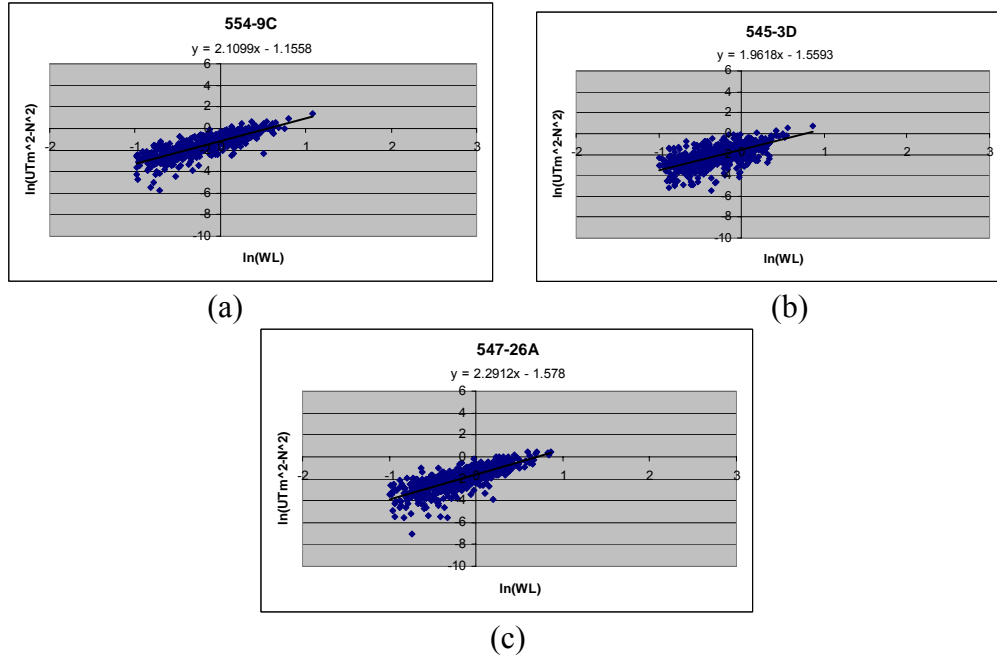
Figure 5.1-4. *Plots of ln(UT$_m{}^2$ – N^2) versus ln(WL) for 1.5-hour exposure data on AF1410 Set B specimens: (a) 554-9C, (b) 545-3D, and (c) 547-26A.*

The trend line is shown in each plot with the equation for this line displayed underneath the title. Figure 5.1-5 contains the 3-hour exposure fits and Figure 5.1-6 shows the 6-hour exposure data. Table 5.1-1 shows all of the slopes and intercepts for these fits.
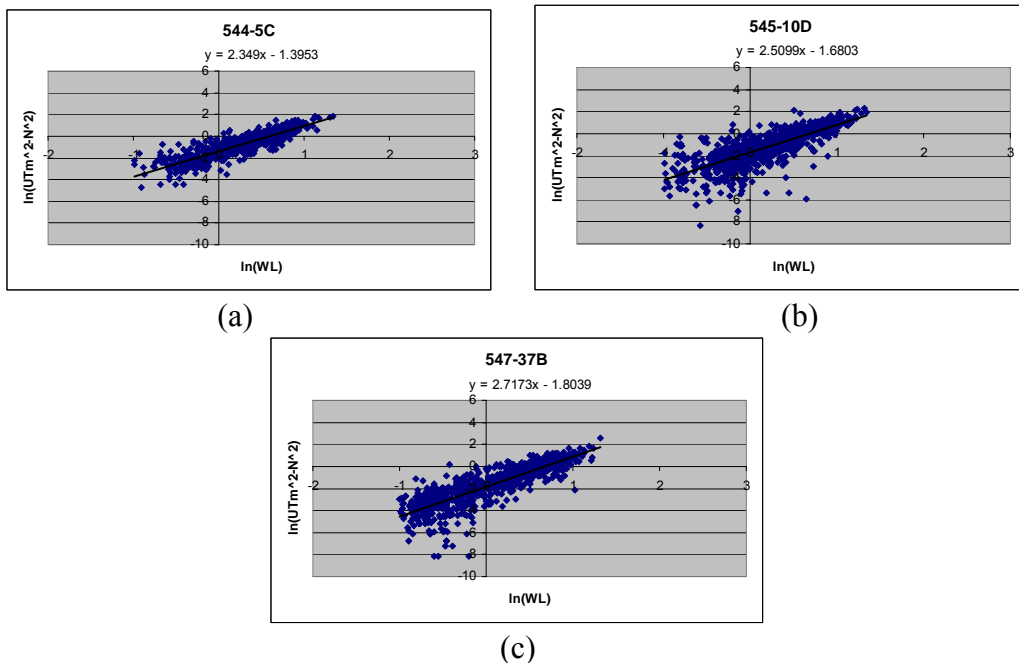
Figure 5.1-5. *Plots of ln(UT$_m{}^2$ – N^2) versus ln(WL) for 3-hour exposure data on AF1410 Set B specimens: (a) 554-5C, (b) 545-10D, and (c) 547-37B.*

79
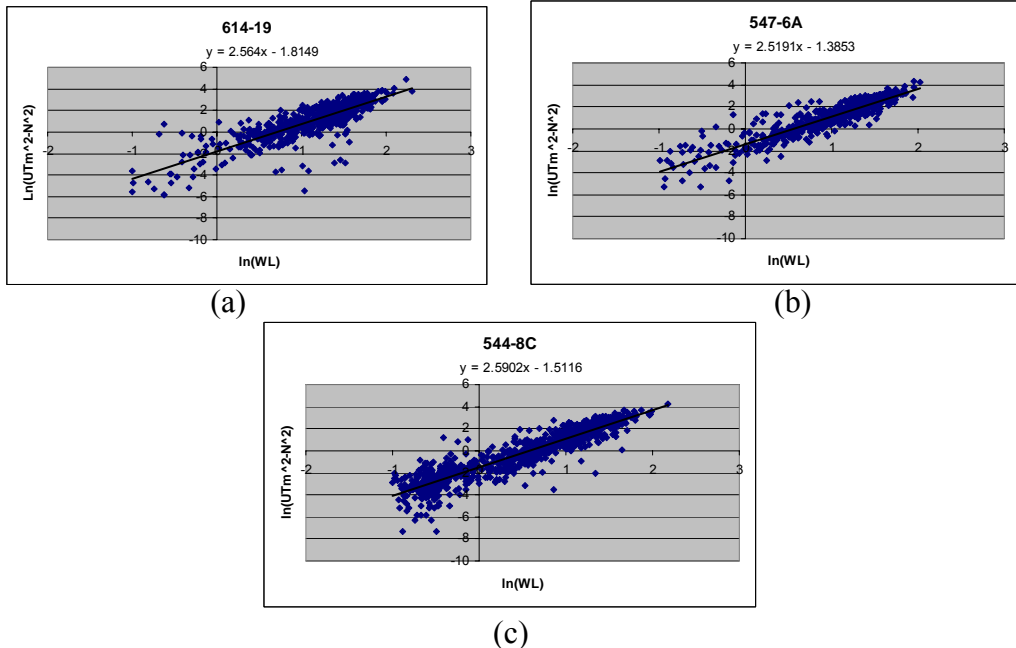
Figure 5.1-6. Plots of $\ln(UT_m^2 - N^2)$ versus $\ln(WL)$ for 6-hour exposure data on AF1410 Set B specimens: (a) 614-19, (b) 547-6A, and (c) 544-8C.

Table 5.1-1. Slopes and Intercepts of Fits

Run	Exposure	Slope	Intercept
554-9C	1.5 hours	2.11	-1.16
545-3D	1.5	1.96	-1.56
547-26A	1.5	2.29	-1.58
544-5C	3	2.35	-1.40
545-10D	3	2.51	-1.68
547-37B	3	2.72	-1.80
547-6A	6	2.52	-1.39
544-8C	6	2.59	-1.51
614-19	6	2.56	-1.81

The slope does vary some, but not in a consistent manner. While the slope is slightly higher for the longer exposures, there are problems with defining a clear trend. The largest slope is actually for a set of 3-hour data and there is a 1.5-hour set of data that is not much different than one of the 3-hour sets of data. It is even harder to establish a trend in the intercept data. The above plots are all shown with the same scales; to the eye, these data sets could very well belong to the same population. There are similar slopes, intercepts, and even scatters between the plots. With this observation in mind, all of the data has been plotted on a single graph as one set of data. In this plot, only data points from the above plots where ln(WL) is greater than –0.5 have been plotted. This was due to the apparent increase in scatter at the smaller WL values. As will be seen below, this limit on the data, while apparently justified, may not have been high enough.

Figure 5.1-7 shows all data, limited as described in the previous paragraphs, as $\ln(UT_m{}^2 - N^2)$ versus $\ln(WL)$.
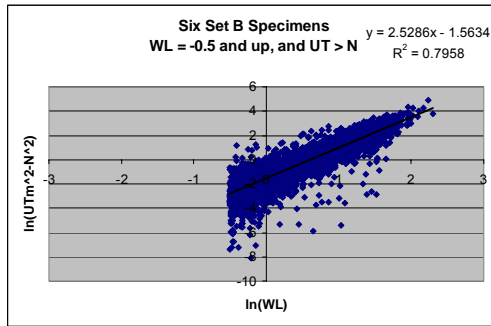
Figure 5.1-7. *Plot of $\ln(UT_m{}^2 - N^2)$ versus $\ln(WL)$ for all specimens.*

The equation of the fit is given in the upper right corner of the figure. It is seen that the slope and intercepts are within those given in Table 5.1-1. In order to better understand the scatter in the data, the standard deviation of the differences from the fit had been calculated: 0.78. The plot seems to show that the variance is increasing with WL. To test this, the data was partitioned into bins as follows: -0.5 to zero, zero to 0.5, 0.5 to 1.0, 1.0 to 1.5, and 1.5 to 2.0. The standard deviations for each bin are given in Table 5.1-2.

Table 5.1-2. Standard Deviations of the Difference Between the Data and the Fit

Bin	Standard Deviation
-0.5 to zero	0.93
Zero to 0.5	0.71
0.5 to 1.0	0.65
1.0 to 1.5	0.76
1.5 to 2.0	0.65

From this table, it is apparent that the standard deviation does not change much, if at all above $\ln(WL)$ equals zero. Below this value, the scatter increases with decreasing $\ln(WL)$. It is hypothesized that this is due to the fact that the UT data is small and can actually be less than the noise. While these points have been removed, there are still others that approach the noise value and, therefore, will fall at large negative values on this plot. These points increase the scatter in the plot. The limit of zero for $\ln(WL)$ means that only WL R_q values greater than 1 micron are being considered. The uncorroded surface has an Rq value that is significantly smaller than this, which is evident in the data in figures 5.1-1 through 5.1-3 where the smallest white light Rq values are in grid elements outside of the corrosion patch.

With this model in hand, the UT R_q measurements can be inverted to find the WL R_q value. However, it must be assumed that the WL values are the independent variable and the UT is a measurement of this value. Therefore, the WL value that gives a high probability that the UT value is above some other value must be found, such as the line that defines a 90% probability. That is, for a given WL R_q value, this limiting line says that there is a 90% probability that the UT R_q value will be above this line. Inverting the UT data will give us a conservative value for the WL R_q value. To get the 90% curve, the fit line must be shifted down by 1.28 standard deviations. The 90% line is then:

$$\ln(UT_m^2 - N^2) = 2.53\ln(WL) - 1.56 - 1.28 * 0.78$$
$$= 2.53\ln(WL) - 2.56$$

Or,

$$2.75(UT_m^2 - N^2)^{1/2.53} = WL$$

Alternatively, the 50% line could be used as the model and then a random variable would need to be introduced to account for the scatter, and the net effect on life would be determined through a Monte Carlo technique.

In summary, an approach was proposed for estimating surface roughness for grid elements from ultrasonic time-of-flight measurements. The grid statistics can then be used in the roughness metric (grid model) to make life predictions and, therefore, corrosion severity decisions.

Section 6
Verification and Validation

6.0   Introduction

An important component of this program has been verification and validation of the life prediction models. Verification refers to steps to confirm that the software code accurately reflects the physics being modeled (code verification) and that the calculations conducted by that code are correct (calculation verification). Validation refers to the steps taken to confirm that the model predictions are experimentally correct. A verification and validation plan was created and considerable work accomplished on this program. Of particular importance were two sets of validation experiments conducted on this program. A set of fatigue specimens were created with micromachined features produced in the gauge section of each specimen. The features were designed to have identical stress concentration factors, but of different shapes. The test specimens were all identical in order to have replicate tests so as to reveal feature and material effects. The second test was a blind validation experiment on AF1410 cadmium plated corrosion-fatigue specimens. Each plated specimen was sanded in a small patch in the center of the gauge section in order to compromise the cadmium plate (otherwise, corrosion would not grow), and then the specimens were exposed to a salt fog containing SO_2 for a set period of time (a different method of growing corrosion than previously used in the corrosion-fatigue tests on this program). Subsequently, the corrosion products were removed, surface height profiles determined, and specimens fatigue tested until failure. Each fracture surface was examined to ascertain the number of cycles to crack initiation. The surface height profiles were used to make life predictions to compare to the actual, experimentally determined fatigue lives. Validation tests and their results are reported in Section 3. Other verification and validation tasks are discussed here.

6.1   Verification and Validation Framework and Tasks

The purpose of this description is to define the framework for Verification and Validation (V&V) of the various components of the NAVAIR Corrosion-Fatigue modeling effort. The framework uses the format suggested in the ASME 29 March 2006 draft, "Guide for Verification and Validation in Computational Solid Mechanics." A bottom-up approach to V&V was utilized for this

program. The current corrosion modeling and test program for AF1410 steel was broken down into elemental building blocks (B1-B4) of increasing model complexity, as shown in Figure 6.1-1.

F/A-18C/D Arresting Shank

Prediction of Corroded Component Life
Fleet Corrosion
Coated Part
Gradient Stress Field

B4

C-F Plated Specimens

Prediction of C-F Lab Test Data
Coated Plate
Uniform Stress Field

B2

Micromachined Plates

Prediction of Lab Test Data
Replicate Large Notches
Bare Plate
Uniform Stress Field

B3

C-F Test Specimens

Prediction of C-F Lab Test Data
Bare Plate
Uniform Stress Field

B1

Figure 6.1-1. *Hierarchical structure of C-F life characterization complexity.*

V&V activities were carried out in each building block of the hierarchical structure, with flowcharts showing how the various modeling and testing activities relate to each other in the following pages. Block 1 is divided into Sub-blocks A and B for the ESR and roughness metric prediction methods, respectively. Figures 6.1-2 through 6.1-6 provide additional detail.
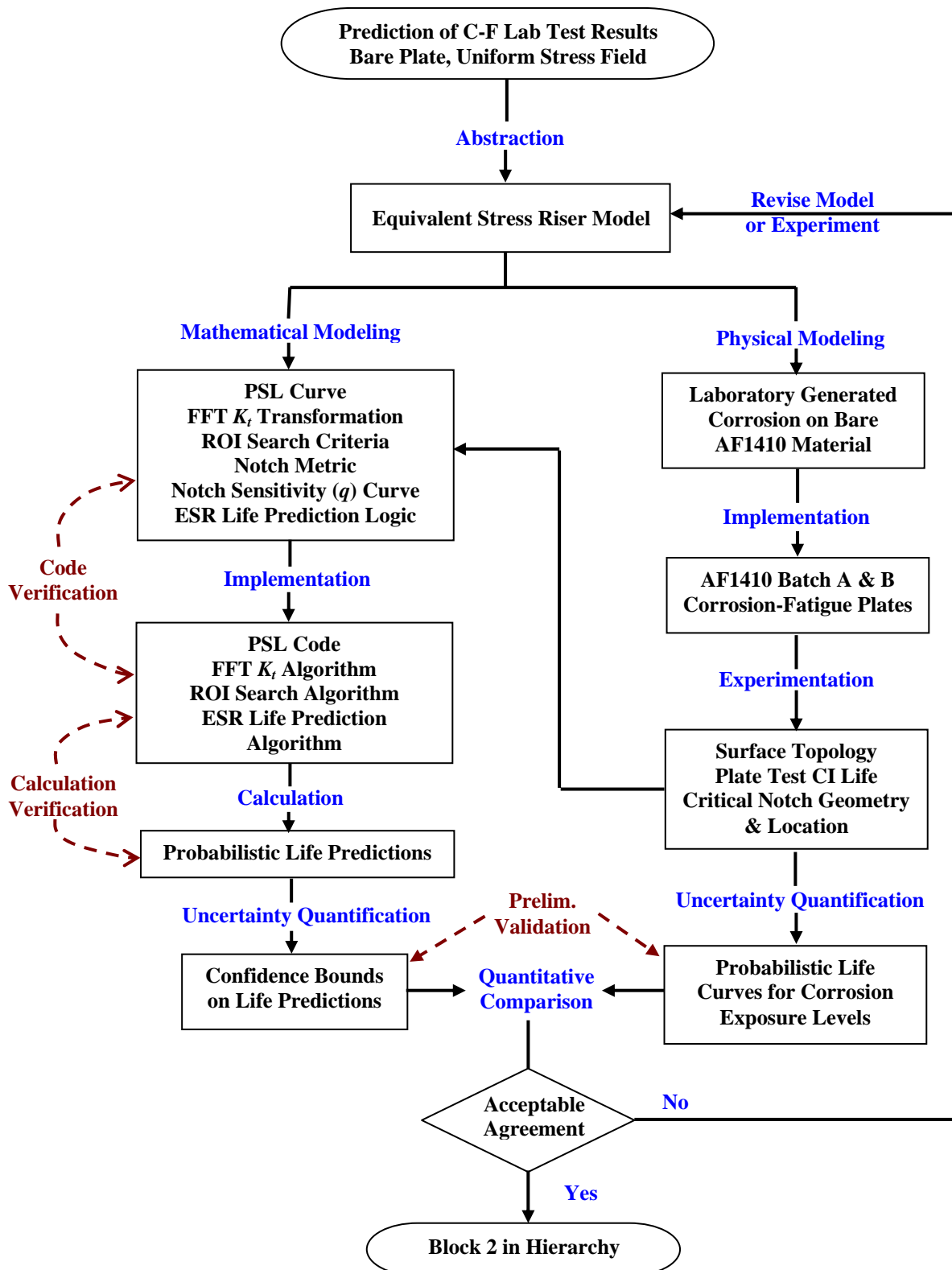
Figure 6.1-2. *V&V framework for Block 1A of C-F life characterization hierarchy.*
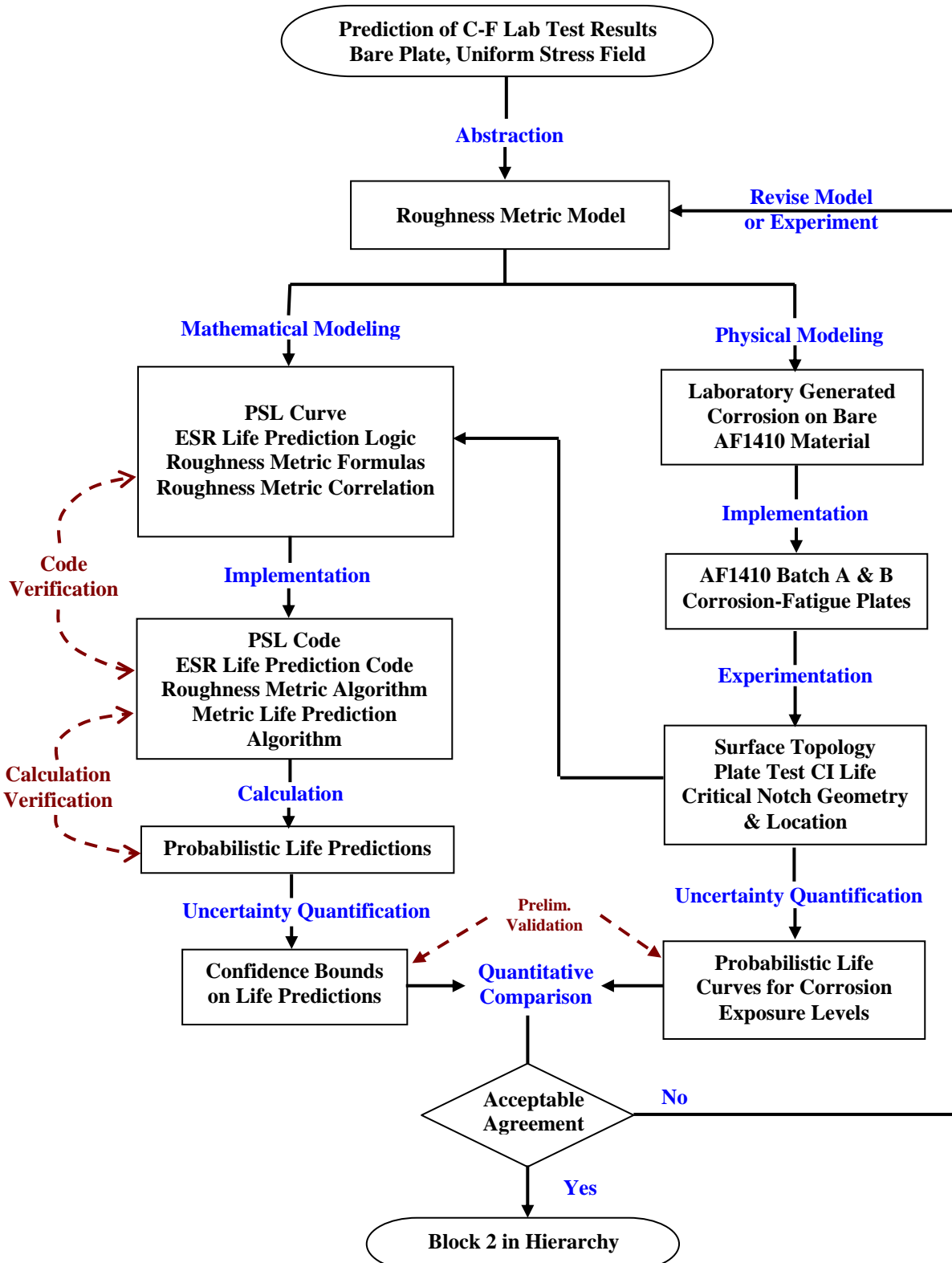
Figure 6.1-3. *V&V framework for Block 1B of C-F life characterization hierarchy.*
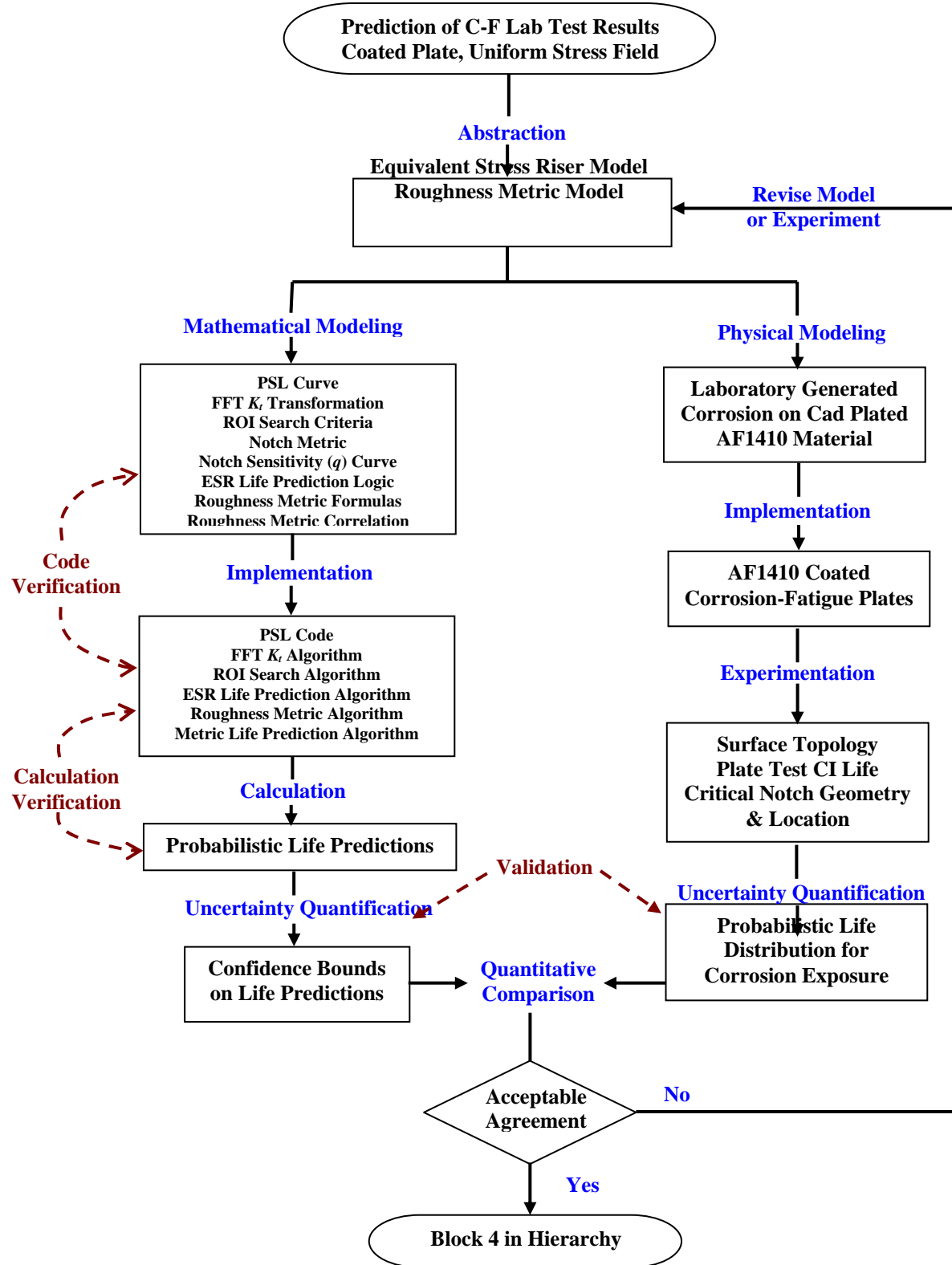
Figure 6.1-4. *V&V framework for Block 2 of C-F life characterization hierarchy.*
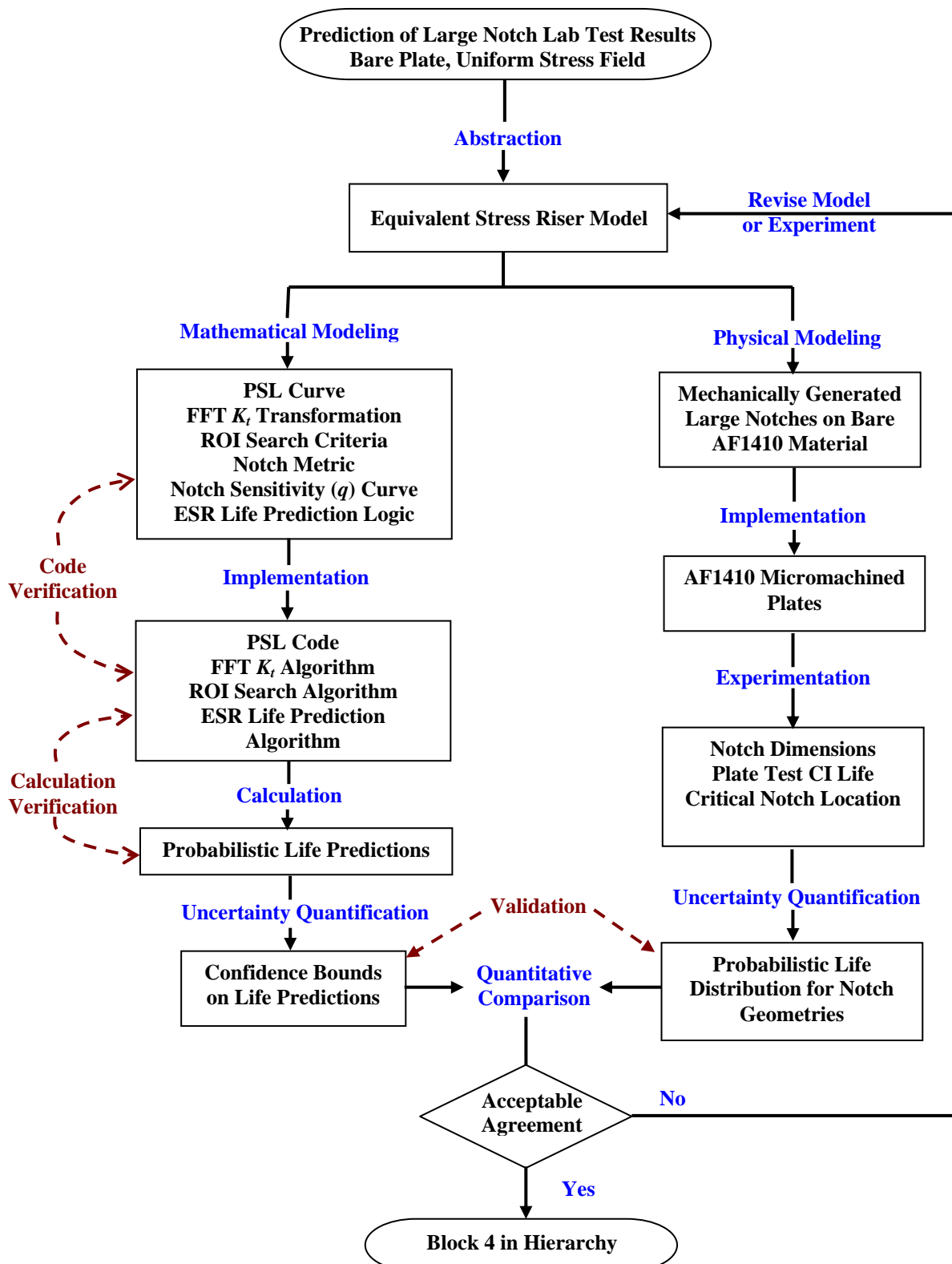
Figure 6.1-5. *V&V framework for Block 3 of C-F life characterization hierarchy.*
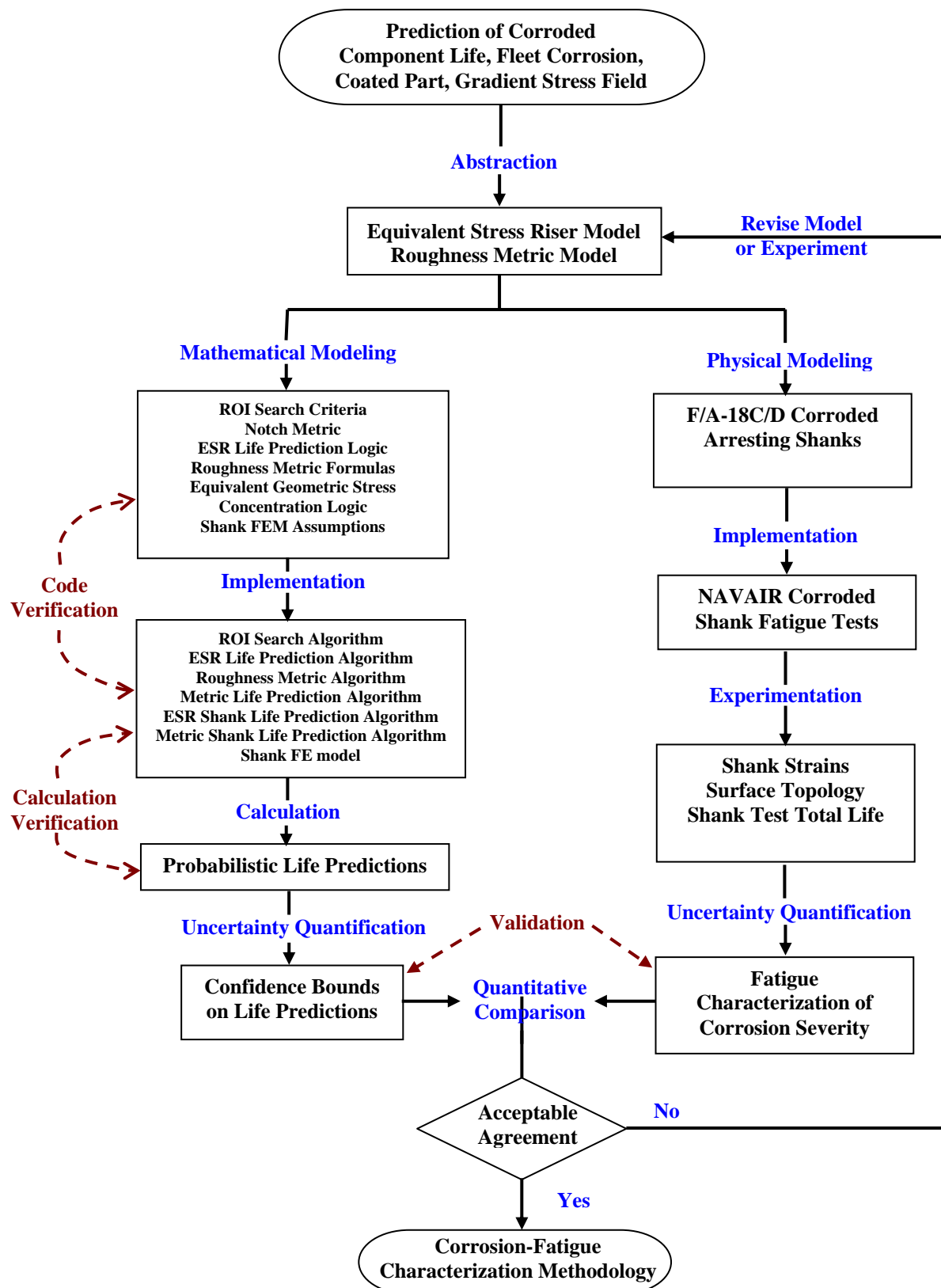
Figure 6.1-6. *V&V Framework for Block 4 of C-F life characterization hierarchy.*

Verification Tasks

Code verification tasks:

1. PSL Curve to PSL Code
2. FFT K_t Transformation to FFT K_t Algorithm
3. ROI Search Criteria to ROI Search Algorithm
4. Notch Metric to ESR Life Prediction Algorithm
5. Notch Sensitivity Curve to ESR Life Prediction Algorithm
6. ESR Life Prediction Logic to ESR Life Prediction Algorithm
7. Roughness Metric Formulas to Roughness Metric Algorithm
8. Roughness Metric Correlation to Roughness Metric Algorithm
9. Equivalent Geometric Stress Concentration Logic to ESR Shank Life Prediction Algorithm
10. Equivalent Geometric Stress Concentration Logic to Metric Shank Life Prediction Algorithm
11. Shank FEM assumptions to Shank FE Model

Calculation verification tasks:

1. PSL Code to ESR Probabilistic Life Predictions
2. FFT K_t Algorithm to ESR Probabilistic Life Predictions
3. ROI Search Algorithm to ESR Probabilistic Life Predictions
4. ESR Life Prediction Algorithm to ESR Probabilistic Life Predictions
5. Roughness Metric Algorithm to Metric-Based Probabilistic Life Predictions
6. Metric Life Prediction Algorithm to Metric-Based Probabilistic Life Predictions
7. ESR Shank Life Prediction Algorithm to ESR Probabilistic Life Predictions
8. Metric Shank Life Prediction Algorithm to Metric-Based Probabilistic Life Predictions
9. Shank FE model to ESR and Metric-Based Probabilistic Life Predictions

Validation Tasks:

1. Confidence bounds on ESR Probabilistic Life Predictions
2. Comparison of ESR Probabilistic Life Predictions with AF1410 Batch A & B C-F test results
3. Confidence bounds on Metric-Based Probabilistic Life Predictions
4. Comparison of Metric-Based Probabilistic Life Predictions with AF1410 Batch A & B C-F test results

5. Confidence bounds on ESR and Metric-Based Probabilistic Life Predictions for Cad-Plated C-F Specimens

6. Comparison of ESR and Metric-Based Probabilistic Life Predictions with Cad-Plated C-F test results

7. Confidence bounds on ESR Probabilistic Life Predictions of Large Notch Plates (micromachine specimens

8. Comparison of ESR Probabilistic Life Predictions with Large Notch plate test results

9. Shank FE model to Shank Strain Survey Results

10. Confidence bounds on ESR and Metric-Based Probabilistic Shank Life Predictions

11. Comparison of ESR and Metric-Based Probabilistic Shank Life Predictions with Corroded Shank test results.

Table 6.1.1-1 details tasks for each team member.

Table 6.1.1-1. Detailed Verification and Validation Tasks

Owner	Verification & Validation Task Assignments
NAVAIR	*Code Verification:* None
	Calculation Verification: None

	Validation:
	1. Confidence bounds on ESR Probabilistic Life Predictions
	     a. Identification of sources of uncertainty (mostly complete)
	     b. Input uncertainty distributions (mostly complete)
	     c. Sensitivity analysis (not started)
	     d. Confidence bounds on Life Predictions (preliminary results)
	3. Confidence bounds on Metric-Based Probabilistic Life Predictions
	     a. Identification of sources of uncertainty (not started)
	     b. Input uncertainty disruptions (not started)
	     c. Sensitivity analysis (not started)
	     d. Confidence bounds on life predications (not started)
	5. Confidence bounds on ESR and Metric-Based Probabilistic Life Predictions of Cad-plated C-F specimens (not started)
	7 Confidence bounds on ESR Probabilistic Life Predictions of Large Notch Plate test (micro-machine specimens)
	     a. Identification of sources of uncertainty (mostly complete)
	     b. Input uncertainty disruptions (mostly complete)
	     c. Sensitivity analysis (not started)
	     d. Confidence bounds on life predications (not started)
	10 . Confidence bounds on ESR and Metric-Based Probabilistic Shank Life Predictions
	     a. Identification of sources of uncertainty (not started)
	     b. Input uncertainty disruptions (not started)
	     c. Sensitivity analysis (not started)
	     d. Confidence bounds on life predications (not started)

Owner	Verification & Validation Task Assignments
UDRI	*Code Verification:* 2. FFT K_t Transformation to FFT Kt Algorithm 3. ROI Search Criteria to ROI Search Algorithm
	Calculation Verification: 2. FFT K_t Algorithm to ESR Probabilistic Life Predictions 3. ROI Search Algorithm to ESR Probabilistic Life Predictions

	Validation:
	2. Confidence bounds on ESR Probabilistic Life Predictions
	    a. Identification of sources of uncertainty
	    b. Input uncertainty distributions
	    c. Sensitivity analysis
	3. Confidence bounds on Metric-Based Probabilistic Life Predictions
	    a. Identification of sources of uncertainty
	    b. Input uncertainty disruptions
	    c. Sensitivity analysis
	7. Confidence bounds on ESR Probabilistic Life Predictions of Large Notch Plate test micro-machine specimens)
	    a. Identification of sources of uncertainty
	    b. Input uncertainty disruptions
	    c. Sensitivity analysis
	10. Confidence bounds on ESR and Metric-Based Probabilistic Shank Life Predictions
	    a. Identification of sources of uncertainty
	    b. Input uncertainty disruptions
	    c. Sensitivity analysis

Boeing	*Code Verification:* 1. PSL Curve to PSL Code 4. Notch Metric to ESR Life Prediction Algorithm 5. Notch Sensitivity Curve to ESR Life prediction 6. ESR Life Prediction Logic to ESR Life Prediction Algorithm 7. Roughness Metric Formulas to Roughness Metric Algorithm 8. Roughness Metric Correlation to Roughness Metric Algorithm 9. Equivalent Geometric Stress Concentration Logic to ESR Shank Life Predication Algorithm 10. Equivalent Geometric Stress Concentration Logic to Metric Shank Life Prediction Algorithm
	Calculation Verification: 1. PSL Code to ESR Probabilistic Life Predictions 4. ESR Life Prediction Algorithm to ESR Probabilistic Life Predictions 5. Roughness Metric Algorithm to Metric-Based Probabilistic Life Predications 6. Metric Life Predication Algorithm to Metric-Based Probabilistic Life Predictions 7. ESR Shank Life Prediction Algorithm to ESR Probabilistic Life Predications 8. Metric Shank Life Predication Algorithm to Metric-based probabilistic Life Predictions 9. Shank FE model to ESR and Metric-Based Probabilistic Life Predications

Owner	Verification & Validation Task Assignments

	Validation:
	1. Confidence bounds on ESR Probabilistic Life Predictions
	    a. Identification of sources of uncertainty
	    b. Input uncertainty distributions
	    c. Sensitivity analysis
	3. Confidence bounds on Metric-Based Probabilistic Life Predictions
	    a. Identification of sources of uncertainty
	    b. Input uncertainty disruptions
	    c. Sensitivity analysis
	7. Confidence bounds on ESR Probabilistic Life Predictions of Large Notch Plate test (micromachine specimens)
	    a. Identification of sources of uncertainty
	    b. Input uncertainty disruptions
	    c. Sensitivity analysis
	10. Confidence bounds on ESR and Metric-based Probabilistic Shank Life Predictions
	    a. Identification of sources of uncertainty
	    b. Input uncertainty disruptions
	    c. Sensitivity analysis

ESRD	*Code Verification:* 11. <u>Shank FEM assumptions to shank FE model</u>: ESRD will verify all the geometric, material and boundary conditions parameters incorporated into the FE description of the shank for the two load cases analyzed (arrestment and damper loads). All the data needed for this task is already available.
	Calculation Verification: 9. <u>Shank FE model to ESR and metric-based probabilistic life predictions</u>: ESRD will verify that the carpet plot of the strains and stresses in the corroded region of the shank are correctly extracted. A different technique will be used to identify the angular position of each extraction point. All the data needed for this task is already available.
	Validation: 2. <u>Comparison of ESR probabilistic life predictions with AF1410 Batches A & B C-F test results</u>: ESRD will compare the ESR predictions with the experimental results once all the data is available. Currently, we have the fatigue corrosion data for AF1410 Batches A & B, but still need to get the latest predictions from NAVAIR using the most recent procedures. 4. <u>Comparison of metric-based probabilistic life predictions with AF1410 Batches A & B C-F test results</u>: ESRD will compare the metric-based predictions with the experimental results once all the data is available. Currently, we have the fatigue corrosion data for AF1410 Batches A & B, but the metric-based prediction model is still under development, so no predictions are available. We need to get the prediction data from NAVAIR to complete this task. 6. <u>Comparison of ESR and metric-based probabilistic life predictions with cad-plated C-F specimens</u>: Experimental and prediction data for the cad-plated experiments are not ready yet. This task will start once the experiments are completed and NAVAIR makes the predictions. 8. <u>Comparison of ESR probabilistic life predictions with large notch plate test</u>: Experimental and prediction data for the micro-machining specimens are not ready yet. This task will start once the evaluation of the experimental results is completed and NAVAIR provides the revised predictions. 9. <u>Shank FE model to shank strain survey results</u>: ESRD will compare the results of the latest FE analyses of the shank and the corresponding strain gage data for the two load cases. Additional modification to the FE model may be required 10. <u>Confidence bounds on ESR and metric-based probabilistic shank life predictions</u>: ESRD will work with NAVAIR to collect the needed bibliographic references to establish confidence bounds. ESRD will determine the K_t values for the notched specimens found in the literature search as requested by NAVAIR. 11. <u>Comparison of ESR and metric-based probabilistic shank life predictions with corroded shank test results</u>: This task will start once NAVAIR provides the revised predictions and the metric-based model is developed.

6.2   Status of Verification and Validation Tasks

Considerable progress has been made on the various verification and validation tasks. Progress accomplished by ESRD and Boeing is documented in the respective final reports given in Appendices A and B. NAVAIR progress is reported in blue in Table 6.1.1 and UDRI progress is described below. The several tasks that remain unfinished and the issues raised in the various descriptions of Verification and Validation progress must be addressed in the future on a subsequent program.

Efforts by UDRI to verify and validate the model have been directed at comparisons of stress concentration estimated from the elasticity approach to that of finite element analysis; review of the code for the elasticity approach, including comparing results from an independently written software implementation of this algorithm; identification of sources of uncertainty in the elasticity and ROI analysis; and simulating a white light surface height profile with artificial features to determine the effectiveness of the ROI algorithm to find and characterize these features.

Several test cases were used to verify that the elasticity approach determined acceptable estimates of the stress concentration factors when compared to finite element analysis of these same test cases. These tests and results are given in Reference 1.

Researchers at UDRI attempted to independently duplicate the algorithm used to implement the elasticity model. The algorithm was able to calculate stress concentration maps that were quite similar to those determined from the original set of code. Unfortunately, the results did not match exactly. This could have been attributed to a slight difference in round-off error from one computer to another, or from differences in the subroutine versions used for the two implementations. That is, different Fast Fourier Transforms were used in the two implementations of the elasticity algorithm and use memory in different ways. While the differences were small, they do merit additional study to confirm that the sources of error are due to implementation and to quantify (and limit) those errors.

In order to better understand the sources of uncertainty in the input to the ESR model, UDRI conducted an analysis of the various steps in the process of generating ROI statistics and stress concentration maps. Table 6.2-1 summarizes the various key steps, the source of uncer-

tainty, and the output affected. There are internal and external sources of uncertainty. Internal sources include uncertainty in output of one step transferring to uncertainty in the input of the next step and the number of pixels passing a threshold, which affects the ROI parameters (size, length, height, depth, and orientation with respect to the load direction). External sources are independent of processing steps and all are traceable to an uncertainty in the digitization of the surface heights (and are shown in red in Table 6.2-1).

Table 6.2-1. Sources of Uncertainty in the ESR Model Input

Process Step	Source of Uncertainty	Output Affected
Kt threshold	Kt amplitude	# of pixels above threshold
WLIM threshold	WLIM depths	# of pixels below threshold
AND images	# of pixels passing threshold in these maps	# of resulting pixels
Define ROIs	# of pixels from AND map	#, shape and size of ROIs
Area Filter	Size of ROIs	# of ROIs
Calc L, H, θ	Size, shape of ROIS	ΔL, ΔH, Δθ
Calc D	WLIM depths, reference plane height	ΔD
Calc R	ΔH, ΔD	ΔR

Based on the results of the analysis described above, a simulation was constructed of the white light interference microscopy measurement of a surface containing a number of randomly generated artificial features. The process started with a field of ellipsoidal pits of various sizes and orientations in a random pattern. This surface was artificially digitized to represent white light interference microscopy (WLIM) data. The digitization uncertainty was selected to approximate the uncertainty expected in the surface height measurements of the white light instrument. In addition, the simulation attempted to account for spatial resolution limitations of the WLIM by sampling the surface randomly within in a grid that matched the WLIM sampling size (pixel sizes of 7.66 microns). Next, the simulated WLIM was processed to determine number of ROIs and their statistics. The goal was to determine the effect of the uncertainty in the digitization step.

A set of 2000 ellipsoidal pits was computer-generated. Rough parameters to define these pits were determined by trial and error to approximate the range of parameters found in AF1410 Set B corrosion-fatigue test specimens. This field of ideal pits was digitized, as described above, to introduce uncertainties and randomness in the surface height profiles. A stress concentration map was generated from this simulated WLIM data, ROI analysis was performed, and 1713 ROIs were identified. It was found that, in many cases, overlapping ROIs were lumped together into one ROI. This accounts for the fact that the total number of ROIs found is less than the total created in the simulation. Figure 6.2-1 shows a small patch of ROIs in the original simulation and how the stress concentration calculation and subsequent ROI analysis find these ROIs.

(a)   (b)
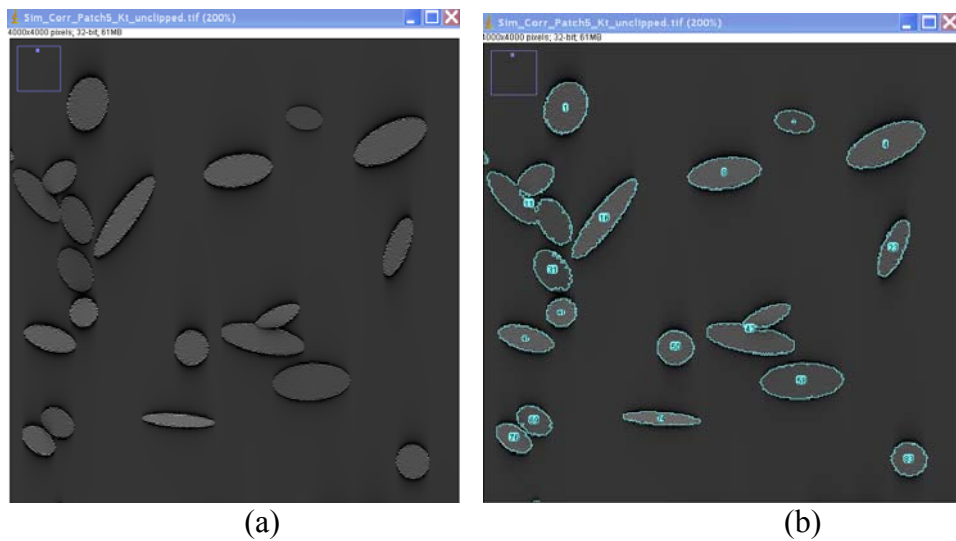
Figure 6.2-1. *Small region showing several ROIs in (a) original simulation and (b) ROIs found by routine.*

Fifty non-overlapping ROIs were selected for more-detailed comparisons to the original ROI statistics: major and minor axes of the ellipse, orientation of the ellipse relative to the loading direction, the shifted depth, and the X and Y locations. Figure 6.2-2 shows a plot of both the original and ROI algorithm output for the major and minor axes of the simulated elliptical features. Figure 6.2-3 shows a plot comparing the original and ROI algorithm output for orientation of the elliptical features. The ROI algorithm depth and coordinates (X and Y) are compared to the original values in Figures 6.2-4 and 6.2-5, respectively. These plots show the level of accuracy of the ROI algorithm in finding and characterizing these features. This calculation verification demonstration shows that the algorithm is functioning as desired for the special case of elliptical features in the corrosion surface.
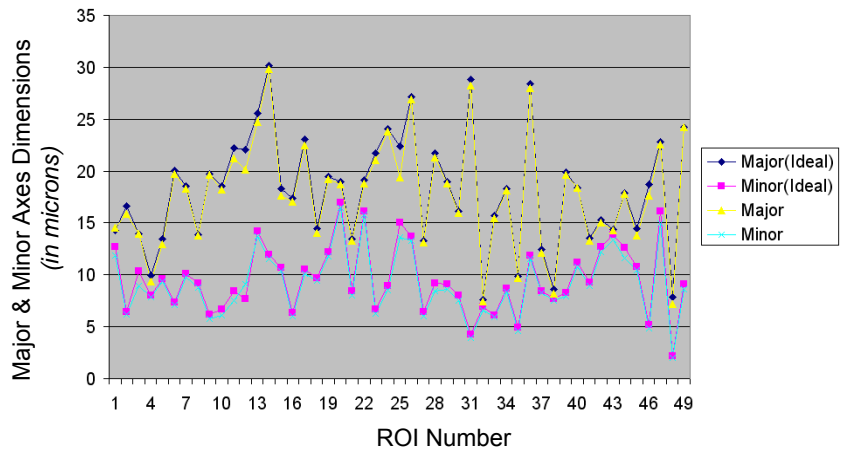
Figure 6.2-2. *Comparison of calculated major and minor axes to ideal.*
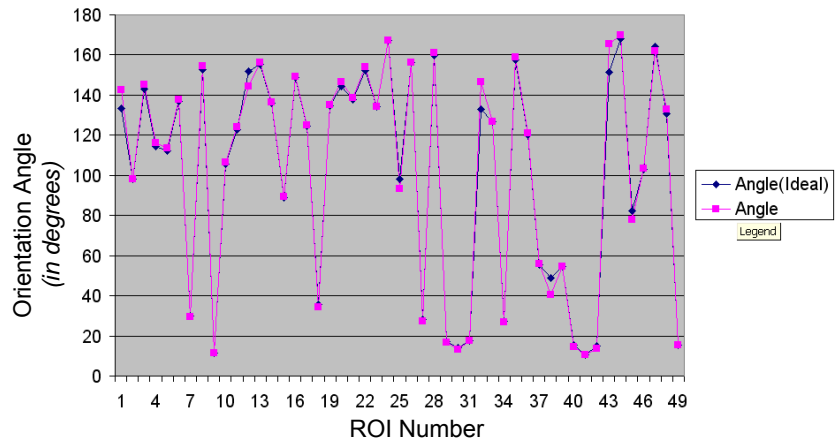
Figure 6.2-3. *Comparison of calculated orientation angle to ideal.*
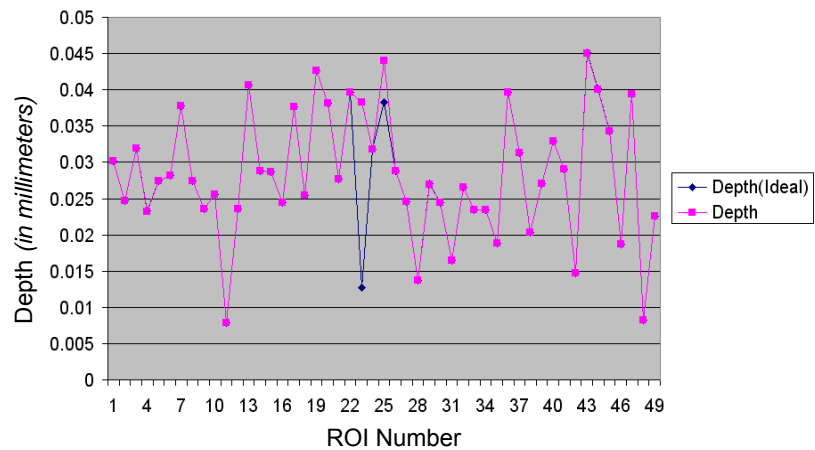
Figure 6.2-4. *Comparison of calculated depth to ideal.*

97
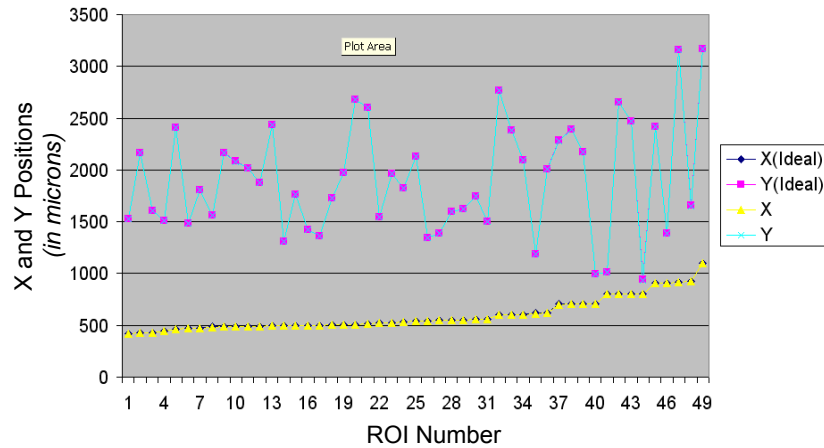
Figure 6.2-5. *Comparison of calculated X and Y positions to ideal.*

While much has been accomplished to verify and validate the models proposed on this program, a number of items are left to be accomplished. This must await further research.

Section 7
Summary, Conclusions, and Recommendations

The objectives of this program and its associated contracts have been met. Specifically:

- A corrosion severity classification scheme (i.e., cosmetic, mild, and severe), tied to component reliability or reduction in fatigue life, has been proposed based on surface roughness statistics calculated for elements of a grid overlaying the corrosion patch and a modification of the equivalent stress riser model.

- Corrosion metrics associated with these corrosion classifications have been identified, which includes R_a and R_q defined over the grid elements. The grid model must include the effects of local applied stresses.

- Nondestructive inspection (NDI) methods, requirements, and procedures for measuring corrosion severity via these corrosion metrics have been outlined. Additional studies have considered the effects of resolution on the determination of the metric statistics and correlations of the NDE-determined grid statistics and those determined from the white light interference profiles over the grid elements.

- Component disposition tools and procedures to make engineering disposition decisions based on detailed corrosion profiles have been developed. In particular, the equivalent stress riser model has been created and tested in a number of ways. Life predictions from this model have been found to be conservative. Additional development, verification, and validation are warranted.

The plan to meet these overall objectives consisted of the following activities

- Determining the effect of corrosion on fatigue life of high-strength steels through corrosion-fatigue experiments supported by other baseline tests,

- Developing corrosion metrics based on surface profiles, correlating metrics to life reduction, and using these results to develop corrosion classification criteria,

- Investigating and developing NDI methods and procedures that can determine corrosion severity via correlations of NDI to corrosion metrics, and

- Developing notched-based analysis methods to determine effective stress concentration factors for corrosion and correlating the analysis predictions to corrosion-fatigue tests and validating on cadmium plated corrosion-fatigue tests.

Initial investigation of the ESR model demonstrates that an empirical approach to corrosion surface damage that builds on traditional notched fatigue analysis methods can be utilized to generate probabilistic life predictions that have substantial engineering value in assessing the residual fatigue life of corroded AF1410 steel components. Further work to refine the ROI search algorithm methods and to investigate the sensitivity to varying levels of corrosion and white light interference microscopy scan resolution is warranted. However, the approach does capture the significant corrosion features that cause fatigue cracking in most cases, especially for more severely corroded surfaces.

Overall, there has been much progress in developing tools for characterization and quantification of the effects of corrosion-induced surface roughness on fatigue life. A master implementation plan was developed and reported in the final report of the second contract [2]. Several of the objectives need additional development in order to be ready for implementation in the fleet.

- Further development and test is needed on the surface roughness metric (grid) model, including setting realistic corrosion classification limits.
- Verification and validation must be completed for the model and all associated components of the model.
- Inspection technologies must be developed that can be implemented in the field or aircraft carrier that meet or exceed the requirements demonstrated on this program.
- The methods developed on this program should be extended to other materials, particularly Aermet 100, by performing corrosion-fatigue tests and making life predictions using the specimens manufactured on this program.
- A method is needed to rapidly inspect shank replicas in the depot with a resolution that rivals the white light interference microscope.

Section 8
References

1. Hoppe, W., et. al., "Navy High-Strength Steel Corrosion-Fatigue Modeling Program", Final Report, UDR-TR-2007-00039, October 2006.

2. Hoppe, W., et. al., "Improved Navy Maintenance Through Corrosion-Fatigue Assessment Program", Final Report, UDR-TR-2008-00064, March 2008.

3. Rusk, D., et. al., "Modeling and Prediction of Corrosion-Fatigue Failure in AF1410 Steel Test Specimens", Navy report: NAWCADPAX/TR-2008/60

4. Rusk, Pierce, Hoppe, "Analysis and Testing of Fleet Corroded F/A-18C/D Arrestment Shanks," NAWCADPAX/TR-2008/9, May, 2008.

5. Rusk, D., et. al., "Results of Fatigue Tests of Bare AF1410 Steel Unnotched Flat Plates with Surface Corrosion Damage", Navy report: NAWCADPAX/EDR-2008/10.

6. Buhrmaster, D., "Aging Aircraft Corrosion Prevention Compound Standardization Test Development – Final Report 1 – 300M High Strength Steel", Contract Number F42620-00-D0039-0001, December 2003.

Appendix A
ESRD Final Report

US Navy High Strength Steel Corrosion-Fatigue Modeling Program

Final Technical Report FY2007

August 28, 2007

Brent Lancaster, Ricardo Actis and Barna Szabó[2]
Engineering Software Research and Development (ESRD), Inc.
111 West Port Plaza, Suite 825
St. Louis, MO 63146
314-744-5021 ext. 11
Contact: barna.szabo@esrd.com

---

[2] Principal Investigator

TABLE OF CONTENTS

FIGURES

TABLES

1. Scope

This report covers year three of a multi-year effort, the principal objective of which is to achieve significant cost savings and enhanced readiness through the development of definitive corrosion maintenance criteria, the supporting diagnostics and enhanced repair capability to effectively manage structural maintenance of Naval aviation assets. This is a collaborative project among NAVAIR, the University of Dayton Research Institute (UDRI), Boeing Phantom Works in St. Louis and Engineering Software Research and Development, Inc. (ESRD).

1.1 Original terms of reference

ESRD, Inc. was to provide engineering services in support of this collaborative project. Specifically, ESRD was to perform the following tasks:

1. Provide numerical stress analysis services in support of the investigation of the predictability of onset of failure events caused by surface damage resulting from corrosion. The results of preliminary investigation summarized in reference [1] indicate that highly simplified representation of surface damage allows the estimation of stress concentration factors (Kt values) very efficiently. At the present time it is not known however whether the simplifications are permissible from the point of view of successful correlation of computed Kt values based on idealizations of corroded surfaces with onset of failure events. ESRD understands that validation experiments will be performed with the objective to collect statistical information and establish the range of predictability of onset of failure events in an experimental setting. ESRD will undertake to perform interpretation of validation experiments utilizing its software product StressCheck® and apply appropriate quality control procedures with the objective to verify the reliability of computed information.

2. In collaboration with NAVAIR, Boeing and UDRI, ESRD will develop criteria for validation of the predictive capabilities of the mathematical model. The validation protocol is to involve "blind" prediction of experimental results.

3. Based on the results of validation experiments, ESRD will modify the mathematical model as necessary for obtaining improved predictions of failure initiation events.

4. Develop a plan for the distribution the corrosion assessment technology developed under this project to the Navy and its subcontractors, utilizing the COM and Java interfaces of StressCheck®. The development of simple-to-use Windows desktop and web-based (or cross-platform) applications is envisioned. The interfaces are to provide a convenient communication protocol to integrate the necessary functions of other applications (e.g. MatLab probability and statistical functions) needed to quantifiably assess the useful remaining life of a corroded part. ESRD will expand the COM interface to include any new capabilities developed under this contract.

5. Coordinate project activities with the University of Dayton Research Institute, NAVAIR and Boeing Phantom Works in St. Louis.

Note that during the reporting period the state of development of the mathematical model for prediction was such that Tasks 2 and 3 in the original terms of reference could not be completed. Task 3 cannot progress until the completion of Task 2, which is under development at this time.

1.2 Deliverables

1. ESRD will provide monthly engineering status reports. These reports will include technical program status, accomplishments, issues and concerns and planned activities for the following quarter.

2. ESRD will provide a draft of the final engineering report thirty (30) days prior to the end of the contract period. The final engineering report will detail all studies, analyses and accomplishments completed in the course of this project.

3. ESRD will provide documentation of the examples that demonstrate the enhanced capabilities of StressCheck® and provide guidelines for proper application of StressCheck®.

1.3 Accomplishments

The accomplishments are detailed in the body of this report. Certain objectives, originally envisioned at the beginning of the project were modified by mutual agreement at project meetings.

2. Importance

As the naval aviation fleet ages, corrosion and environmental degradation have become major contributors to spiraling naval aviation maintenance costs, burgeoning repair backlog, and increased aircraft failure rates. The corrosion problem is most observable in high strength steels (HSS) which comprise critical aircraft components; AF 1410 is one such HSS. In fact, many recent aircraft losses due to corrosion/environmental degradation failures can be traced to a failure of HSS components. Aircraft including F/A-18, F-14, EA-6B and E-2C have been plagued by these corrosion-load cycle failures, forcing the USN the costly measure of grounding these aircraft for extended periods of time.

Much of the increasing cost and risk are attributable to the lack of definitive, clear-cut corrosion maintenance criteria, necessitating the repair and/or replacement of all corroded parts. Therefore, the U.S. Navy (USN) needs workable corrosion maintenance criteria that can be followed in today's operational environments providing safety and readiness within the limited operations and maintenance resources. With respect to corrosion, maintenance teams must be able to differentiate between corrosion with potential safety impacts and corrosion that does not have substantial impact on life. In other words, maintenance personnel must quickly determine what must be removed immediately and what can be tolerated for some time period. The distinction must be justified quantitatively. The USN needs corrosion maintenance criteria that are accessible for routine assessment of corroded components. In short, a reliable and robust geometrically and mechanically defined metric or directive for quantitatively predicting remaining corroded part lives is necessary for a reliable assessment. This approach must be timely and efficient in order to meet USN maintenance scheduling requirements.

Furthermore, it is imperative that workable metrics or models are properly filtered from those that are not feasible. For example, a proposed model that takes a very long time to compute a valid numerical result may be too costly because time is a crucial variable in terms of quantitative approaches; therefore it cannot be used as part of a maintenance program and has to be rejected. On the other hand, a complex (more detailed) model may be too costly to be used within a maintenance program but it can be used to generate benchmarks in order to avoid selecting an oversimplified model. An ideal model may be defined as one that does not imply extended grounding of aircraft during evaluation, yet produces reliable results.

3. Goals

This project was aimed at establishing intervals of inspection based on sound scientific principles and the latest analytical technology to reduce the number of occurrences of in-service failures. It was also hoped that unnecessary inspection procedures could be reduced or eliminated, leading to increased safety and reduced cost. Thus, the focus was on quantitative USN high strength steel corrosion-cycle fatigue modeling and the formulation of reliable predictions for remaining fatigue life. Specifically, developments of prediction models focus on current states of corrosion, as long-term corrosion is highly unpredictable in terms of both extent of damage and location.

In order to achieve these goals, methodical testing involving validation of proposed metrics and models must be performed both through laboratory testing and through numerical methods, such as the finite element method (FEM). Verification is a process by which the quality of the numerical solution is ascertained, and validation is a process by which the predictive capabilities of mathematical models are tested. Validation of a model is performed through comparison with independently obtained experimental data.

FEM is a numerical method useful for obtaining approximate solutions to the equations of continuum mechanics. The accuracy of the approximate solution can be estimated. The technological prerequisites for verification of stresses in pristine (uncorroded) components, specifically in locations where corrosion occurs or is expected to occur, are currently available through the capabilities of StressCheck[®].

StressCheck[®] is the finite element software product of ESRD Inc., of St. Louis, MO. It was chosen as the primary investigative analytical tool for the function of extracting potential mechanical relationships between corrosion and fatigue life. ESRD was to provide detailed mathematical corrosion model verification and validation for the project team, as well as to provide recommendations for improving the USN mathematical corrosion model.

4. Numerical Simulation

Mathematical models are mathematical problems formulated so as to capture the essential characteristics of some physical system with the expectation that the data computed from the solution of a mathematical model will be a reliable predictor of the data of interest. Proper selection of a mathematical model is the most important decision when undertaking a numerical simulation task. Formulation of a mathematical model involves a theoretical formulation, specification of input data and a statement of objectives.

1. Theoretical formulation. The applicable physical laws, together with certain simplifications, are stated as a mathematical problem in the form of ordinary or partial differential equations, or extremum principles.

2. Specification of input data. The input data are comprised of the following:

   - Data that characterize the solution domain.

   - Physical properties (elastic moduli, yield stress, coefficients of thermal expansion, thermal conductivities, etc.)

   - Boundary conditions (loads, constraints, prescribed temperatures, etc.) Information or assumptions concerning the reference state (initial conditions).

   - Uncertainties. It is useful to distinguish between two types of uncertainties: When some information needed in the formulation of a mathematical model is unknown then the uncertainty is said to be cognitive (also called epistemic). For example, the magnitude and distribution of residual stresses is usually unknown, some physical properties may be unknown, In addition, there are statistical uncertainties (also called aleatory uncertainties): Even when the average values of needed physical properties, loading and other data are known, there may be very substantial statistical variations. Consideration of uncertainties is necessary in the interpretation of computed data.

3. Statement of objectives. Definition of the data of interest and the corresponding permissible error tolerances.

Associated with each mathematical model is a modeling error. The process by which a mathematical model is evaluated and modified to ensure that it meets necessary conditions for acceptance is called validation. The goal of validation is to ensure that the model is a sufficiently accurate mathematical description of the physical system or process it is supposed to represent[3]. Validation involves calibration and prediction. The determination of physical properties and other model parameters through correlation with experiments is called calibration. The use of a model to foretell the data of interest corresponding to some set of input data is called prediction.

Mathematical models are solved by numerical means, most commonly by the finite element method. In this process the exact solution is approximated. Determination of the accuracy of data computed from the approximate solution of a particular mathematical model is called verification In verification accuracy is understood to be with respect to the exact solution of the mathematical model, not with respect to physical

---

[3] American Institute of Aeronautics and Astronautics, Guide for Verification and Validation of Computational Fluid Dynamics Simulations AIAA G-077-1998 (1998).

reality. Verification is concerned with estimation and control of the discretization error; errors associated with iterative solution procedures and determination that the program is functioning properly.

5. Planning

As stated, the main objective of this study is the development of metric(s) that characterize HSS corrosion with respect to structural integrity providing viable maintenance guidelines with respect to fatigue life. In the US Navy, the effective stress concentration factor (Kt_{eff}) is used as a basis for estimating the FLE[4]. The basic assumption adopted by the corrosion project group was that the onset of crack initiation, defined by the first appearance of a 0.01 inch long crack, can be correlated with Kt_{eff}. This assumption implies that (a) heterogeneities occurring in the material do not contribute to crack initiation, only the averaged properties of the heterogeneities are important; (b) corrosion progresses along a sharp front and (c) the surface features that determine the critical values of Kt_{eff} can be reliably measured. In this context averaging is understood to be over length scales that are not larger than the corrosion features. Progression along a sharp front means that once the corrosion products were removed by cleaning, the remaining material has the same mechanical properties as the uncorroded material. Given this assumption, estimation of the maximum effective stress concentration factor of a corroded part is required. StressCheck® is well suited for both computation and verification of Kt_{eff} for idealizations of corrosion features. The definition of Kt_{eff} in reference to this study is the ratio of the first principal stress in a corroded part to the local first principal stress in a pristine, or uncorroded, part. The stress concentration in a pristine part will be referred to as Kt.

The effects of corrosion damage on fatigue life expended (FLE) depend on the location of the damage. Therefore inspection must be focused not only on regions of high corrosion, but also where Kt is high in the pristine part. Cases in point are the bench-tested F-18 tailhook shanks, in which the regions where corrosion damage was observed were not the regions with the highest Kt.

Since it would be impractical to perform detailed analysis on the effects of corrosion on each part, it is necessary to develop methods that involve two processes: (a) the determination of Kt in an uncorroded (pristine) part, and (b) based on corrosion metrics obtainable by field observations, or experience based on exposure to various operating environments, estimation of Kt_{eff} . These methods would provide a basis for evaluating the effects of corrosion on the number of cycles to crack initiation for a given part configuration and load history. Estimation of the rate of corrosion is not within the scope of this project.

---

[4] Kt_{eff} is a characteristic input for the determination of the fatigue notch factor (K_f), which is applied to FLE probabilistic strain life calculations.

Process (a) can be readily solved using StressCheck$^®$; process (b) poses a challenging problem in that computation of Kt_{eff} in a corroded part is possible only if the surface details are known with sufficient accuracy and multi-scale methods are properly applied. The available information on the details of the corroded surface is limited by the resolution of the system used for mapping the surface features. Additionally, the usability of the available information is limited by our ability to represent highly irregular surface features in a form suitable for computation. An uncertainty is therefore introduced between the computed and "actual" Kt_{eff} for a given surface profile, the extent of which is not clearly defined.

The Kt_{eff} for a given corroded profile is but one input into the probabilistic strain life (PSL) model proposed by NAVAIR. Each additional component used by the model will have some uncertainty as well as a range of applicability. It is primarily for this reason that on March 18, 2007 ESRD prepared a verification & validation (V&V) framework to identify and test the components dictated by the proposed PSL model (see Appendix, Section 9.1 for the complete proposal). Each component represents the mathematical process applied to convert an input or set of inputs into an output; for instance, the transfer function that converts the measured dimensions of a feature into a Kt_{eff}. This framework provides a means to identify and quantify the uncertainties associated with each of the model inputs and associated transfer functions such that the model output can be subjected to proper validation experiments. The goal of validation experiments in this context is to test the predictive capability of the metric, (the mean cycles to crack initiation), with respect to a given criterion. The criterion will determine whether the model passes or fails the validation experiments. If it does not pass then the model must be rejected and another one proposed. The process is then repeated until the model meets the established criteria.

Upon acceptance of this framework, each organization involved was assigned V&V tasks. The description of the V&V tasks assigned to ESRD and the status of completion are contained in this document. Detailed reports for each completed task are incorporated in the Appendix.

6. Approaches/Methodologies

As identified in Section 5 ("Planning"), the primary focus during the reporting period has been establishing and executing the framework for the verification and validation (V&V) of the proposed PSL model. The following task table (Table 1) was developed by NAVAIR in April 2007 and distributed to all organizations.

Table 1. PSL Model Verification and Validation (V&V) Task List as of April 2007

Owner	Verification & Validation Task Assignments
NAVAIR	**Code Verification:** None
	Calculation Verification: None

	Validation:
	3. Confidence bounds on ESR Probabilistic Life Predictions
	   a. Identification of sources of uncertainty
	   b. Input uncertainty distributions
	   c. Sensitivity analysis
	   d. Confidence bounds on life predictions
	3. Confidence bounds on Metric-Based Probabilistic Life Predictions
	   a. Identification of sources of uncertainty
	   b. Input uncertainty disruptions
	   c. Sensitivity analysis
	   d. Confidence bounds on life predications
	5. Confidence bounds on ESR and Metric-Based Probabilistic Life predictions of Cad-Plated C-F Specimens
	7. Confidence bounds on ESR Probabilistic Life predictions of Large Notch plate test (micromachine specimens)
	   a. Identification of sources of uncertainty
	   b. Input uncertainty disruptions
	   c. Sensitivity analysis
	   d. Confidence bounds on life predications
	10. Confidence bounds on ESR and Metric-based Probabilistic Shank Life predictions
	   a. Identification of sources of uncertainty
	   b. Input uncertainty disruptions
	   c. Sensitivity analysis
	   d. Confidence bounds on life predications

UDRI	**Code Verification**: 2. FFT Kt Transformation to FFT Kt Algorithm 3. ROI Search Criteria to ROI Search Algorithm
	Calculation Verification: 2. FFT Kt Algorithm to ESR Probabilistic Life Predictions 3. ROI Search Algorithm to ESR Probabilistic Life Predictions

Owner	Verification & Validation Task Assignments

	Validation:
	4. Confidence bounds on ESR Probabilistic Life Predictions
	   a. Identification of sources of uncertainty
	   b. Input uncertainty distributions
	   c. Sensitivity analysis
	3. Confidence bounds on Metric-Based Probabilistic Life Predictions
	   a. Identification of sources of uncertainty
	   b. Input uncertainty disruptions
	   c. Sensitivity analysis
	7. Confidence bounds on ESR Probabilistic Life predictions of Large Notch plate test (micromachine specimens)
	   a. Identification of sources of uncertainty
	   b. Input uncertainty disruptions
	   c. Sensitivity analysis
	10. Confidence bounds on ESR and Metric-based Probabilistic Shank Life predictions
	   a. Identification of sources of uncertainty
	   b. Input uncertainty disruptions
	   c. Sensitivity analysis

Boeing	**Code Verification:** 1. PSL Curve to PSL Code 4. Notch Metric to ESR Life Prediction Algorithm 5. Notch Sensitivity Curve to ESR Life prediction 6. ESR Life Prediction Logic to ESR Life Prediction Algorithm 7. Roughness Metric Formulas to Roughness Metric Algorithm 8. Roughness Metric Correlation to Roughness Metric Algorithm 9. Equivalent Geometric Stress Concentration Logic to ESR Shank Life Predication Algorithm 10. Equivalent Geometric Stress Concentration Logic to Metric Shank Life Prediction Algorithm **Calculation Verification:** 1. PSL Code to ESR Probabilistic Life Predictions 4. ESR Life Prediction Algorithm to ESR Probabilistic Life Predictions 5. Roughness Metric Algorithm to Metric-Based Probabilistic Life Predications 6. Metric Life Predication Algorithm to Metric-Based Probabilistic Life Predictions 7. ESR Shank Life Prediction Algorithm to ESR Probabilistic Life Predications 8. Metric Shank Life Predication Algorithm to Metric-based probabilistic Life Predictions 9. Shank FE model to ESR and Metric-Based Probabilistic Life Predications

Owner	Verification & Validation Task Assignments
	Validation: 1. Confidence bounds on ESR Probabilistic Life Predictions a. Identification of sources of uncertainty b. Input uncertainty distributions c. Sensitivity analysis 3. Confidence bounds on Metric-Based Probabilistic Life Predictions a. Identification of sources of uncertainty b. Input uncertainty disruptions c. Sensitivity analysis 7. Confidence bounds on ESR Probabilistic Life predictions of Large Notch plate test (micromachine specimens) a. Identification of sources of uncertainty b. Input uncertainty disruptions c. Sensitivity analysis 10. Confidence bounds on ESR and Metric-based Probabilistic Shank Life predictions a. Identification of sources of uncertainty b. Input uncertainty disruptions c. Sensitivity analysis
ESRD	**Code Verification:** 11. <u>Shank FEM assumptions to shank FE model</u>: ESRD will verify all the geometric, material and boundary conditions parameters incorporated into the FE description of the shank for the two load cases analyzed (arrestment and damper loads). All the data needed for this task is already available.
	Calculation Verification: 9<u>. Shank FE model to ESR and metric-based probabilistic life predictions</u>: ESRD will verify that the carpet plot of the strains and stresses in the corroded region of the shank are correctly extracted. A different technique will be used to identify the angular position of each extraction point. All the data needed for this task is already available.

Owner	Verification & Validation Task Assignments
	Validation:
	2. <u>Comparison of ESR probabilistic life predictions with AF1410 batch A & B C-F test results</u>: ESRD will compare the ESR predictions with the experimental results once all the data is available. Currently have the fatigue corrosion data for AF1410 batch A & B, but still need to obtain from NAVAIR the latest predictions using the most recent procedures.
	4. <u>Comparison of metric-based probabilistic life predictions with AF1410 batch A & B C-F test results</u>: ESRD will compare the metric-based predictions with the experimental results once all the data is available. Currently have the fatigue corrosion data for AF1410 batch A & B, but the metric-based prediction model is still under development, so no predictions are available. Need to obtain the prediction data from NAVAIR to complete this task.
	6. <u>Comparison of ESR and metric-based probabilistic life predictions with Cad-plated C-F specimens</u>: Experimental and prediction data for the cad-plated experiments not ready yet. This task will start once the experiments are completed and NAVAIR makes the predictions.
	8. <u>Comparison of ESR probabilistic life predictions with large notch plate test</u>: Experimental and prediction data for the micro-machining specimens are now available. Preliminary results are under investigation.
	9. <u>Shank FE model to shank strain survey results</u>: ESRD will compare the results of the latest FE analyses of the shank and the corresponding strain gage data for the two load cases. Additional modification to the FE model may be required.
	10. <u>Confidence bounds on ESR and metric-based probabilistic shank life predictions</u>: ESRD will work with NAVAIR to collect the needed bibliographic references to establish confidence bounds. ESRD will determine the Kt values for the notched specimens found in the literature search as requested by NAVAIR.
	11. <u>Comparison of ESR and metric-based probabilistic shank life predictions with corroded shank test results</u>: This task will start once NAVAIR provides the revised predictions and the metric-based model is developed.

Tasks were organized based on three (3) categories: Code Verification, Calculation Verification and Validation. ESRD was assigned one (1) task in Code Verification, one (1) task in Calculation Verification and seven (7) tasks in Validation. The progress of these tasks is indicated in the following subsections.

Additionally, ESRD continued to provide numerical stress analysis services and support by using StressCheck® to investigate several topics. These topics primarily included a parametric Kt study of a frustum with a variable blend radius at the base, and an elastic-plastic local strain analysis of idealized interacting notch geometries. The former study was intended to determine the influence of an additional characterizing parameter not included in the notch metric Kt, while the latter study was intended to develop a load versus local notch strain relationship for AF1410 Set A Specimen #36 crack initiation site.

6.1 ESRD Verification and Validation (V&V) Tasks

6.1.1 ESRD V&V Task Status

Table 2 summarized the state of completion of the tasks assigned to ESRD as of July 31, 2007. Tasks identified as "Completed" have a full report in the Appendix section. The remainder of the tasks, with the exception of Validation Task #8, could not be completed due to unavailability of data at reporting time.

Table 2. ESRD V&V Task Progress

	Task	Complete?	Comments
Code Verification	11	Yes	Completed
Calculation Verification	9	Yes	Completed
Validation	2	No	Waiting for Data
	4	No	Waiting for Data
	6	No	Waiting for Data
	8	Yes	Completed
	9	Yes	Completed
	10	Yes	Completed
	11	No	Waiting for Data

6.1.2 Code Verification Task #11: Shank FEM Assumptions to Shank FE Model

ESRD completed Verification Task #11 from the ESRD V&V Task List. This task pertained to the verification that the inputs into the StressCheck models used for the two load cases (arrestment and hook bounce) were correct. A report was sent to NAVAIR on July 10, 2007 titled "ESRD Tailhook Modeling Verification Task11.doc." This report is included in the Appendix, Section 9.2.

6.1.3 Calculation Verification Task #9: Arrestment Shank Extraction Algorithm Verification

ESRD completed Calculation Verification Task #9 from the ESRD V&V Task List. This task pertained to the verification that the carpet plot of the strains and stresses in the corroded region of the shank were correctly extracted. A report was sent to NAVAIR on June 28, 2007 titled "ESRD_FE_Shank_Extraction_Methodology.doc." This report is included in the Appendix, Section 9.3.

6.1.4 Validation Task #8: ESR Prediction vs. AF1410 Large Notch Test Results

ESRD completed Validation Task #8 from the ESRD V&V Task List. This task pertained to the preliminary comparison between ESR probabilistic strain life predictions and micro-machined (large notch) AF1410 plates. A report was sent to NAVAIR on August 6, 2007 titled "ESRD Prediction Validation Task8.doc." This report is included in the Appendix, Section 9.4.

6.1.5 Validation Task #9: Shank FE Model Results vs. Shank Strain Survey Results

ESRD completed Validation Task #9 from the ESRD V&V Task List. This task pertained to the comparison of arrestment shank load case StressCheck FEA results with available strain survey results. Additionally, the modeling assumptions for each load case (damper load and arrestment load) are described, and FEA results for each load case presented. A report was sent to NAVAIR on June 26, 2007 titled "ESRD Tailhook Modeling Validation Task9.doc." This report is included in the Appendix, Section 9.5.

6.1.6 Validation Task #10: ESR & Metric-Based Prediction Confidence Bounds

ESRD completed Validation Task #10 from the ESRD V&V Task List. This task pertained to providing assistance in locating bibliographic references necessary to establish confidence bounds for the PSL model. Additionally, StressCheck FEA Kt's were computed for sets V-notch specimens in order to populate the Peterson notch sensitivity factor (q) database. This database is critical in converting Kt information into a K_f, which is the ~~corrosion~~ fatigue notch factor representing the degradation of life. A report was sent to NAVAIR on May 7, 2007 titled "ESRD_Vnotch_Kt_summary_update.doc." This report is included in the Appendix, Section 9.6.

6.2 StressCheck® Investigation Topics

6.2.1 StressCheck Parametric Kt Study: Cylindrical Bore with Variable Blend Radius

A study was performed to ascertain the effect on Kt for a cylindrical feature with a variable blend radius at the base of the feature (see Figure 1). A cylinder of depth D=1.0 units and radius R=1.0 units was Boolean-Subtracted from a plate of depth=10 units. The resulting bore was then blended at the base, with radii varying from 0.1 units to 0.95 units. The notch metric Kt of this feature is ~2.0. Since the notch metric Kt is based on three (3) parameters (W, H, and D), it will be independent of the fourth parameter, the blend radius. Figure 2 is a summary of Kt versus blend radius: When the blend radius is < 0.4 units, then the Kt increases very rapidly. Plots of Kt values are shown for blend radii 0.1-0.6 in the Appendix, Section 9.7.
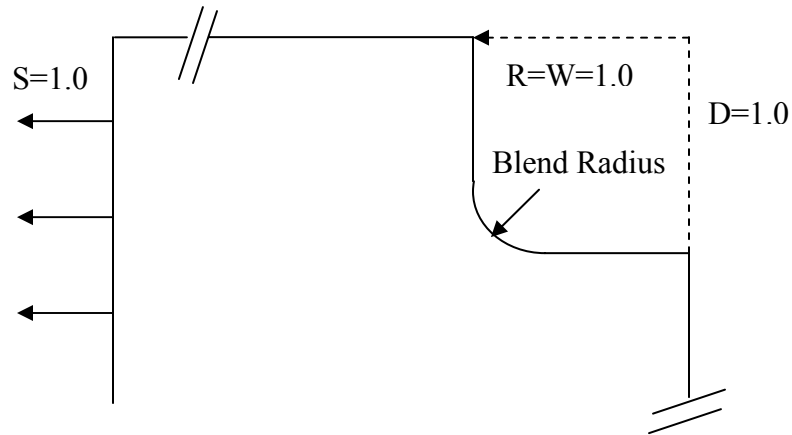
Figure 1: Cylinder with Blended Radius
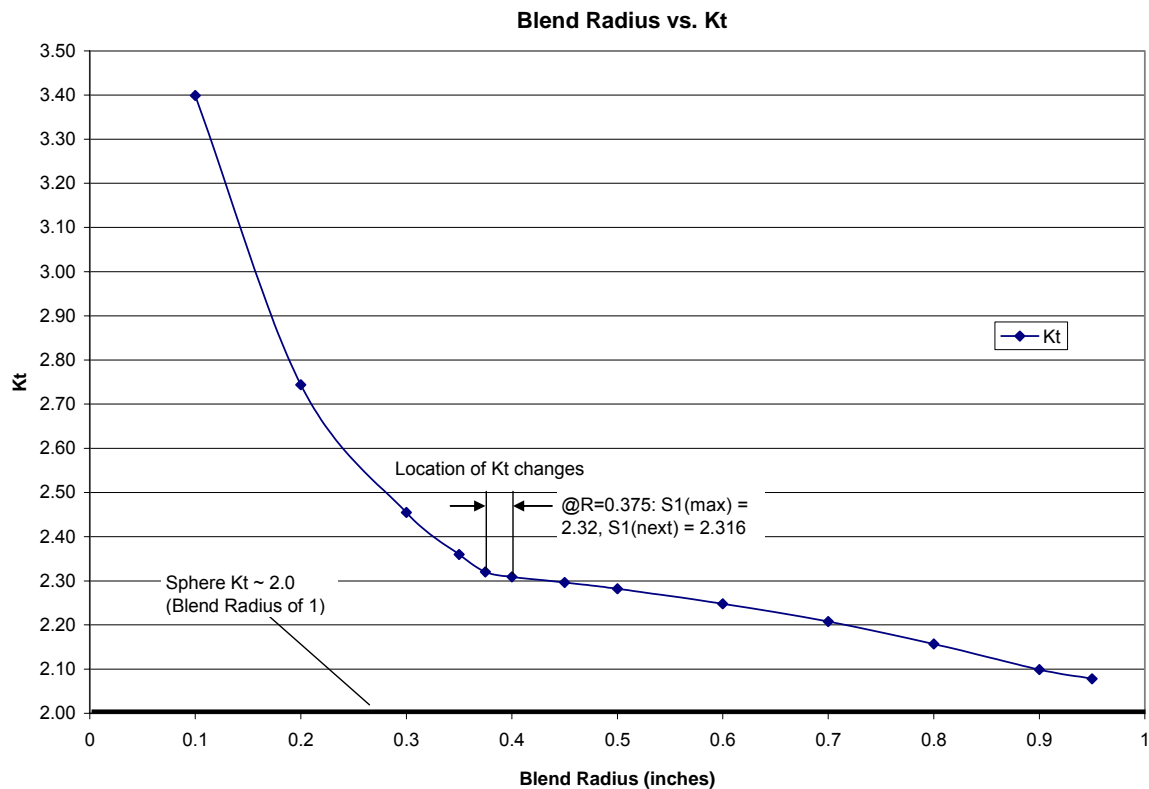
Figure 2: Summary of Kt versus Blend Radius

6.2.2 StressCheck Elastic-Plastic Local Strain Analysis of Idealized Interacting Notch Geometries

An elastic-plastic local strain versus far field stress analysis of the idealization of the AF1410 Set A Specimen 36 interacting pit geometry was performed via incremental load step application. This study was performed at the request of Dave Rusk of NAVAIR. The interacting pit geometry was idealized by formulas in StressCheck, and was placed on the surface of the center of a plate with dimensions 1.0 x 1.0 x 1/8 inches in size. This plate represents the gage section of the specimen, and it is assumed that the loads on the boundaries of the gage section are not affected by other local features resulting from corrosion. An image of the finite element mesh used for the analysis is shown in Figure 3.
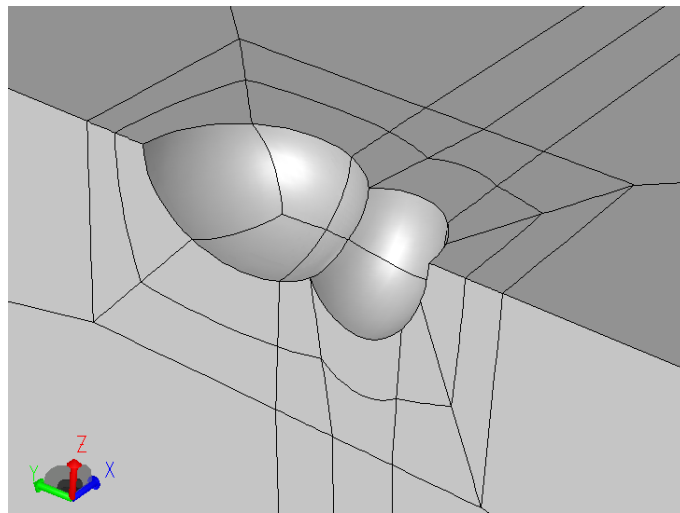
Figure 3: Finite Element Mesh of Interacting Pit Geometry

The far field stress (S0) was applied by imposed displacement, and was determined during post-processing of each load step solution. The range of imposed displacement was from 2e-4 to 6e-3 inches. The maximum first principal local stress (S1) and strain (E1) at the pit intersection was extracted from each load step solution. A summary of the S0 vs. E1 relationship is shown in Figure 4.
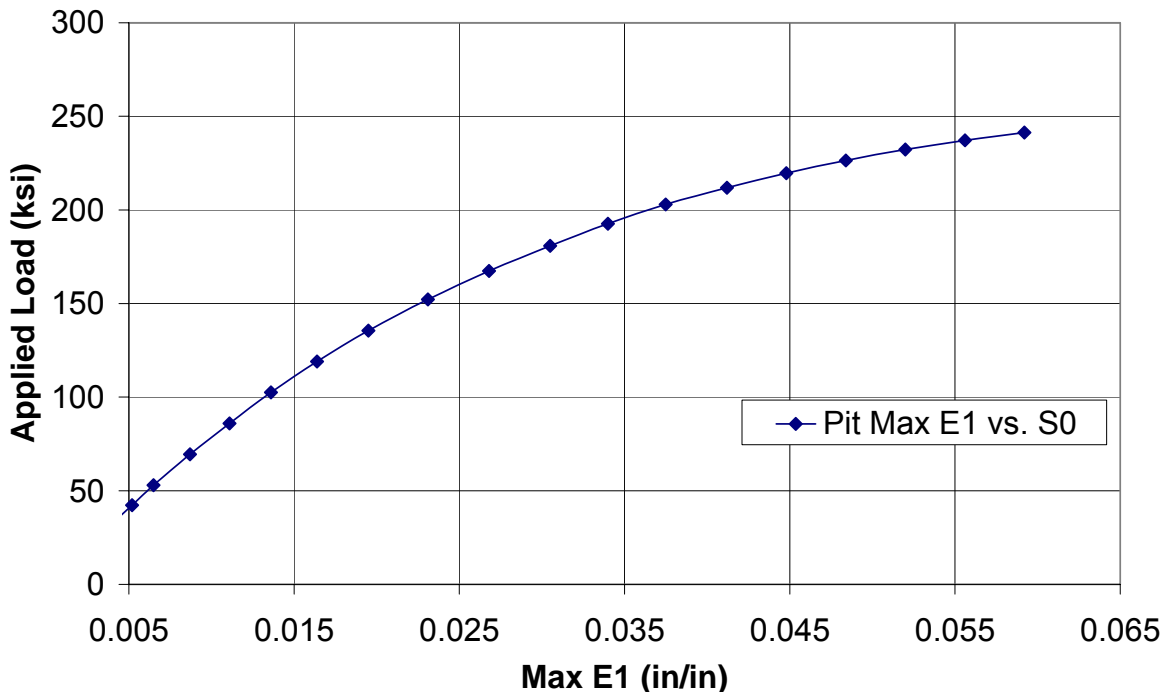
Figure 4: Summary of S0 versus E1 for Interacting Pit Geometry

7. Plan for Deployment

ESRD is engaged in the development of a framework for the distribution the corrosion assessment technology developed under this project to the USN and its subcontractors, utilizing the COM and Java interfaces of StressCheck®. The COM and Java interfaces are to provide a convenient communication protocol that integrates the necessary functions of other applications (e.g. MATLAB probability and statistical functions). The development of simple-to-use Windows desktop and web-based (or cross-platform) applications is envisioned. Web-based deployment of StressCheck capabilities is employed in Web Book, which has been updated to use StressCheck 7.1 technology. These desktop and web-based (or cross-platform) applications comprise the StressCheck FEA Toolkit. A description of the StressCheck FEA Toolkit was given in the final technical report submitted in 2005.

8. Summary

At the close of the fourth year of the USN High-Strength Corrosion Fatigue Modeling Program progress can be reported in the following areas: (a) A plan was defined for verification and validation (V&V) of the NAVAIR PSL model, with key V&V tasks identified and execution of tasks by each organization in progress, (b) ESRD performed several finite element analysis studies in support of the V&V plan as well

for the investigation of the effects of an additional parameter on the Kt, (c) ESRD completed all V&V tasks for which enough information was available; reports from these tasks are included in the Appendix.

9. Appendix

The following appendix contains all ESRD documentation relevant to the NAVAIR PSL model verification & validation (V&V) process. These documents include the ESRD proposal for the V&V of the current model (Section 9.1), as well as the reports corresponding to the completed ESRD V&V tasks (Sections 9.2-9.6). Additionally, the appendix contains a set of fringe plots corresponding to the parametric Kt study for variable blend radii (Section 9.7) and the sensitivity study for the WLI-measured micro-machined dimensions (Section 9.8), and selected references for V&V background material (Section 9).

9.1 ESRD PSL Model Verification & Validation (V&V) Proposal

Plan for Validation of a Notch-Based Model for the Prediction of Crack Nucleation Events in AF1410 Steel

Barna Szabó, Ricardo Actis and Brent Lancaster

ESRD, Inc.

Scope

This document outlines a plan for validation of a mathematical model designed to predict the number of load cycles to crack nucleation in AF1410 steel specimens. Crack nucleation is defined as the first occurrence of a 0.01 inch (0.254 mm) crack.

This validation plan is based on the recently issued Guide for Verification and Validation in Computational Solid Mechanics [1]. The Guide was approved by the American National Standards Institute in November, 2006.

The mathematical model

By definition, a mathematical model is a transformation of one set of data, the input, into another set, the output. In this case the input data consist of the metric that characterizes the degree of corrosion damage, the magnitude and spectrum of the load cycles, the location of the corrosion damage, the geometric description of the corroded part, the material properties and constraint conditions. The output is the estimated number of load cycles to crack nucleation. *The goal is to determine the number of load cycles at which the probability of crack nucleation is 1/1000.*

The proposed mathematical model is based on the assumption that crack nucleation can be correlated with the corrosion-fatigue notch factor, denoted by K_{fc}, which is related to the geometric stress concentration factor K_t. This relationship involves a notch sensitivity index q ($0 \leq q \leq 1$):

$$K_{fc}= q(K_t-1)+1 \tag{1}$$

where q is defined by one of several alternative empirical equations. In the present project the following definitions for q were considered.

Peterson: $$q=1/(1+\alpha/r) \tag{2}$$

Neuber: $$q=1/(1+(\rho'/r)^{1/2}) \tag{3}$$

NAVAIR: $$q=1/(1+(a/r)^2) \tag{4}$$

where α, ρ' and *a* are positive material constants. These constants were determined by calibration experiments. In the first set of corrosion-fatigue experiments (Batch A), 54 specimens, loaded by 160, 165, 180 and 200 ksi nominal stress were tested. Prior to testing, the specimens were exposed to a corrosive environment for 0, 3, 6 and 12 hrs. The constants were found by least squares fitting to be α=0.0608 mm, ρ'=0.1134 mm, *a*=0.0451 mm. In the following we will refer to the alternative mathematical models as the Peterson, Neuber and NAVAIR models. The relationship between the notch radius and the three definitions of q are shown in Figure 5. It is seen that at r~0.033 mm the Peterson, Neuber and NAVAIR models yield very nearly the same value for q. The second set of experiments (Batch B) are in progress.

The Batch A specimens had been surface treated, which introduced residual stresses. It was estimated that compressive residual stresses, of the order of 100 ksi, exist in a very thin layer at the surface. The effects of the residual stresses are included with other relevant features of corrosion in the results of calibration. The batch B specimens were stress relieved prior to testing.
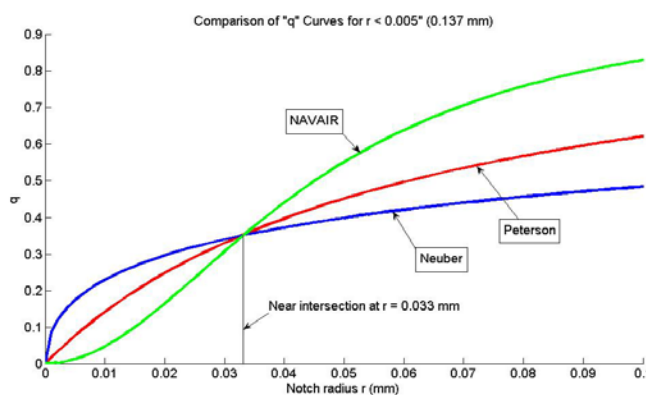
Figure 5: Dependence of the notch sensitivity index q on the notch radius r.

The idea that the geometric stress concentration factor K_t needs to be adjusted for notch radii is well established in machine design. The proposed models extend this methodology to estimated fatigue notch radii that are approximately two orders of magnitude smaller than those for which the empirical formula (1) was originally proposed. In extending the methodology to very small notch sizes, the following basic assumptions are implied:

1. Heterogeneities occurring in the material do not contribute to crack nucleation, only the physical properties averaged on a scale of the notch radii being considered, are important.
2. The notch parameters that determine the critical value of K_{teff} can be reliably and accurately measured.
3. Corrosion progresses along a sharp front, that is, once the corrosion products were removed, the material properties at the corroded surface are the same as those of the intact material.

Uncertainties that affect the predictions based on the mathematical model are associated with each of these assumptions. Those uncertainties, together with the effects of residual stresses, influence the results of calibration.

Validation

The purpose of validation experiments is to test the predictive capabilities of mathematical models. Validation experiments involve a *metric* and a *criterion*. In this case the metric is the number of load cycles to crack nucleation.

If the predictions based on a mathematical model do not meet the established criterion then the model is rejected, otherwise the model is said to have passed the validation test. Of course, setting the criterion depends on the intended use of the model. Passing validation tests shows only that the model meets *necessary* conditions for acceptance. Sufficient conditions that would guarantee that a mathematical model is valid for all admissible input cannot be established. In other words, a model cannot be validated, it can be invalidated only. Confidence in a mathematical model increases with the number of validation tests passed. Mathematical models on which decisions that relate to safety of flight are based must be tested through a series of carefully designed validation experiments.

Since there are uncertainties in model parameters, the prediction of the outcome of an experiment must be understood in a statistical sense. Let us assume that, having considered the aleatory uncertainties in the input data, we predicted a log-normal probability density function (pdf) of the number of cycles to crack initiation characterized by the mean value μ_{mod} and standard deviation σ_{mod}. Let us assume further that the criterion for rejection was set at the 95% confidence interval. We make an experimental observation N_{exp}. Let us assume that N_{exp} falls within the 95% confidence bounds. This shows that the experiment is

consistent with the prediction based on the model *at the 95% confidence level*. If N_{exp} would lie outside of the 95% confidence bounds then the model would be rejected. Using this criterion, the chance that a *valid model* would be rejected is 5%. This does not mean that we are 95% confident that the model is valid when N_{exp} falls within the 95% confidence bounds. The chances of rejecting a valid model could be reduced by setting the confidence interval at (say) 99%, however the chances of not rejecting an invalid model would be increased.

Validation protocol

The validation protocol requires that a clear statement of the criterion for rejection must be formulated in advance of the validation experiments and the model predictions must be produced before the results of the experiments become available. See, for example, [2]. For this reason, the Batch A and Batch B experiments are properly classified as calibration experiments, not validation experiments.

Test of micro-machined specimens[5]

A set of experiments were designed for the purpose of determining the statistical characteristics of crack initiation under very nearly ideal conditions. These experiments also serve the purpose of testing the predictive capabilities of the model with respect to the first occurrence of a 0.01-inch crack under uniaxial loading. The surface features were of simple geometric shape designed such that each feature would have approximately the same geometric stress concentration (K_t) and therefore roughly the same probability of failure. Owing to limitations in micro-machining, the notch radii of the micro-machined features were an order of magnitude larger than the notch radii of the corrosion features and fall within the range of the Peterson and Neuber models. The layout of the micro-machined features and the results of finite element analysis based on StressCheck, showing the computed stress contours for the normal stress Sx (x being the direction of load), is shown in Figure 6.

---

[5] Called Block 3 of C-F Life Characterization Hierarchy in the Draft Verification & Validation Framework for Corrosion-Fatigue Modeling, written by D. Rusk, 2/26/07.
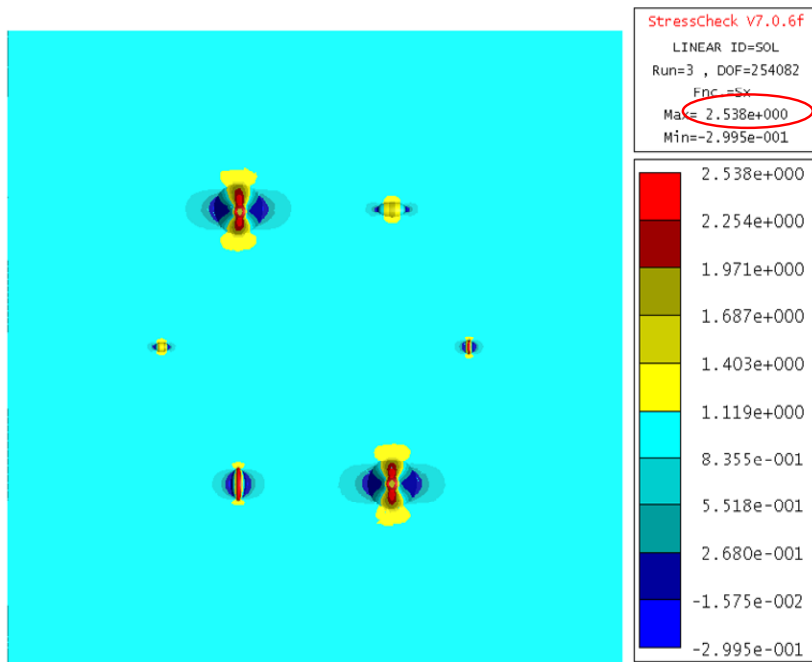
Figure 6: Arrangement of micro-machined features and stress contours for Sx.

At the time of writing, only preliminary results are available for four of the ten test specimens. The four specimens were tested at 200 ksi and the number of cycles to failure have been reported. In the absence of the results of fractographic examination, we make the rough assumption that 75% of the total number of cycles produced the crack nucleation and the pdf is lognormal. The mean μ_{exp} and the standard deviation σ_{exp} were estimated to be 7953 and 1093 cycles respectively. The estimated lognormal pdf based on the NAVAIR model and the estimated lognormal pdf based on the preliminary results of the experiments are plotted in Figure 7. If the results of fractographic examination fall in the same range then, by any reasonable criterion, the model has to be rejected.
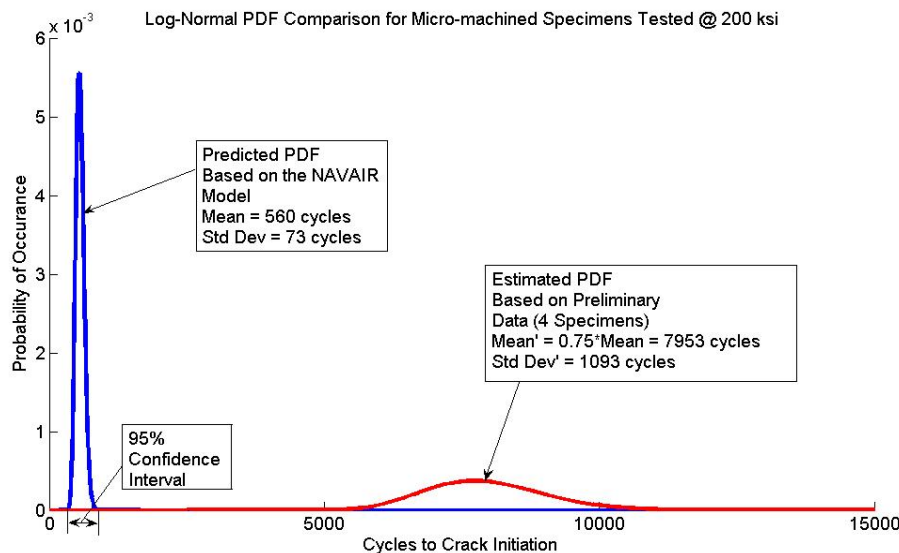
Figure 7: Estimated probability density functions for the predicted and experimental cycles, based on preliminary results of the experiments.

One very likely reason for the large differences between the predicted and observed data is that the parameter *a* in the expression for q (see eq. 4), is dependent on the notch radius, and therefore it cannot be extended far beyond the range for which it was calibrated. In other words, the parameters α, ρ' and *a* are not just material-dependent, but also depend on certain attributes of corrosion damage. Therefore the notch radii of the micro-machined specimens are not in the admissible set of input data for the model.

In considering the difference between the prediction and the experiment, we have to take into account the effects of residual stresses. In the preparation of the micro-machined specimens care was taken to minimize residual stresses through gentle polishing of the surfaces. Nevertheless, high compressive residual stresses, of the order of 100 ksi, were measured on the polished surfaces and some residual stresses were introduced by the micro-machining operation, the sense and magnitude of which are unknown. It is very likely that the distribution of the machining-induced residual stress is very different from that in the surface-treated specimens. One of the purposes of calibration experiments is to determine how far from the existing experimental data one can make predictions and still retain an acceptable level of confidence in the prediction [2], [3], [4]. The preliminary results indicate that the micro-machined specimens are well beyond the predictive capabilities of the model.

Fatigue experiments on three arrestment shanks

Three arrestment shanks were fatigue tested by NAVAIR. Failure occurred outside of the corroded area at a much larger number of cycles than predicted. Microscopic examination following the tests found no evidence of crack nucleation in the corroded region. This result is unexpected because the notch sizes

were roughly the same as the notch sizes on the basis of which the model was calibrated. One potentially significant difference between the laboratory specimens and the arrestment shanks is that the corrosion of the arrestment shanks occurred under field conditions. This result appears to support the hypothesis that the notch parameter q depends not only on the notch radius but also on other attributes of the corrosion damage.

Validation experiments using cadmium-plated specimens[6]

The forthcoming validation experiments of cadmium-plated specimens will provide additional information on the predictive capabilities of the model in the range of notch radii considered to be representative of corrosion damage under field conditions.

Formulation of the criterion

The criterion for the validation test is based on the intended use of the model. In this case the goal is to predict the number of cycles at which the probability of a crack nucleation event is 1/1000. The difficulty is that small probability events are sensitive to the assumed pdf. Wildly different results can be obtained with various plausible choices of pdf and there is not a sufficiently large number of experimental data available to justify selection of a particular pdf.

The only possibility is to measure the difference between model predictions and experimental results in terms of the characterizing statistical parameters. Ideally, the predicted and experimental data should have the same pdf, mean and standard deviation. The question to be decided is what the largest permissible difference should be. For example, the criterion could be stated as follows: Reject the model if μ_{mod} falls outside of the 95% confidence interval of the prediction, or $\sigma_{exp} > 2\sigma_{mod}$. The validation protocol requires that criterion must be established prior to undertaking validation experiments.

It would not be correct to say that, as long as the predictions are consistently conservative, the model passes the validation test. This statement would imply that a new parameter, the factor of safety, is introduced to compensate for the differences between the predicted and observed crack nucleation events, once the results of validation experiments are known. Factors of safety are properly applied to models that pass validation tests, not to those that fail.

What happens if the model fails the validation test? This demonstrates that the model failed to account for one or more attributes of the physical system, therefore it has to be revised in the light of the results of the validation experiments. Consequently the validation experiments must be re-classified as calibration experiments and new validation experiments have to be designed and executed for the revised model, subject to the validation protocol.

---

[6] Called Block 4 of C-F Life Characterization Hierarchy in the Draft Verification & Validation Framework for Corrosion-Fatigue Modeling, written by D. Rusk, 2/26/07.

Verification

Verification is a process by which it is assured that the computer code and the computational procedures used for making predictions perform their function as intended. Verification is a prerequisite to validation.

The procedures used for filtering white light interferometry data and computing K_{fc} are relatively simple, and easily checked. The computation of stresses in parts, such as the arrestment shanks, was performed with StressCheck. StressCheck has intrinsic error estimation and error control capabilities, therefore the errors of approximation are known to be small.

References

[1] ASME V&V 10-2006: Guide for Verification and Validation in Computational Solid Mechanics. The American Society of Mechanical Engineers, ISBN No. 0-7918-3042-X (2006).

[2] W. L. Oberkampf. What are validation experiments? *Experimental Techniques* **25** pp. 35-40 (2001).

[3] K. M. Hanson and F. M. Hemez. A framework for assessing confidence in computational predictions. *Experimental Techniques* **25** pp. 50-55 (2001).

[4] R. G. Hills and T. G. Trucano. Statistical validation of engineering and scientific models: Background. Report SAND99-1256, Sandia National Laboratory (1999).

9.2 ESRD Code Verification Task #11 Final Report

StressCheck Arrestment Hook Model
Summary of Model Input Checks
Verification Task #11
July 10, 2007
Report Prepared By: Brent Lancaster

1) Introduction

ESRD performed finite element analyses of the AF1410 arrestment hook shank, for typical arrestment and hook bounce load cases, with the purpose of determining the stress distribution for a specific region inside the bore of the shank. Additionally, the strains on the outer shank surface were of interest because these could be directly compared with experimental strain surveys for the validation of the models. The details of the activities for the validation of the mathematical models for each load case are summarized in the document "StressCheck Arrestment Hook Model, Summary of Development and Validations Efforts, Validation Task 9" dated June 27, 2007 (File: ESRDTailhookModelingValidationTask9.doc).

This report documents the verification that the input parameter of the models conform to the original drawings and other data provided by NAVAIR. Verification was performed by a different person than the

one that built the models. The input checks were broken into five (5) major groups: geometry, mesh, material properties, load and constraints. The goal was to determine if there was incorrect or inadmissible data stored in the model. Each of these input checks is examined in the following.

2) Check #1: Geometric Dimensions
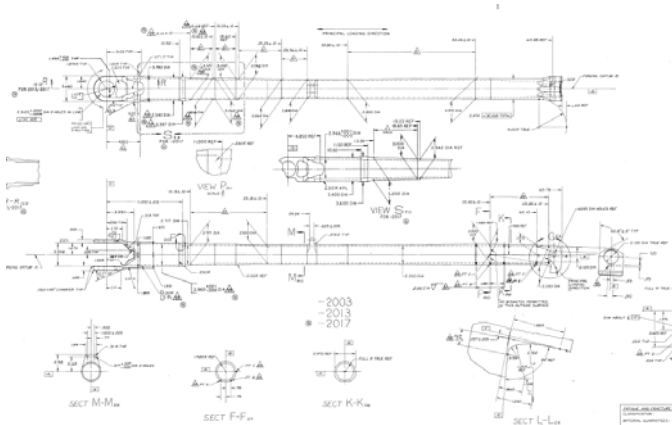
Figure 8: Drawing 74A480617# - Arresting hook (tail hook) assembly

The geometric dimensions in the finite element model were compared directly with the drawing given in Figure 8 (74A480617) as well as with drawing 74A480001. It was found that all relevant dimensions were as indicated in the drawing. Any dimensions not noted in the above drawings were not compared.

3) Check #2: Mesh Continuity and Quality

The mesh shown in Figure 9 was checked for mesh continuity (i.e. disconnected nodes and edges) as well as element quality (i.e. distortion and volume). An element free edge/face check was performed, and no cracks or discontinuities were found to exist in the model.
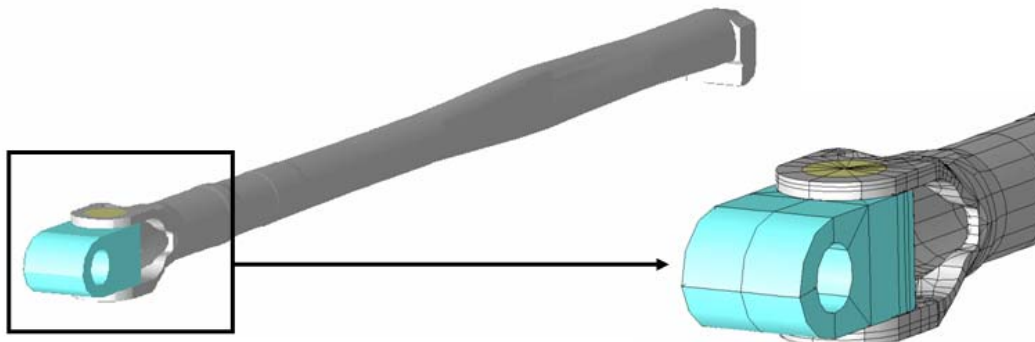
Figure 9: Arresting hook (tail hook) full 3D-model for the arresting load case

The result of the element distortion check shown in Figure 10 indicate that 1240 elements have vertex angles inside the range of 5.0 and 175.0 degrees, and 42 elements with vertex angles outside that range. These distorted elements were located outside of the region of primary interest, their vertex angles were within acceptable limits (>0 & <179), and therefore the elements are acceptable if they pass the property check.

```
Element Distortion Report
================================================================================
Testing for valid element vertex angles in the range  5.0 to 175.0.
Set DISTORT_WARN contains distorted elements.
Set DISTORT_FAIL contains illegal elements.
Define parameter _warn_distort to report distortion warnings.
Check/Mesh/Properties to determine whether model can be solved.
--------------------------------------------------------------------------------
1282 element(s) selected, 1240 acceptable, 42 distorted, 0 rejected.
Smallest angle found in element 2023 = 1.223631e+000
Largest angle found in element 2235  = 1.650120e+002
================================================================================
```

Figure 10: Element distortion report

Figure 11 shows the result of the element property check. The check consists in computing the volume of the mesh as the sum of the volumes of the individual elements. The volume computation fails if an element is badly distorted. All of the elements passed the volume computation, and therefore the mesh is considered acceptable.

```
Element Property Report
================================================================================
Total elements                        ... 1282
Total SELECTED elements               ... 1282
Total volume                          ... 2.1724e+002
X-coord. of center                    ... 2.1354e+001
Y-coord. of center                    ... -9.8507e-002
Z-coord. of center                    ... -2.9200e-005
================================================================================
```

Figure 11: Element properties report

4) Check #3: Material Properties

The material properties assigned to the models were checked for consistency by comparing the elastic modulus and Poisson's ratio used for the solution of the StressCheck models with test data provided by UDRI for AF1410 (Figure 12). It was found that the elastic modulus used in the StressCheck models (E=2.94e7 psi), is the same as the average of several test results given in STL414-4. However, the Poisson's ratio used in StressCheck model (v=0.31), was 4% higher than the average of the test results given in STL414-6 (v=0.297). A sensitivity study was performed with the full 3D-model to assess the

influence of Poisson's ratio in the stress distribution in the region of primary interest. No significant changes in the strain or stress distribution (< 1%) were observed when Poisson's ratio was changed from 0.31 to 0.29, and therefore it was concluded that there was no need to perform the FE analyses again with ν=0.297.
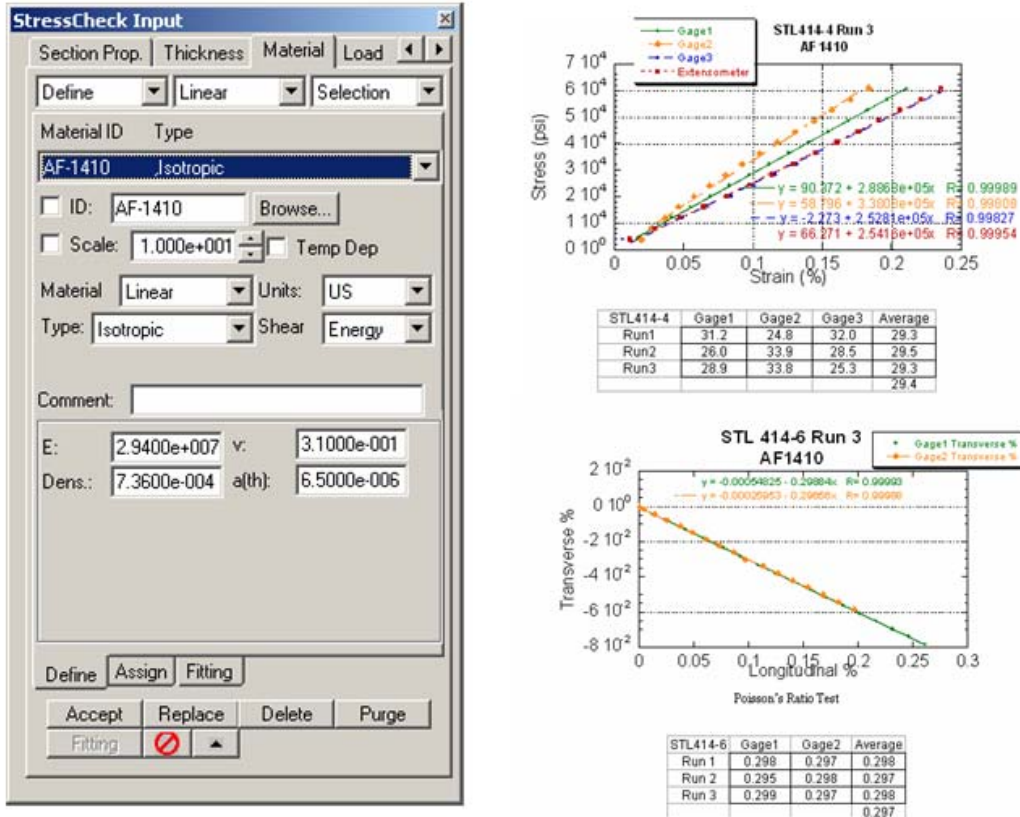
Figure 12: Material properties check

5) Check #4: Resultant Load

5a) Arrestment Load Case

For the arrestment load case, a 140 kip axial load was originally applied to the tail hook model as shown in Figure 13. Later on, to compare the FEA results with the strain gage data, an axial load of 136912 lb was used for the analysis. The check was performed for the second load.
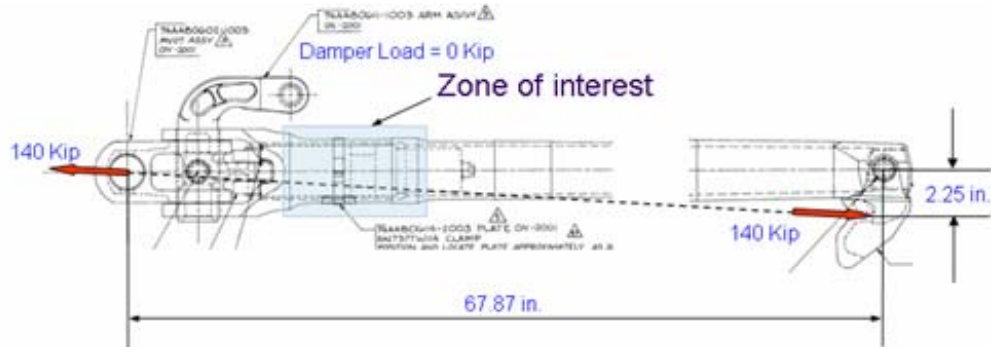
Figure 13: Arrestment load case

The load was applied to the faces of several elements on the hook end as distributed tractions (Figure 14) in the direction of the x-axis of a local coordinate system parallel to the dotted line indicated in Figure 13. Figure 15 shows the load summary after a resultant check was performed. It can be seen that the intended load, 136912 lb, is practically the same as the output of 136917 lb. The outputs of the load check are the global force components computed as the integral of the applied tractions over the faces.
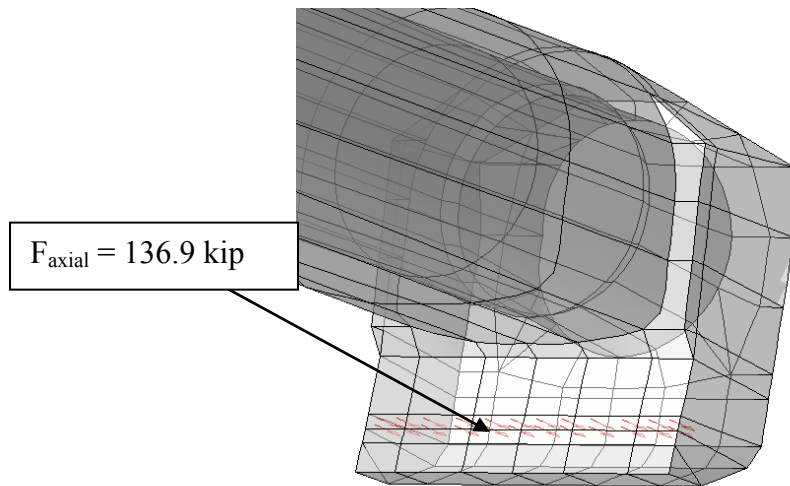
Figure 14: Arrestment load applied as a distributed traction at the hook end

```
                             Load Summary
                 F-18 Arresting Hook Shank Assy - 74A480617
                       Load ID: Load, Elements=1282
            Moment center:  (-3.750000e+000,0.000000e+000,0.000000e+000)
-------------------------------------------------------------------------------
     Fx            Fy            Fz            Mx            My            Mz
-------------------------------------------------------------------------------
 1.3685e+005  -4.2758e+003   0.0000e+000  -1.0766e-010  -3.4852e-009   2.7354e-010
-------------------------------------------------------------------------------
```

$$F = \sqrt{\left((Fx)^2 + (Fy)^2\right)} = \sqrt{\left((136850lb)^2 + (-4276lb)^2\right)} = 136917lb$$

Figure 15: Arrestment load resultant check

5b) Hook Bounce (Damper) Load Case

In the hook bounce load case a damper load of 18.5 kip is applied to the pivot arm at a 27 degree angle to the horizontal as shown in Figure 16. For this load case, a local 3D-model of the full arrestment hook was used (Figure 17). The damper load at the arm cross section and the resultant shear and moment at the shank cross section are shown were applied as distributed tractions as shown in Figure 17. The resultant shear (2017 lb) and moment (92700 lb-in) for the local model cross-section were determined from the full 2D-model shown in Figure 18 and converted into equivalent formula-based tractions. For more detail on the assumptions for the transformation from 2D to 3D loads, see "StressCheck Arrestment Hook Model, Summary of Development and Validations Efforts, Validation Task 9".
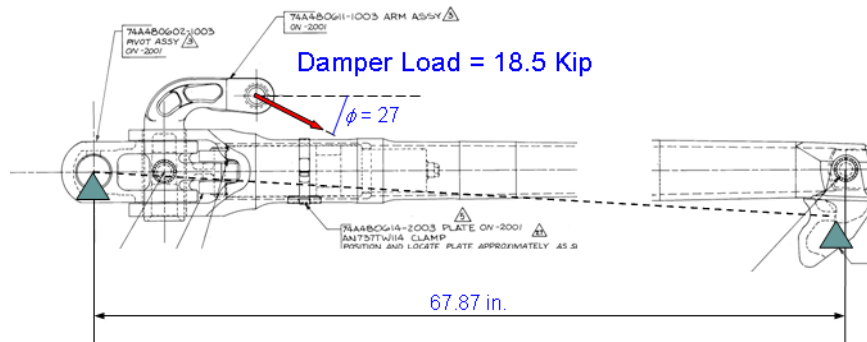
Figure 16: Damper load case

3D Local contact
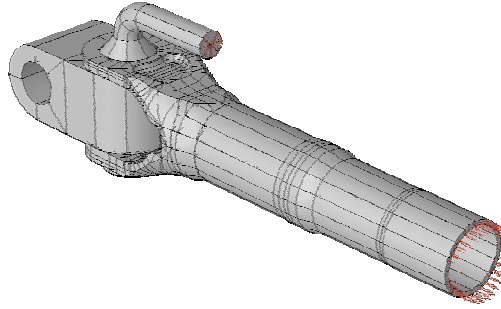
Figure 17: Arrestment hook local 3D-model for the damper load case

Fastener constraint and load

Node constraint and load
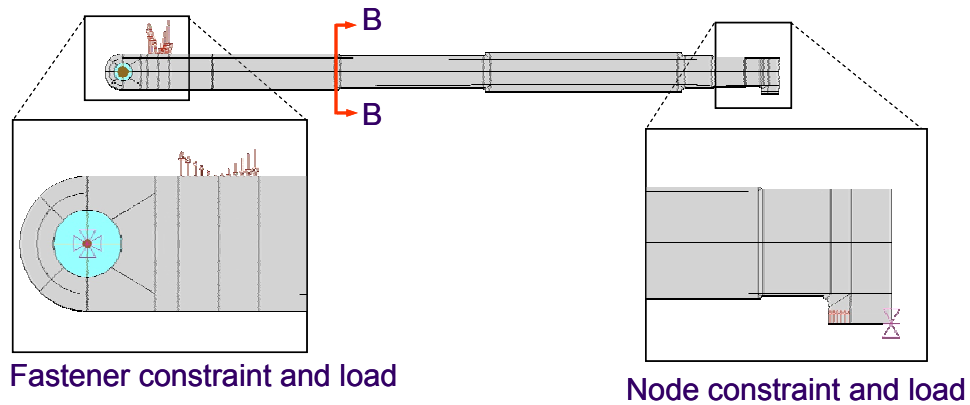
Figure 18: Arrestment hook full 2D-model for the damper load case

Figure 19 shows the load summary after a resultant check was performed for the loads at the circular cross section of the local 3D-model. The moment center was taken to be at the center of the cross-section (x=18.65, y=0.0, z=0.0). It can be seen that the resultants computed as the integral of the tractions for the shear (Fy=2017 lb) and the moment (Mz=92698 lb-in) are practically the same as the intended loads (Fy=2017 lb and Mz=92700 lb-in, respectively), and the other components are very close to zero.
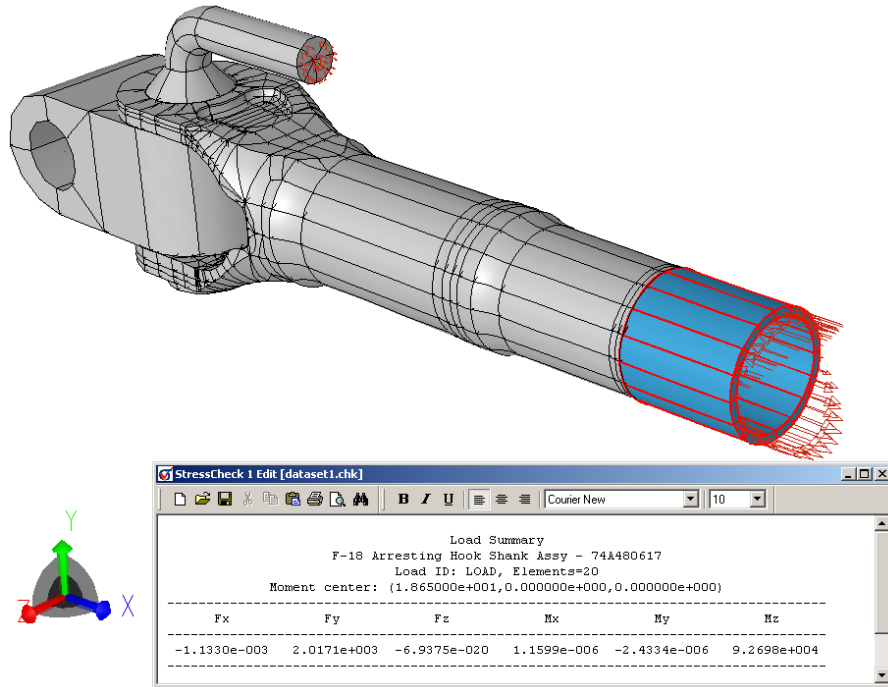
Figure 19: Resultant check of the local 3D-model (circular cross-section)

Additionally, the resultant at the arm must be checked to ensure that the intended damper load of 18.5 kip at an angle -27 degrees to the horizontal is properly applied (Figure 20). In this case, the moment center was taken to be at the center of the arm cross section (x=4.833, y=3.966, z=0.0). It can be seen that the resultants are the same as the intended loads.

$$F = \sqrt{\left(F_x^{\,2} + F_y^{\,2}\right)} = \sqrt{\left((16484)^2 + (-8399)^2\right)} = 18500 lb = 18.5 kip$$

$$\theta = \tan^{-1}\!\left(F_x \Big/ F_y\right) = \tan^{-1}\!\left(-8399 \Big/ 16484\right) = -27^0$$
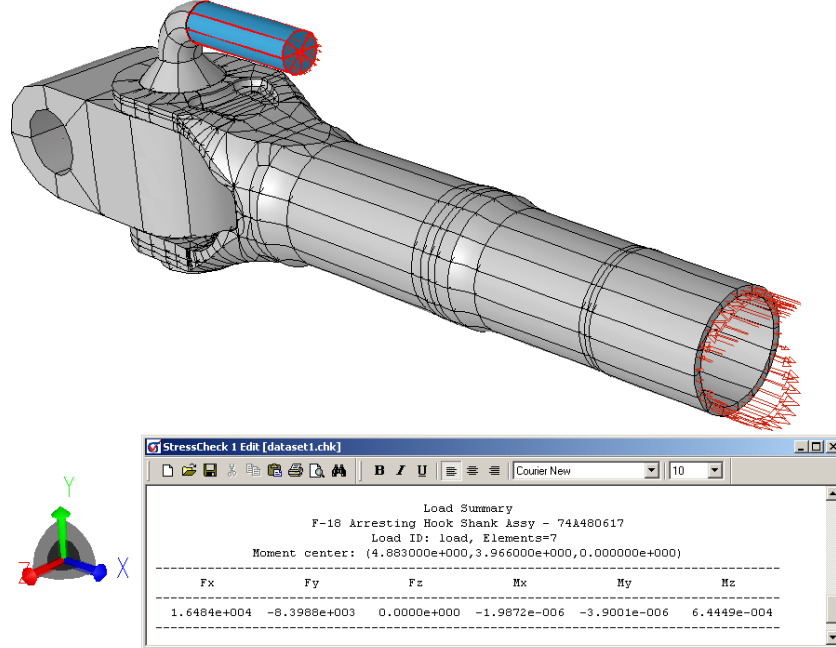
Figure 20: Resultant check for the damper load

A bearing load was specified at the bore of the pivot end so that the system of forces was in equilibrium. Figure 21 shows the resultant check for all the elements satisfying this requirement with minor unbalance in the forces in the x- and y-directions and in the moment Mz.
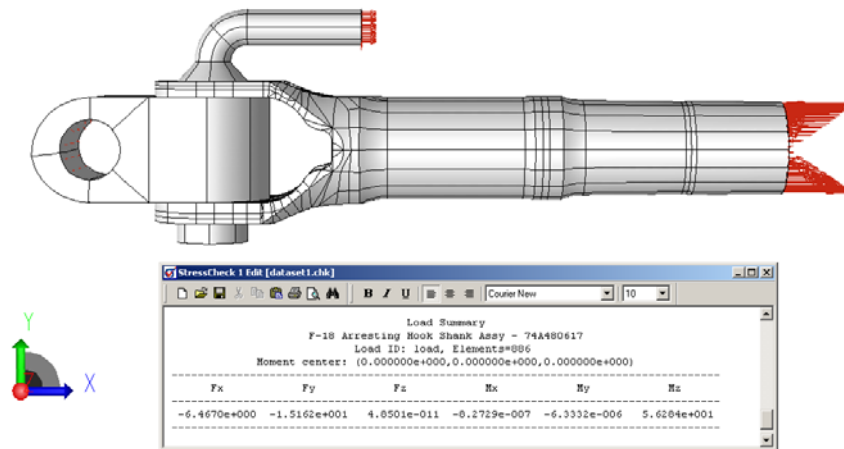
Figure 21: Resultant check for all the elements

A-36

6) Check #5: Constraint Assumptions

6a) Arrestment Load Case

The constraints used in the full 3D-model of the arrestment hook were checked for consistency with the actual restrictions of the shank during arrestment and found to be acceptable. To simulate the pin-constraint for the tail hook during arrestment, normal springs with a constant K=1e8 psi/in, were specified in half the bore of the pivot block as shown in Figure 22. The distributed spring is attached to the faces of the elements at one end and fixed at the opposite end, allowing rotation of the shank about the pivot centerline, and reacting to axial load when in compression, and therefore capable of simulating the effect of a pin. Additionally, to constrain the tail hook from lateral motion (and prevent rigid body displacement), a softer spring (K=1e4 psi) was used on the sidewalls of the pivot block. A nodal constraint was also specified at the hook end to prevent rigid body rotation about the pivot point centerline.
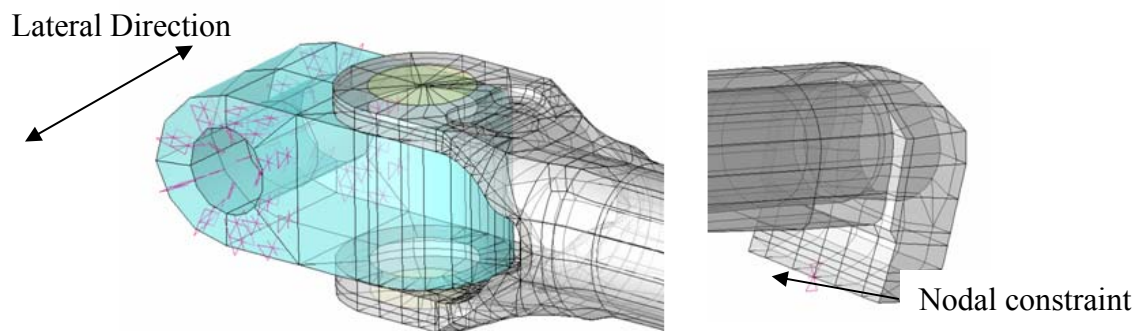
Figure 22: Constraints for the arrestment load case

6b) Hook Bounce (Damper) Load Case

The constraints used in local 3D-model of the arrestment hook were checked for consistency with the actual restrictions of the shank during the damper load. The pivot block and arm were fused into a single body and contact conditions were specified between the shank clevis and the pivot block. Contact constant values of Kc=1e7 psi/in were specified between all contact pairs (lug bore-pivot arm, lug faces-pivot block). The contact specifications can be observed in Figure 23. Additionally, because the assembly was in equilibrium due to the applied loads, rigid body motions were restricted by fixing lateral nodal displacements on the pivot block and arrestment hook.
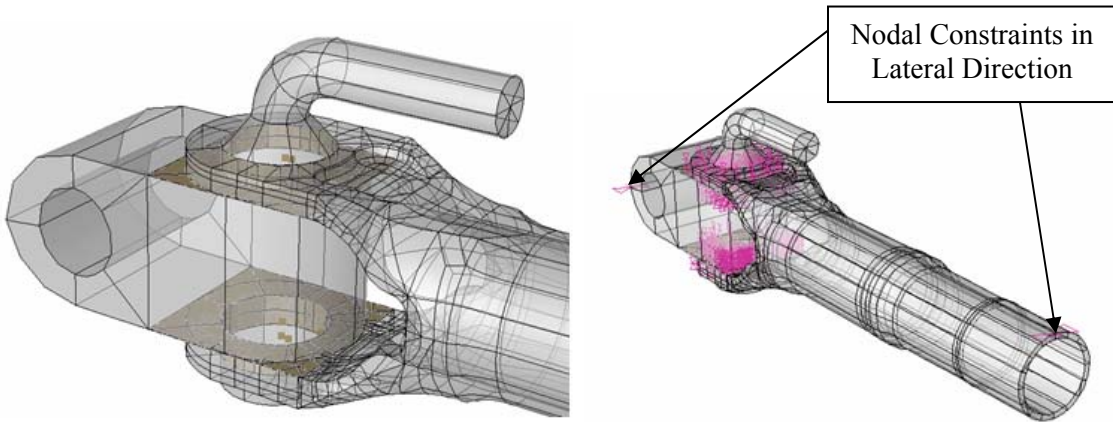
Figure 23: Constraints for the hook bounce (damper) load case

7) Summary

The verification of the input data for the full 3D arrestment hook model used for the arrestment load case and the local 3D-model used for the bounce load case was completed successfully. No discrepancies were found between the input parameters of the models and the original drawings and other data provided by NAVAIR.

9.3 ESRD Calculation Verification Task #9 Final Report

FE Arrestment Hook Model
Automated Shank Extractions Using VBA
Calculation Verification Task #9
May 10, 2007

1. Background

In September 2006, NAVAIR requested the development of a procedure to automatically extract point-wise stress/strain values from the StressCheck solutions of AF1410 arrestment hook load cases, in a pre-determined grid of point in the inner bore of the region of interest. These extractions were automated by an Excel macro, programmed in VBA, and were written to a text file which could be read into MATLAB. This document outlines the extraction process and establishes the reference conventions agreed upon by Dave Rusk and ESRD, Inc.

2. Conventions and Data Format

The reference conventions were established based on a document produced by Dave Rusk on September 13, 2006 entitled "Zone-Based Corrosion-Fatigue Life Prediction for F/A-18 Arresting Shank." Conventions for both axial and circumferential directions and locations on the shank are described in Figure 24. The total number of points is 14580, evenly spaced in the axial direction from x=4.0-in to x=10.7-in (0.08375-in increments) and in the circumferential direction from 0° to 358° (2° increments).
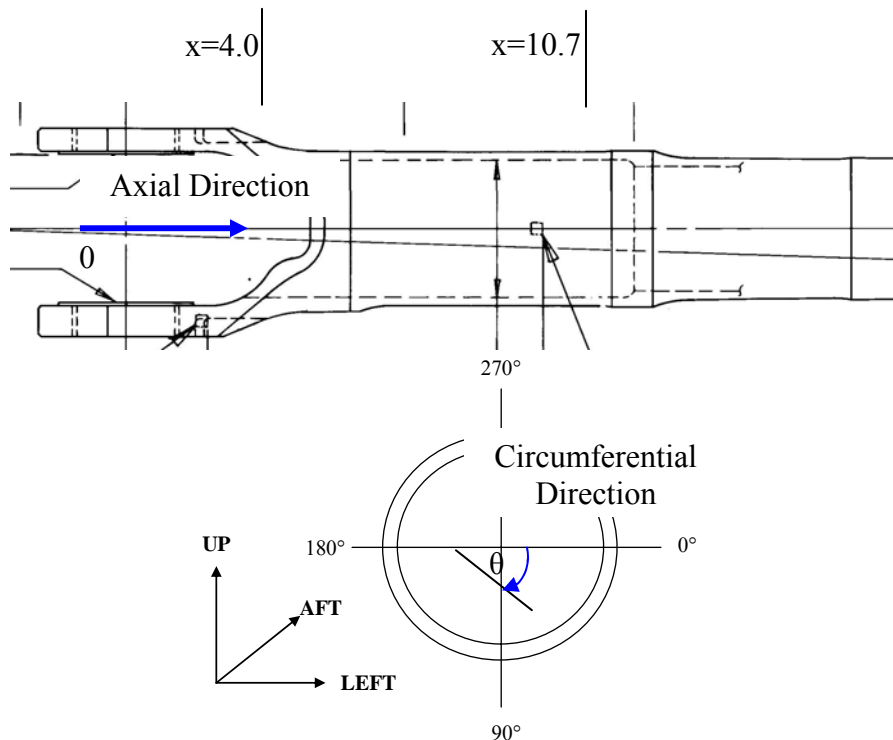
Figure 24: Reference Conventions for Shank Extractions

The format of the data extracted from the finite element solutions is as follows:

4, 0, 8.314E-05,-688.24

Axial Location (inches)   Circumferential Location (Degrees)   Axial Strain (in/in)   Axial Stress (psi)

3. Process Map for Arrestment Shank Automated Extractions
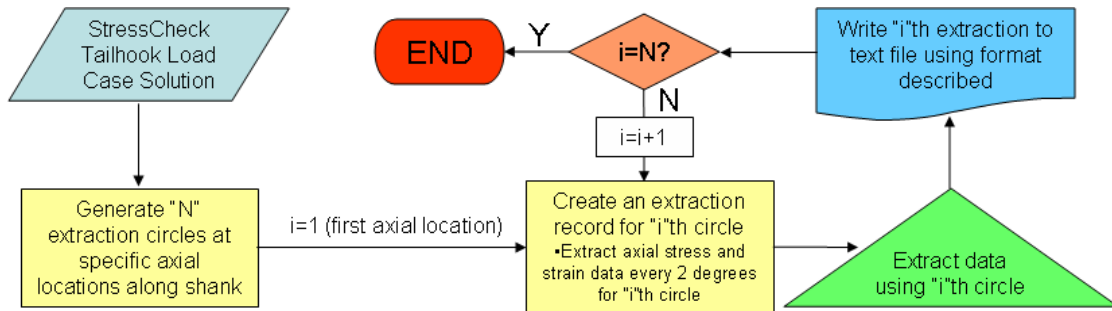
Figure 25: Process Map for Axial Stress and Strain Automated Extractions

The process map given in Figure 25 outlines the algorithm written to perform the extraction tasks. The algorithm was written in VBA such that Excel could be used to automate the tasks. The extractions, output in the format described, are then written to an ASCII file (.txt) for processing via MATLAB or a similar software package. Figure 26 shows an example plot generated by MATLAB to display a contour plot of the axial stresses extracted at the grid point locations.
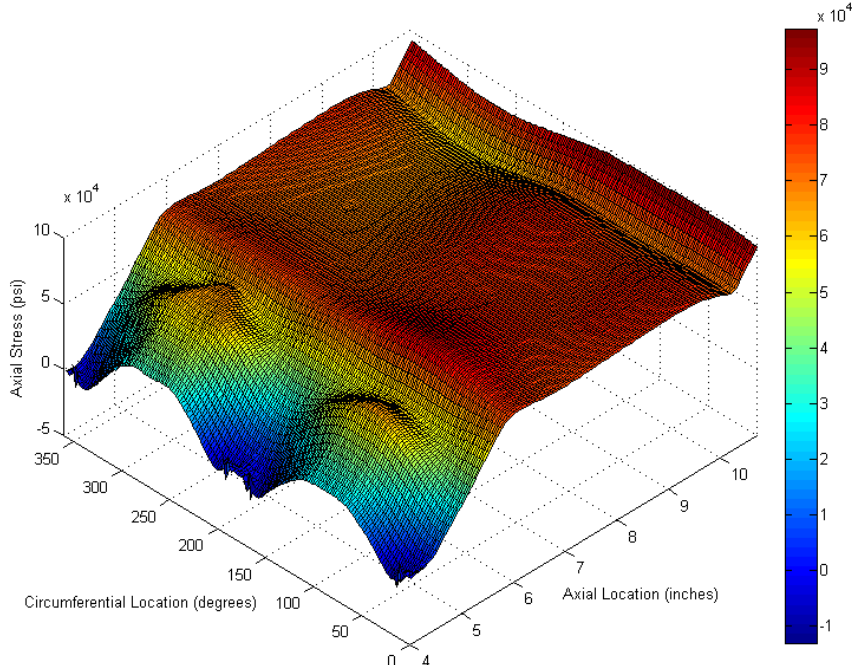
Figure 26: Example MATLAB Plot of Arrestment Shank Axial Stresses

4. Extraction Algorithm Modifications and Corrections

In April 2007, parts of the original algorithm described by the process map in Figure 25 were modified in order to improve performance and overcome inconsistencies with design specifications. These modifications are described in the following:

1) Changed independent variable from extraction point # to an angular degree function computed internally in StressCheck. This modification was made in order to represent exactly the location of the extraction along the circle and avoid potential transformation mistakes of the angular coordinate.

2) Changed number of extraction mid-points from 180 to 179 per circle, or one extraction every 2 degrees. This modification was made because in StressCheck the end points of the boundary are always included in the extraction, so that a total of 181 points are computed in the range 0 and 360 degrees with the first and last point at the same location.

3) Changed the local coordinate system orientation of each circle such that the extraction order matches the circumferential direction described in Figure 24. While previous extractions do not differ substantially from corrected extractions, the correction must be made to keep consistent with convention.

5. Independent Code Verification

An independent verification of the data generated by the automatic extraction procedure consisted of performing the extractions interactively in StressCheck by a different person. Three extraction circles were created at X=4.8375-in, X=5.675-in and X=7.76875-in with a radius R=1.481-in. The strain and stress components in the axial direction were extracted along each circle by selecting 179 points in the Points extraction interface, and the local coordinate system of the corresponding circle. The tabular data in StressCheck was compared with ASCII file generated by the automatic process shown in Figure 25. The coordinates, strain and stress values for several points along each circle were checked and all found to be the same in both tables.

9.4 ESRD Validation Task #8 Final Report

Comparison of ESR Probabilistic Life Predictions with
Large Notch Plate Tests
Validation Task #8
August 6, 2007
Report Prepared By: Brent Lancaster

1) Introduction

For Validation Task #8, ESRD compared NAVAIR ESR probabilistic life predictions with large notch (micro-machined) plate fatigue test results. For each specimen, the number of cycles to crack initiation (CI), which is defined as the number of cycles to generate a 0.01" long crack, was determined by Scanning Electron Microscope (SEM) examination of marker band sequences performed by Boeing. ESRD then used the specimen by specimen marker band sequence, provided by Jennifer Pierce of UDRI and titled "Micro-machine Specimen Test Records 200ksi 031907 JLP.xls", to determine the number of R=0.1 cycles for each specimen. The R=0.7 cycles were removed from the CI cycle count for two reasons: 1) A continuous Cumulative Probability Distribution (CDF) for ESR life prediction could not be produced with variable R values, and 2) the R=0.7 cycles were assumed to have little influence on the overall crack growth even though the number of R=0.7 cycles is nearly twice that of the R=0.1 cycles. This was justified by NAVAIR and is discussed in Section 4 of this document.

2) Large Notch (Micro-machined) Plate Geometric Description

The geometric features described in Figure 27 were designed by ESRD and machined by Boeing. The conical features and the features perpendicular to the load were designed for a Kt of ~2.5. After the machining was performed for two wafers with the same sequence as the specimens, UDRI examined each feature using White Light Interferometry (WLI) measurements; these measurements were approved by ESRD before fatigue testing was begun. Figure 28, Figure 29 and Figure 30 show the blueprint design dimensions, along with the relative differences between the design and WLI-measured dimensions, for each micro-machined feature. Based on these differences, a StressCheck sensitivity study of Kt was performed, and it was found that the Kt of the conical feature increased by 8% (Kt ~2.7) while the other two features were not affected. Also studied was the sensitivity of the Kt to irregularity in the pill-shaped feature. A rounded parallelepiped was subtracted from one-half of the pill feature to resemble to surface profile given in Figure 30; it was discovered that this change in geometry had no effect on Kt. Fringe plots of Kt for both sensitivity studies are included in the Appendix, Section 9.8. Additionally, in Figure 31 a Kt map from a StressCheck analysis of the specimen with the blueprint features is shown along with a representative micro-machined specimen.
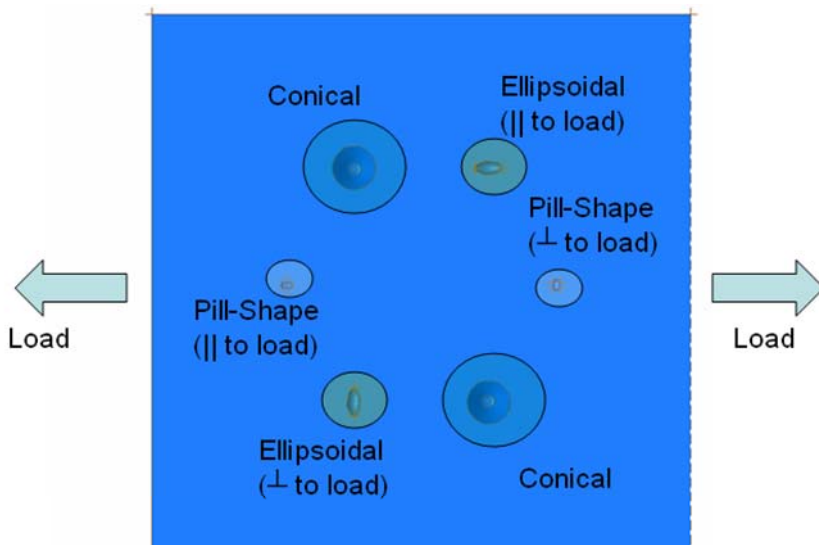
Figure 27: Large Notch (Micro-machined) plate geometric description

R1=4.0e-002"
R2=1.2993e-002"
R3=5.4007e-003"
R_fillet=1.0e-002"
H=3.5e-002"

Relative Difference: Conical Feature 1			
(mils)	CAD Model	Machined	%Difference
H	35.00	37.30	-6.57
R1	40.00	42.00	-5.00
R2	13.00	12.30	5.38
R3	5.40	6.70	-24.07
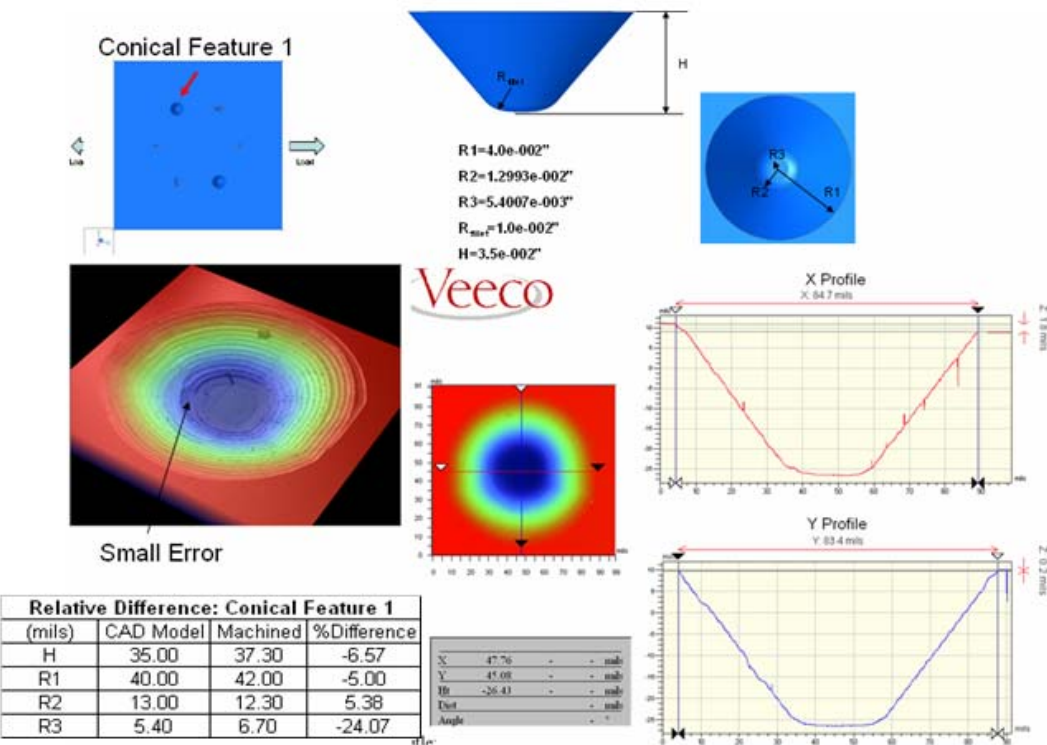
Figure 28: Conical feature blueprint dimensions and corresponding WLI measurements

Ellipsoidal Feature 2

R1= 2.5e-002"
R2= 1.25e-002"
H= 1.25e-002" (same as R2)

Very Well Made

Relative Difference: Ellipsoid Feature 2			
(mils)	CAD Model	Machined	%Difference
H	12.50	14.20	-13.60
R1	25.00	25.50	-2.00
R2	12.50	13.65	-9.20
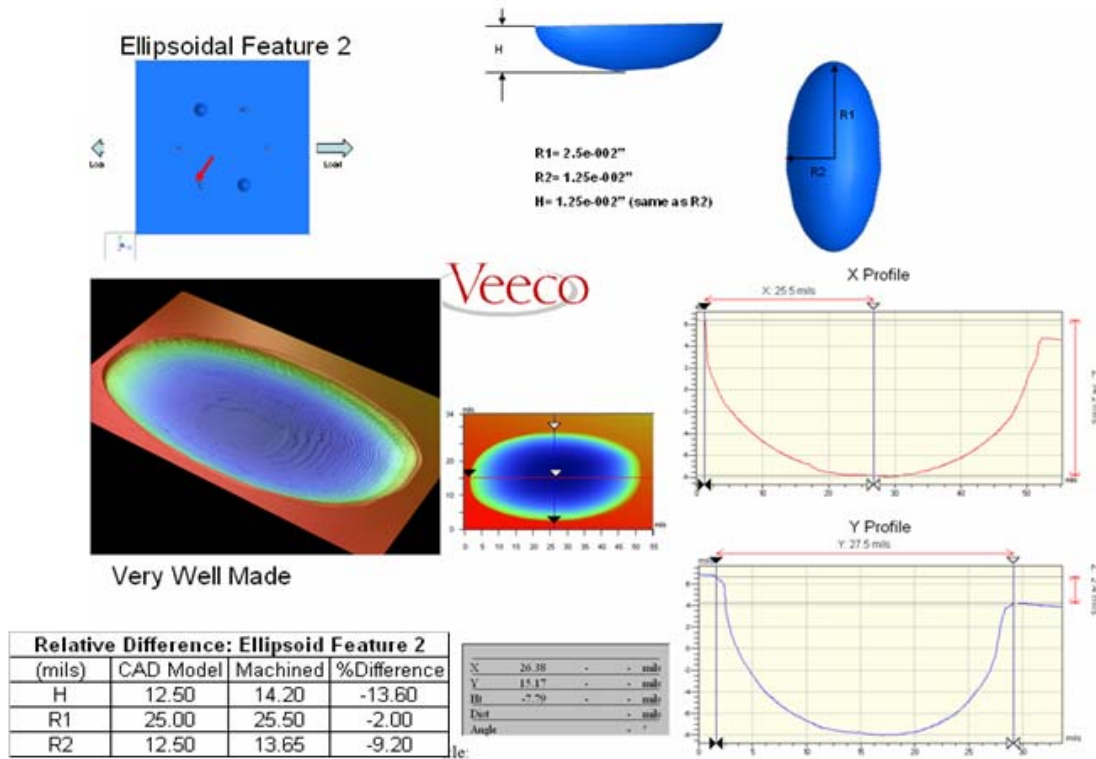
Figure 29: Ellipsoidal feature blueprint dimensions and corresponding WLI measurements

Pill Feature 1

R1=H=7.0e-003"
L=8.4e-003"
L overall = 22.4 mils

Feature is a bit oblong.

Measurements

Relative Difference: Pill Feature 1			
(mils)	CAD Model	Machined	%Difference
H	7.00	8.40	-20.00
R1	7.00	8.30	-18.57
L	8.40	7.10	15.48
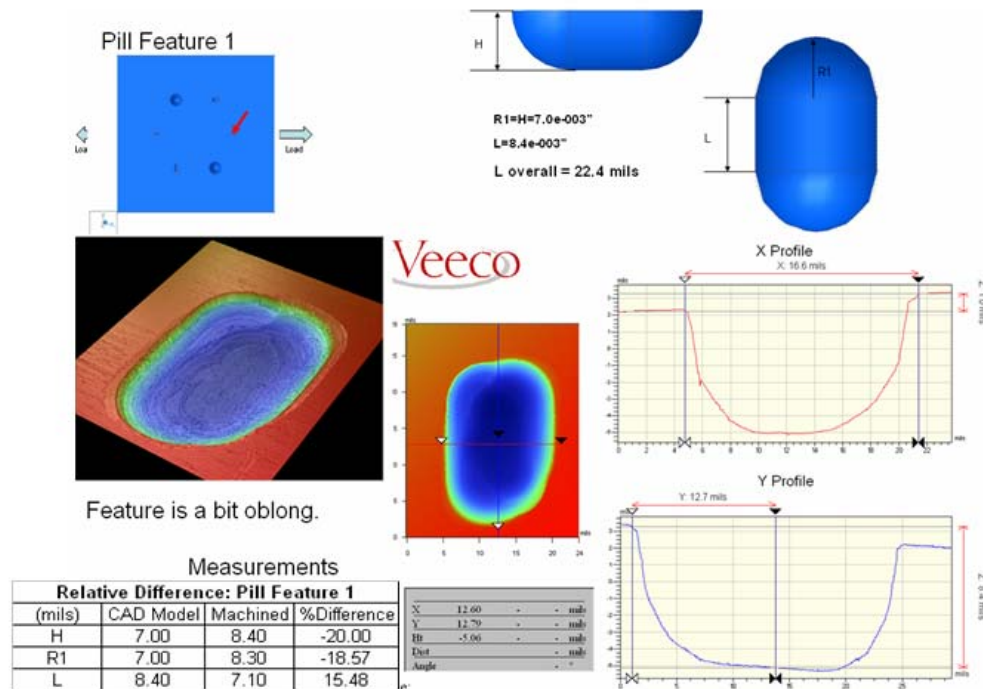
Figure 30: Pill feature blueprint dimensions and corresponding WLI measurements
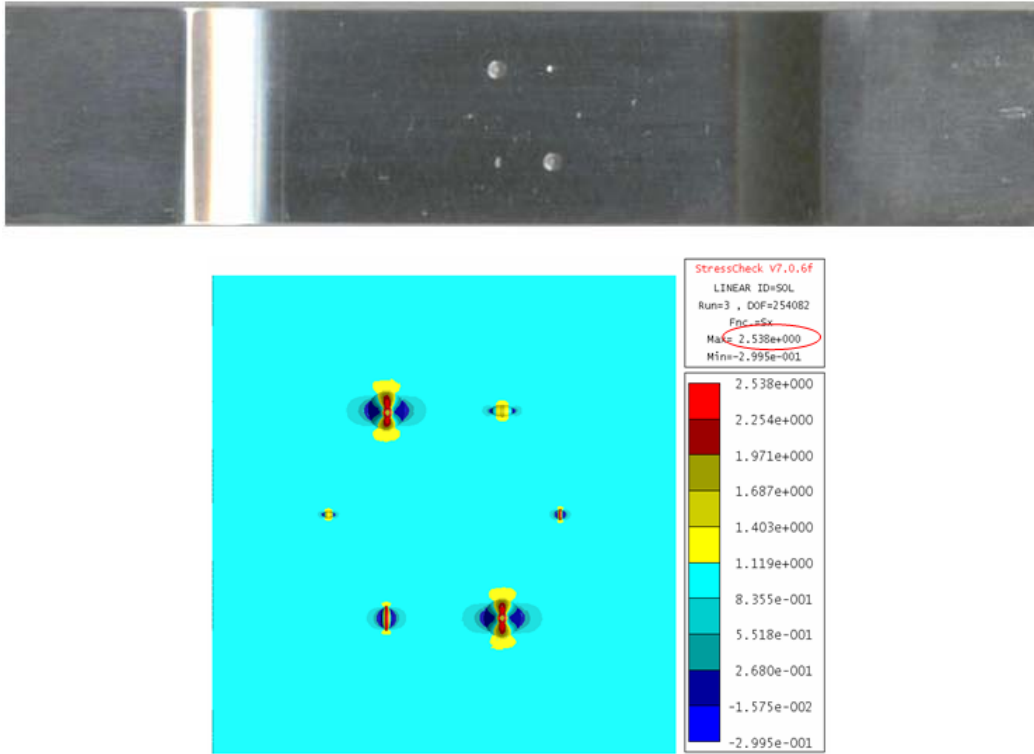
Figure 31: StressCheck Kt map for micro-machined plate geometry

From the evaluation of the WLI results it was concluded that the micro-machining process produced features very close to the blueprint design in terms of shape and dimensions. In all, nine (9) micro-machined specimens were produced by Boeing and sent to UDRI for testing. Three (3) un-notched specimens were also fatigue-tested by UDRI to establish baselines.

3) NAVAIR ESR Probabilistic Life Predictions vs. SEM Measured CI Cycles

Table 3 contains the predicted CI cycles vs. measured CI cycles for nine (9) micro-machined specimens. The predictions were made using two kinds of distributions: Peterson nominal and Peterson Beta. The details of these distributions are given in a document by NAVAIR entitled "Micromachined Specimen Life Predictions" and dated July 9, 2007. These specimens were tested at 200 ksi maximum, with parts of the spectrum using stress ratios of R=0.7 and R=0.1. The R=0.7 cycles were removed from the CI cycles count in order to compare with the predictions. Each specimen used a different marker band sequence, so the R=0.1 cycles had to be counted for each specimen using as a basis the cycle count spreadsheet provided by UDRI. A verification of the cycle count was then performed by a different person than the author. The average value of the number of measured R=0.1 cycles was determined to be 1727. The column labeled 'Ratio' in Table 3 is the ratio between the actual and predicted CI cycles.

Table 3: **Large Notch ESR Predictions vs. Measured CI Cycles**

		Stress Level (ksi)	Total Cycle Count	CI Cycle Count	R=0.1 CI Cycle Count	Peterson Nominal Prediction	Ratio	Peterson Beta Prediction	Ratio
Micro-machined Specimen Crack Initiation Life: SEM Measured vs. NAVAIR Prediction									
	Specimen ID								
Micro-machined	598-1	200	11110	6,567	1767	1040	1.70	1700	1.04
Micro-machined	598-5	200	12433	5,760	1521	1040	1.46	1700	0.89
Micro-machined	598-2	200	9279	3,300	1700	1040	1.63	1700	1.00
Micro-machined	598-8	200	9595	4,660	1869	1040	1.80	1700	1.10
Micro-machined	598-10	200	8416	3,100	1500	1040	1.44	1700	0.88
Micro-machined	598-9	200	11435	5,700	1878	1040	1.81	1700	1.10
Micro-machined	598-3	200	10351	4,371	1971	1040	1.90	1700	1.16
Micro-machined	598-12	200	8726	4,700	1550	1040	1.49	1700	0.91
Micro-machined	598-13	200	12697	6,502	1790	1040	1.72	1700	1.05
			Average	4962	1727	1040	1.66	1700	1.02
			STD	1268	171	n/a	n/a	n/a	n/a

An important characteristic of all nine (9) specimens was that the fracture was dominated by the conical features. Figure 32 provides a representative fracture surface, in this case specimen 598-5. Additionally, Figure 33 provides the pre- and post-fracture top view of specimen 598-5.

Figure 32: Fracture surface for micro-machined specimen 598-5

Figure 33: Pre- and post-fracture top view of specimen 598-5

In all cases, one of the two conical features was the feature from which the cycles were measured. At the July 18, 2007 meeting at UDRI, it was decided by the group to continue examination of the fracture surfaces of all features, not just the feature which reached CI first. Each feature can then be independently represented in terms of CI cycles, providing additional experimental data.

4) Note on the Influence of R=0.7 Cycles on Crack Propagation

The following quote is a justification by NAVAIR for the removal of the R=0.7 cycles from the prediction ("Micromachined Specimen Life Predictions", dated July 9, 2007):

"For the constant-amplitude marker cycle spectrum block used in the micromachined specimen tests, the R = 0.1 load cycles result in an equivalent fatigue damage rate that is about 5 times greater than the R = 0.7 load cycles. Therefore, the life predictions shown here only represent the damage accumulated from R = 0.1 cycles, with the R = 0.7 cycles ignored. When comparing test results to the life predictions, all of the R = 0.7 cycles must be eliminated from the final cycle count to crack initiation for each test."

To verify this statement, ESRD performed a simple evaluation of the relative influence in crack propagation rates for the R=0.1 and R=0.7 cycles. The results are summarized in Figure 34, in which v_1 represents the crack propagation rate associated with the R=0.1 cycles and v_2 with the R=0.7 cycles. The value of n in the crack propagation law was determined experimentally by UDRI for the AF1410 steel to be $n = 1.944$. Using the average values of cycles shown in Table 3, it was found that the contribution of the R=0.7 was approximately 1/5th of the R=0.1 cycles.

$$v_1 = \left(\frac{da}{dN}\right)_1 = C(\Delta K_1)^n \qquad\qquad v_2 = \left(\frac{da}{dN}\right)_2 = C(\Delta K_2)^n$$

$$\Delta K_1 = \Delta\sigma_1\sqrt{\pi a} \qquad\qquad\qquad \Delta K_2 = \Delta\sigma_2\sqrt{\pi a}$$

For $R = 0.1 \rightarrow \Delta\sigma_1 = 0.9\sigma_{max}$ *For $R = 0.7 \rightarrow \Delta\sigma_2 = 0.3\sigma_{max}$*

$$\frac{v_1}{v_2} = \left(\frac{0.9}{0.3}\right)^n = 3^{1.944} = 8.46$$

Average total cycles = 4962
Average R=0.1 cycles = 1727 -> 0.010" crack
Average R=0.7 cycles = 3254 -> 0.002" crack (or 20%)

Figure 34: Estimation of the contribution of the R=0.7 cycles to crack initiation

5) Summary

The micro-machined specimens were originally designed to serve a discovery experiment. All the features perpendicular to the load were designed to have the same Kt, however the fatigue failure initiated in the same feature type (conical) in all 9 fatigue tests, clearly indicating that the Kt alone is not the characterizing parameter for failure initiation. As expected, the fatigue notch factor Kfc is the characterizing parameter in determining the life reduction when compared with an un-notched specimen. It should be noted however that the Kfc of the conical feature (crack initiation site for all 9 fatigue specimens, Kfc = 1.888 for Peterson Beta) is smaller than that of the ellipsoidal feature (Kfc=1.977 for Peterson Beta). One possible explanation for this apparent inconsistency is that the specimens had a thin layer of surface compressive residual stresses before micro-machining the features and the cones (0.035-in deep) penetrated that residual stress layer more that the ellipsoid (0.0125-in deep) and therefore the crack initiation site was located in a region with less beneficial compressive residual stresses than that of the ellipsoidal features.

Later in the project it was decided that the tests of micro-machined specimens could be viewed as a validation experiment, to test the predictive capabilities of the ESR probabilistic life prediction model. Both predictions (Peterson Nominal and Peterson Beta) are consistent with the observed crack initiation cycles, with a ratio of measured (N_m) and predicted (N_p) greater than one (N_m/N_p=1.66 for Peterson Nominal and N_m/N_p=1.02 for Peterson Beta). Even though the CI life prediction was very close to the measured life, the ESR model identified the ellipsoidal feature as the main contributor while the experiments showed the conical feature to be dominant. Again, one possible explanation for this is that the ESR model does not account for residual stresses in the computation of Kfc. An additional source of uncertainty is that the micromachined specimens were taken from the tabs of previously fatigue tested specimens.

9.5 ESRD Validation Task #9 Final Report

StressCheck Arrestment Hook Model
Summary of Development and Validation Efforts
Validation Task #9
June 27, 2007
Report Prepared By: Brent Lancaster, Ricardo Actis & Barna Szabo

1) Introduction

ESRD performed finite element analyses of the AF1410 arrestment hook shank, for typical arrestment and hook bounce load cases, with the purpose of determining the stress distribution for a specific region inside the bore of the shank. For each load case, the prediction of the strains at gage locations was compared against experimental strain data provided by NAVAIR. For each load case, a mathematical model was constructed to determine the strain and stress distributions in the region of interest. For the arrestment load case, the original model was not acceptable because it could not represent the strain-gage test data well (see Section 4). The model was revised and the results compared with the experimental data. The modeling approaches, assumptions and FEA results are described in the following. The p-version FEA code StressCheck was used for all of the calculations. The geometric description of the arrestment shank was obtained from drawings provided by NAVAIR (reference drawings 74A480001 and 74A480617), and the following material properties were used for the analyses: E=29.4e6 psi, ν=0.31.

2) Modeling Case 1: Arrestment Load
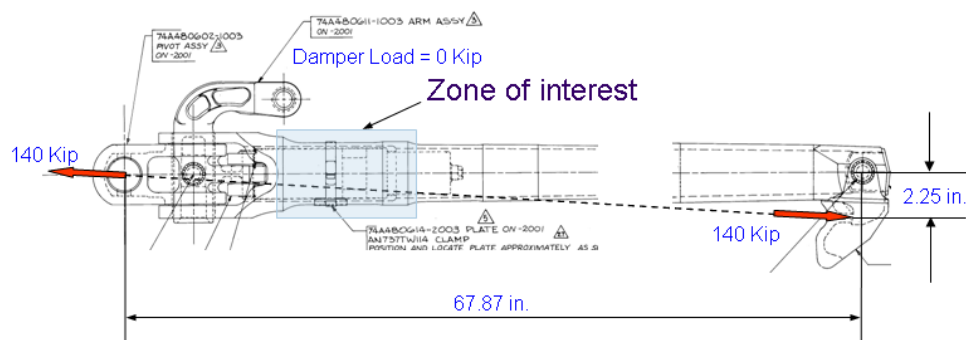
Figure 35: Arrestment load case configuration

2.1) Modeling Approach & Results

In the arrestment load case, a 140 kip axial load is applied to the hook end and reacted through the assembly connection. The model consisted in a 2D representation of the complete shank to determine the moment (M), shear (V) and normal (N) forces at a location close to the region of interest (Section B-B in Figure 36).
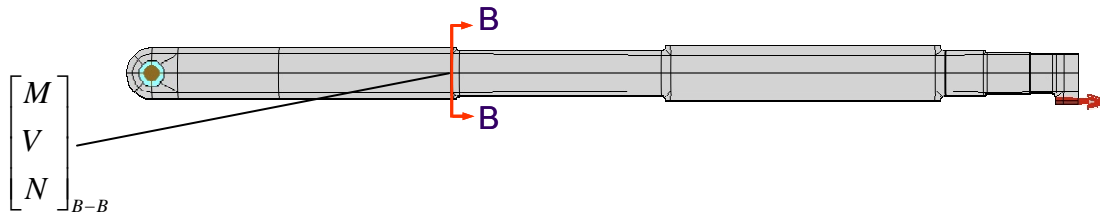
Figure 36: 2D representation of the tail hook for the arrestment load case.

In this 2D model (plane strain) the height and thickness of each section was determined so as to maintain the same cross-sectional area and moment of inertia of the different regions of shank. Figure 37 shows the thickness variation to accomplish this. This model is appropriate to obtain the deformed configuration, the moment, axial force and shear force at Section B-B.
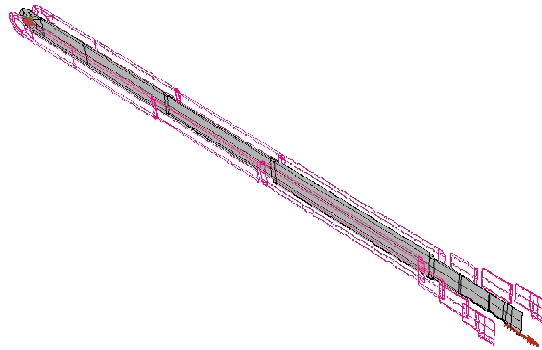
Figure 37: Thickness variation for the 2D model of the tail hook.

The prescribed boundary conditions for the 2D representation of the arrestment load case are given in Figure 38. A fastener element was used to simulate the pinned connection while a distributed traction was used to apply an axial load of 140100 lb to the hook end. A nodal constraint was used to prevent rigid body motion (RBM). The center of the fastener was constrained in two orthogonal directions.

Fastener constraint

Node constraint and load
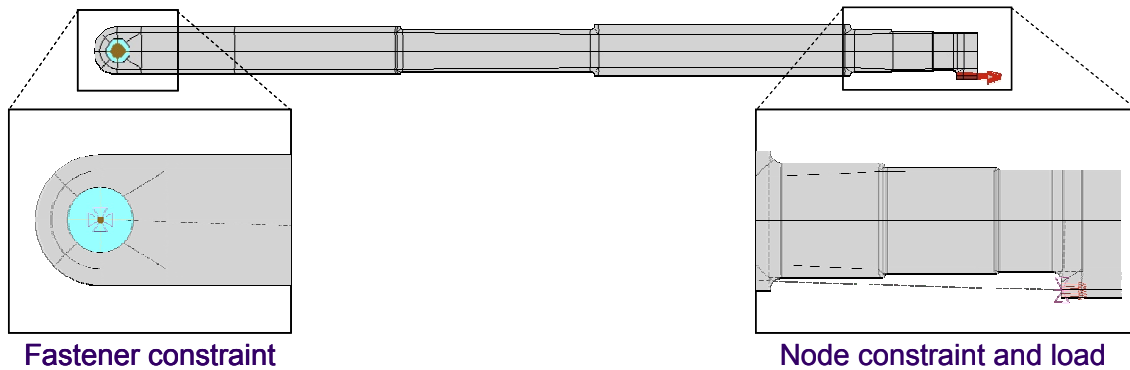
Figure 38: Boundary conditions for 2D representation of the arrestment load case.

First, a linear analysis was performed by p-extension. After a linear analysis was performed, it was determined from the results that geometric nonlinear effects could not be ignored. Therefore, a geometric nonlinear analysis was performed in order to account for the redistribution of load due to the coupling between axial and bending. The moment diagram and vertical displacements for the linear and geometric nonlinear solutions are shown in Figure 39. Additionally, the moment, shear force and normal force at Section B-B located at 22.4-in from the center of the fastener are shown in the table of Figure 39.

Section B-B (x = 22.4 in)		
Load		
Axial (N)	Shear (V)	Moment (M)
140100 lb	-4203 lb	23750 lb in

Moment diagram

Deformed configuration
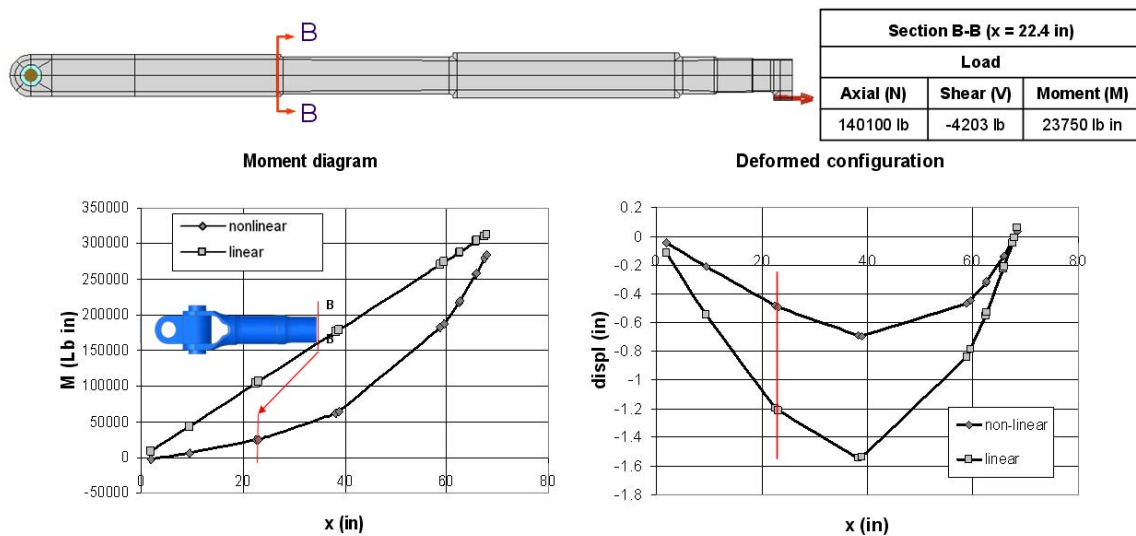
Figure 39: Moment diagram and deformed configuration for the arrestment load case.

A-51

Since the moment variation is nearly linear from the center of the fastener to Section B-B, it was assumed that the stress distribution in the region of interest could be determined by solving a local 3D-contact problem of the shank. The solution for the local 3D model was obtained using as loads the moment, shear and axial forces computed from the 2D solution at Section B-B (Figure 40). These loads were applied as distributed tractions and the local model included the nonlinear effect of contact between the pivot and arm assemblies. Since the loads obtained from the 2D nonlinear solution were computed from the deformed configuration, and the local 3D-contact solution considers the undeformed configuration, the shear force was adjusted so that the net moment at the center hole of the pivot was zero. This was expected to introduce no significant changes in the magnitude and distribution of the stresses in the region of interest, since the shear force obtained from the 2D geometric nonlinear analysis (-4203 lb) is a small fraction (3%) of the applied axial load (140100 lb).
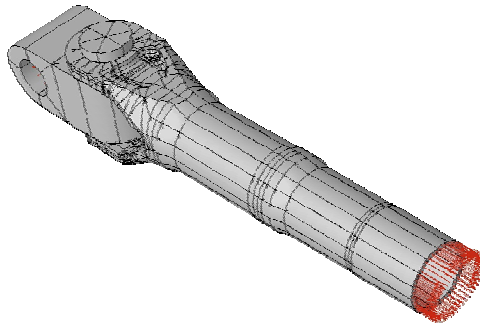
Figure 40: 3D Local model of the shank with loads applied at section B-B.

As is shown in Figure 40, the moment (23750 lb-in), adjusted shear force (-1060 lb) and normal force (140100 lb) at Section B-B have been converted into the equivalent traction distributions over the circular cross section. To enforce equilibrium conditions, a sinusoidal bearing load of axial resultant 140100 lb was assigned to the bore of the pivot. Contact zones were specified between the pin and clevis of the shank, and between clevis and pivot. A contact solution was performed, and the stress distribution in the region of interest was extracted. Figure 41 shows the maximum first principal stress ($\sigma_{1\max}$) in the inner bore of the shank while Figure 42 shows the $\sigma_{1\max}$ on the outer surface of the shank in the region of interest.

Max = 1.289e+005
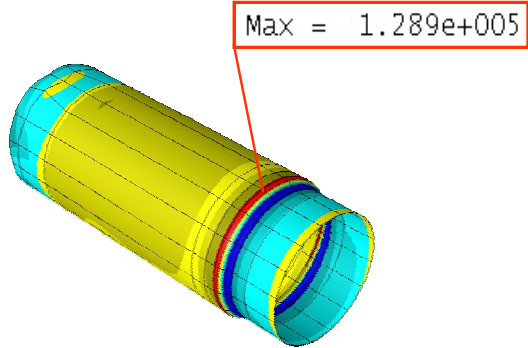
Figure 41: Value of $\sigma_{1\max}$ in the inner bore of the region of interest for the local contact model.

Max = 1.363e+005
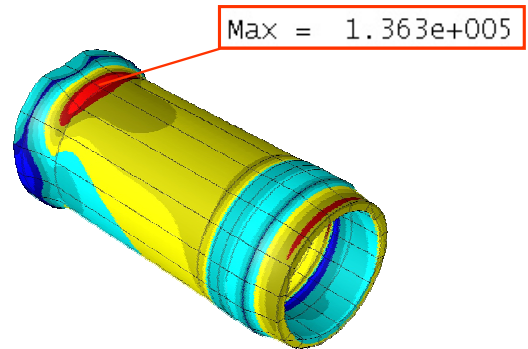
Figure 42: Value of $\sigma_{1\max}$ in region of interest for the local contact model.

Two more cases were considered for the local model to determine whether the complexity of the model could be reduced without significantly affecting the stress distribution in the region of interest. The second model involved the removal of contact considerations in favor of distributed springs at the clevis (Figure 43). In doing so, the model complexity was significantly reduced as it is no longer a nonlinear problem due to the contact. The goal was to determine if the effect of this additional modeling reduction was significant on the inner bore $\sigma_{1\max}$. As can be seen in Figure 44 and Figure 45, the effect is not significant and therefore the simpler model without contact could also be used for the local analysis.
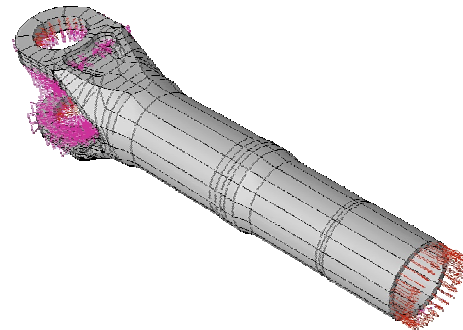
Figure 43: 3D local model without contact.
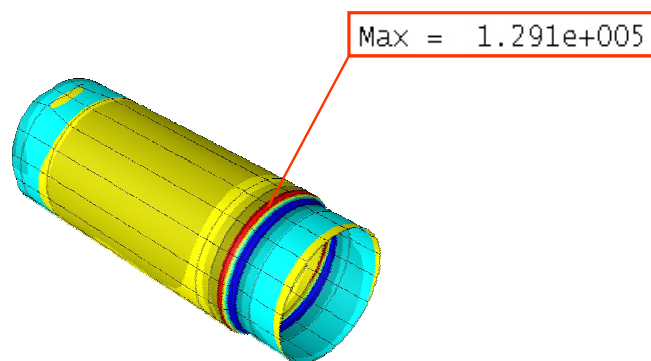
Figure 44: Value of $\sigma_{1\max}$ in the inner bore region for the local model without contact.
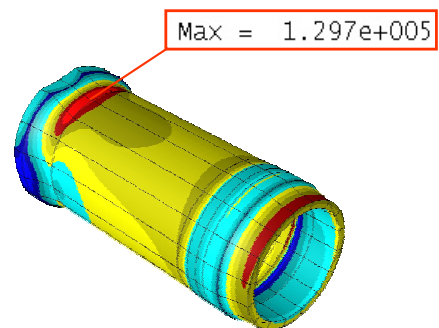
Figure 45: Value of $\sigma_{1\max}$ in the region of interest for the local model without contact.

One more simplification of the local model was considered, consisting of the removal of the entire clevis portion of the model in favor of distributed springs at the cross-section. Again, the goal was to compare the results with those obtained for the local contact model to determine the effect on the stress distribution in the region of interest. As can be seen in Figure 46, the influence of the simplification does not affect the value of $\sigma_{1\max}$ substantially.
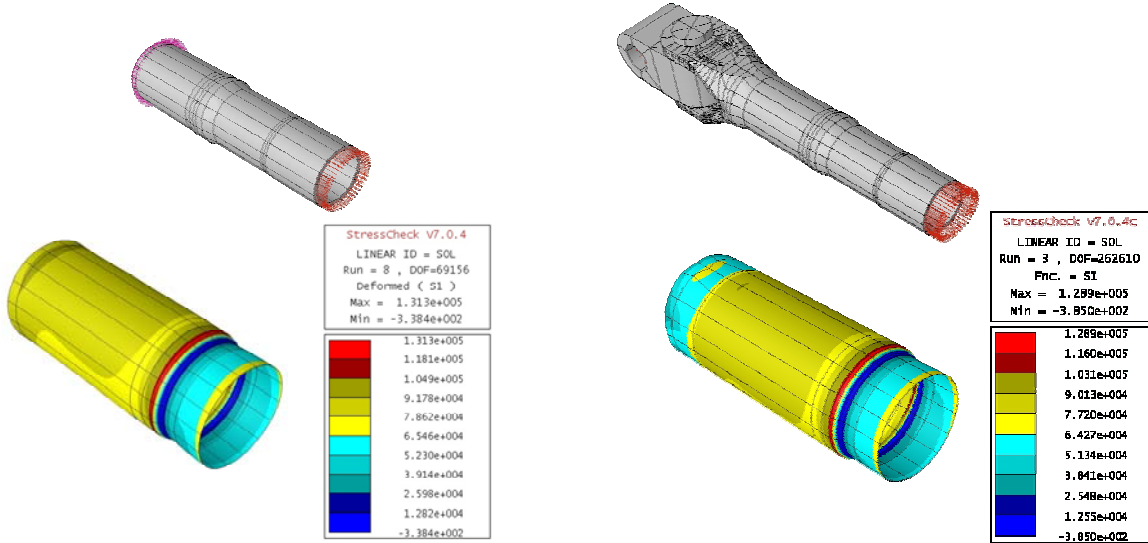
Figure 46: Comparison of $\sigma_{1\max}$ in the inner bore: Contact model (right) and simplified model (left).

In summary, it is shown that for the arrestment load case, the local contact model and the two local models without contact will give an approximation for the axial stress distribution (in the region of interest) very close to one another.

3) Modeling of Case 2: Hook Bounce Load
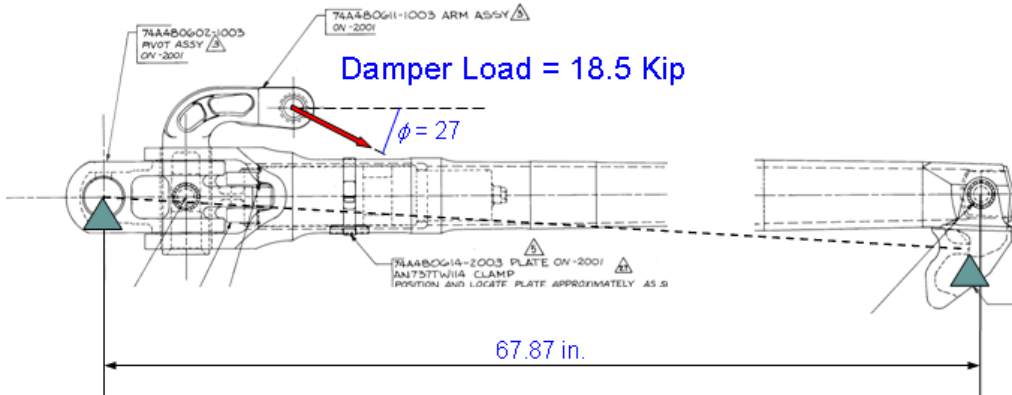
Figure 47: Hook bounce load case configuration.

3.1) Modeling Approach & Results

In the hook bounce load case an 18.5 kip damper load is applied to the pivot arm at a 27 degree angle to the horizontal as shown in Figure 47. The modeling approach for the hook bounce load case was very similar to the arrestment load case. A 2D model of the complete shank was used to determine the resultants at Section B-B and these loads were applied as traction distributions in a 3D local model of the clevis end. To simulate the forces and moments generated at the arm assembly, a set of equivalent traction distributions were applied at section B-B. A vertical traction was then introduced at the hook end to represent a simply-supported reaction condition, and a fastener element was used to simulate the contact between assemblies. The 2D model for the hook bounce load case is shown in Figure 48. The resultant moment and shear force at section B-B are shown in Table 4. As expected, the moment at Section B-B is far more dominant in the hook bounce load case than for the arrestment load case (92700 lb-in versus 23750 lb-in, respectively).

Fastener constraint and load

Node constraint and load
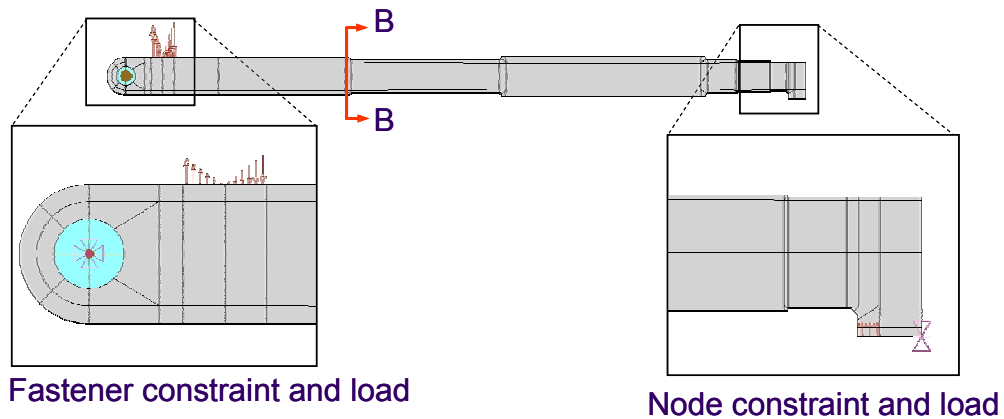
Figure 48: 2D model for the hook bounce load case.

Table 4: Resultant moment and shear force at section B-B for the hook bounce load case

Section B-B (x = 22.4 in)		
Load		
Axial (N)	Shear (V)	Moment (M)
0 lb	2016 lb	92700 lb in

Similar to the modeling approach used in the arrestment load case, the loads given in Table 4 were converted to equivalent tractions and applied to 3D local models at Section B-B. The most complex of the 3D local models included contact at the clevis end between the pivot, damper arm, and clevis (Figure 49). The least complex of the 3D localized models did not consider contact or the clevis geometry as distributed springs were used to model the stiffness at the clevis end (Figure 50). Again, the goal was to determine if the simplified local model could accurately capture the inner bore $\sigma_{1\max}$ given by the local model with contact. Comparing Figure 51 and Figure 52, both cases give practically the same value for $\sigma_{1\max}$ (108 ksi). It will also be shown in the Validation section, that the axial strains given by the model are strongly correlated with available experimental strain information.
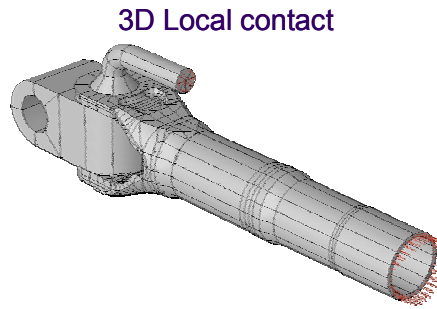
Figure 49: 3D Local model with contact for the hook bounce load case.
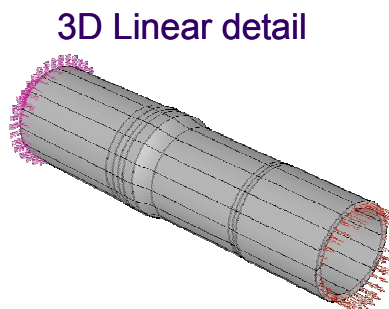
Figure 50: Simplified 3D local model for the hook bounce load case.
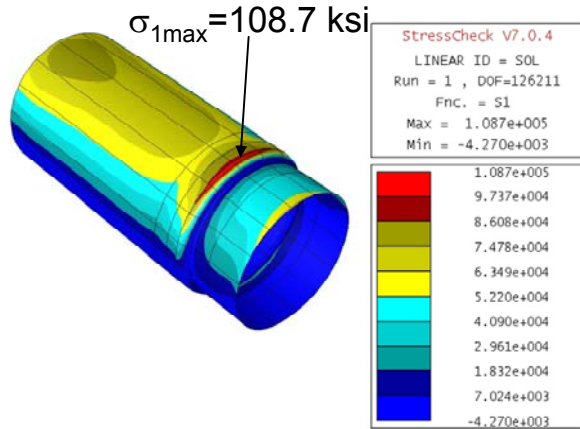
Figure 51: Extraction of $\sigma_{1\max}$ **in the inner bore region for the local contact model.**
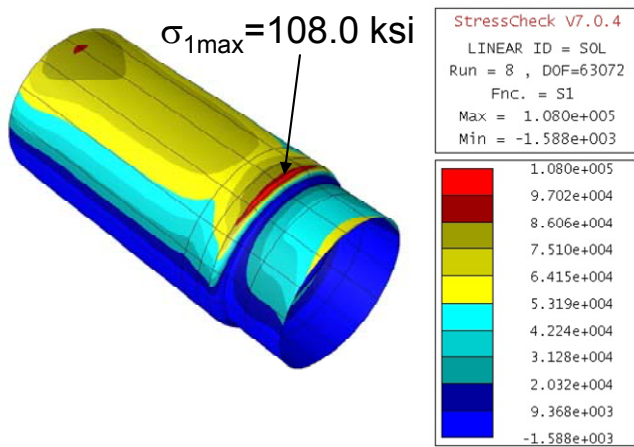
Figure 52: Extraction of $\sigma_{1\max}$ **in the inner bore region for the simplified local model.**

4) Validation: Comparison of StressCheck results with experimental strain surveys

Validation involves one or more metrics and corresponding criteria. In this case the metrics are the strain gage readings at certain location within the region of primary interest (Figure 53). The criteria should be understood as criteria for rejection. Formulation of the criteria depends on the intended use of the model and the accuracy required. The model is rejected if any one of the criteria is not met. Setting the criteria properly for a validation experiment is very important. If the criteria are overly stringent then a valid model may be rejected. If the criteria allow large differences between the predicted and measured metrics then invalid models may not be rejected. In this case the criteria were based on the estimated repeatability of experimental data. Specifically

1. In regions of shallow strain gradients, differences between measured and predicted strains must be 5% or less.

2. In regions of large strain gradients, differences between measured and predicted strains can be larger than in item 1 above, and are to be evaluated on a case-by-case basis. The intent is to estimate the repeatability of strain measurements.
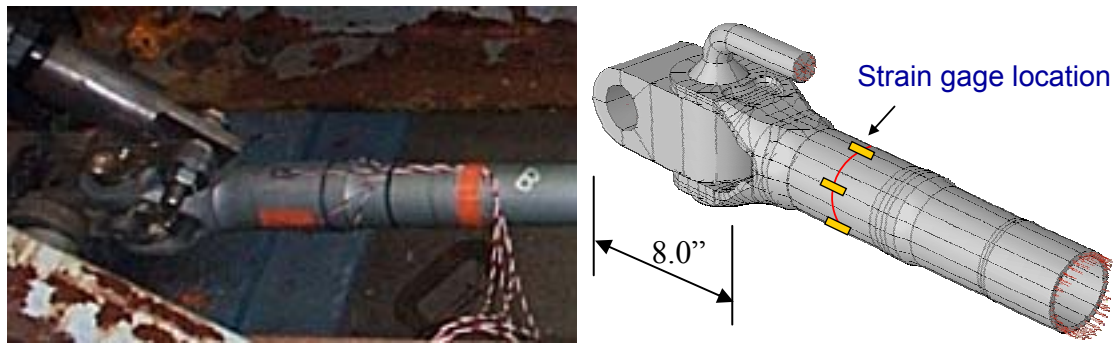
Figure 53: Strain Gage Locations

4.1) Hook Bounce Load Case Validation

For the hook bounce load case, the numerical predictions based on the 3D local model shown in Figure 53 compared well against available experimental results (Figure 54). These results give confidence that the mathematical model used for representing the hook bounce load meets criterion 1.
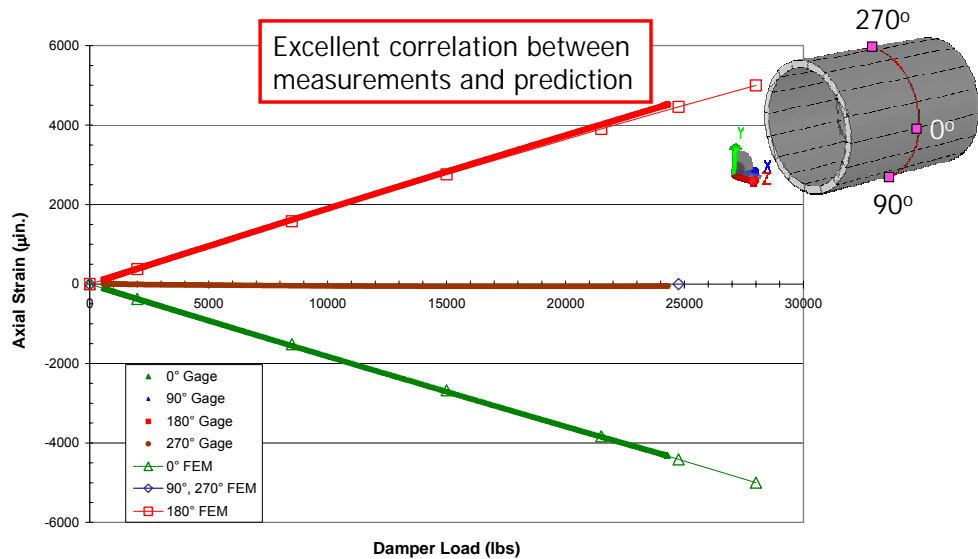
Figure 54: Model validation - Comparison of predicted and measured axial strains at 4 locations for several values of the hook bounce (damper) load.

For example, at a compressive damper load of -24293 lbs, the average strain gage reading for the 0 deg. gage was -4312 μ, while the FEM prediction was -4331 μ (a difference of only 0.44%). The strain gage readings for the maximum test load (-24293 lb) and the comparison with the predictions are summarized in Table 5.

Table 5: Strain gage readings and FEM predictions at two locations for a damper load of -24293 lb

	Strain [μ in/in]	
Condition	**0° gage**	**180° gage**
Run #1 reading	-4318	4518
Run #2 reading	-4312	4512
Run #3 reading	-4306	4512
Average	-4312	4514
FEM Result	-4331	4381
(FEM-Avg)/Avg *100	0.44%	-2.95%

4.2) Arrestment Load Case Validation

For the arrestment load case, the numerical predictions of the axial strains given by the 3D local model shown in Figure 55 and the strain gage survey at 8 circumferential locations for an arrestment axial load of 137 kip are shown in Figure 56. There is substantial difference between predicted and experimental strain values for the locations in the upped half of the shank, with a maximum difference of 19% for the strain gage located at the top. Therefore, based on the stated criteria, the model has to be rejected.
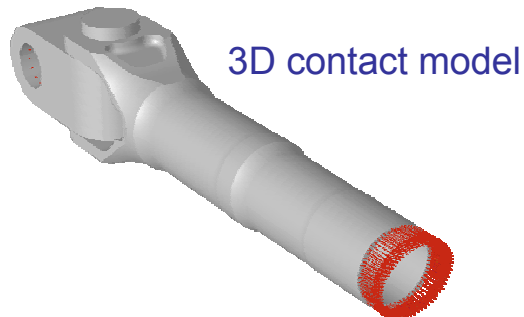
3D contact model

Figure 55: Arrestment load case 3D local contact model.
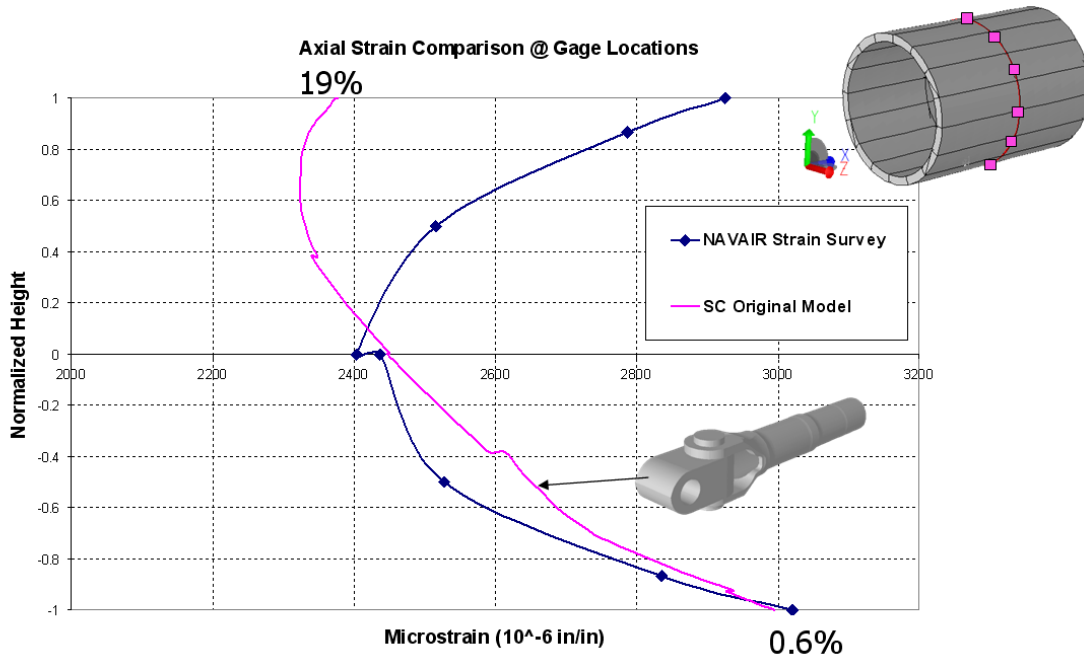
Figure 56: Validation of Arrestment Load Case (3D local contact model). Axial Strains for 137 kip axial load.

The model was reevaluated to determine the reason for rejection. A modification to the original modeling approach was investigated as described in the following.

5) Updated Model: Full Arrestment Hook with Geometric Nonlinearities

The evaluation of the modeling strategy indicated that the combination of a 2D geometric nonlinear model with a 3D local contact model was responsible for the observed difference between prediction and experiments. Because the bending moment computed from the 2D-model, from Section B-B to the pinned connection, decreased to zero linearly, it was assumed that the shear at section B-B of the local 3D-contact model could be adjusted proportionally to equilibrate the moment (Figure 39). This implied that a linear model, albeit with boundary conditions resulting from a geometric nonlinear analysis, was sufficient to represent the behavior of the shank from Section B-B to the pinned connection. However, at the axial location of the strain gages the magnitudes of the axial strains were not consistent with prediction, with significant underestimations occurring at the top of the shank (Figure 56). Therefore, this linear model does not adequately capture the axial strain distribution between Section B-B and the pinned connection given this loading condition due to the strong coupling between bending and membrane strains.

To overcome this problem, the full tail hook must be modeled and solved incorporating both contact and geometric nonlinear analysis. Because geometric nonlinear analysis with contact is outside the current capabilities of StressCheck, a simplified approach was considered. A full 3D-model of the tail hook assembly was created with the components in the contact region "fused" together (all elements connected), and a geometric nonlinear analysis performed for the arrestment load case. The updated StressCheck arrestment hook model is shown in Figure 57. The elements of the gold-colored region are fused to the clevis bore, and a 137 kip axial load was applied to the element faces at the hook end as shown in the figure.
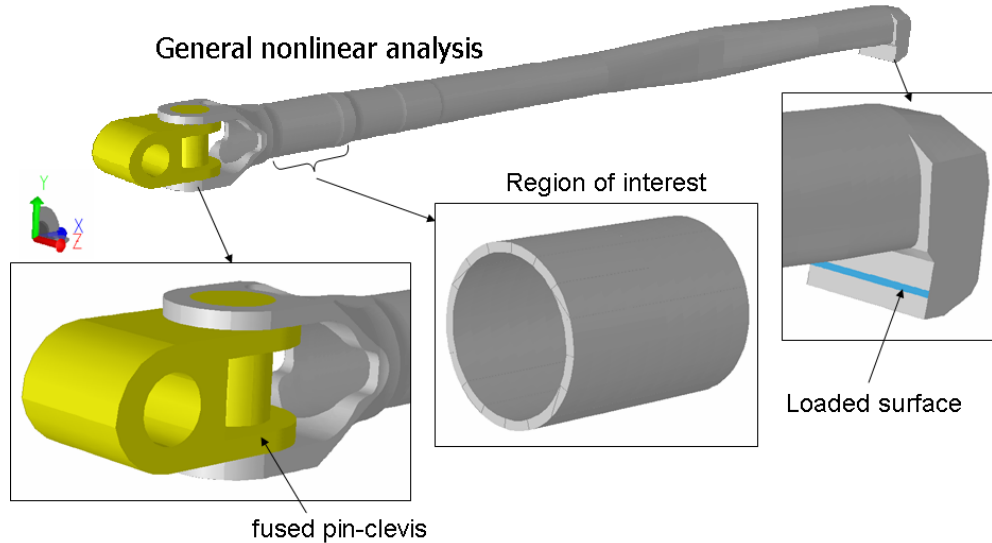
Figure 57: Full 3D arrestment hook model with fused pin-clevis.

The solution to the updated model, which included geometric nonlinear effects, was compared to the previous solutions for the arrestment load case (Figure 58). Observe that the incorporation of the geometric nonlinear effects (light blue curve) improved the overall shape of the axial strain distribution when compared to the strain survey results. For example, at the bottom surface the strain gage measurement was 3017 μ in/in while the FEM prediction was 2940 μ in/in (a difference of 2.6%), and at the top surface the strain gage measurements was 2922 μ in/in while the FEM prediction was 2570 μ in/in (a difference of 12%). These are regions of high stress gradient through the shank thickness and therefore the second criterion is applicable. Also superimposed in the graph are the predicted strains from the 3D-local contact model in which the bending moment was removed and only the axial load was applied at section B-B (green curve). This was studied as a limiting case in order to show the influence of bending in the strains values at the survey location. The results for the top, bottom and center locations are summarized in Table 6, where the % difference between the average strain gage reading and the

prediction of a particular model is shown bracketed next to the prediction. The % difference is computed as (Avg. reading - prediction)/Avg. reading x 100.
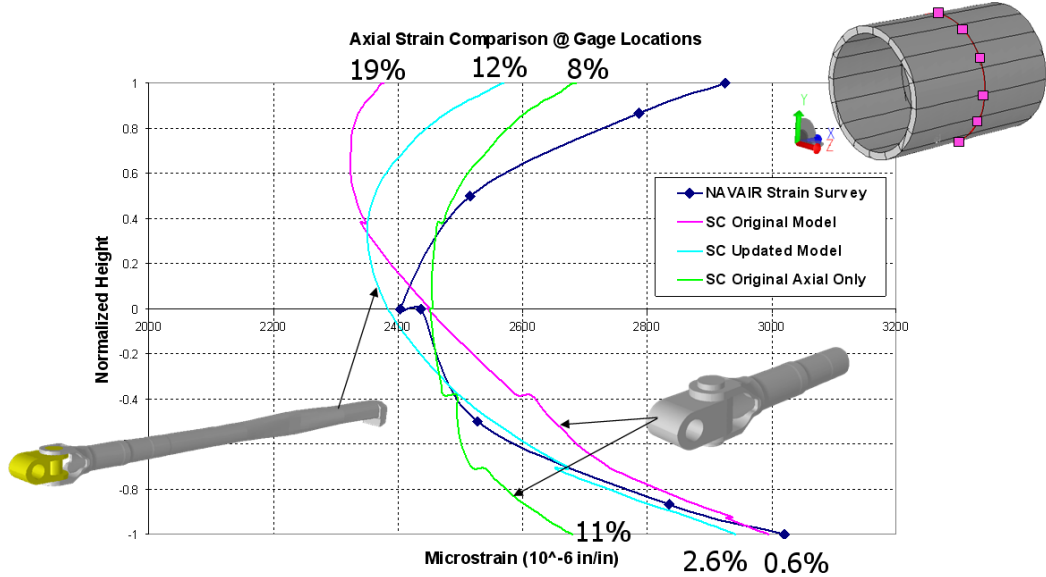
Figure 58: Comparison of predicted axial strains and strain survey results (axial load of 137 kip).

When comparing the axial stress distributions in the region of primary interest of the updated model with the original 3D-local contact model, it can be seen that there is a small difference in both the distribution of the stress and the magnitudes (Figure 59). Therefore, though the maximum predicted axial strains on the outer surface of the shank are quite different for both models, the magnitude and distribution of axial stresses in the inner bore are not as sensitive to the modeling assumption (less than 1% difference).

Table 6: Strain gage reading and FEM predictions at three locations. Arrestment load case (137 kips)

Condition	Strain [μ in/in]			
	Top	**Center 1**	**Center 2**	**Bottom**
Run #1 reading	2922	2432	2400	3013
Run #2 reading	2921	2430	2400	3018
Run #3 reading	2922	2429	2400	3019
Average	2922	2430	2400	3017
FEM original	2380 (19%)	2450 (-0.8%)	2450 (-2.1%)	3000 (0.6%)
FEM original - Axial only	2690 (8%)	2460 (-1.2%)	2460 (-2.5%)	2680 (11%)
FEM modified	2570 (12%)	2380 (2.1%)	2380 (0.8%)	2940 (2.6%)
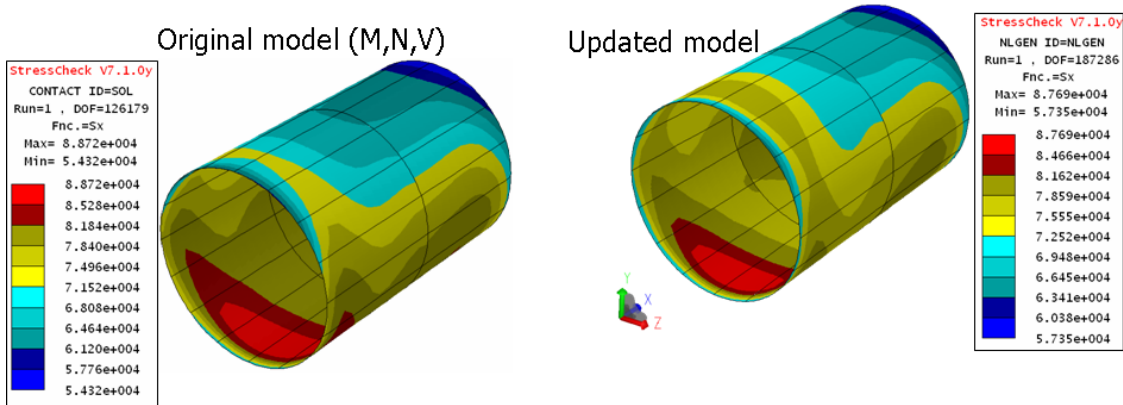
Figure 59: Inner bore axial stress distribution for the original and updated models.

Finally, Figure 60 shows convergence information in the region of primary interest. The general nonlinear solution of the full 3D-model of the assembly was obtained for p-levels 5, 6, and 7, and the axial strain distribution along a circumference and maximum axial stress σ_x inside the bore of the region of interest were extracted for all three runs. Figure 60(a) shows the strain distribution along a circle on the outer surface of the shank (at the strain gage location) for all three runs. The results indicate a strong convergence of the strain for all the points. Figure 60(b) shows the convergence of the maximum axial stress at the inner bore of the shank in the region of interest as a function of the number of degrees of freedom (DOF). The estimated maximum for σ_x differs only by 0.14% with the value computed from the finite element solution corresponding to run #3 (p=7).

(a) ε_x strain distribution for p=5 to 7 Outside circumference

(b) Maximum stress σ_x for p=5 to 7 Inside bore
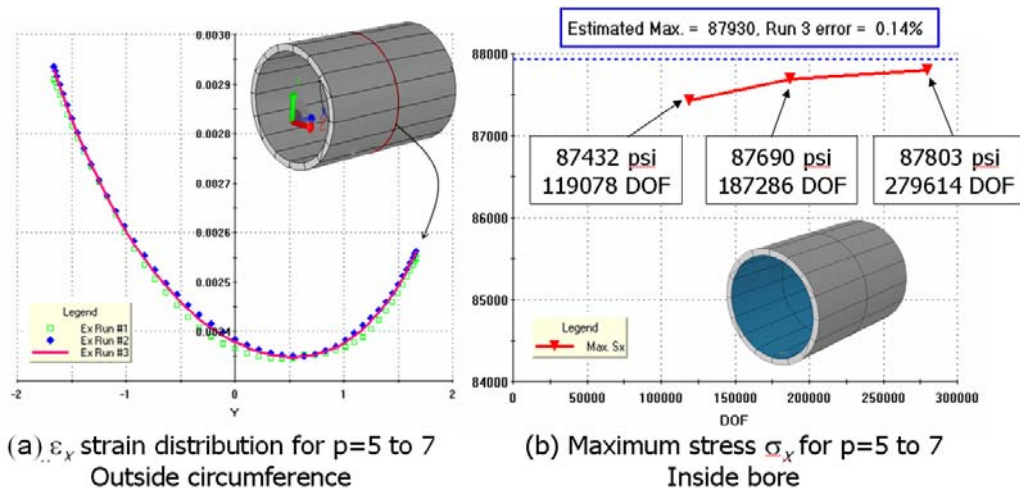
Figure 60: Convergence information for the updated 3D-model. (a) Axial strain on the outside surface for 3 FEA runs; (b) maximum axial stress in the inner bore for 3 FEA runs.

6) Summary

Verification and validation (V&V) procedures were used to evaluate the effect of modeling considerations on the axial stress distributions in the region of primary interest of the arresting hook for two load cases. Verification was accomplished by p-extension, that is, by increasing the number of degrees of freedom while keeping the mesh fixed and checking that the quantities of interests (strain and stresses) were substantially independent of the discretization parameters (mesh and polynomial order of the elements). For both load cases, the modeling approach consisted of solving a global 2D-model including contact and geometric nonlinearities, extracting stress resultants and applying them to a local 3D-contact model that did not include large deformations. The validation task consisted of comparing the predicted strains at specific locations with experimental results. It was found that while for the hook bounce load case the agreement between predicted and experimental strains was very good (within the requirements of the first criterion), the discrepancy for the arrestment load case was not acceptable.

The model for the arrestment load case was revised and modified by solving a complete 3D tail hook assembly accounting for geometric nonlinearities but ignoring the effect of contact. With the modified model the comparison between predicted and measured strains were much closer than previously and considered to have satisfied the second criterion because the strain survey area is located in a high strain gradient region. It must be noted also that while the axial strains were not as close as in the case of the bounce load, the shank inner bore axial stresses in the region of interest were very insensitive to the modeling assumptions.

The writers believe that correlation between experiment and prediction could be further improved for the arrestment load case if geometrical nonlinearities and mechanical contact could be represented in the mathematical model. The current implementation of StressCheck does not support that capability, however. It is expected that this limitation will be removed in a future version of StressCheck. Nevertheless, within the accuracy range considered useful from the point of view of the intended use of the model, no reason was found to reject the simplified model described in this report.

V-Notch Cylindrical Specimen
Computation of Kt using StressCheck
Validation Task #10
May 3, 2007

1. Background

Dave Rusk requested computation of geometric stress concentration factors (Kt) for a set of V-notch cylindrical specimen geometries and for axial and bending load cases (Figure 61). The V-notch cylindrical specimen is characterized by three (3) parameters (D1, D2, and R) and a constant value for the V-notch angle (60 degrees). The V-notch cylindrical specimen configurations considered for analysis are given in

Table 7.
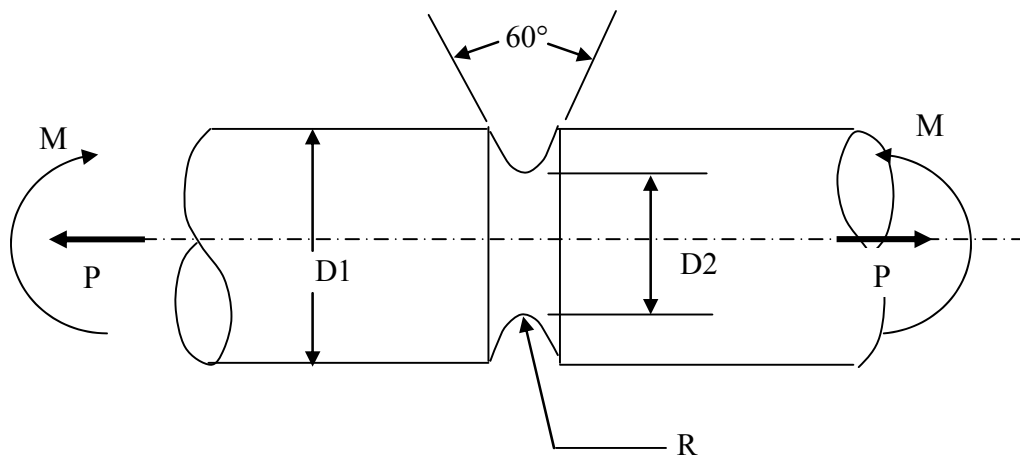
Figure 61: V-notch cylindrical specimen geometry and loading

Table 7: V-notch cylindrical specimen configurations

Case #	D1 (in.)	D2 (in.)	R (in.)	Loading
1	0.221	0.160	0.0080	axial & bending
2	0.290	0.220	0.0150	bending
3	0.400	0.215	0.0250	bending
4	0.400	0.270	0.0250	bending
5	0.220	0.180	0.0055	axial & bending
6	0.500	0.480	0.0050	bending
7	0.300	0.200	0.0120	axial
8	0.270	0.220	0.0100	axial & bending
9	0.450	0.400	0.0100	axial & bending
10	0.500	0.250	0.0400	axial
11	0.500	0.250	0.0145	axial
12	0.500	0.250	0.0042	axial
13	0.300	0.220	0.0300	axial & bending

Parametric handbook models for the V-notch specimen were developed in StressCheck (vnotchcase_quarter.sci & vnotchcase12_quarter.sci). Case 12 required an alternative meshing strategy. For each case number, and loading configuration, a Kt was computed and the quality of approximation verified by p-extension. Because of symmetry, only one-quarter of the specimen was discretized, as shown in Figure 62.
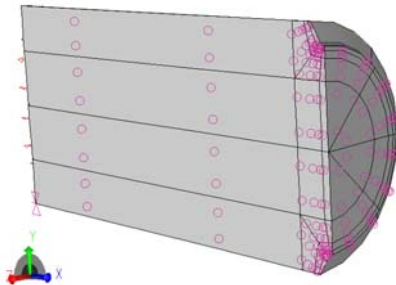
Figure 62: StressCheck Parametric Model of V-notch Specimen (One-Quarter)

The stress concentration factor is defined by the following equations:

Kt Axial: $Kt = \dfrac{\sigma_1}{\sigma_0}$ (1)

Kt Bending: $Kt = \dfrac{\sigma_1}{\sigma_b}$ (2)

Where: σ_1 is the maximum first principal stress at the notch root, σ_0 is the net section stress due to the axial load ($\sigma_0 = \dfrac{4P}{\pi D_2^2}$), and σ_b is the maximum bending stress in the net section ($\sigma_b = \dfrac{32M}{\pi D_2^3}$).

The Kt for each load case is given in Table 8. The estimated error in Kt was computed from the convergence information provided by StressCheck during the extraction of the maximum first principal stress.

Table 8: V-notch Specimen Kt Computation and Verification

Case #	Kt Axial	Kt Axial %Error	Kt Bending	Kt Bending %Error
1	3.307	0.109	2.683	-0.050
2	2.849	-0.117	2.348	-0.018
3	2.404	0.108	1.937	0.122
4	2.597	0.007	2.107	0.061
5	3.792	0.100	3.183	0.050
6	3.754	0.020	3.533	0.030
7	3.127	-0.027	2.507	0.055
8	3.219	0.060	2.705	0.040
9	3.661	0.040	3.193	0.080
10	2.107	0.015	1.727	0.021
11	3.282	0.070	2.545	0.110
12	5.849	0.070	4.448	0.170
13	2.191	0.040	1.823	0.050

9.7 StressCheck Parametric Kt Study: Cylindrical Bore with Variable Blend Radius

The following images show Kt values for various blend radii.
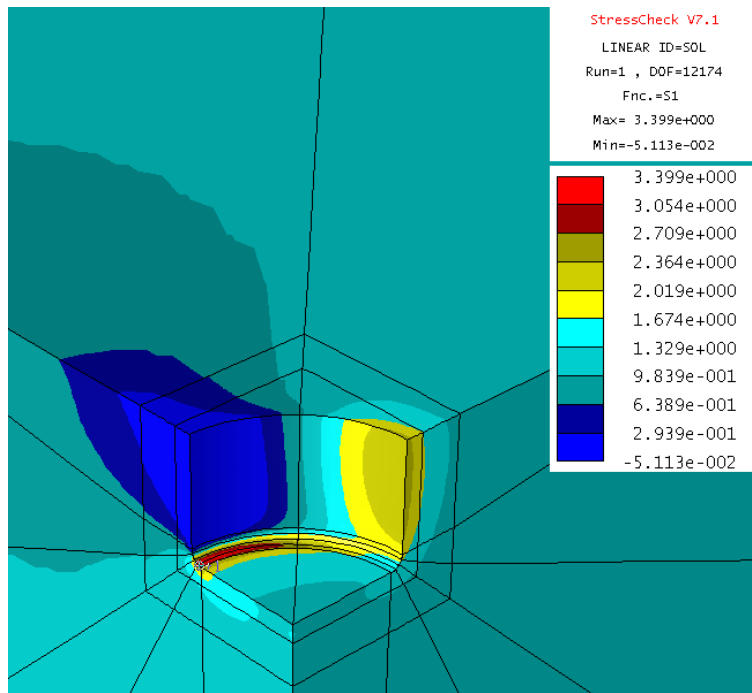
Figure 63: Kt-value for R=0.1
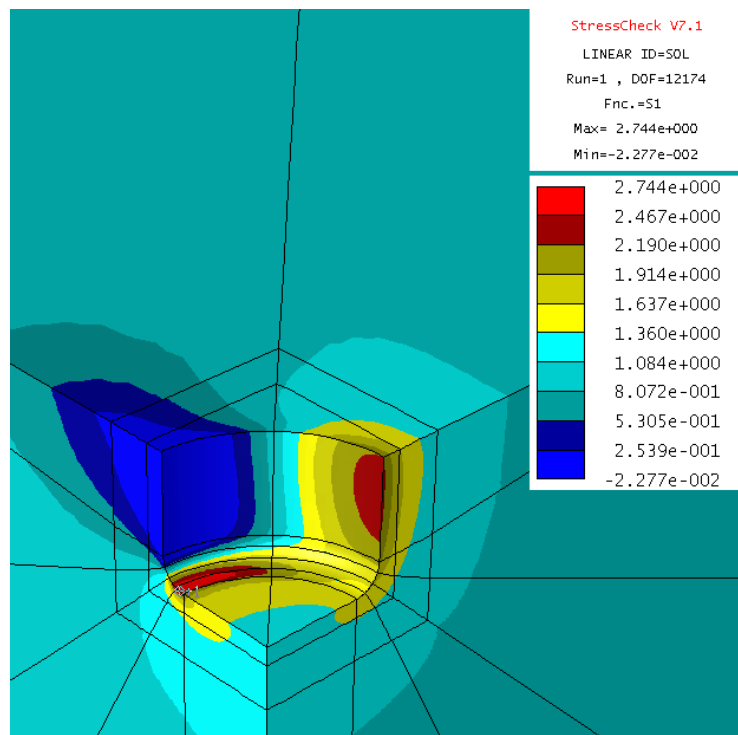
Figure 64: Kt-value for R=0.2
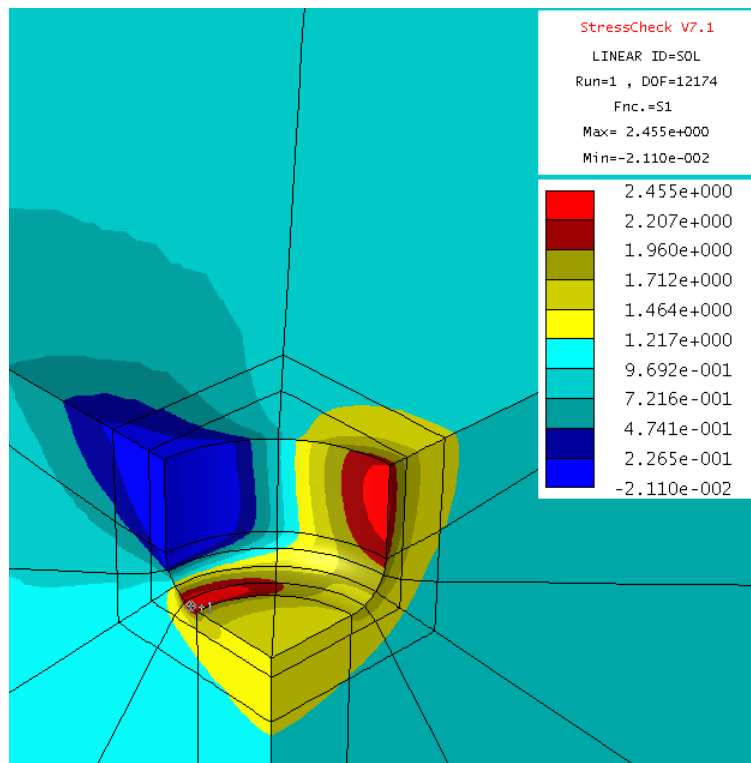
Figure 65: Kt-value for R=0.3
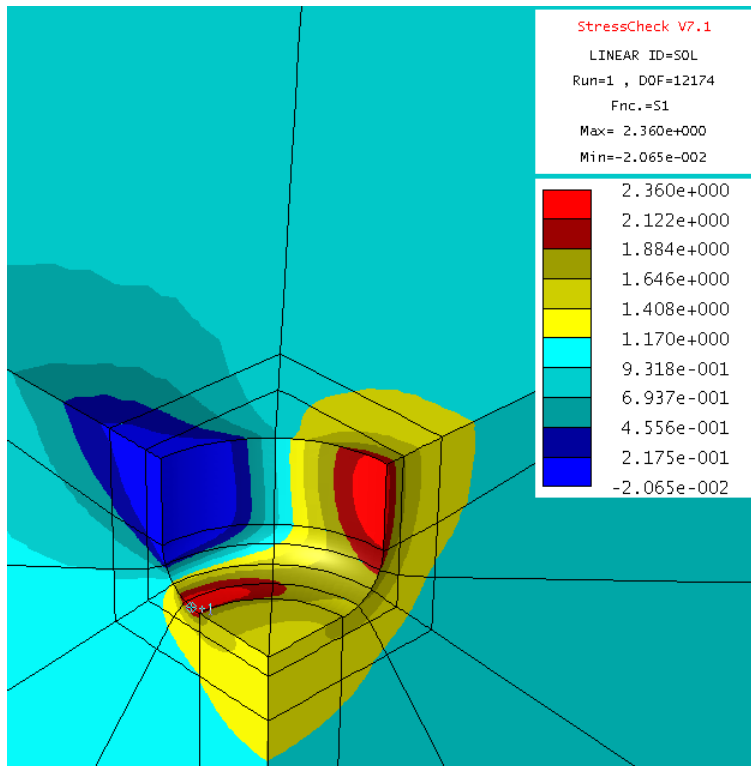
Figure 66: Kt-value for R=0.35
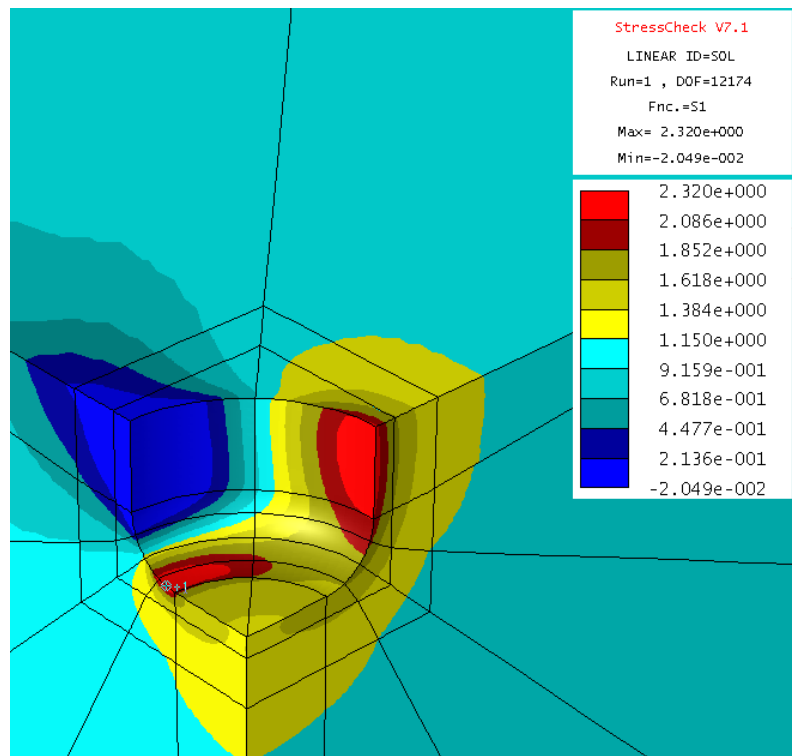
Figure 67: Kt-value for R=0.375
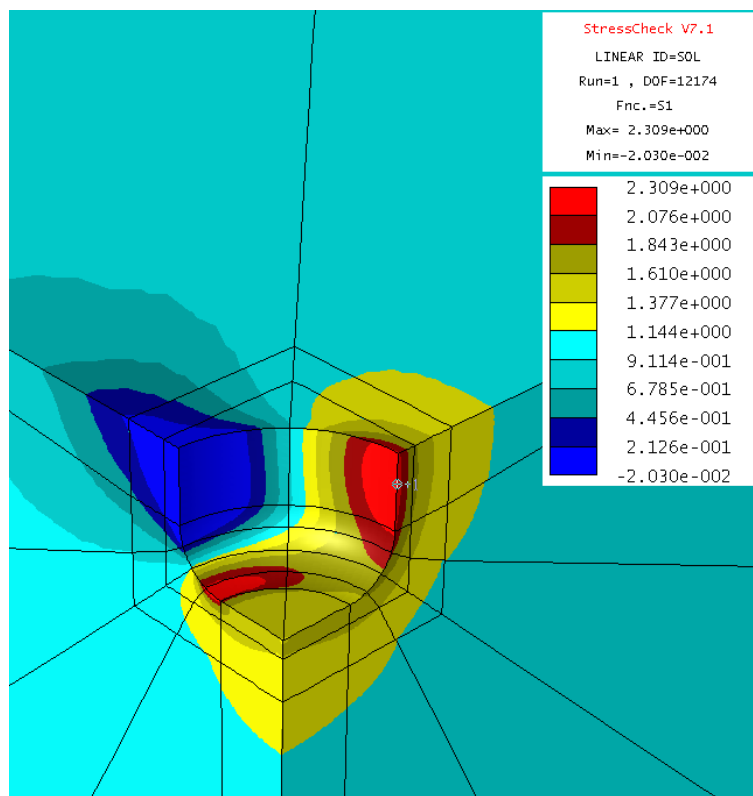
Figure 68: Kt-value for R=0.4
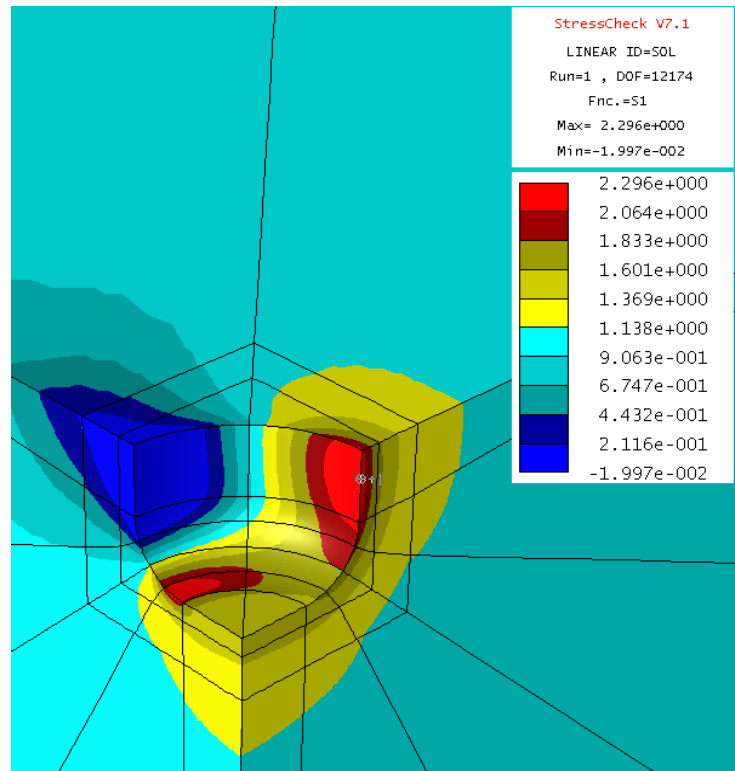
Figure 69: Kt-value for R=0.45
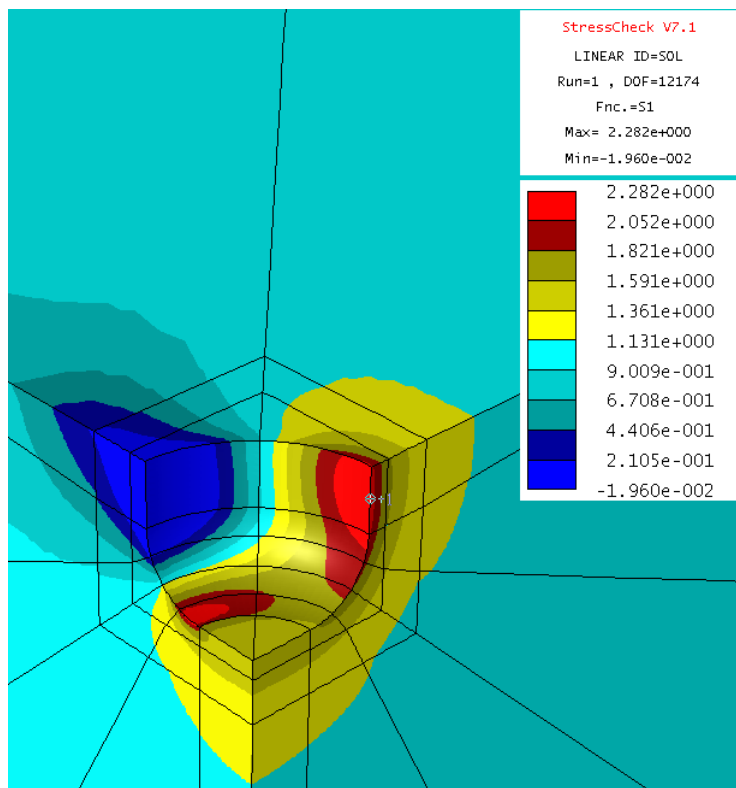
Figure 70: Kt-value for R=0.5
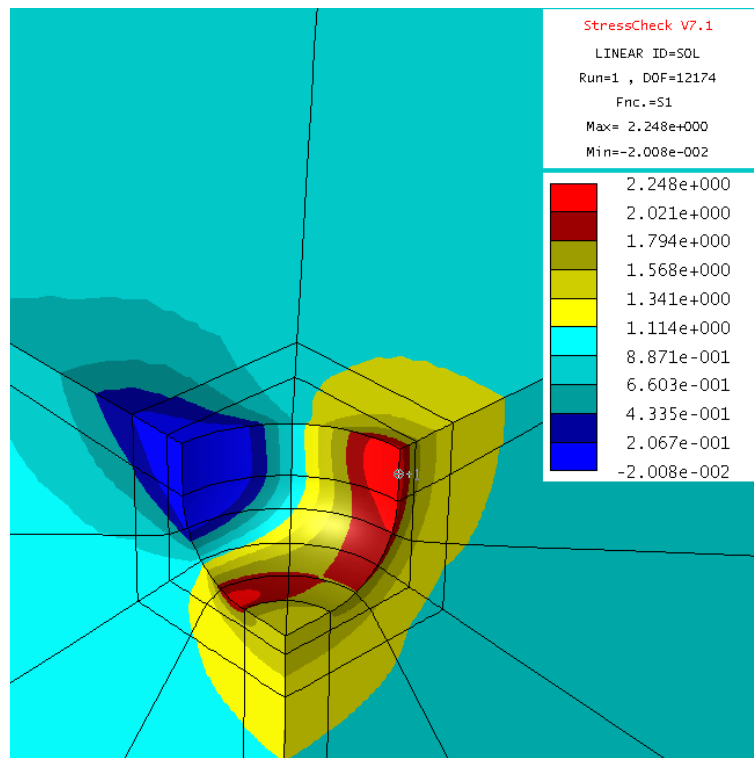
Figure 71: Kt-value for R=0.6

9.8 Kt Sensitivity Study Fringe Plots for WLI-Measured Micro-machined Dimensions
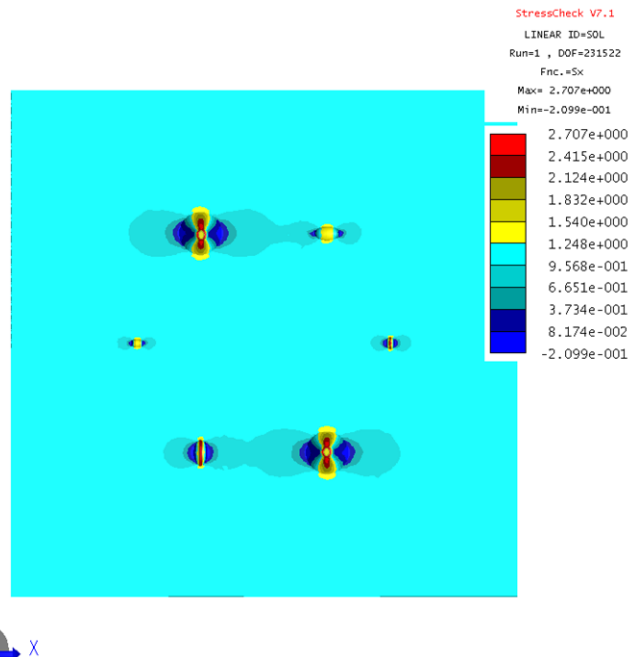
Figure 72: Fringe Plot of Kt for WLI-Measured Dimensions
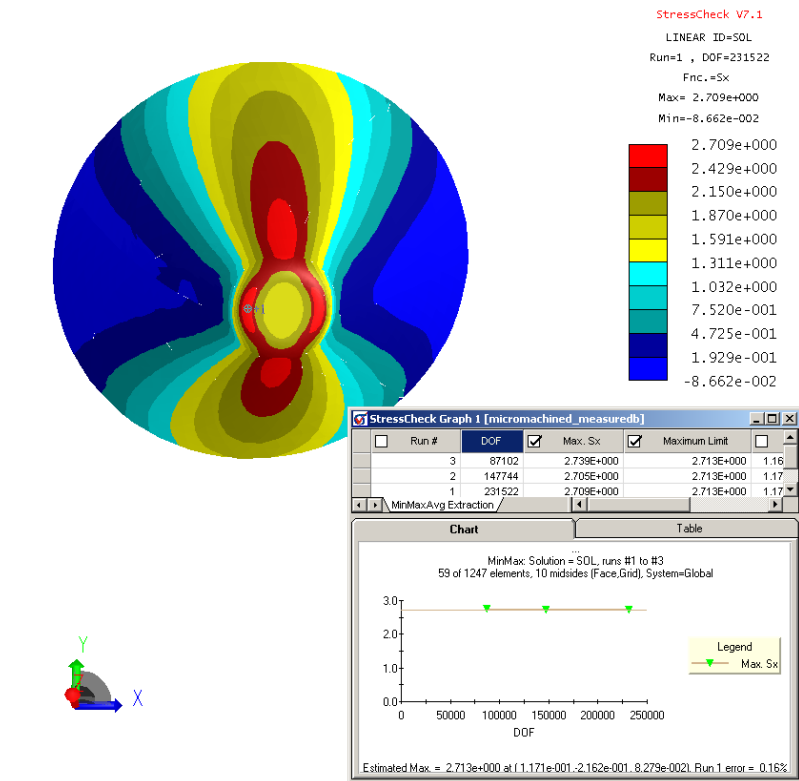
Figure 73: Convergence of Kt for the WLI-Measured Conical Feature
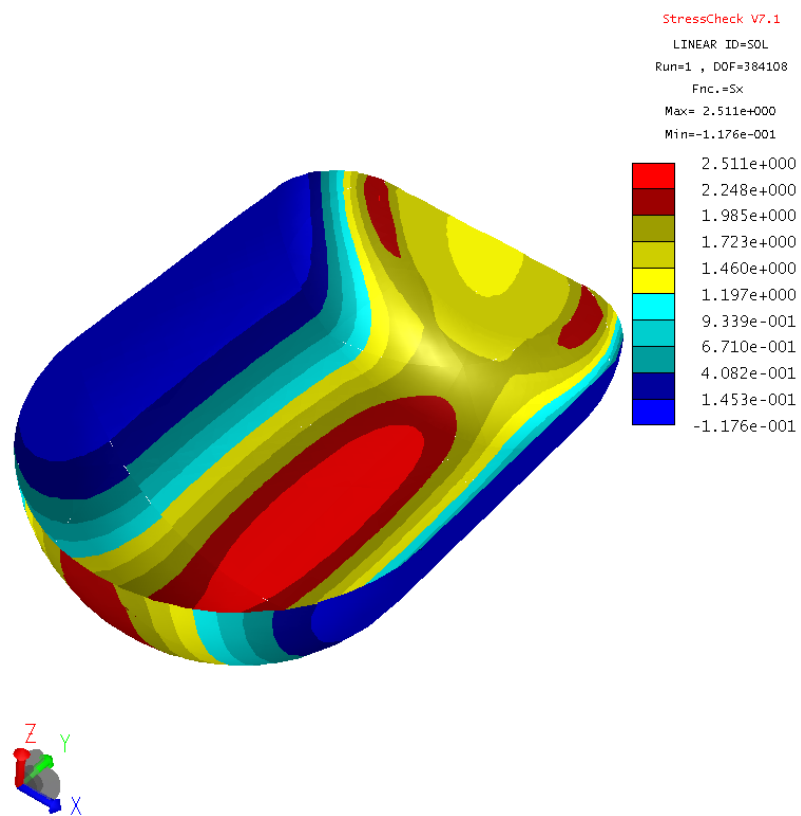
Figure 74: Fringe Plot of Kt for the Irregularity in Pill Feature

9.9 Selected References on Verification and Validation

1. Roach, P. J. *Verification and Validation in Computational Science and Engineering,* Hermosa Publishing, Albuquerque, 1998.

2. Trucano, T. G., Swiler, L.P., Igusa, T., Oberkampf , W. L. and Pilch, M. Calibration, validation and sensitivity analysis: What is what. *Reliability Engineering and System Safety* 91 (2006) 1331-1357.

3. Oberkampf, W. L. and Barone, M. F. Measure of agreement between computation and experiment: Validation Metric. Journal of Computational Physics 217 (2006) 5-36.

4. Post, D. E. The coming crisis in computational science. Los Alamos National Laboratory Report LA-UR-04-0388, 2004.

5. Babuška, I. and Oden, J. T. The reliability of computer predictions: Can they be trusted? International Journal for Numerical Analysis and Modeling. 1 (2005) 1-18.

6. Szabó, B. Validation of working models with StressCheck®. ESRD Technical Brief 01/02/07, St. Louis, 2007.

Appendix B

Boeing Final Report

HIGH STRENGTH STEEL CORROSION - FATIGUE

MODELING

Final Report

K. K. Sankaran, H. G. Smith, Jr., A. L. Neal, C.W. Scott, S. P. Gaydos, G. E. Weaver

The Boeing Company
St. Louis, Missouri

February 2008

Final Report for the Period August 2007 – February 2008

Table of Contents

Acknowledgments

1.0 Introduction

1.1   Overall Program Background

Corrosion increases the stress in an airframe part by reducing the effective cross sectional area of the structure carrying the load. Corrosion also causes stress concentrations, which can result in premature fatigue crack initiation. Therefore, the presence of corrosion reduces fatigue life and can result in greater risk of component failure.   The prevention and repair of corrosion is a major maintenance cost for the U.S. Armed Services.

Corrosion-fatigue modeling and analysis are essential to determining the impact of corrosion on structural integrity. Efforts have focused principally on aluminum alloy applications and more recently on steel alloys (Reference 1). This report documents the results of the Boeing effort between August 2007 and February 2008 under Subcontract RSC06048, which is part of a high strength steels corrosion-fatigue modeling program conducted by UDRI. Boeing's efforts under the earlier subcontracts covered the following tasks and have been described in References 2 through 4.

1. Assisting UDRI in corrosion simulation, exposure and characterization procedures including specimen preparation and masking to avoid crevice corrosion.

2. Characterizing the magnitude of corrosion on specimens provided by UDRI by laser profilometry and spot check measurements using microscopy.

3. Determining the adequacy of laser profilometry to obtain valid corrosion metrics for use in life prediction models and developing software tool to provide these metrics.

4. Examining the laser profilometry data obtained previously and performing a comparative statistical and probabilistic fatigue life prediction analysis to determine the efficacy and adequacy of using this technique.

5.   Defining the requirements for finite element analysis methods, which use the metrics to calculate stress concentrations caused by corrosion. These stress concentrations shall be applicable in fatigue life analysis procedures.

6. Identifying aircraft parts that have corroded in service, defining issues involved in correlating various corroded parts removed from in-service aircraft and selecting an in-service part for component testing with UDRI/USN concurrence.

7. Developing plans for testing the in-service parts and gathering of corroded and non-corroded parts for use in simulation tests.

These activities supported the overall program goal to quantify corrosion and conduct sufficient tests to obtain lives from specimens with various levels of corrosion. Presently different and inconsistent definitions of corrosion exist. The approach is to determine Kt's and distributions/grouping of Kt's and to analytically accomplish the following:

- Define corrosion categories with respect to Kt grouping
- Define characteristics for each corrosion category
- Correlate NDI signals to corrosion metrics, and
- Develop maintenance plans/practices/processes based on categories

1.2   Subcontract RSC06048 (August 2007 – February 2008)

The Boeing's company's SOW under subcontract RSC06048 (August 2007 – February 2008) included:

1.2.1 Statement of Work (Revised November 2007)

1. Perform additional fracture analysis on micromachined specimens to determine number of cycles to crack initiation (0.010 inch crack) at all practical locations that have not been characterized if sufficient funds and task priorities allow.

2. Provide engineering support to evaluate, verify, and validate corrosion life prediction model.

3. Provide support to the validation effort by corroding CAD plated test specimens as required.

4. Participate in program meetings, reviews, and planning as required.

2.0 Fractography of Fatigue Specimens with Micro-machined Features

Twelve AF 1410 fatigue specimens tested at 200 ksi maximum stress were provided by UDRI. Three of the specimens (baseline) had no micro-machined features and nine had such features, as shown in Figure 2-1. Fracture in all the specimens with the micro-machined features resulted from a crack that originated in one (designated the primary feature) of the two conical features with significant growth also occurring in the crack that initiated from the other (designated the secondary feature) conical feature. Under this subcontract, we performed additional quantitative fractography using scanning electron microscopy with the objective to determine the number of cycles to initiate a 0.01" size flaw from the secondary conical feature.

The fracture surfaces showing the crack growth from the secondary feature and the crack advance determined from the fractography are shown in Figures 2-2 through 2-19 for the nine specimens with the micromachined features.

Table 2-1 compares the crack initiation lives for the cracks growing from both the conical features. As expected, the presence of a flaw as simulated by the micro-machined feature reduces the initiation lives by an order of magnitude. For those specimens with the micro-machined features, the initiation lives are very close for both the features in a given specimen as well as for all the specimens.

Specimen Number	Crack Initiation at 0.01 in. (cycles)	
	Primary Feature	Secondary Feature
598-1	6, 567	6, 600
598-2	3, 300	5, 822
598-3	4, 371	4, 368
598-5	5, 760	6, 173
598-8	4, 209	4, 660
598-9	5, 700	5, 808
598-10	3, 100	3, 433
598-12	4, 700	4, 633
598-13	6, 502	6, 682
Baseline Specimens		
598-4	83, 467	
598-11	80, 212	
598-14	49, 374	

Table 2-1 Initiation lives for 0.01 in. crack

(Specimens 598-4, 598-11 and 598-14 are the baseline specimens without the micromachined features)
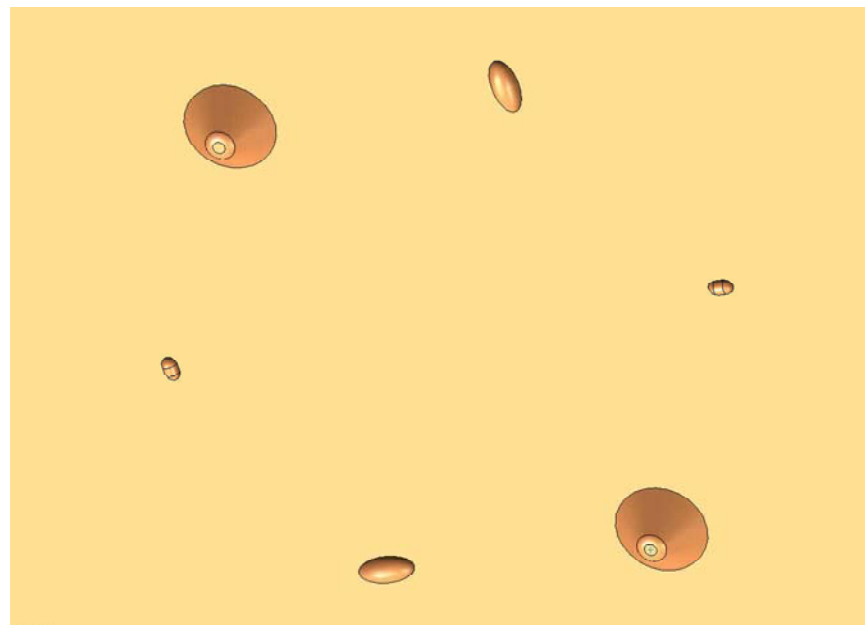
Figure 2-1 Micro-machined Features on AF 1410 Steel
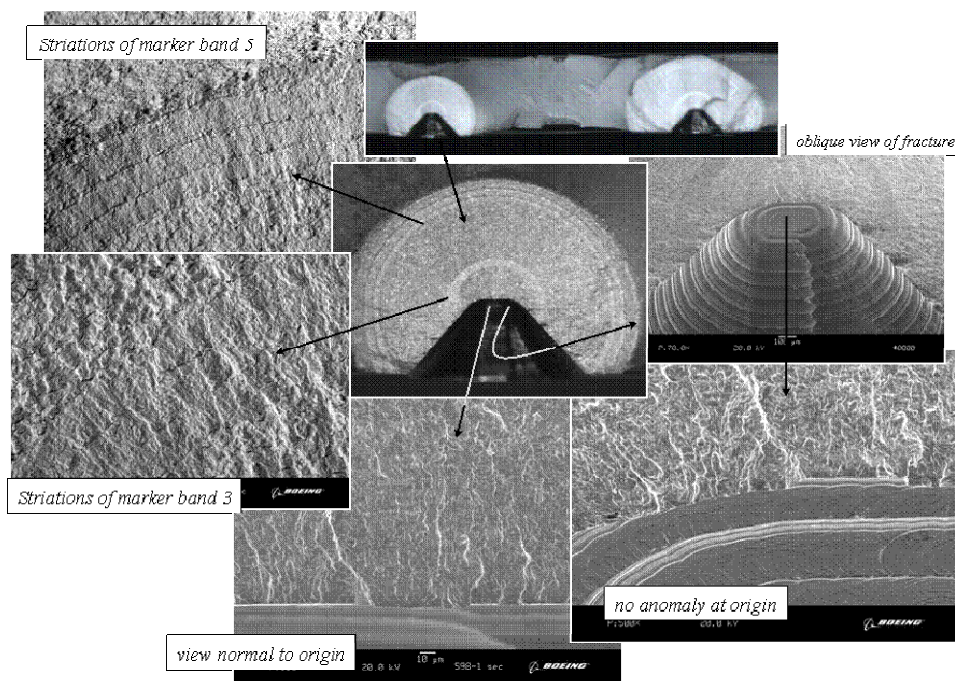
Figure 2-2 Fracture Surface of Specimen 598-1
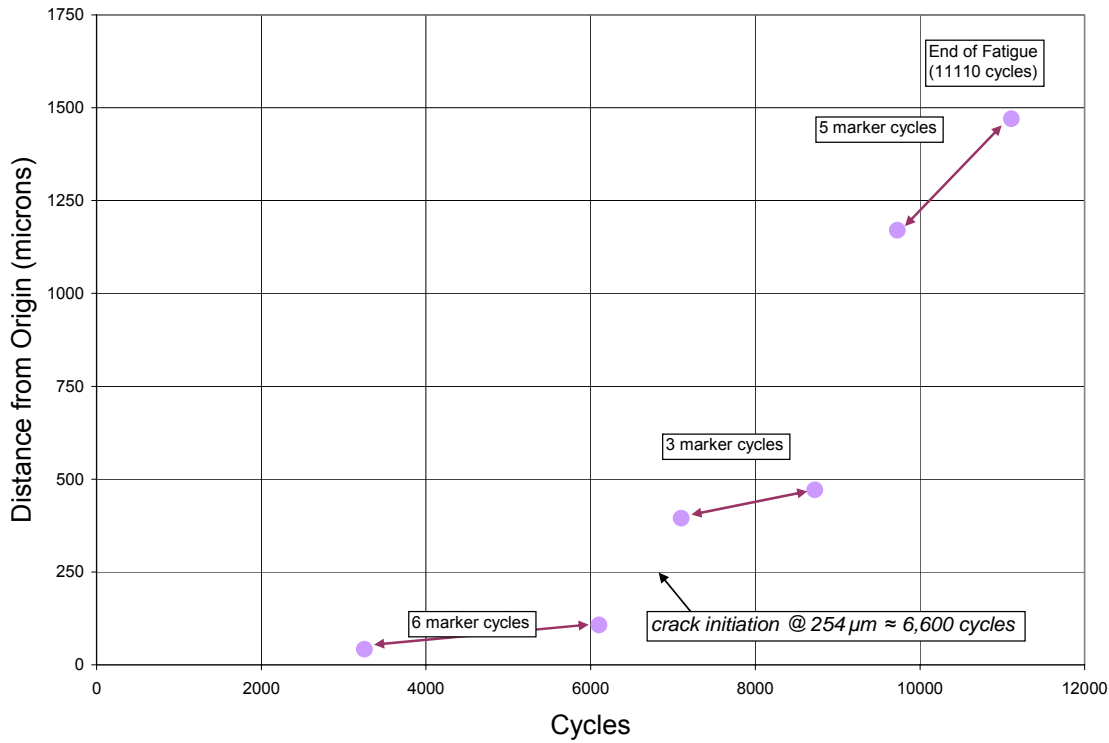
Figure 2-3 Crack Advance in Specimen 598-1 Determined from Fractography
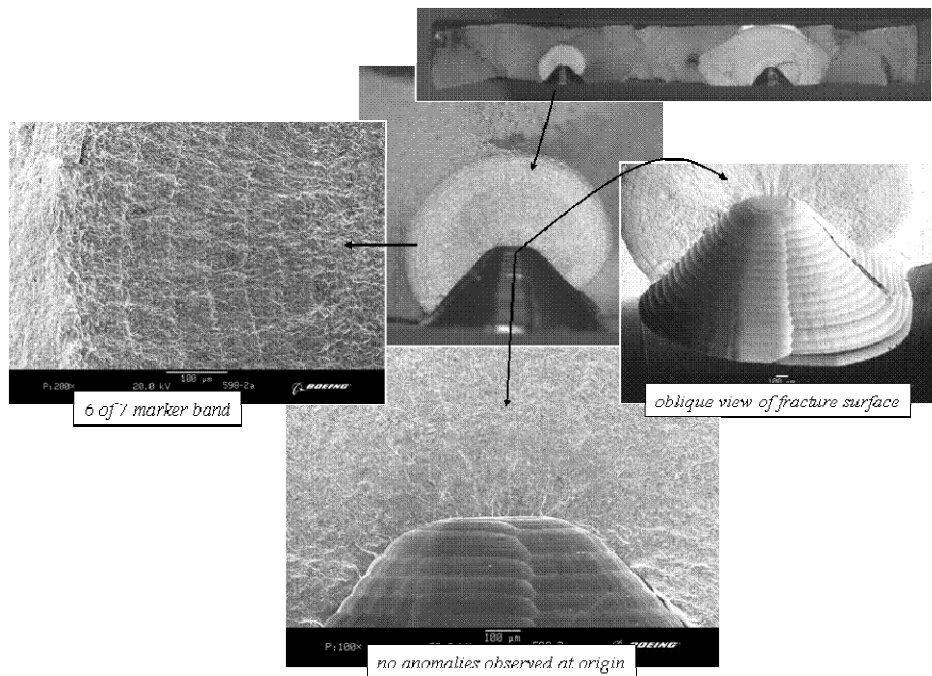
Figure 2-4 Fracture Surface of Specimen 598-2
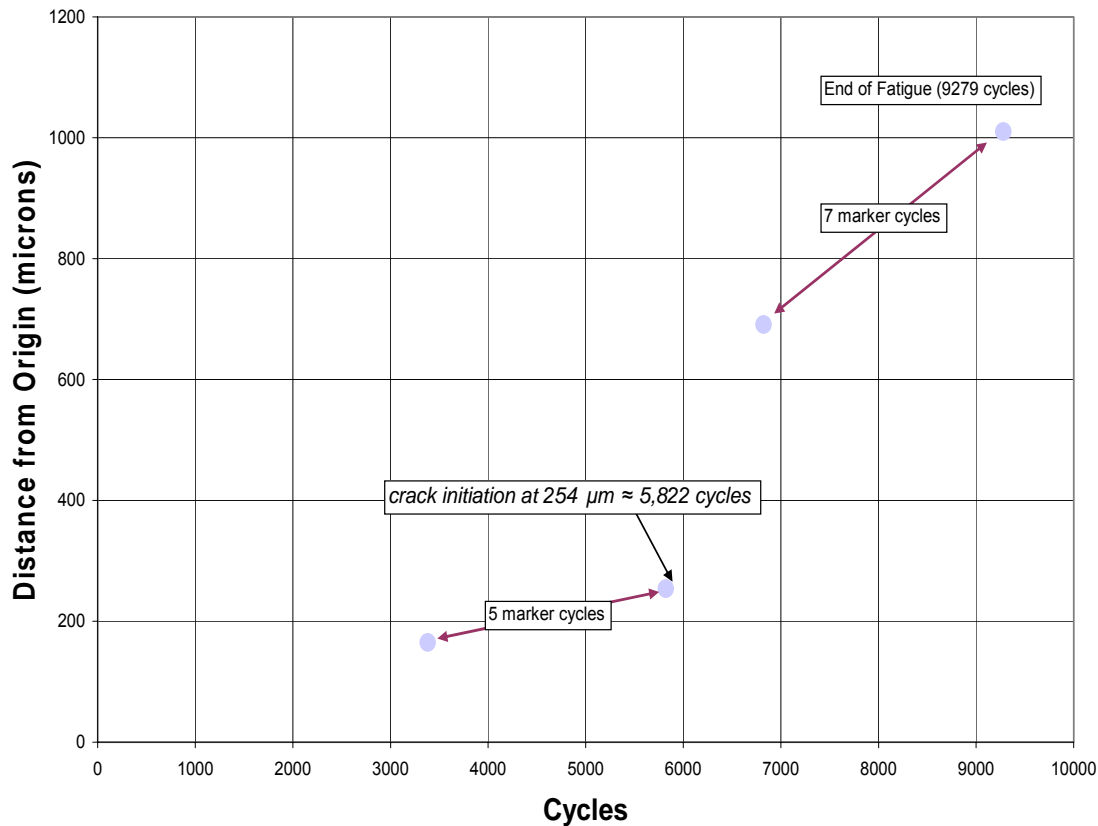
Figure 2-5 Crack Advance in Specimen 598-2 Determined from Fractography
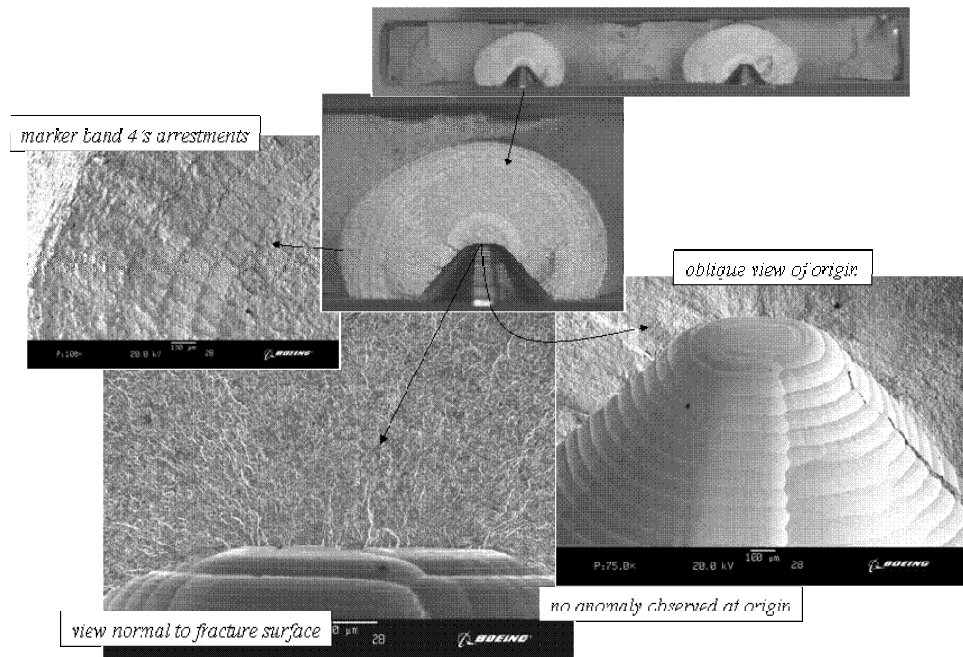
Figure 2-6 Fracture Surface of Specimen 598-3
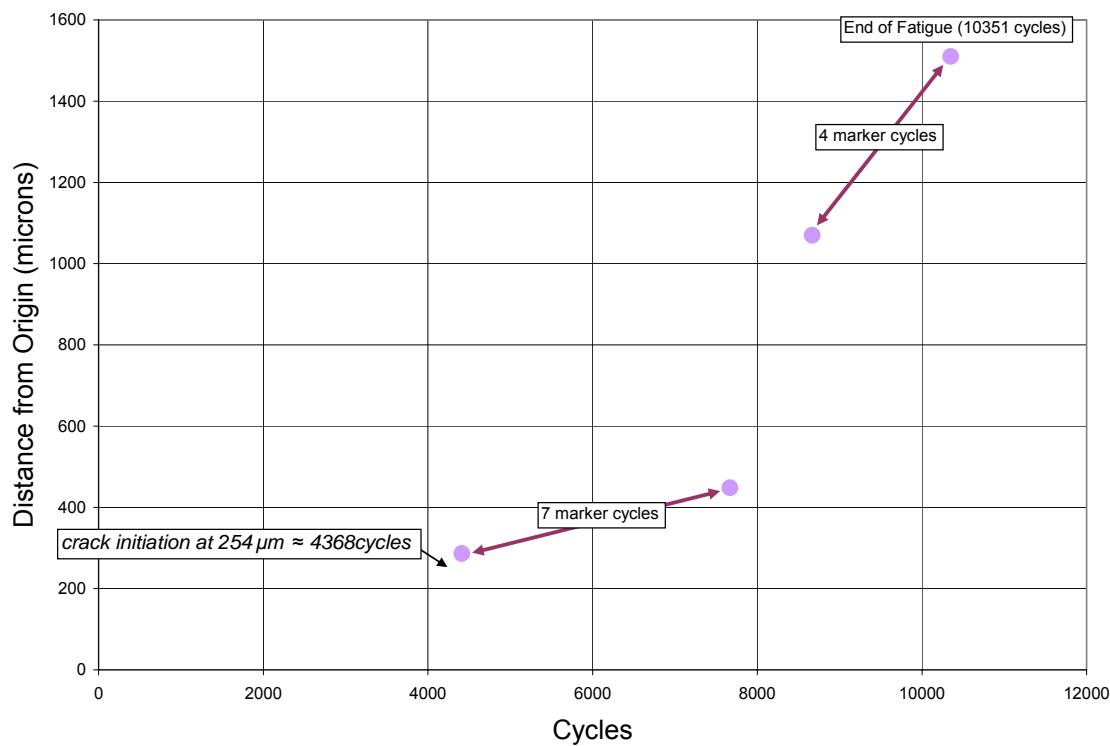
Figure 2-7 Crack Advance in Specimen 598-3 Determined from Fractography
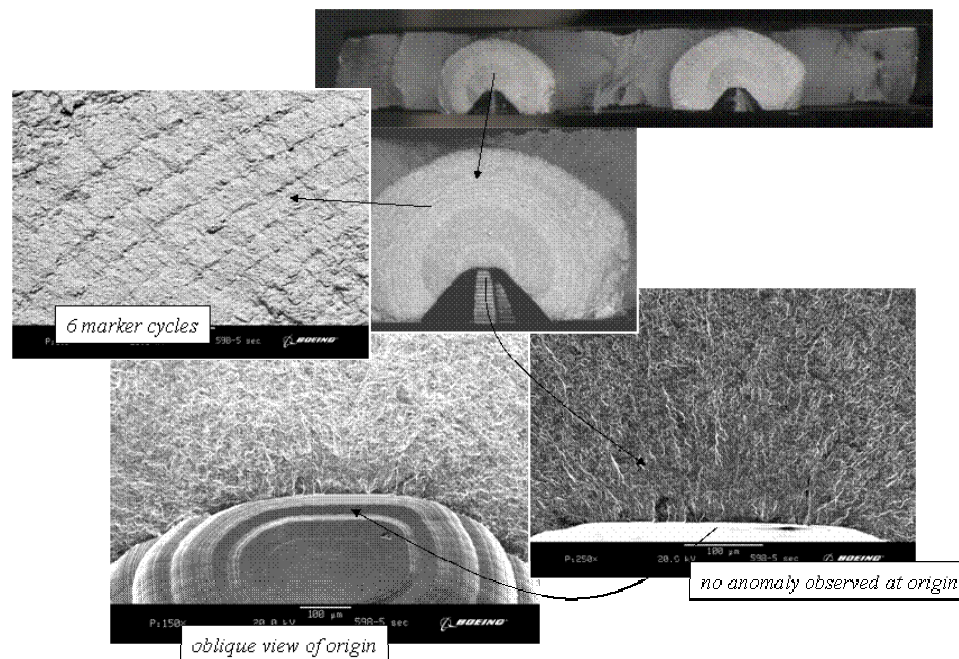
Figure 2-8 Fracture Surface of Specimen 598-5
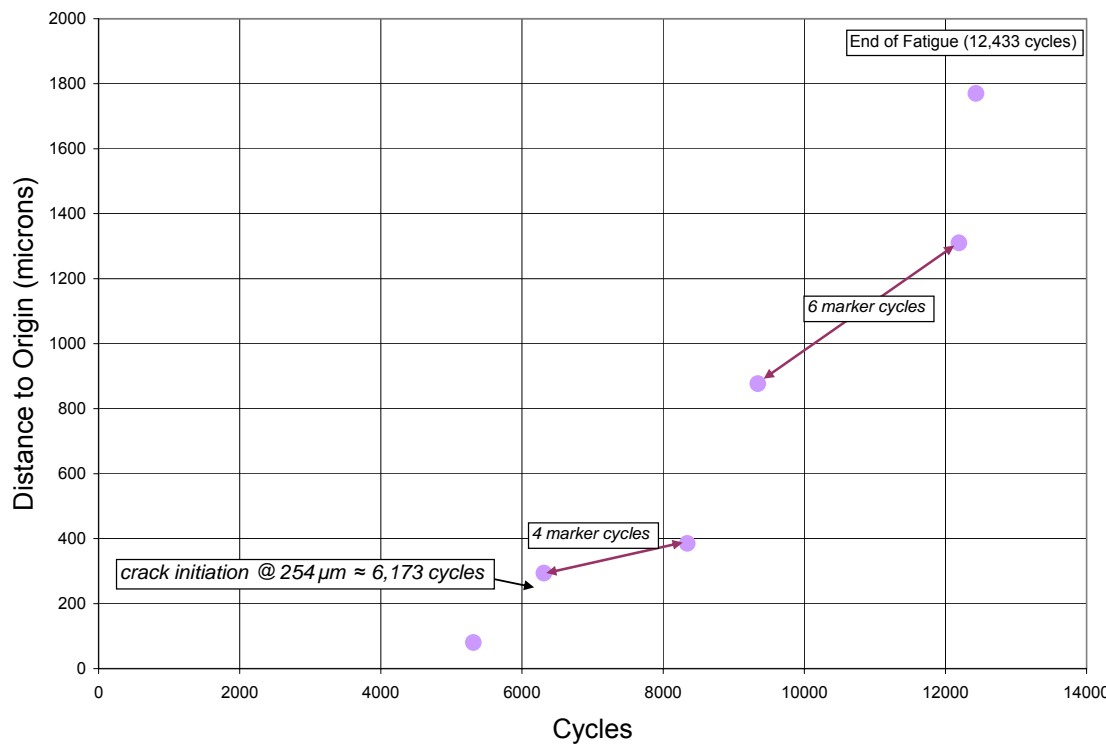
Figure 2-9 Crack Advance in Specimen 598-5 Determined from Fractography
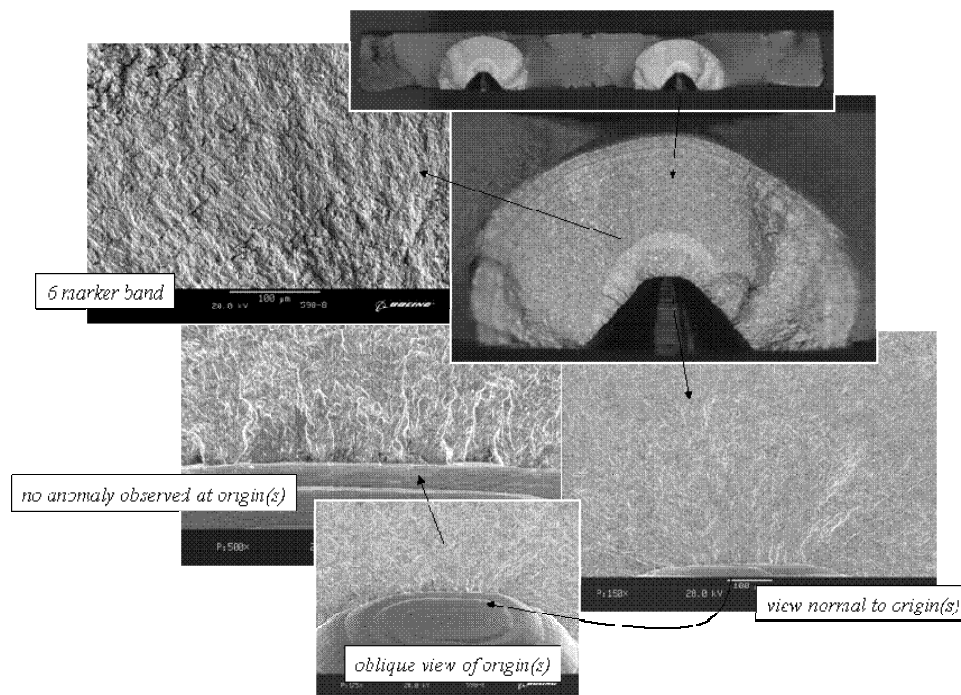
Figure 2-10 Fracture Surface of Specimen 598-8
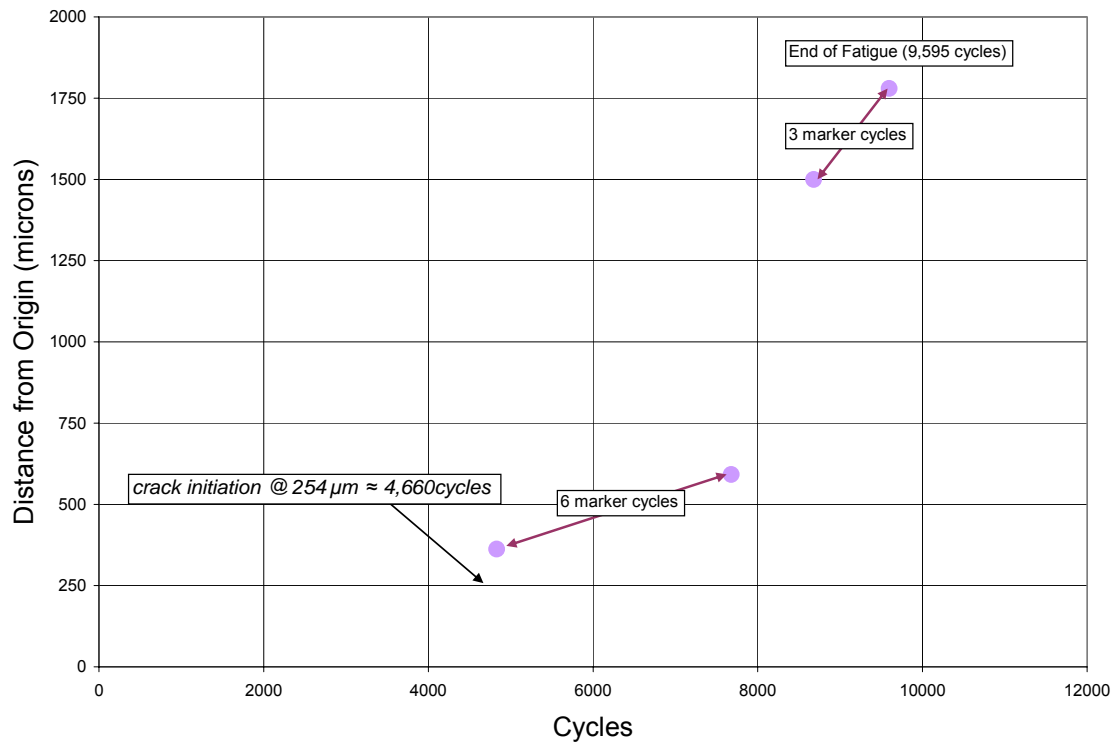
Figure 2-11 Crack Advance in Specimen 598-8 Determined from Fractography
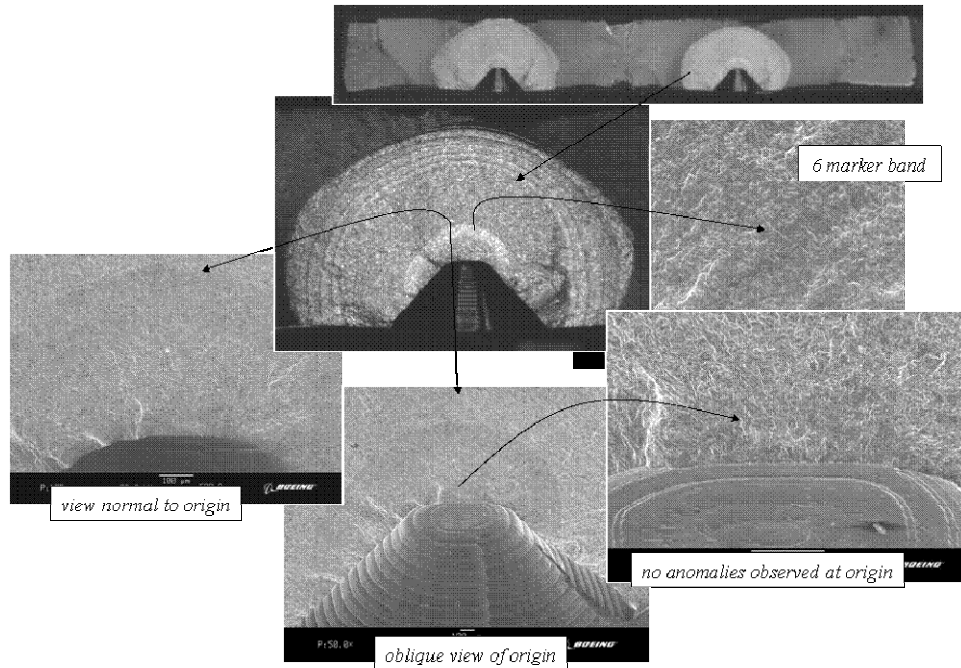
Figure 2-12 Fracture Surface of Specimen 598-9
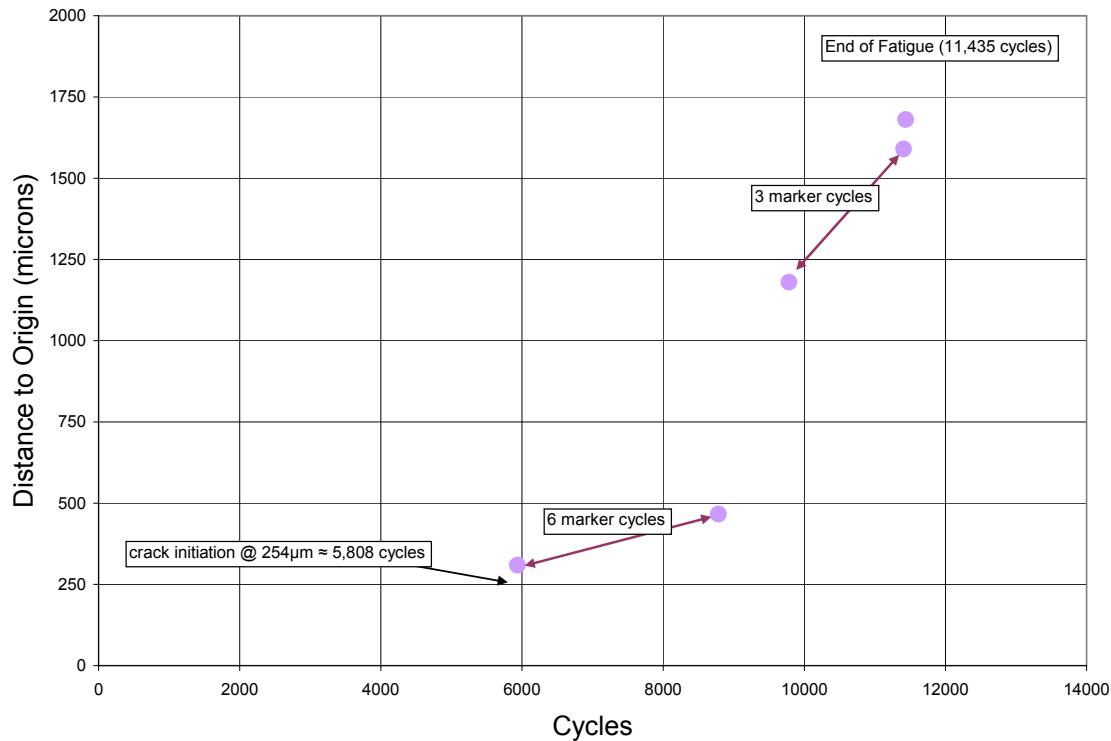
Figure 2-13 Crack Advance in Specimen 598-9 Determined from Fractography
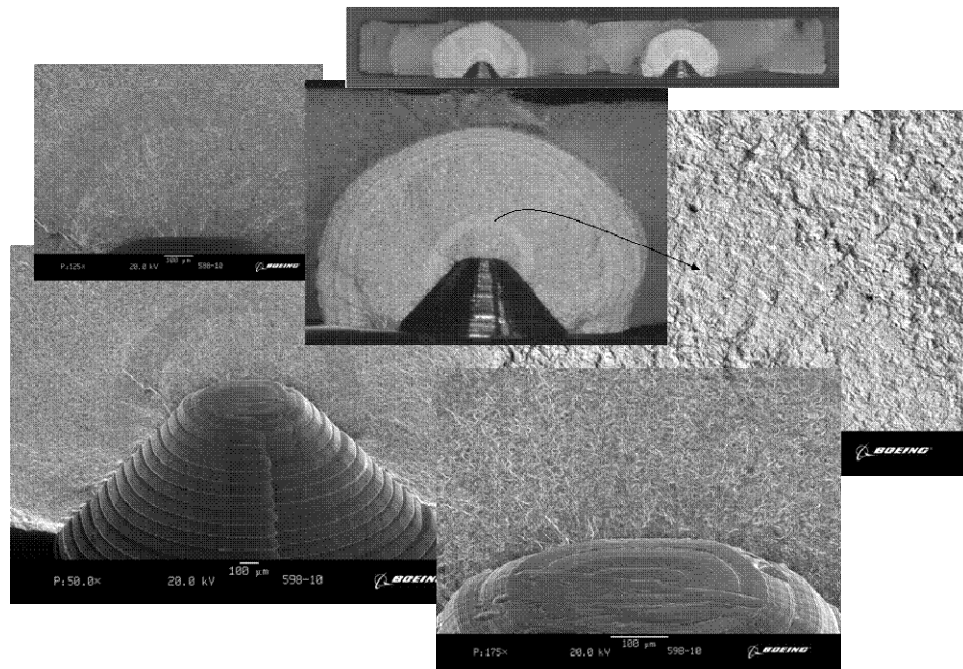
Figure 2-14 Fracture Surface of Specimen 598-10
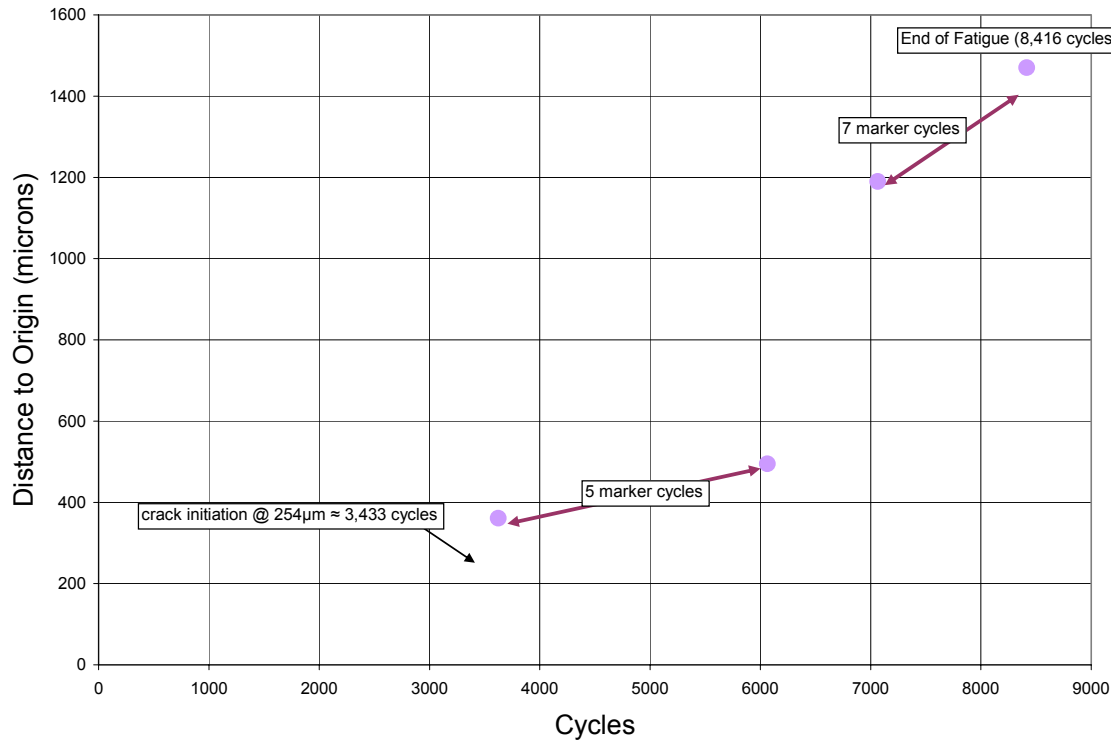
Figure 2-15 Crack Advance in Specimen 598-10 Determined from Fractography
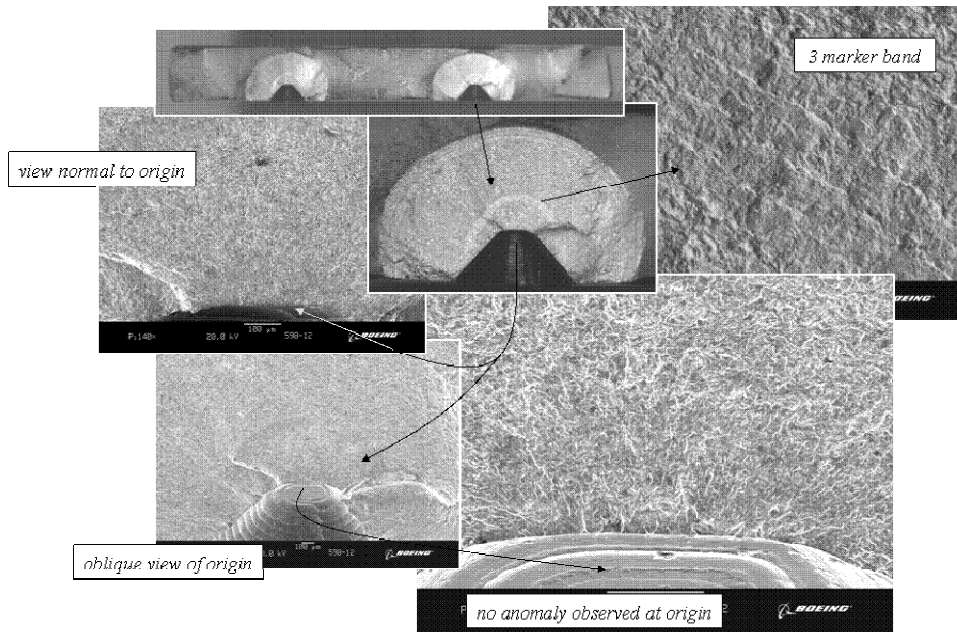
Figure 2-16 Fracture Surface of Specimen 598-12
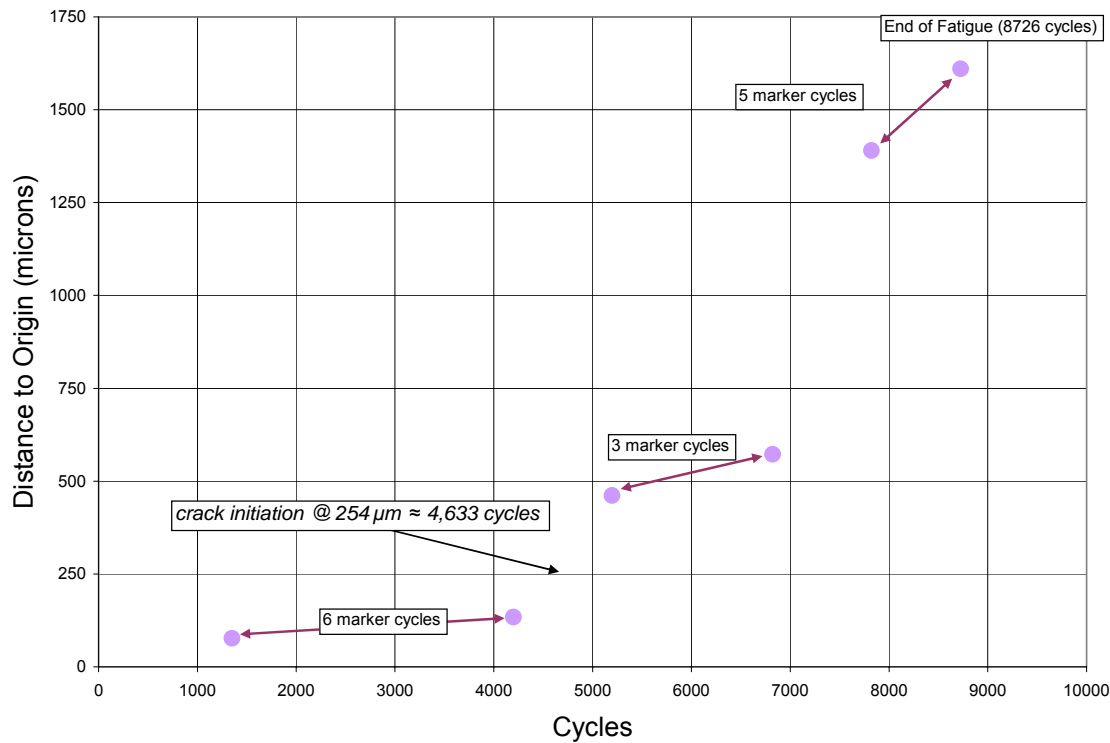
Figure 2-17 Crack Advance in Specimen 598-12 Determined from Fractography
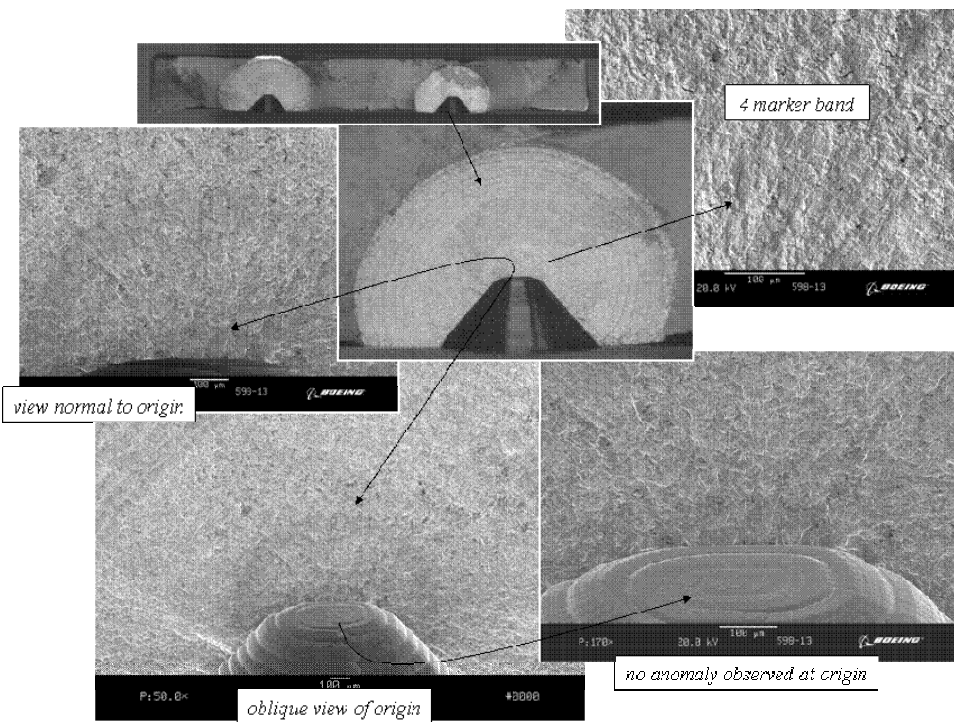
Figure 2-18 Fracture Surface of Specimen 598-13
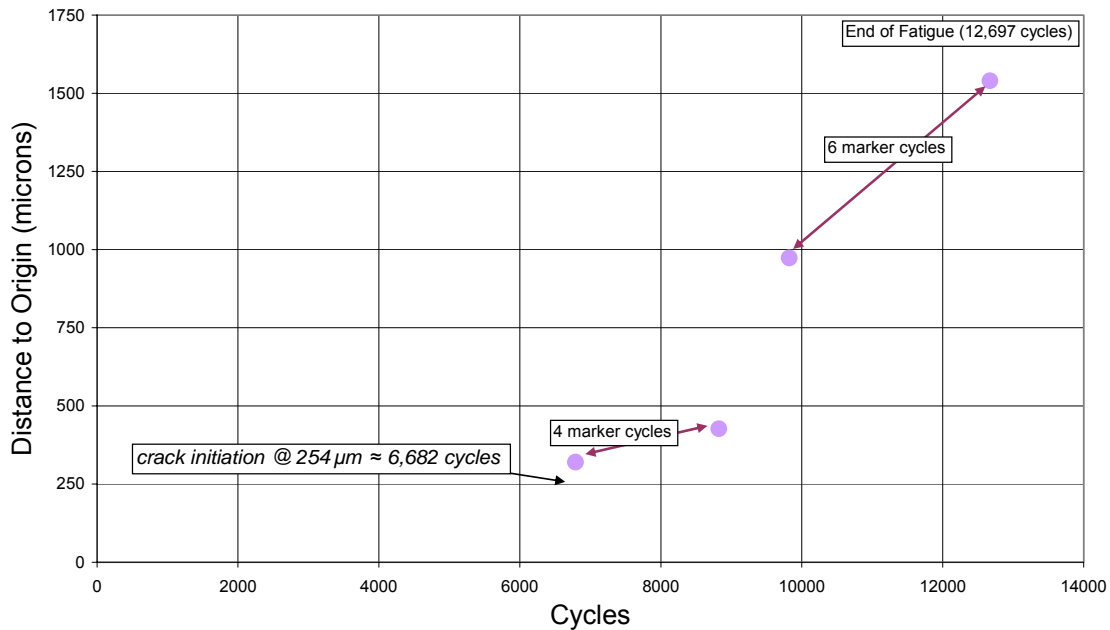
Figure 2-19 Crack Advance in Specimen 598-13 Determined from Fractography

3.0 Life prediction software verification.

3.1 Software Verification

Some of the individual components of the ESR software were evaluated individually in an effort to determine if they were performing as expected. The initial work on this was reported in the previous contract report. That initial result is repeated here for continuity.

The first module that was investigated was a routine titled PSLcurveAF1410_UG02. This function computes the probabilistic strain life curve. The result, for a range of the standard normal pdf value for the prediction bounds from -3 to +3 is shown in Figure 3.1-

1.
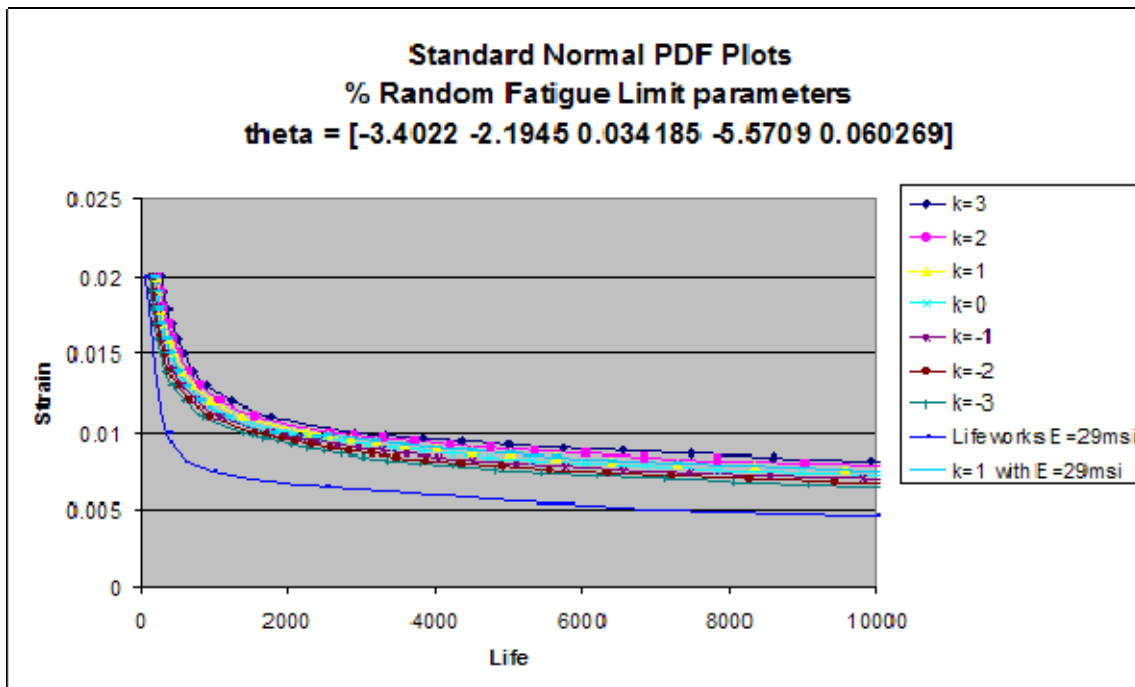
Figure 3.1-1 Predicted Strain Life Curves Compared to LifeWorks

Comparison is made to the curve obtained from Boeing's proprietary life prediction code called Lifeworks. The Lifeworks code is somewhat conservative. The same data plotted on a log plot is shown in Figure 3.1-2. Initially it was thought that a difference in elastic modulus might be the cause for the difference as the Matlab predictions were based on the 27.5 MSI value from the test data. The Lifeworks result was based on a stated modulus of 29 MSI. A Matlab prediction was run for a 29 MSI modulus and, as can be seen in the figures, has no significant effect. Further investigation revealed that the Lifeworks predictions are based on representative data from the Aerospace Materials Handbook and it is unclear exactly what the product form of the material was. The curve did show the same trend as a function of strain which would seem to indicate that the Matlab routine was indeed correctly modeling the behavior of the AF1410 material. It is recommended that the curves generated to match the test data be used as correctly representing the coupon material behavior.
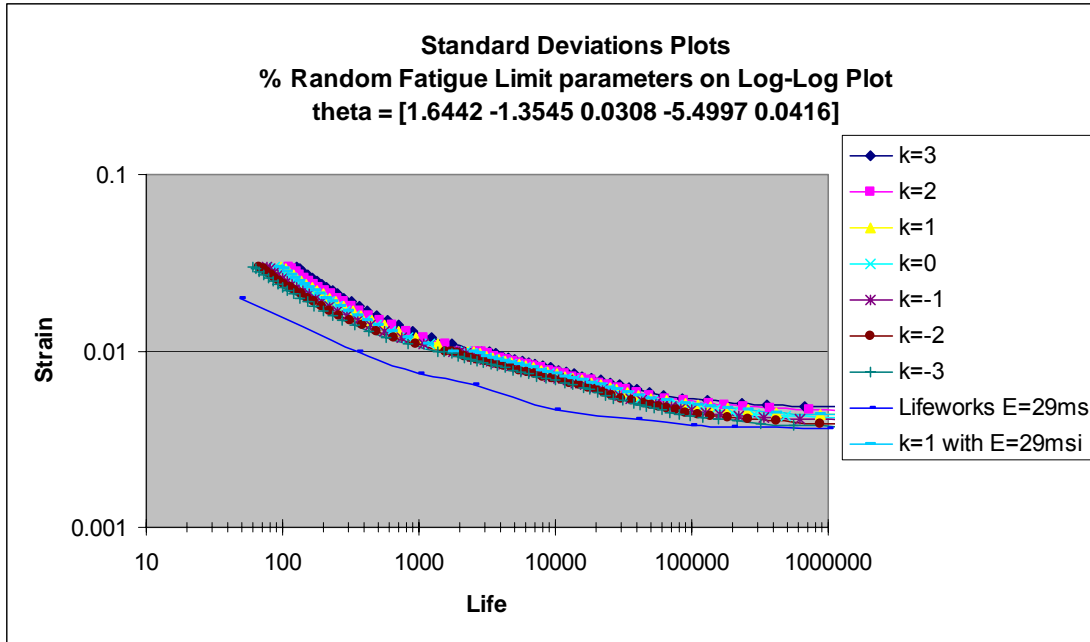
Figure 3.1-2 Predicted Strain Life Curves Compared to LifeWorks – Log Plot

The second routine evaluated was Kfc_fitNeu1 which produces converged Kfc values for various test coupons. These results are shown in Figures 3.2-3 through 3.2-6.
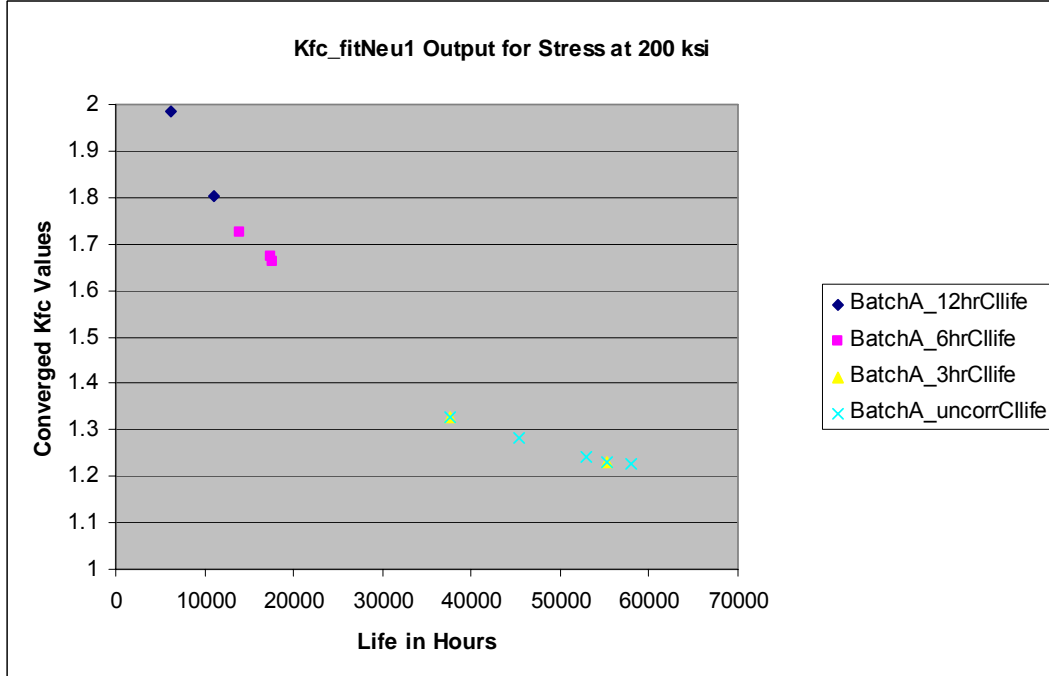
Figure 3.1-3 Predicted Kfc Values versus Life for 200 ksi
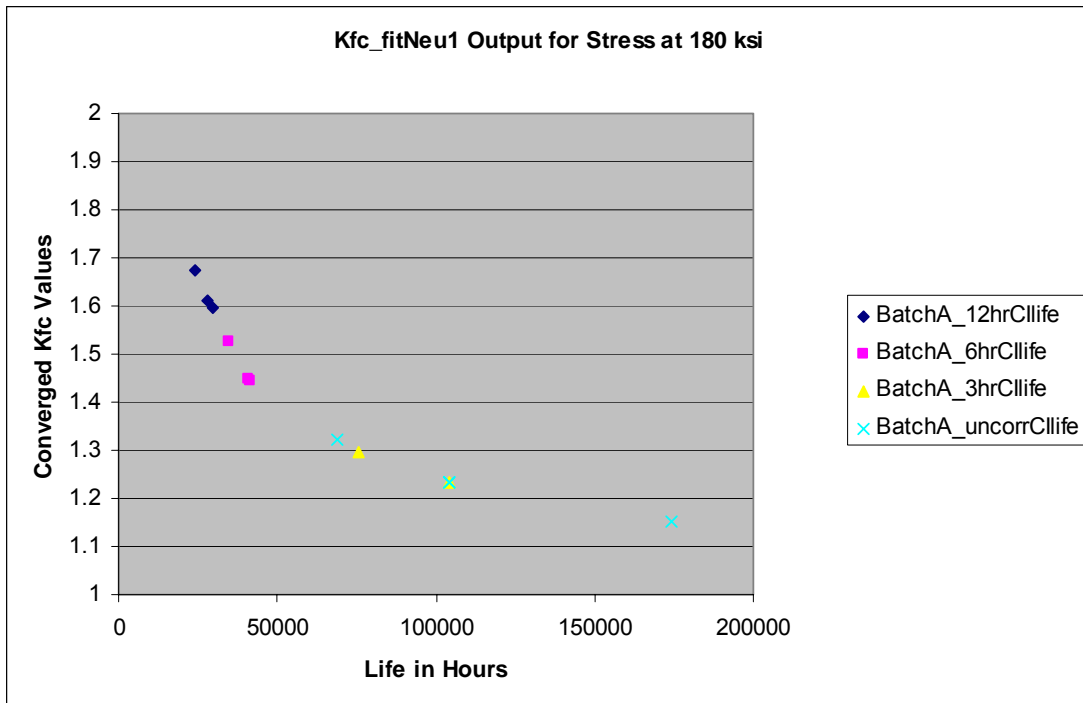
Figure 3.1-4 Predicted Kfc Values versus Life for 180 ksi
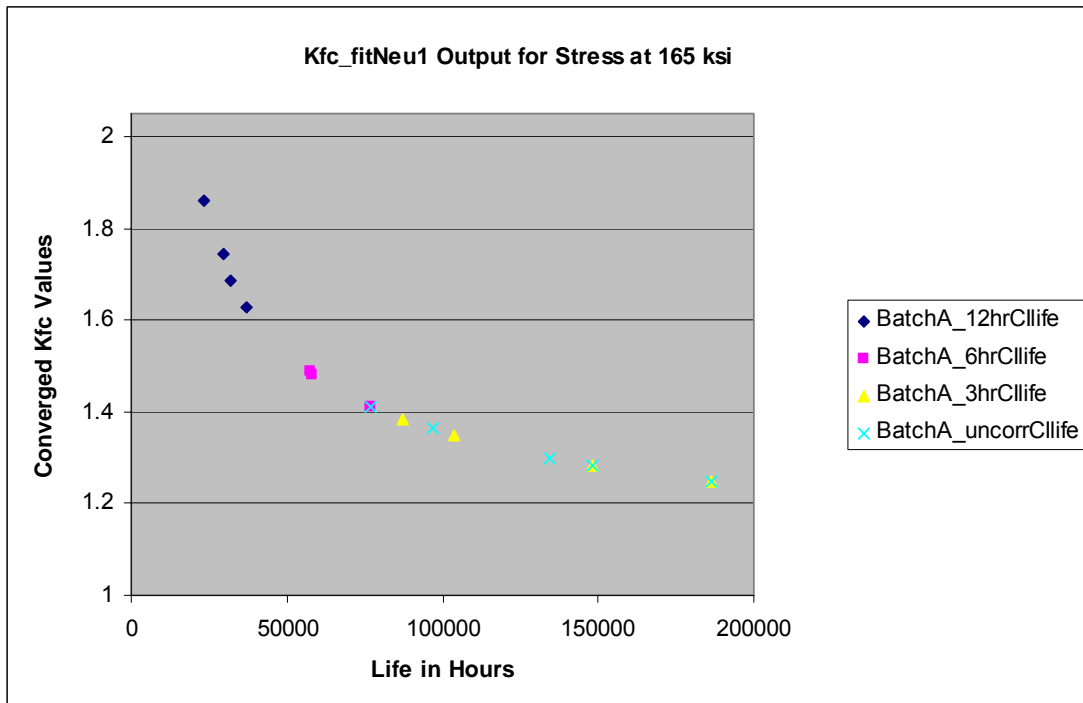
Figure 3.1-5 Predicted Kfc Values versus Life for 165 ksi
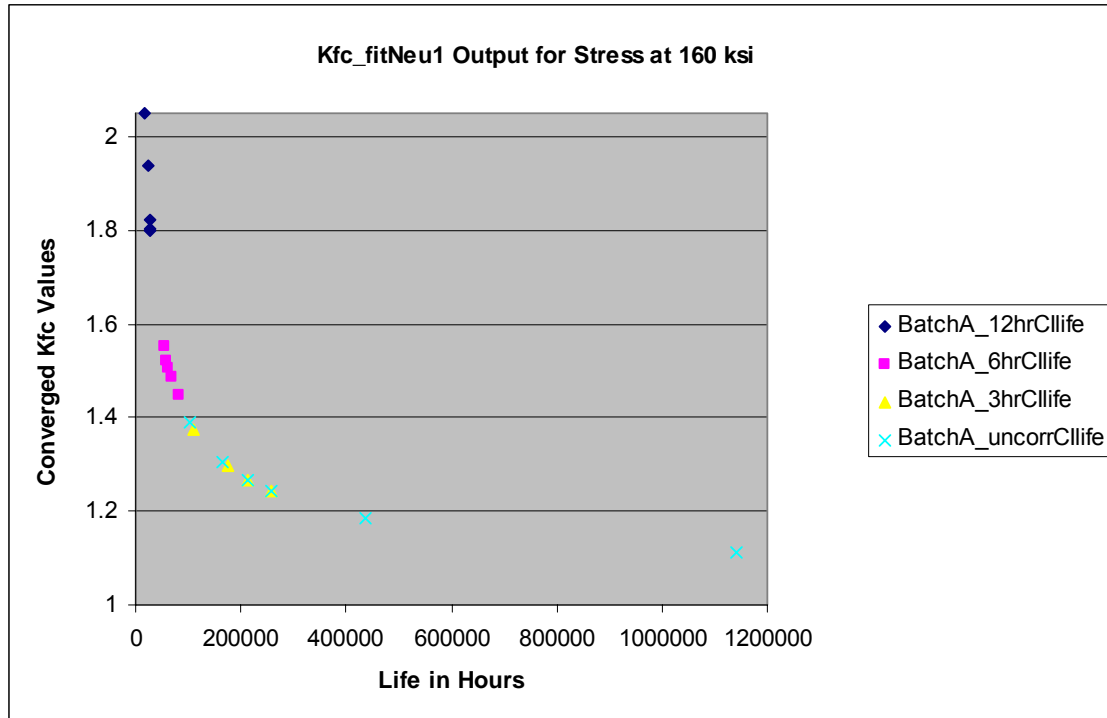
Figure 3.1-6 Predicted Kfc Values versus Life for 160 ksi

The Kfc values generally behave as would be expected. Previous corrosion work showed that equivalent notch factors were in the 1.0-2.0 range and this seems consistent with that. It might have been expected that the uncorroded specimens should have Kfc values at 1.0, but the 3 hour specimens and the uncorroded seem to be clustered together as was seen in other results.

A third procedure, PCF_Kfcpred2, is used to build the CDF showing the cumulative probability of crack initiation for a given specimen. A typical result from this routine is shown in Figure 3.1-7. The unusual shape is due, somehow, to the presence of the marker band cycles in the spectrum. This may be a correct representation due to the way that marker bands are handled; however, it is unclear how this effect a prediction in a service-related case.
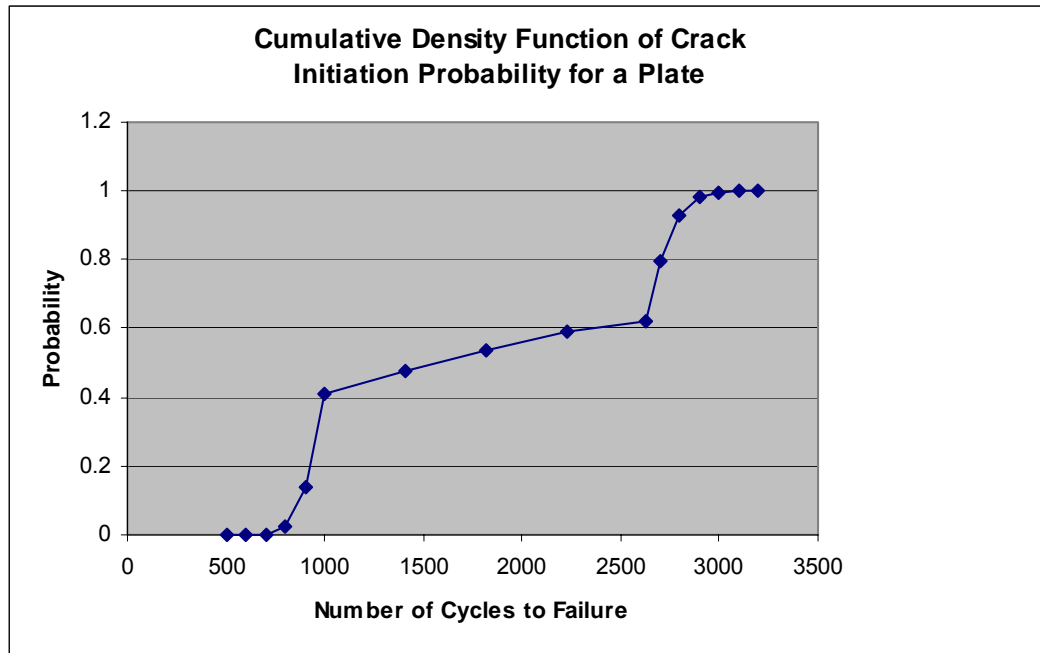
Figure 3.1-7 Predicted CDF for a Typical Case.

3.2 Data and Prediction Analysis

The focus of the effort in this task was running the ESR software on Matlab to generate predictions for the Batch B specimens.

The results for the cases that were generated by the ESR software are shown in Figures 3.2-1 to 3.2-3.

	1.5 Hr. Exposure										ESR Pred.		
		Critical	Critical	Critical	Critical	Critical	Critical	Plate	Max.	Critical	Life	Test CI Life	Test/Pred
Specimen	Total ROI's	Notch ROI #	ROI K_t	Meas. K_t	ROI q_c	Meas. q_c	ROI K_{fc}	Test K_{fc}	ROI K_{fc}	K_{fc} %	50% Prob.	(cycles)	Life Ratio
544-9C	547	343	1.7912	2.044	0.3768	0.434	1.2981	1.453	1.368		71732	79374	1.106535
545-3D	306	71	1.4102	2.026031	0.536	0.323407	1.2199	1.331825	1.4715		65395	140711	2.151709
547-7B	345	None		1.933802		0.328386		1.306648					
547-26A	548	311	1.3731	1.501133	0.7228	0.818115	1.2697	1.409984	1.6325		45041	96069	2.132923
547-44C	443	None		2.913244		0.196433		1.375823					
545-2A	493	270	1.1695	2.159408	0.8362	0.359245	1.1418	1.416511	1.3914		54500	64581	1.184972
547-39D	353	None		1.849153		0.395241		1.33562					
547-46C	510	None		2.134946		0.407267		1.462226					
547-50B	251	177	1.2636	2.072525	0.6979	0.251193	1.184	1.269411	1.4141		57706	127432	2.208297
614-2	743	None		2.06564		0.310733		1.331129					
614-22*								1.305594					
614-25*								1.312548					
614-7	517	258	1.4002	2.00939	0.5898	0.299503	1.2361	1.302316	1.3441		34400	41141	1.195959
614-11	875	551	1.3843	1.903794	0.855	0.347622	1.3286	1.314179	1.3837		31100	40591	1.305177
614-17	907	None		2.270189		0.232221		1.294964					

Figure 3.2-1 Prediction vs. Test Results for 1.5 Hour Corrosion Exposure

												ESR Pred.		
3 Hr. Exposure												Life	Test CI Life	Test/Pred
		Critical	Critical	Critical	Critical	Critical	Critical	Plate	Max.	Critical				
Specimen	Total ROI's	Notch ROI #	ROI K_t	Meas. K_t	ROI q_c	Meas. q_c	ROI K_{fc}	Test K_{fc}	ROI K_{fc}	K_{fc} %	50% Prob.	(cycles)	Life Ratio
545-6A	1700	913	1.5022	1.864961	0.7749	0.429886	1.3891	1.371835	1.4876				
545-10D	1809	1759	1.222	2.18545	0.9405	0.476625	1.2088	1.565015	1.6405		45220	51988	1.149668
547-22C	2691	2016	1.3564	1.979497	0.743	0.480696	1.2648	1.47084	1.8758		28099	72125	2.566817
547-37B	2243	1366	1.4614	1.879274	0.7059	0.504285	1.3257	1.443404	1.4814		54474	82424	1.513089
547-9M	1748	1133	2.121	1.824362	0.2623	0.477241	1.294	1.393419	1.6221		45220	103392	2.286422
547-5A	1584	1140	2.0539	2.832712	0.2354	0.213622	1.2481	1.391507	1.5563		38024	71468	1.87955
547-48D	2075 None			2.450762		0.309494		1.449003					
547-23B	2180	866	1.3087	2.675416	0.6566	0.308746	1.2027	1.517278	1.8142		23764	44960	1.891937
544-5C	1405	645	1.5117	2.212711	0.5139	0.363926	1.263	1.441337	1.4753		45220	57903	1.280473
614-4	1933	321	1.4374	2.1175	0.628	0.348776	1.2747	1.389757	1.6861		24014	52069	2.168277
614-12	2365	1685	1.1792	1.805702	0.8558	0.485004	1.1534	1.390764	1.708		23764	52009	2.188563
614-21	2086	1898	1.2438	1.803863	0.9354	0.434296	1.228	1.349114	1.765		20574	62035	3.015213
614-1	2225	1448	1.4303	1.984978	0.7319	0.394578	1.3149	1.388651	1.6303		17886	34403	1.92348
614-15	1739	117	1.266	1.818839	0.911	0.417148	1.2423	1.341577	1.5189		24014	37046	1.542683
614-18*								1.355055					

Figure 3.2-2 Prediction vs. Test Results for 3.0 Hour Corrosion Exposure

												ESR Pred.		
6 Hr. Exposure												Life	Test CI Life	Test/Pred
		Critical	Critical	Critical	Critical	Critical	Critical	Plate	Max.	Critical				
Specimen	Total ROI's	Notch ROI #	ROI K_t	Meas. K_t	ROI q_c	Meas. q_c	ROI K_{fc}	Test K_{fc}	ROI K_{fc}	K_{fc} %	50% Prob.	(cycles)	Life Ratio
544-8C	2777	584	1.5923	2.16157	0.8735	0.501695	1.5174	1.582754	2.0303				
544-10C	3674	1376	1.4486	1.877541	0.7158	0.626418	1.3211	1.549708	2.4427				
547-6A	3706	3086	1.3166	1.723492	0.9426	0.664496	1.2985	1.480758	2.0195				
547-20B	2839	1124	1.3055	2.240592	0.9374	0.384752	1.2864	1.477321	2.1515		13850	71566	5.16722
547-36B	3777	3391	1.3089	3.805012	0.9566	0.204634	1.2955	1.574001	1.9807				
544-3B	3459	3362	3.0016	1.988534	0.5624	0.753124	2.1258	1.744488	4.7236				
547-16B	2933	1857	1.3389	1.924151	0.9497	0.594511	1.3219	1.549418	2.504				
547-2C	3484	85	1.1741	1.912094	0.9826	0.506323	1.1711	1.461815	2.4436				
547-31B	3065	1924	1.1541	2.099044	0.9784	0.420571	1.1507	1.462226	2.2917				
614-3	4182	515	1.422	2.227501	0.8718	0.340037	1.3678	1.417396	2.2958		3400	46378	13.64059
614-8	4548	2270	1.3677	1.833982	0.9139	0.581904	1.3361	1.485298	2.0865		9200	37236	4.047391
614-13	4655	730	1.2903	1.766731	0.9611	0.71065	1.279	1.544878	2.1761		6500	32523	5.003538
614-5	4109	3065	1.4805	1.899403	0.8599	0.569391	1.4132	1.512111	2.5161		***		
614-6	4291	2139	1.1606	2.793347	0.9872	0.346506	1.1586	1.621406	2.0944		3230	18178	5.627864
614-19	4668	4234	1.3302	1.63621	0.9221	0.768658	1.3044	1.489028	2.2533		2900	27389	9.444483

Figure 3.2-3 Prediction vs. Test Results for 6.0 Hour Corrosion Exposure

No predictions were made for some cases as the results from the interferometery were not available. In each case, the last three columns give the ESR predicted life, the test life, and the ratio of the test to predicted values for exposure times of 1.5 hours, 3.0 hours, and 6.0 hours respectively.

Several observations can be made from these results; however, first a comparison of the initiation lives from testing of uncorroded, 1.5 hour and 3.0 hour data is examined. This data is shown in Figure 3.2-4.
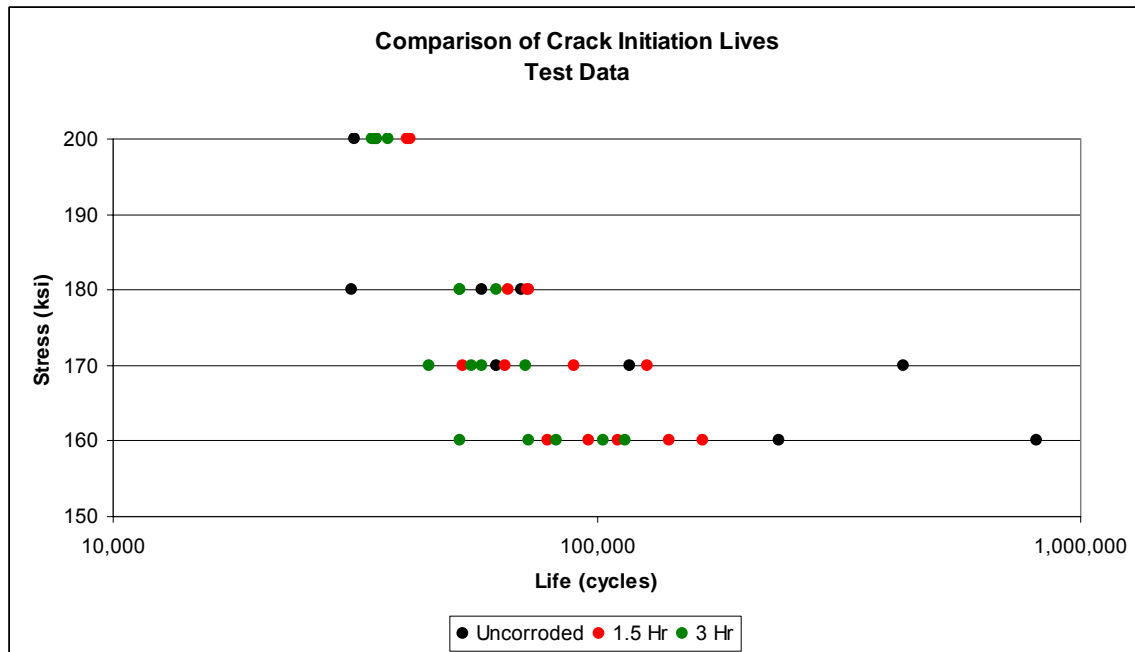
Figure 3.2-4 Comparison of Crack Initiation Lives from Test Data

It is clear from Figure 3.2-4 that there seems to be little or no effect on the crack initiation life from corrosion at these levels of exposure except at the very lowest stress level where 3 of the uncorroded specimens experienced run-out. This is made even clearer when it's noticed that some of the coupons at these corrosion levels did not initiate their failures in the corroded area.

The predictions vary considerably from the test data with the ratio of test life to prediction life varying from a minimum of 1.11 to a maximum of 13.6. The 1.5 and 3.0 hour exposure coupons had a test to prediction ratio average of 1.9 and 1.95 respectively while the 6.0 hour coupons had an average ratio of 7.2. The standard deviation of the 1.5 and 3.0 hour coupons was about the same at approximately 0.53, however the standard deviation of the 6.0 hour coupons was 3.68.

A plot of the error factor versus the corrosion level is shown in Figure 3.2-5. The test life to prediction life ratio seems to be growing exponentially with exposure time. Data at higher levels of corrosion exposure would obviously be needed to determine if the trend continues.
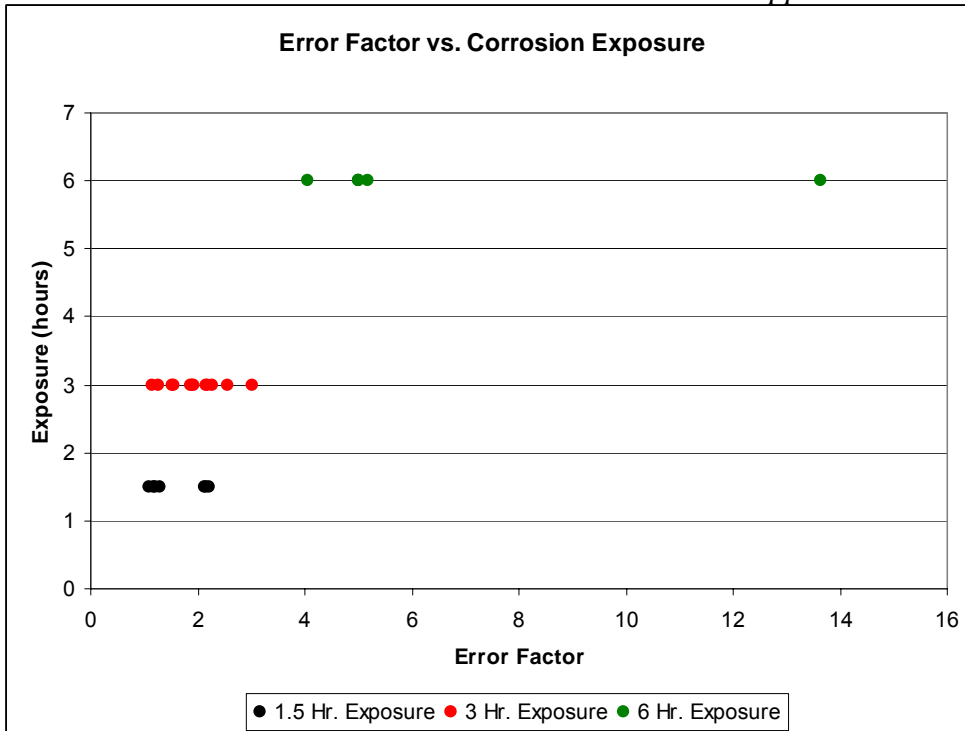
Figure 3.2-5 Prediction Error versus Corrosion Level

3.2 Prediction Summary

There is clearly a significant difference between the predictions and the test data. The software under-predicts the life by an average factor of approximately 2 for the very lowest levels of corrosion. In the case of more significant corrosion, such as the 6 hour exposure cases, the software under-predicts by a factor of anywhere from 4 to 13.

It is unclear where this discrepancy originates as there are a number of analytical steps that make it difficult to pinpoint. It is obviously related to corrosion level, but due to the lack of any information at higher corrosion levels it's not clear whether it would continue to increase along with the corrosion severity. The efficacy of these individual steps in the analysis would need to be established individually in an effort to determine if the error is coming from one of the prior steps in the process. In addition, it is unclear how this methodology would perform in a case where the stress state is more complex and not just a uniaxial load. A full validation of the methodology would need to include predictions and test results for a more complex geometry incorporating a multi-axial stress state and complicating factors such as holes or other stress risers. Proceeding in that direction, however, would not be advised until the simpler uniaxial cases are resolved.

In its current form, the software is a series of Matlab applications. This is perhaps a useful tool for development work, however, the software would need to be rewritten in a form where it could be operated from a simple graphical user interface (GUI). This would be essential for any sort of field application.

4.0 Validation coupon preparation

During this period Boeing completed three phases of activities:

1. Evaluation Of Test Methods To Simulate Field Corrosion Using Wafer Specimens

2. Tests Of An Actual Fatigue Bar To Verify Corrosion Matches Field Corrosion

3. Corrode Fatigue Bars For Future Tests.

4.1 Evaluation of Test Methods to Simulate Field Corrosion Using Wafer Specimens

Six samples of AF 1410 wafers, with cadmium plating that was sanded by UDRI to remove some of the plating thickness, were received at Boeing. These samples were then subjected to three types of corrosion tests in order to determine if corrosion attack from these tests could simulate what was seen on F/A-18 parts in the field. The corrosion tests being performed were: ASTM B117 Neutral Salt Spray, ASTM G85 Prohesion testing and ASTM G85 SO2 Salt Spray.

Wafers were vibratory etched with the identification provided on the individual package and both thinned areas and full plating thickness was recorded.

ASTM B117 Neutral Salt Spray					
Panel ID		**2**		**4**	
		Side A (Brown Spot)	**Side B**	**Side A (Brown Spot)**	**Side B**
Coating Thickness	Surrounding	0.4 mils	0.5 mils	0.4 mils	0.5 mils
	Test Area	0.10	0.15	0.15	0.15

ASTM G85 SO2 Salt Spray					
Panel ID		**5**		**7**	
		Side A (Brown Spot)	**Side B**	**Side A (Brown Spot)**	**Side B**
Coating Thickness	Surrounding	0.55 mils	0.65 mils	0.5 mils	0.65 mils
	Test Area	0.15	0.20	0.05	0.15

ASTM G85 Prohesion testing					
Panel ID		**10**		**12**	
		Side A (Brown Spot)	**Side B**	**Side A (Brown Spot)**	**Side B**
Coating Thickness	Surrounding	0.6 mils	0.7 mils	0.45 mils	0.5 mils
	Test Area	0.10	0.12	0.15	0.15

Table 4-9 - Wafer Cd Thicknesses

For the Phase I tests, a sheet of polypropylene was applied to the backside of the wafer with maskant tape per the test matrix. For the Phase II tests, the wafers were de-masked and cleaned. Another sheet of polypropylene was applied to the backside of the wafer with maskant tape to protect the Phase I test data. Wafers were identified with permanent marker on the maskant tape. Wafers were solvent wiped to clean the test surfaces prior initial photographing and putting into test chambers. Below is a representative sample of the pre-test photographs.
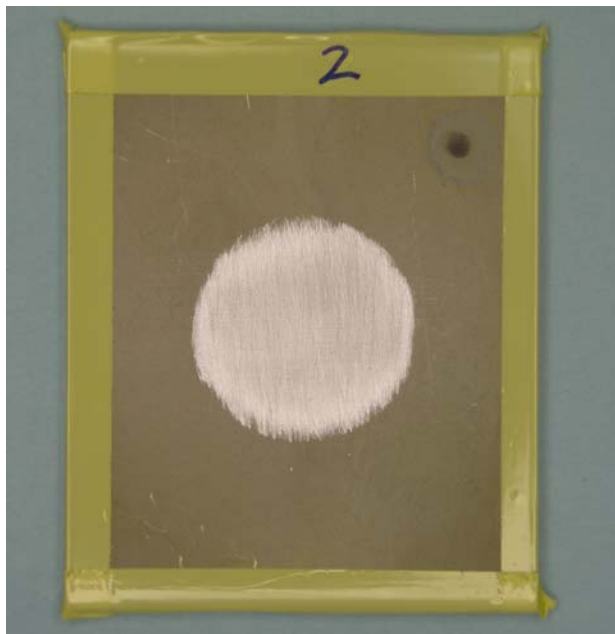
Figure 4-75 – Wafer #2 Spot Side Pre-Test Photo

4.1.1 ASTM B 117 Neutral Salt Spray – Phase I

Wafers #2 spot side and #4 no spot side were placed in the Neutral Salt Spray cabinet Monday August 6, 2007. Approximately every 24 hours during standard work days the wafers were inspected for corrosion or other changes. Photos were taken to documents changes. During the first two weekends of testing the test was suspended and the panels were forced air dried and protected from contamination in an air conditioned environment. The test was restarted on the following Monday. Due to the relatively slow corrosion rate, the wafers were left in the Neutral Salt Spray cabinet over the weekend beginning August 19, 2007.

After 573 hours in ASTM B 117 Neutral Salt Spray the wafers failed to achieve the required corrosion level as defined by UDRI. Therefore this test was terminated and the test method was eliminated from the test matrix. A scheduled second ASTM B 117 Neutral Salt Spray test was never started.
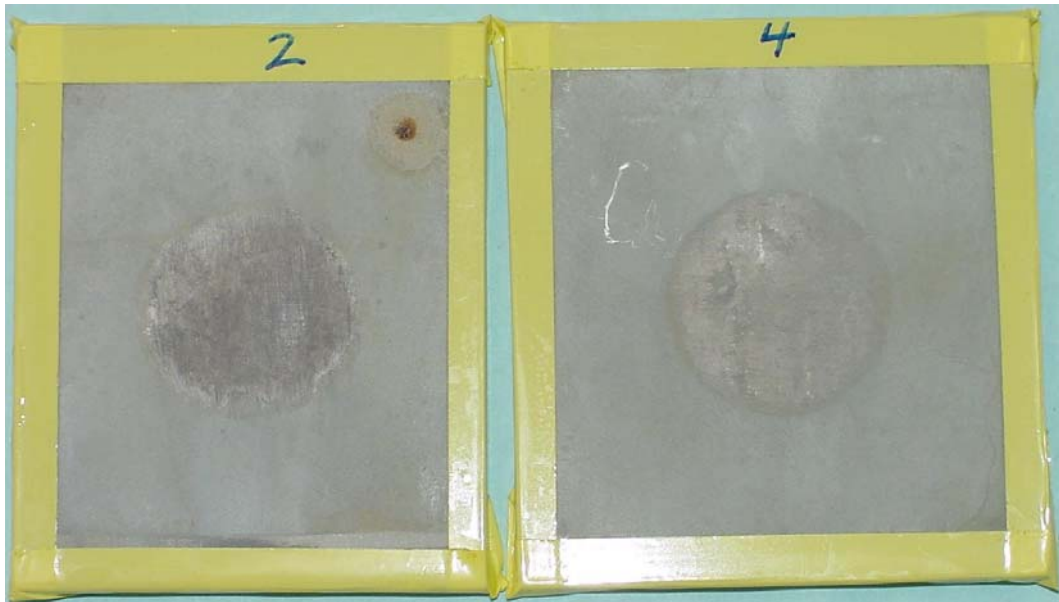
Figure 4-2 – Wafer #2 Spot Side and #4 at 339 hours Neutral Salt Spray

4.1.2 ASTM G 85 Prohesion testing – Phase I

Wafers #10 spot side and #12 no spot side were placed in the Prohesion cabinet Tuesday August 7, 2007. Inspections for red rust were scheduled for early in the morning and late in the afternoon during standard work days. During weekends the wafers were to be removed from the test.

At 48 hours into (70 hours total elapsed time) the Prohesion test a large red area appeared in the thin Cd area of wafer #12 no spot side. Wafer #12 continued to cycle in the chamber.
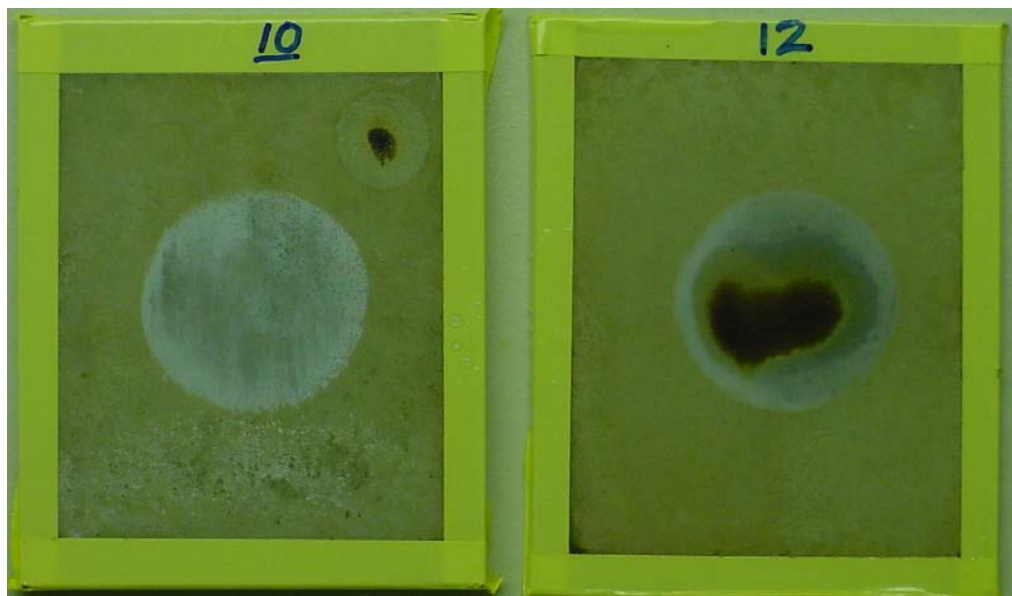
Figure 4-76 - Wafers #10 spot side and #12 no spot side at 48 hours in Prohesion Test I

Testing in the Prohesion cabinet continued till August 15, 2007 when UDRI determined requested the test be stopped. This amounted to 109 hours into (196 hours total elapsed time) the testing.
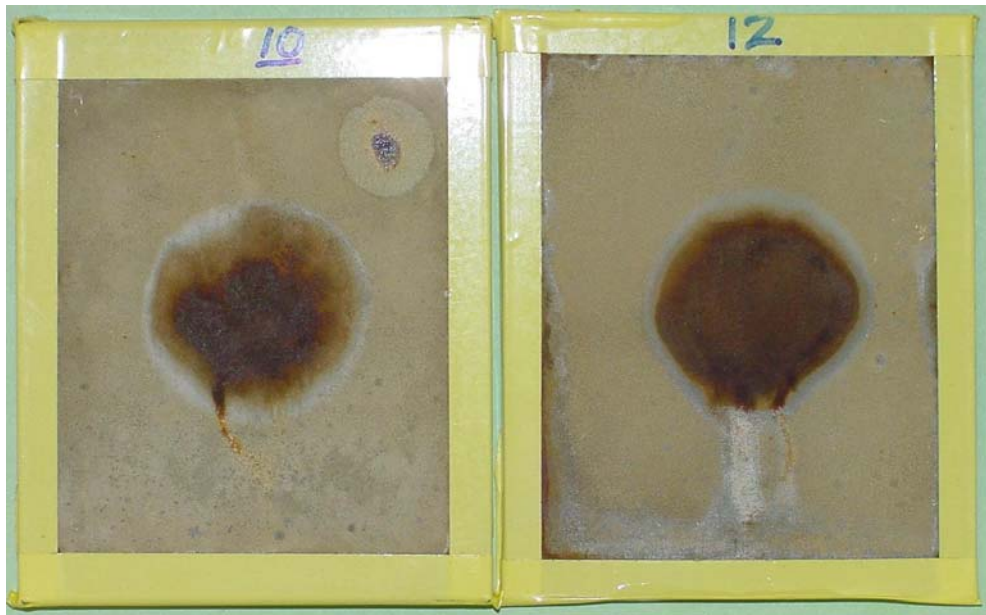
Figure 77-4 Wafers #10 spot side and #12 no spot side at 109 hours – Test Termination

4.1.3 ASTM G 85 Prohesion testing – Phase II

Based on the observations of how quickly the wafers showed corrosion in Phase I, the test was restarted using the alternate side of the wafers and changing the test methodology. The original test side was protected with polypropylene and maskant tape to preserve the results. Wafers #10 no spot side and #12 spot side were placed in the Prohesion cabinet Tuesday August 21, 2007. The wafers were inspected the next morning and allowed to continue in the test. The wafers were inspected again at the end of the shift and then rinsed, dried and protected from contaminants. The next morning at the beginning of the shift the wafers were put into the Prohesion cabinet for the shift. This daily cycle continued during standard working days till red rust corrosion was found.

At 37 hours into (72 hours total elapsed time) the Prohesion test a large red area appeared in the thin Cd area of wafer #12 spot side. Wafer #12 was removed from further testing and wafer #10 no spot side continued to cycle in the chamber.
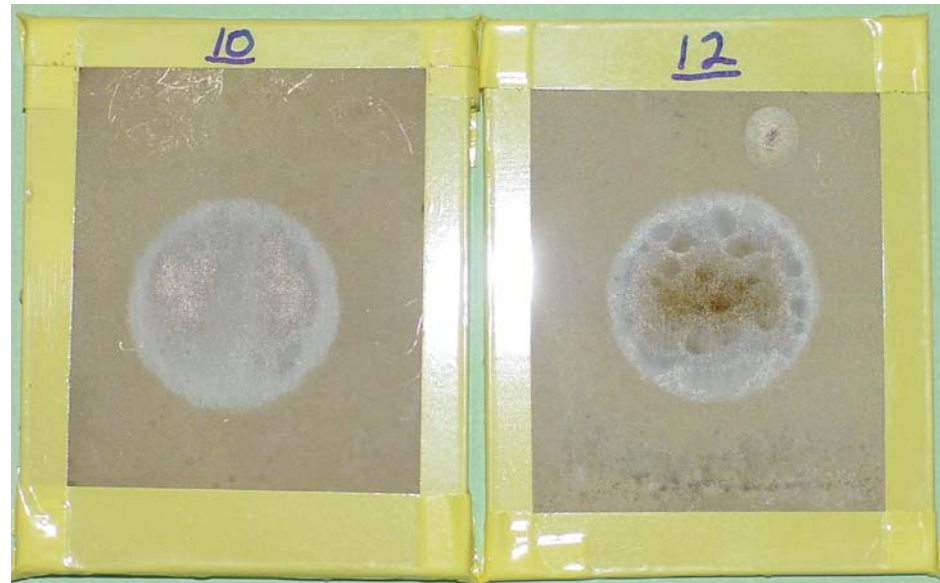
Figure 4-5 – Wafer #10 No Spot Side and #12 Spot Side at 37 in Prohesion Test II

At 50 hours into (167 hours total elapsed time) the Prohesion test significant red rust appeared in the thin Cd area of wafer #10 no spot side. Wafer #10 was removed from further testing.
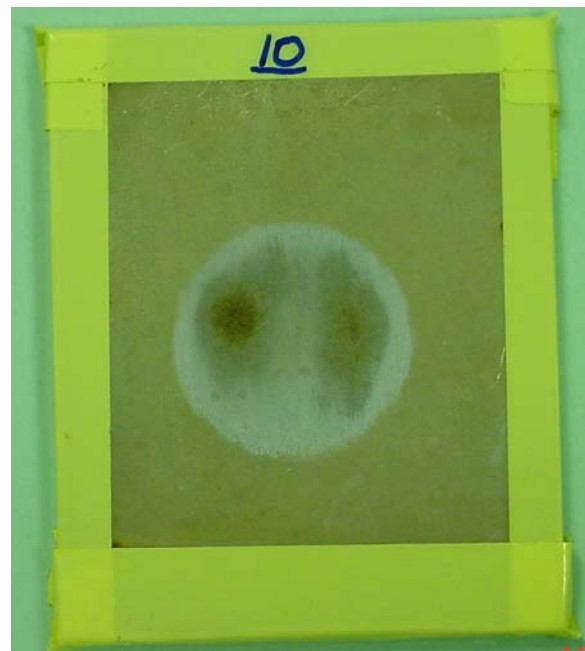
Figure 4-6 - Wafer #10 No Spot Side and #12 Spot Side at 50 hours in Prohesion Test II

4.1.4 ASTM G 85 SO2 Salt Spray – Phase I

Wafers #5 spot side and #7 no spot side were placed in the SO2 Salt Spray cabinet Monday August 13, 2007. Approximately 6 hours later the wafers were inspected for corrosion or other changes.
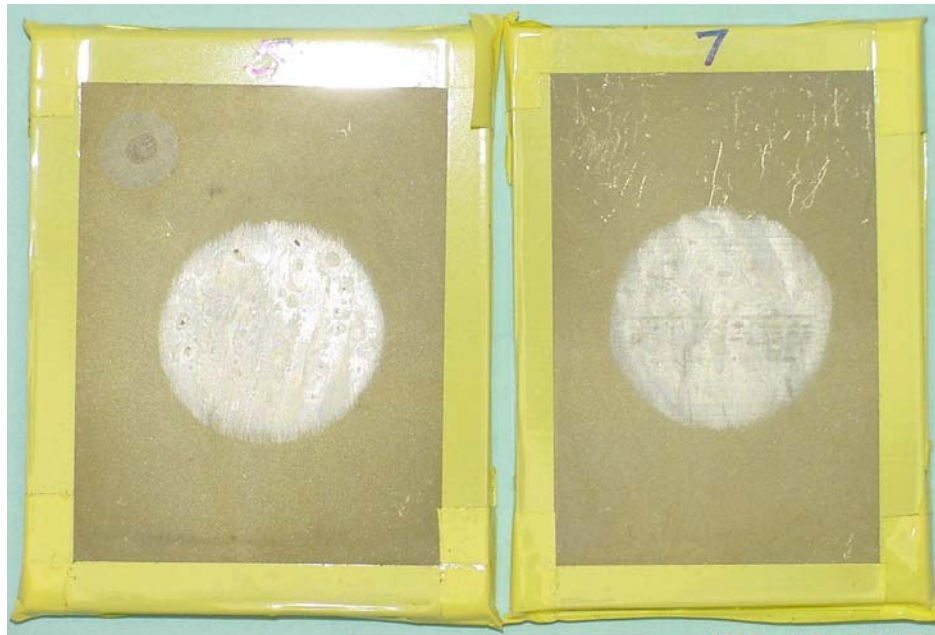
Figure 4-7 – Wafer #5 Spot Side and #7 No Spot Side at 6 hours SO2 Salt Spray I

Wafers were kept in the SO2 Salt Spray cabinet over night. The next morning 23 hours into the test, the wafers were inspected to find a major red rust area in the thinned Cd area.

Figure 4-8 – Wafer #5 Spot Side and #7 No Spot Side at 23 hours SO2 Salt Spray I

This test was terminated at 54 hours at Jenifer Pierce's direction. Also at Jenifer Pierce's direction the wafers were rinsed with tap water and brushed with a used soft toothbrush and photographed. The photos below provide a comparison of the not brushed and brushed surfaces.
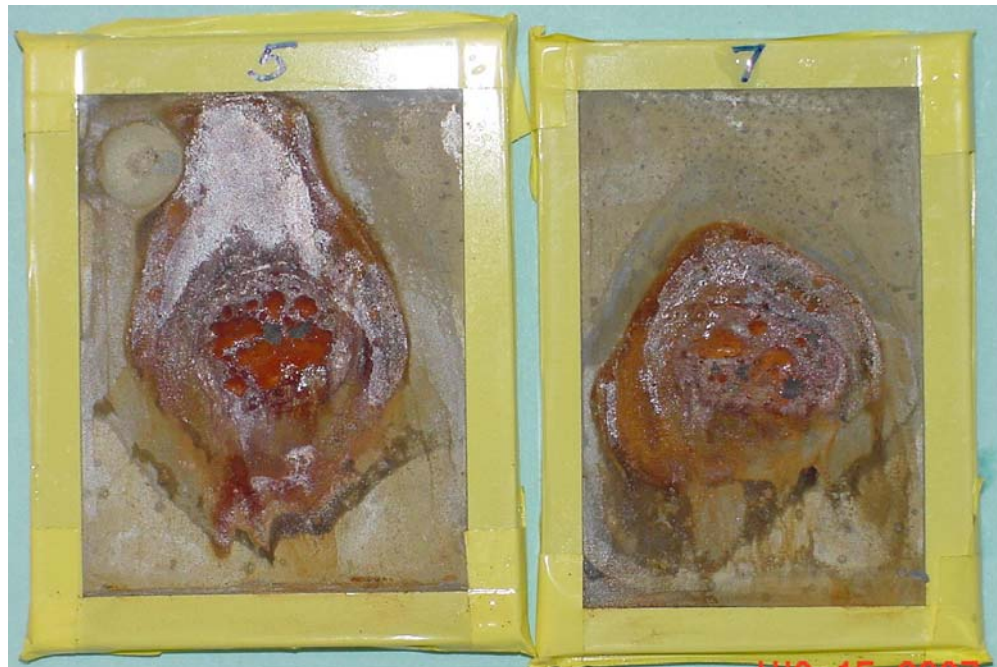
Figure 4-9 – Wafer #5 Spot Side and #7 No Spot Side Not Brushed at 54 hours SO2 Salt Spray I – Test Termination
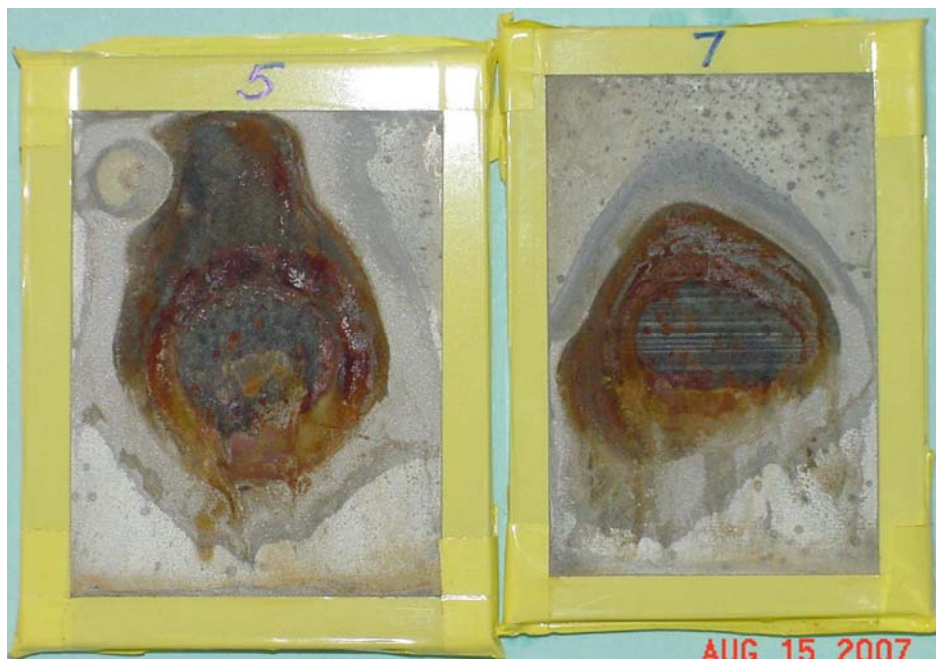
Figure 4-10 – Wafer #5 Spot Side and #7 No Spot Side – Rinsed and Brushed at 54 hours SO2 Salt Spray I – Test Termination

4.1.5 ASTM G 85 SO2 Salt Spray – Phase II

Based on the observations of how quickly the wafers showed corrosion in Phase I, the test was restarted using the alternate side of the wafers and changing the test methodology. Wafers #5 no spot side and #7 spot side were placed in the SO2 Salt Spray cabinet at Tuesday August 21, 2007. The wafers were inspected after a single 6 hour SO2 Salt Spray cycle and then rinsed, dried and protected from contaminants. The next morning the wafers were put into the SO2 Salt Spray cabinet for another single cycle followed by inspection. This one cycle per day was continued during standard working days till red rust corrosion was found.

The test of Wafer #7 Spot Side was terminated after 2 cycles at Steve Gaydos' direction. Wafer #5 is continuing to cycle in the SO2 cabinet.
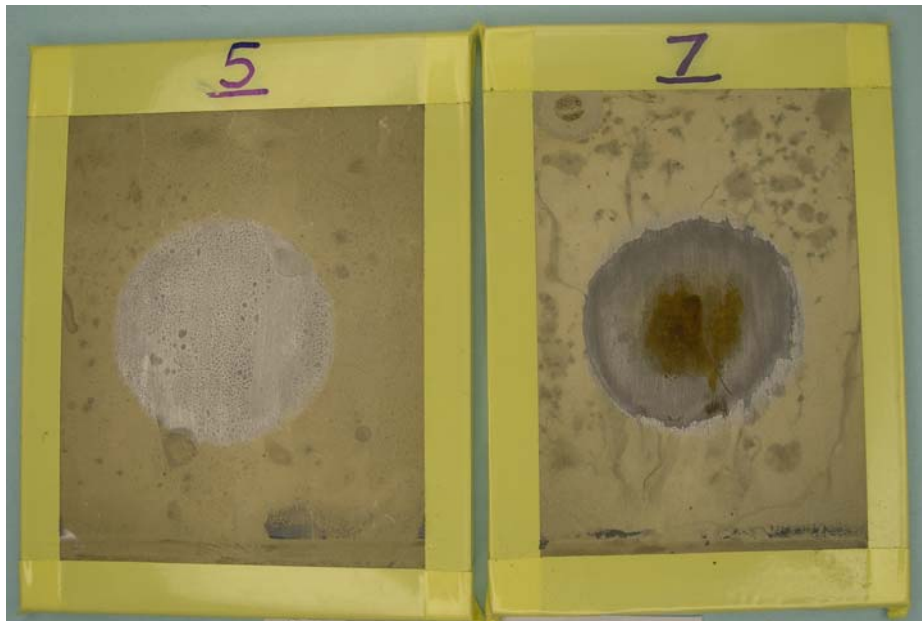
Figure 4-11 - Wafer #5 No Spot Side and #7 Spot Side at 12 hours SO2 Salt Spray II – Wafer #7 Spot Side Test Termination

4.2 Tests Of An Actual Fatigue Bar To Verify Corrosion Matches Field Corrosion

4.2.1 Fatigue Bar Test I

A WebEx meeting was held on 19 November 2007. It was decided to run a dummy fatigue bar to verify the procedures developed during previous tests. Craig Scott prepared written procedures to be followed in the verification test. These procedures were reviewed and accepted by the team.

A fatigue bar was received at Boeing on 28 November 2007 from UDRI. Measurements and photographs were taken and the fatigue bar was prepared for the SO_2 Salt Fog chamber.

Cd Thickness Measurements of Fatigue Bar 545-7B

Specimen ID	Location	Cd Thickness (mils)	
		Test Side	Back Side
544-7B	1	0.87	1.07
	2	0.93	0.89
	3 Avg	0.11	0.63
	3a	0.10	
	3b	0.12	
	3c	0.07	
	3d	0.13	
	3e	0.08	
	3f	0.17	
	3g	0.09	
	4	0.97	1.10
	5	0.86	0.84
	6	0.96	0.93
	7	0.85	0.72
	8	1.06	1.10
	9	1.06	1.02
	10	0.96	0.99
	11	0.95	0.97
Average		0.95	0.93

NOTE (1) Specimen 545-5C had to be degaussed prior to taking measurements.
(2) Locations per J Pierce provided drawing, approximate locations only.
(3) Locations 3a through 3g were within the reduced Cd area.

Table 4-2 – Fatigue Bar 545-7C Cd Thickness Measurements
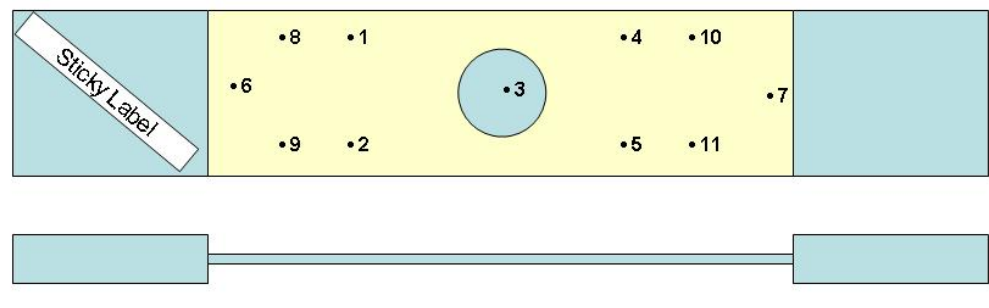
Figure 4-12 – Typical Locations for Cd Thickness Measurements for all Fatigue Bars

In addition to the fatigue bar that was received at Boeing on 28 November 2007, two cadmium coated wafers were also in the package. After photographing of the specimens, the thickness of the cadmium plating was measured using a DeFelsko magnetic induction gauge. The thicknesses were not consistent between the wafers and the fatigue bar. This prompted an investigation that found the fatigue bar was received with residual magnetism. The fatigue bar was demagnetized and the measurements were re-measured.

Cd Thickness Measurements of Wafer #6 & #9					
Specimen ID	Side	Location	Cd Thickness (mils)		
			Avg	Min	Max
6	A	Outer Area	0.73	0.50	0.76
6	A	Test Area	0.25	0.21	0.28
6	B	Outer Area	0.71	0.60	0.85
6	B	Test Area	0.26	0.23	0.29
9	A	Outer Area	0.71	0.56	0.82
9	A	Test Area	0.30	0.26	0.42
9	B	Outer Area	0.77	0.62	0.90
9	B	Test Area	0.31	0.26	0.38

Table 4-3 - Wafers #6 & # 9 Measured Cd Plating Thicknesses

Craig Scott prepared a test matrix/procedure document for developing corrosion on the fatigue bar. Upon approval of the test matrix/procedure document from UDRI, the fatigue bar was placed into the SO_2 Salt Fog chamber on 05 December 2007. Cycling the fatigue bar in the SO_2 Salt Fog chamber continued through 13 December 2007. At this point, a consensus of the team reviewing the daily photographs recommended stopping SO_2 Salt Fog testing.
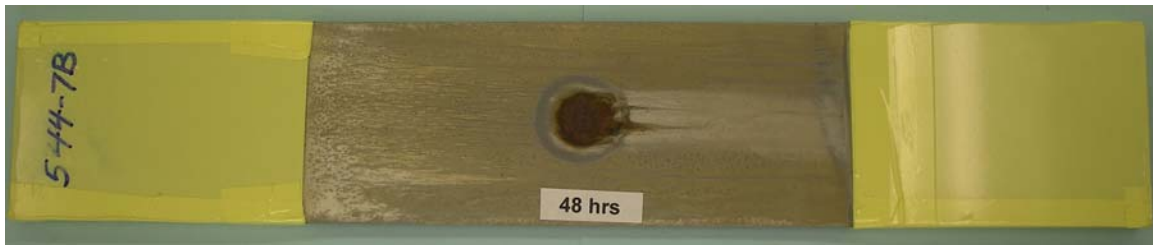
Figure 4-13 –Fatigue Bar 544-7BCorrosion at 48 Hours

The fatigue bar was prepared for shipping to UDRI and hand carried to the local FedEx office for shipment on 14 December 2007.

4.2.2 Fatigue Bar Test II

A test matrix/procedure document for developing corrosion on the fatigue bar was created. Upon approval of the test matrix/procedure document from UDRI, the fatigue bar was placed into the SO_2 Salt Fog chamber on 18 January 2008. Cycling the fatigue bar in the SO_2 Salt Fog chamber continued through 24 January 2008. At this point, a consensus of the team reviewing the daily photographs recommended stopping SO_2 Salt Fog testing on this specimen.

Cd Thickness Measurements of Fatigue Bar 545-5C

Specimen ID	Location	Cd Thickness (mils)	
		Test Side	Back Side
545-5C	1	0.63	0.77
	2	0.61	0.60
	3 Avg	0.16	
	3a	0.18	
	3b	0.20	
	3c	0.21	
	3d	0.12	
	3e	0.17	
	3f	0.01	
	3g	0.22	
	4	0.70	0.69
	5	0.65	0.70
	6	0.63	0.65
	7	0.89	0.73
	8	0.59	0.75
	9	0.70	0.50
	10	0.89	0.75
	11	0.83	0.69
Average		0.71	0.68

NOTE (1) Specimen 545-5C had to be degaussed prior to taking measurements.
(2) Locations per J Pierce provided drawing, approximate locations only.
(3) Locations 3a through 3g were within the reduced Cd area.

Table 4-4 - Fatigue Bar 545-5C Cd Thickness Measurements
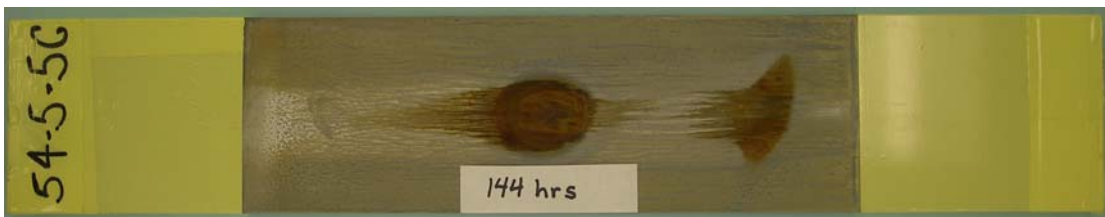
Figure 4-14 –Fatigue Bar 545-5CCorrosion at 144 Hours

The fatigue bar was prepared for shipping to UDRI and hand carried to the local FedEx office for shipment on 24 January 2008.

4.3 Corrode Fatigue Bars For Future Test

Due to the corrosion through the Cd plating, the test matrix/procedure document for developing corrosion was modified to mask the entire fatigue bar to with in a ¼ inch of the test area. Upon approval of the test matrix/procedure document from UDRI, the fatigue bar was measured for Cd plating thickness and a Chem Mill maskant (AC Products, Inc., AC-854-GEL-NF) was painted on in two coats and allowed to cure for 24 hours.

Figure 4-15 - Fatigue Bar 614-14 showing typical application of Chem Mill Maskant

Cd Thickness Measurements of Fatigue Bar 545-C1

Specimen ID	Location	Cd Thickness (mils)	
		Test Side	Back Side
545-C1	1	0.92	0.89
	2	0.84	0.89
	3 Avg	0.12	0.63
	Inner Dot	0.05	
	Inner Ring	0.07	
	Outer Ring	0.25	
	4	0.74	0.86
	5	0.85	0.84
	6	0.89	0.85
	7	0.81	0.78
	8	0.87	0.96
	9	0.87	1.00
	10	0.64	0.98
	11	0.88	0.82
Average		0.83	0.89

NOTE (1) Locations per J Pierce provided drawing, approximate locations only.
(2) Location 3 is within the reduced Cd area.

Table 4-5 - Fatigue Bar 545-C1 Cd Thickness Measurements

Cd Thickness Measurements of Fatigue Bar 614-10

Specimen ID	Location	Cd Thickness (mils)	
		Test Side	Back Side
614-10	1	0.80	0.82
	2	0.80	0.69
	3 Avg	0.08	0.55
	Inner Dot	-0.02	
	Inner Ring	-0.02	
	Outer Ring	0.28	
	4	0.73	0.81
	5	0.81	0.70
	6	0.79	0.81
	7	0.85	0.75
	8	0.85	0.98
	9	0.82	0.75
	10	0.52	0.88
	11	0.82	0.49
Average		0.78	0.77

NOTE (1) Locations per J Pierce provided drawing, approximate locations only.
(2) Location 3 is within the reduced Cd area.

Table 4-6 - Fatigue Bar 614-10 Cd Thickness Measurements

Cd Thickness Measurements of Fatigue Bar 614-14

Specimen ID	Location	Cd Thickness (mils)	
		Test Side	Back Side
614-14	1	0.70	0.79
	2	0.72	0.65
	3 Avg	0.03	0.51
	Inner Dot	-0.02	
	Inner Ring	-0.02	
	Outer Ring	0.12	
	4	0.67	0.67
	5	0.74	0.63
	6	0.74	0.78
	7	0.75	0.77
	8	0.87	0.92
	9	0.85	0.87
	10	0.65	0.76
	11	0.68	0.70
Average		0.74	0.75

NOTE (1) Locations per J Pierce provided drawing, approximate locations only.
(2) Location 3 is within the reduced Cd area.

Table 4-6 - Fatigue Bar 614-14 Cd Thickness Measurements

Cd Thickness Measurements of Fatigue Bar 614-23

Specimen ID	Location	Cd Thickness (mils)	
		Test Side	Back Side
614-23	1	0.56	0.71
	2	0.53	0.70
	3 Avg	0.03	0.52
	Inner Dot	-0.05	
	Inner Ring	-0.05	
	Outer Ring	0.19	
	4	0.60	0.76
	5	0.56	0.79
	6	0.61	0.67
	7	0.79	1.04
	8	0.74	0.91
	9	0.66	0.74
	10	0.80	0.90
	11	0.76	0.76
Average		0.66	0.80

NOTE (1) Locations per J Pierce provided drawing, approximate locations only.
(2) Location 3 is within the reduced Cd area.

Table 4-7 - Fatigue Bar 614-23 Cd Thickness Measurements

The fatigue bar was placed into the SO_2 Salt Fog chamber on 11 February 2008. Cycling the fatigue bar in the SO_2 Salt Fog chamber continued through 22 January 2008. Photos were delivered via email to team members to review the fatigue bars progress. A consensus of the team reviewing the daily photographs recommended removing the fatigue bars from the SO_2 Salt Fog chamber after 198 hours.
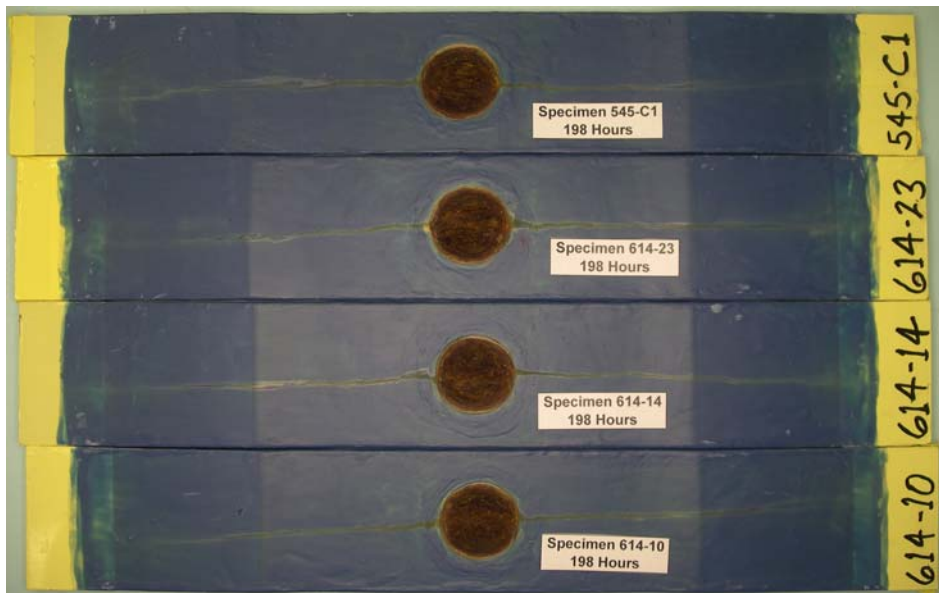
Figure 4-16 - Fatigue Bars Corrosion at 198 Hours

The fatigue bars were prepared for shipping to UDRI and hand carried to the local FedEx office for shipment on 25 February 2008.

5.0 Summary and Conclusions

This report summarizes the final effort in this program. Each section explains their work on the program during the period of performance. This effort was a first step in creating a way to determine the true impact that corrosion has on the fatigue life of a steel aircraft part. The engineers learned a lot during this effort, more work needs to be done on the prediction technique, but again, it was a first step. It did show that there had to be a significant amount of corrosion to dominate the failure mechanism of the tensile coupons.

References

[1] Perez, R. Sankaran, K. K., and Smith, Jr., H. G. "Structural Life Enhancement -Corrosion Impact on Airframe Total Life Analysis", The Boeing Company, Final Report submitted to NAVAIR, October 2003.

[2] Perez, R. Rich, D. Sankaran, K. K., and Smith, Jr., H. G. "High Strength Steel Corrosion-Fatigue Modeling ", The Boeing Company, Final Report (Period January 2004 – April 2006), Sub Contract RSC03024, submitted to UDRI, April 2006.

[3] Easley, S.J., Neal, A.L., Sankaran, K. K., and Smith, Jr., H. G. "High Strength Steel Corrosion-Fatigue Modeling ", The Boeing Company, Final Report (Period January 2004 – February 2007), Sub Contracts RSC03024 (January 2004 – April 2006) and RSC06014 (August 2006 – January 2007), submitted to UDRI, February 2007.

[4] Easley, S.J., Neal, A.L., Sankaran, K. K., and Smith, Jr., H. G. "High Strength Steel Corrosion-Fatigue Modeling ", The Boeing Company, Final Report (Period August 2006 - August 2007), Sub Contracts RSC06014 submitted to UDRI, August 2007.

Appendix C
Aermet100 Test Plan

Ref: (a) ASTM Designation: E8, "Standard Test Methods for Tension Testing of Metallic

Materials," ASTM.

(b) ASTM Designation: E9, "Standard Test Methods of Compression Testing of Metallic

Materials at Room Temperature," ASTM.

(c) ASTM Designation: E606, "Standard Practice for Strain-Controlled Fatigue Testing,"

ASTM.

(d) ASTM Designation: E646, "Standard Test Methods for Tensile Strain-Hardening

Exponents (n – Values) of Metallic Sheet Materials," ASTM.

(e) ASTM Designation: E111, "Standard Test Method for Young's Modulus, Tangent

Modulus and Chord Modulus," ASTM.

(f) ASTM Designation: E466, "Standard Practice for Conducting Constant Amplitude

Axial Fatigue Tests of Metallic Materials," ASTM.

1. The NAVAIR Airframe Technology Team (AIR 4.3.3.5) requests the services of the University of Dayton Research Institute to perform fabrication and material property testing of Aermet100 steel coupons. The required tests are static tensile, compression, incremental step and strain-controlled & load-controlled fatigue. Fabrication requirements are for (30) round, small-size tensile test specimens with 0.25 in. nominal diameter per Ref. (a), (30) solid cylindrical compression test specimens per Ref. (b), and (375) uniform-gage strain-life specimens per Ref. (c), with 0.25 in. nominal diameter and 0.75 in. reduced section length.

2. Tensile testing requirements are as follows:

   a. All tensile coupons are to be tested in accordance with Ref. (a), (d) & (e), at room temperature in laboratory air. A minimum of 10 coupons are to be tested under replicated test conditions.

   b. Speed of testing is to be specified in terms of strain rates. A nominal strain rate of 0.005 in./in.· min. is specified for the elastic portion of the tests, and a nominal strain rate of 0.2 in./in.· min. is specified for the plastic portion of the tests. The transition point for switching to the higher strain rate during the test is at an engineering strain value above the 0.2% offset yield strain of the test coupons.

   c. At least three elastic tensile pulls below the proportional limit should be performed before the start of tensile testing to collect data for the determination of Young's modulus (Ref. (e)).

   d. Test results to be reported include those listed in Ref. (a), Section 8.2 and 8.3. A complete history of the test coupon response from test initiation until necking is also to be digitally recorded in a format that can be transformed in to an ASCII data file. Variables to be recorded are time, load, axial strain and displacement. After necking, the variables to be recorded are time, load and displacement up to and including final failure. The sampling rate for the elastic portion of the test should be 1 sample per second. The sampling rate for the plastic portion of the test should be 1 sample per 0.1 second.

3. Compression testing requirements are as follows:

   a. All compression coupons are to be tested in accordance with Ref. (b), and will be performed to measure the compressive stress-strain curve and compressive elastic modulus at room temperature in laboratory air. A minimum of 10 coupons are to be tested under replicated test conditions.

b. At least three elastic compression cycles below the proportional limit should be performed before the start of compression testing to collect data for the determination of compressive Young's modulus (Ref. (e)).

c. A history of the test coupon response from test initiation until the end of test is to be digitally recorded in a format that can be transformed in to an ASCII data file. Variables to be recorded are time, load, axial strain and displacement. The sampling rate for the test should be 1 sample per second.

4. Incremental step testing requirements are as follows:

a. All incremental step coupons are to be tested in accordance with Ref. (c), at room temperature in laboratory air. A minimum of 10 coupons are to be tested under replicated test conditions.

b. Standard round uniform-gage strain-life test coupons conforming to the geometry recommended in Ref. (c) should be used, with a nominal gage diameter of 0.25 in., and a nominal reduced section length of 0.75 in.

c. Incremental step tests are to be performed under strain control, using a strain history block file provided by NAVAIR. The test blocks have an initial maximum peak strain amplitude of 2.0%, with subsequent tensile peaks stepped down in increments of 0.05% strain, and then stepped up in increments of 0.05% strain to 2.0% strain amplitude. The block file should be repeated until coupon failure, or until 10 complete blocks have been applied.

d. Testing is to be conducted at a constant axial strain rate of 0.02 in/in/sec.

e. Test data is to be digitally recorded in a format that can be transformed into an ASCII data file. Variables to be recorded are time, load, axial strain and load segment. A sampling rate of 0.005 seconds per sample is specified for each test. All cycle data for the complete test should be recorded.

5. Strain-controlled fatigue testing requirements are as follows:

a. Perform (180) strain-controlled fatigue tests per Ref. (c). Tests to be performed are fully reversed (R = -1.0), constant amplitude at various maximum strain values where inelastic deformation is present. A triangular waveform is to be used, with initial straining in the tension direction. All testing is to be conducted at a constant axial strain rate of 0.02 in/in/sec, at room temperature in laboratory air.

b. Some specimens at lower strain amplitudes are to be subjected to initial overstraining of approximately 20 cycles before the start of constant-amplitude testing. Initial overstraining is to be performed in strain control, with a waveform and duration specified by AIR 4.3.3.5.

c. Failure is defined as complete fracture of the specimen. All fractured specimens, including untested spares, are to be kept and returned to AIR 4.3.3.1 at the conclusion of testing.

d. Test data is to be digitally recorded in a format that can be transformed in to an ASCII data file. Variables to be recorded are time, load, axial strain and load segment or cycles. A sampling rate of 0.01 seconds is specified for all tests. All cycle data for the complete test should be recorded, unless a method is used to record selected cycles from the strain history. In such a case, all peak load and strain values for each cycle shall be recorded for the entire test.

e. A test matrix, which includes the number of specimens to be tested and the strain levels, will be provided by AIR 4.3.3.5. A Randomized Complete Block (RCB) test structure is used, in which the test specimens, strain levels and test order have been randomized. All tests should thus be conducted according to the test matrix, in the order specified. If multiple test machines are to be used, each test machine should be assigned one complete block of specimens to test. Tests within a block should not be divided between test machines. The machine used to test each block of specimens should be recorded.

f. Anomalies that occur during the course of testing that may impact the observed results, such as strain-gage recalibration, fixture realignment, hardware failure, etc., should be reported to AIR 4.3.3.5 as they occur. Events should be referenced to the test number in which the event occurred, or to the last successful test completed prior to the event.

6. Load-controlled fatigue testing requirements are as follows:

a. Perform (155) load-controlled fatigue tests per Ref. (f). Tests to be performed are fully reversed (R = -1.0), constant amplitude, load controlled fatigue tests at various maximum load amplitudes. A sine waveform is to be used, with initial loading in the tension direction. All testing is to be conducted at the frequency specified in the test plan, at room temperature in laboratory air. Runout is to be at 1×10^7 cycles.

b. Test specimens will be subjected to initial overstraining of approximately 10 cycles before the start of constant-amplitude testing. Initial overstraining is to be performed in strain control, with a waveform and duration specified by AIR 4.3.3.5. Periodic overstrains are to be introduced at every 2.5×10^5 cycles during the load-controlled test, using a strain-controlled overstrain profile of approximately 2 cycles, with a waveform and duration specified by AIR 4.3.3.5. Initial and periodic overstrain events are to be conducted at a constant axial strain rate of 0.02 in/in/sec.

c. Failure is defined as complete fracture of the specimen. All fractured specimens, including untested spares, are to be kept and returned to AIR 4.3.3.5 at the conclusion of testing.

d. Data for the initial & periodic overstrain portions of the loading history does not need to be recorded for any tests with initial or periodic overstraining. For the load controlled tests, only the number of cycles to failure needs to be recorded, and a notation if the failure occurs during an overstrain event.

e. A test matrix, which includes the number of specimens to be tested and the strain levels, will be provided by AIR 4.3.3.5. A Randomized Complete Block (RCB) test structure is used, in which the test specimens, strain levels and test order have been randomized. All tests should thus be conducted according to the test matrix, in the order specified. If multiple test machines are to be used, each test machine should be assigned one complete block of specimens to test. Tests within a block should not be divided between test machines. The machine used to test each block of specimens should be recorded.

f. Anomalies that occur during the course of testing that may impact the observed results, such as fixture realignment, hardware failure, etc., should be reported to AIR 4.3.3.5 as they occur. Events should be referenced to the test number in which the event occurred, or to the last successful test completed prior to the event.

Appendix D
Displacement Transducer Calibration Sheet

UDRI Structural Test Laboratory

Displacement Transducer Calibration Sheet   Cat. Item Number _____

Machine Number	2 Calibration Date	7-Jun-07	Temp /Humidity	74°F /48%	Performed by	R. Glett

Transducer Type/Capacity	Extensometer/+.02"	Transducer Conditioner	MTS 458.11	Readout	Console
Manufacturer	MTS	Serial Number	124858	Mfgr	MTS
Model Number	632.27B-30 OPT001	Gage Factor		Model #	458.20
Serial Number	148	Excitation Voltage	6.0V.	Serial #	546975
Allowable tolerance:	1.0% of Standard value	Condition Rec'd./Ret'd:	Good/Good	Cal.Spec.#:	Class B2
Comments: Class B2 calibration. Used Gage blocks with 650.03 calibrator.		1.000" G.L.		Shunt cal.= internal	

Standard Data		Range 1:	0.02 in./in.	=V. full scale	10	Cal Value:	-0.01249
		% of	Transducer Readings		Standard Readings		%Error	
	17/04	Full Scale	Run 1	Run 2	Applied	Blocks used	Pre-Cal	Post-Cal
Standard Used for This Range	Gage blocks w/650.03 calibrator	0%	.00000	.00000	.0000000	.200	0.0000	0.0000
Standard Type	Brown & Sharpe Super A-jo set	10%	.00200	.00200	.0020001	0.1+.102	-0.0035	-0.0035
Standard Capacity	.050" to 4.0"	20%	.00400	.00399	.0040002	0.1+.104	-0.0037	-0.2537
Standard Serial Number	Set F-39	30%	.00601	.00599	.0059992	0.1+.106	0.1795	-0.1539
Standard Calibration Data	3-May-04 Brown & Sharpe	40%	.00800	.00800	.0079963	0.1+.108	0.0461	0.0461
Standard Readout Meter r	Nist trace 821/257390-96	50%	.01004	.01003	.0100004	0.1+.110	0.3962	0.2962
Standard Readout Meter S/N		60%	.01201	.01202	.0120070	.110+.102	0.0253	0.1086
Comments Shunts:		70%	.01402	.01401	.0140055	.110+.104	0.1032	0.0318
		80%	.01601	.01602	.0160036	.110+.106	0.0399	0.1024
		90%	.01800	.01803	.0180027	.110+.108	-0.0149	0.1517
		100%	.02000	.02000	.0200018	0.1+.120	-0.0088	-0.0088
		0%	.00000	.00000	.0000000	.200	0.0000	0.0000
		#VALUE!					#VALUE!	#VALUE!
		#VALUE!					#VALUE!	#VALUE!
		#VALUE!					#VALUE!	#VALUE!

Standard Data	Same	Range 2:	0.02 in.	=V. full scale	10	Cal Value:	-0.01249
		% of	Transducer Readings		Standard Readings		%Error	
		Full Scale	Run 3	Run 4	Applied	Blocks used	Pre-Cal	Post-Cal
Standard Used for This Range		0%	.00000	.00000	.0000000	.200	0.0000	0.0000
Standard Type		10%	.00201	.00200	.0020001	0.1+.102	0.4965	-0.0035
Standard Capacity		20%	.00399	.00401	.0040002	0.1+.104	-0.2537	0.2462
Standard Serial Number		30%	.00600	.00600	.0059992	0.1+.106	0.0128	0.0128
Standard Calibration Data		40%	.00800	.00801	.0079963	0.1+.108	0.0461	0.1712
Standard Readout Meter		50%	.01003	.01004	.0100004	0.1+.110	0.2962	0.3962
Standard Readout Meter S/N		60%	.01201	.01199	.0120070	.110+.102	0.0253	-0.1413
Comments Gain=		70%	.01402	.01400	.0140055	.110+.104	0.1032	-0.0396
DK=		80%	.01601	.01600	.0160036	.110+.106	0.0399	-0.0226
Exc.=		90%	.01803	.01798	.0180027	.110+.108	0.1517	-0.1260
		100%	.02000	.02000	.0200018	0.1+.120	-0.0088	-0.0088
		0%	-.00001	.00000	.0000000	.200	0.0000	0.0000

Standard Data	Same	Range 3:	in.	=V. full scale		Cal Value:	
		% of	Transducer Readings		Standard Readings		%Error	
		Full Scale	Pre-Cal	Post-Cal	Applied	Reading	Pre-Cal	Post-Cal
Standard Used for This Range		#VALUE!					#VALUE!	#VALUE!
Standard Type		#VALUE!					#VALUE!	#VALUE!
Standard Capacity		#VALUE!					#VALUE!	#VALUE!
Standard Serial Number		#VALUE!					#VALUE!	#VALUE!
Standard Calibration Data		#VALUE!					#VALUE!	#VALUE!
Standard Readout Meter		#VALUE!					#VALUE!	#VALUE!
Standard Readout Meter S/N		#VALUE!					#VALUE!	#VALUE!
Comments		#VALUE!					#VALUE!	#VALUE!
		#VALUE!					#VALUE!	#VALUE!
		#VALUE!					#VALUE!	#VALUE!
		#VALUE!					#VALUE!	#VALUE!

Standard Data	Same	Range 4:	in.	=V. full scale		Cal Value:	
		% of	Transducer Readings		Standard Readings		%Error	
		Full Scale	Pre-Cal	Post-Cal	Applied	Reading	Pre-Cal	Post-Cal
Standard Used for This Range		#VALUE!					#VALUE!	#VALUE!
Standard Type		#VALUE!					#VALUE!	#VALUE!
Standard Capacity		#VALUE!					#VALUE!	#VALUE!
Standard Serial Number		#VALUE!					#VALUE!	#VALUE!
Standard Calibration Data		#VALUE!					#VALUE!	#VALUE!
Standard Readout Meter		#VALUE!					#VALUE!	#VALUE!
Standard Readout Meter S/N		#VALUE!					#VALUE!	#VALUE!
Comments		#VALUE!					#VALUE!	#VALUE!
		#VALUE!					#VALUE!	#VALUE!
		#VALUE!					#VALUE!	#VALUE!
		#VALUE!					#VALUE!	#VALUE!

Notes: All Applied standard readings are error and temperature corrected.

Restrictions: For Navair Aermet100 program

Appendix E
Strain-Life Test Results

LABORATORY REPORT

To:	University of Dayton	**Project No.:**	741-85142-1
	Attn: Garry Abfalter		
	Structures and Materials Evaluation Group	**Date:**	August 27, 2007
	300 College Park		
	Dayton, OH 45469-0135	**Authorization:**	N00014-06-C-0643

Project : Low Cycle Fatigue Testing of (40) Aermet 100 Bar Specimens Prepared by Metcut from Material Supplied and Identified by University of Dayton.

All testing was conducted in accordance with the specifications referenced below.
Exceptions to these specifications, if any, are noted in the report.

Material Identity:	Aermet 100
Test Specification:	ASTM E606-04
Machining Finish:	Low Stress Ground & Polished

Test Conditions

Mode:	Longitudinal Strain Control
Extensometer Length:	0.500 in.
Temperature:	75°F
Strain Ratio:	R = -1.0
Frequency:	0.001 in./in./sec.
Waveform:	Triangular
Test Machine:	Closed Loop Servo Controlled Hydraulic System of 50,000 Lbf.
	Capacity (LCF No. 60020)

Crack Initiation (Ni) detection was accomplished by means of a continuous load monitor and represents a discernible deviation from the mean after the stabilized portion of the trace.

Thomas E. Arnold	Kenneth G. Horner
Manager, Engineering	Project Engineer

LABORATORY REPORT

METCUT

To:	University of Dayton	**Project No.:** 0741-85143-2

To: University of Dayton
ATTN: Garry Abfalter
Structures and Materials Evaluation Group
300 College Park
Dayton, OH 45469-0135

Project No.: 0741-85143-2
Date: June 18, 2007
Authorization: R0700926

Project: Tensile Testing of (3) Bar Specimens Prepared by Metcut Research Inc. from Material Supplied and Identified by University of Dayton.

All testing was conducted in accordance with the specifications referenced below. Exceptions to these specifications, if any, are noted in the report.

Material Identification: AerMet 100
Drawing Number: 4013195-603
Nominal Gage Dimensions: 0.25 in. dia. x 1.36 in. egl.
Testing Specification: ASTM E-8(04)
Extensometer Gage Length (in.): 1.0 in.
Strain Rate through 0.2% yield: 0.005 in./in./min.
Head Rate thence to failure: 0.05 in./min.
Test Temperature (°F): 70

Metcut Test Number	Specimen Identification	U.T.S. (ksi)	0.2% Y.S. (ksi)	Elong. (%)(a)	R.A. (%)
T-167008	16-11	293	263	12	67
T-167009	21-4	283	256	12	69
T-167010	23-7	289	259	11	67

Notes: (a) Value based on overall length measurements.

Patrick J. Walling
Project Engineer

Gregory T. Kasten
Testing Specialist

J:\85143\35\reports\85143-2.xls
eld

LOW CYCLE FATIGUE DATA SUMMARY
Axial Strain Measurement and Control

Material: Aermet 100
Strain Ratio: R = -1.0
Waveform: Triangular
Date: 8/27/2007
Ecalc v 8.01

METCUT Project No.: 741-85142-1
METCUT Engineer: Kenneth Horner
METCUT Phone No.: 513-271-5100
Customer Engineer: Garry Abfalter
P.O. Number: N00014-06-C-0643

Specimen Number	Metcut Test No.	Test Mach. No.	Test Temp. (°F)	Freq. (Hz)	R.T. Dim. (in)	R.T. Mod. E x 10^6	E.T. Dim. (in)	Test Area (in²)	Gauge Length (in)	First Cycle Mod. E x10^6	First Cycle $\Delta\varepsilon_t$ (%)	First Cycle σ Max (ksi)	First Cycle σ Min (ksi)	Cycles Data Calc.	Midlife $\Delta\sigma$ (ksi)	Midlife σ Max (ksi)	Midlife σ Min (ksi)	Midlife Mod E x10^6	Midlife $\Delta\varepsilon_{tm}$ (%)	Midlife $\Delta\varepsilon_e$ (%)	Midlife $\Delta\varepsilon_p$ (%)	Midlife $\Delta\varepsilon_{pm}$ (%)	Midlife σ_e/Alt (ksi)	Cycles Switched to Load	Cycles to Initiation	Cycles to Fracture	Results RTL (lbf)	Fracture Location (in) to Ext.
10-8	23-215	60020	75	0.02	0.3750	28.1	0.3750	0.1104	0.500	26.6	3.00	274.6	-301.7	100	553.4	274.4	-279.0	26.0	3.00	2.13	0.87	0.87	390.0	0	163	641	FRACTURE	IX,S,.05
9-13	15-215	60020	75	0.02	0.3750	28.6	0.3750	0.1104	0.500	27.8	2.40	261.0	-290.2	200	539.4	260.6	-278.8	27.5	2.40	1.96	0.44	0.43	330.0	0	503	556	FRACTURE	IX,S,.01
12-8	24-215	60020	75	0.02	0.3751	28.2	0.3751	0.1105	0.500	27.4	2.40	262.5	-288.5	99	543.0	262.4	-280.6	27.0	2.40	2.01	0.39	0.39	324.0	0	489	612	FRACTURE	IX,S,.08
20-6	39-215	60020	75	0.02	0.3751	28.3	0.3751	0.1105	0.500	27.3	2.40	262.4	-286.6	200	534.8	262.1	-272.7	26.8	2.40	2.00	0.40	0.40	321.6	0	670	732	FRACTURE	IX,S,.02
13-3	30-215	60020	75	0.02	0.3748	28.3	0.3748	0.1103	0.500	27.4	2.40	262.9	-289.1	200	538.3	264.8	-273.5	26.9	2.40	2.00	0.40	0.39	322.8	0	546	778	FRACTURE	IX,S,.10
7-8	5-215	60020	75	0.02	0.3749	28.6	0.3749	0.1104	0.500	27.5	2.40	264.3	-286.4	200	520.4	285.1	-235.3	26.3	2.40	1.98	0.42	0.42	315.6	0	430	803	FRACTURE	IX,S,.15
8-9	6-215	60020	75	0.02	0.3750	28.2	0.3750	0.1104	0.500	27.2	2.40	263.0	-283.9	500	528.5	256.6	-271.9	26.6	2.40	1.99	0.41	0.41	319.2	0	821	836	FRACTURE	OX,S,.02
26-2	40-215	60020	75	0.02	0.3750	28.1	0.3750	0.1104	0.500	27.2	2.40	262.2	-285.5	500	530.7	255.3	-275.4	26.6	2.40	2.00	0.40	0.41	319.2	0	763	908	FRACTURE	IX,S,.02
18-9	31-215	60020	75	0.02	0.3750	28.2	0.3750	0.1104	0.500	27.3	2.40	263.7	-287.6	99	534.9	277.5	-257.4	26.6	2.40	2.01	0.39	0.39	319.2	0	428	950	FRACTURE	IX,S,.20
10-11	21-215	60020	75	0.02	0.3750	28.3	0.3750	0.1104	0.500	27.5	2.40	263.0	-290.2	200	537.6	259.3	-278.3	26.9	2.40	2.00	0.40	0.40	322.8	0	423	1,255	FRACTURE	AX,S
11-9	22-215	60020	75	0.02	0.3750	28.1	0.3750	0.1104	0.500	27.3	2.40	263.1	-287.1	312	531.9	270.5	-261.4	26.5	2.40	2.01	0.39	0.39	318.0	0	583	1,624	FRACTURE	IX,S,.10
10-15	18-215	60020	75	0.03	0.3750	28.3	0.3750	0.1104	0.500	27.9	2.00	246.2	-268.8	500	508.5	243.3	-265.2	27.5	2.00	1.85	0.15	0.15	275.0	0	1,256	1,366	FRACTURE	OX,S,.09
9-10	13-215	60020	75	0.03	0.3750	28.7	0.3750	0.1104	0.500	28.2	2.00	247.5	-268.5	500	499.8	266.6	-233.2	27.4	2.00	1.82	0.18	0.17	274.0	0	1,055	1,415	FRACTURE	IX,S,.02
19-7	35-215	60020	75	0.03	0.3746	28.2	0.3746	0.1102	0.500	27.8	2.00	246.4	-268.1	500	508.1	250.6	-257.5	27.4	2.00	1.85	0.15	0.15	274.0	0	1,340	1,471	FRACTURE	AR,S,.14
18-8	33-215	60020	75	0.03	0.3750	28.1	0.3750	0.1104	0.500	27.8	2.00	247.6	-266.2	500	505.2	255.0	-250.2	27.2	2.00	1.86	0.14	0.15	272.0	0	1,302	1,543	FRACTURE	AR,S,.18
13-8	32-215	60020	75	0.03	0.3751	28.2	0.3751	0.1105	0.500	27.7	2.00	247.0	-265.6	1000	496.6	263.4	-233.2	26.9	2.00	1.85	0.15	0.16	269.0	0	1,060	1,565	FRACTURE	AR,S,.09
11-13	19-215	60020	75	0.03	0.3750	28.5	0.3750	0.1104	0.500	28.2	2.00	248.8	-270.1	500	504.3	263.0	-241.3	27.4	2.00	1.84	0.16	0.16	274.0	0	1,172	1,617	FRACTURE	AR,S,.09
12-12	26-215	60020	75	0.03	0.3746	27.9	0.3746	0.1102	0.500	27.6	2.00	245.8	-265.9	500	506.3	252.9	-253.4	27.2	2.00	1.86	0.14	0.13	272.0	0	1,643	1,692	FRACTURE	OX,S,.06
5-B	1-215	60020	75	0.03	0.3749	28.4	0.3750	0.1104	0.500	27.8	2.00	248.8	-261.6	1000	502.3	241.7	-260.6	27.3	2.00	1.84	0.16	0.16	273.0	0	1,287	1,802	FRACTURE	OX,S,.13
7-10	3-215	60020	75	0.03	0.3750	28.6	0.3750	0.1104	0.500	28.2	2.00	247.3	-268.6	500	506.8	244.7	-262.1	27.7	2.00	1.83	0.17	0.17	277.0	0	1,056	3,463	3024	OX,S,.01

Note: Specimen 8-7 experienced a broken rubber band at 209 cycles, causing the stress to shift. Void test, no charge for test.

For Specimen No. 7-10 the test was stopped and the specimen pulled in tension, to complete separation, at room temperature (as per ASTM E606). RTL (Residual Tensile Load) is the load measured.

Descriptors-Fracture Location
IX — Inside Extensometer
— Outside Extensometer in Uniform Gage Section
AX — At Extensometer
AR — At Radius
Descriptors-Preliminary Initiation Site
S — Surface

LOW CYCLE FATIGUE DATA SUMMARY
Axial Strain Measurement and Control

Material: Aermet 100
Strain Ratio: R = -1.0
Waveform: Triangular
Date: 8/27/2007
Ecalc v 8.01

METCUT Project No.: 741-85142-1
METCUT Engineer: Kenneth Horner
METCUT Phone No.: 513-271-5100
Customer Engineer: Garry Abfalter
P.O. Number: N00014-06-C-0643

Specimen Number	Metcut Test No.	Test Mach. No.	Test Temp. (°F)	Freq. (Hz)	R.T. Dim. (in)	R.T. Mod. E x 10^6	E.T. Dim. (in)	Test Area (in²)	Gauge Length (in)	First Cycle Mod. E x10^6	$\Delta\varepsilon_t$ (%)	σ Max (ksi)	σ Min (ksi)	Cycles Data Calc.	Midlife $\Delta\sigma$ (ksi)	σ Max (ksi)	σ Min (ksi)	Mod E x10^6	$\Delta\varepsilon_{tm}$ (%)	$\Delta\varepsilon_e$ (%)	$\Delta\varepsilon_p$ (%)	$\Delta\varepsilon_{pm}$ (%)	σ_e/Alt (ksi)	Cycles Switched to Load	Cycles to Initiation	Cycles to Fracture	Results RTL (lbf)	Fracture Location (in) to Ext.	Test Hours
19-9	25-215	60020	75	0.01	0.3750	28.1	0.3750	0.1104	0.500	26.4	4.00	287.1	-301.4	20	574.8	284.8	-290.0	26.4	4.00	2.18	1.82	1.82	528.0	0	58	61	FRACTURE	IX,S,.02	1.3
13-7	17-215	60020	75	0.01	0.3752	28.2	0.3752	0.1106	0.500	25.9	4.00	284.6	-308.0	48	564.3	279.5	-284.8	25.7	4.00	2.20	1.80	1.80	514.0	0	64	88	FRACTURE	AX,S	1.9
12-10	16-215	60020	75	0.01	0.3749	28.5	0.3749	0.1104	0.500	25.9	4.00	284.5	-303.3	50	561.6	278.7	-282.9	25.9	4.00	2.17	1.83	1.83	518.0	0	88	90	FRACTURE	AX,S	1.9
11-11	14-215	60020	75	0.01	0.3750	28.4	0.3750	0.1104	0.500	26.1	4.00	284.8	-308.0	51	565.2	279.2	-286.0	25.7	4.00	2.20	1.80	1.80	514.0	0	88	95	FRACTURE	IX,S,.05	2.0
10-9	12-215	60020	75	0.01	0.3750	28.5	0.3750	0.1104	0.500	26.1	4.00	285.3	-299.4	49	564.3	279.8	-284.5	25.9	4.00	2.18	1.82	1.82	518.0	0	93	99	FRACTURE	OX,S,.05	2.1
25-2	27-215	60020	75	0.01	0.3750	28.0	0.3750	0.1104	0.500	25.8	4.00	285.5	-309.8	52	567.0	280.5	-286.5	25.7	4.00	2.21	1.79	1.79	514.0	0	64	102	FRACTURE	AX,S	2.2
8-16	7-215	60020	75	0.01	0.3750	28.6	0.3750	0.1104	0.500	25.9	4.00	284.1	-302.6	51	561.8	277.6	-284.2	25.5	4.00	2.20	1.80	1.80	510.0	0	102	105	FRACTURE	AX,S	2.2
27-8	34-215	60020	75	0.01	0.3749	28.4	0.3749	0.1104	0.500	25.9	4.00	285.2	-303.5	51	564.6	279.9	-284.7	25.5	4.00	2.21	1.79	1.78	510.0	0	113	114	FRACTURE	AX,S	2.4
7-9	4-215	60020	75	0.01	0.3750	28.6	0.3750	0.1104	0.500	25.9	4.00	285.3	-296.6	97	557.3	275.3	-282.0	25.4	4.00	2.19	1.81	1.80	508.0	0	133	181	FRACTURE	IX,S,.05	3.9
1-B	2-215	60020	75	0.01	0.3750	28.4	0.3750	0.1104	0.500	25.6	4.00	284.7	-300.9	100	563.4	275.6	-287.8	25.1	4.00	2.24	1.76	1.75	502.0	0	135	269	FRACTURE	AX,S	5.7
11-5	28-215	60020	75	0.02	0.3750	28.0	0.3750	0.1104	0.500	26.7	3.00	275.3	-304.6	100	559.4	276.4	-283.0	26.1	3.00	2.14	0.86	0.86	391.5	0	238	247	FRACTURE	AX,S	4.0
13-14	36-215	60020	75	0.02	0.3750	28.3	0.3750	0.1104	0.500	26.7	3.00	274.3	-302.3	95	555.9	273.5	-282.4	26.3	3.00	2.11	0.89	0.89	394.5	0	225	247	FRACTURE	IX,S,.03	4.0
9-11	20-215	60020	75	0.02	0.3749	28.3	0.3749	0.1104	0.500	27.0	3.00	275.5	-303.0	100	556.3	275.1	-281.2	26.5	3.00	2.10	0.90	0.90	397.5	0	269	276	FRACTURE	IX,S,.05	4.5
12-11	29-215	60020	75	0.02	0.3751	28.0	0.3751	0.1105	0.500	26.7	3.00	275.2	-304.2	100	557.0	278.3	-278.7	26.1	3.00	2.13	0.87	0.86	391.5	0	287	296	FRACTURE	IX,S,.02	4.8
25-8	38-215	60020	75	0.02	0.3751	28.2	0.3751	0.1105	0.500	26.7	3.00	275.6	-300.4	100	555.4	273.5	-281.9	26.0	3.00	2.14	0.86	0.87	390.0	0	268	305	FRACTURE	AX,S	5.0
4-B	9-215	60020	75	0.02	0.3749	28.7	0.3749	0.1104	0.500	26.9	3.00	277.3	-293.4	100	547.4	276.5	-270.9	26.3	3.00	2.08	0.92	0.92	394.5	0	237	358	FRACTURE	IX,S,.05	5.8
7-1	10-215	60020	75	0.02	0.3750	28.4	0.3750	0.1104	0.500	26.9	3.00	275.8	-298.6	100	552.4	279.0	-273.4	26.2	3.00	2.11	0.89	0.89	393.0	0	221	519	FRACTURE	IX,S,.25	8.5
19-6	37-215	60020	75	0.02	0.3751	28.2	0.3751	0.1105	0.500	26.8	3.00	274.5	-302.4	99	556.3	274.0	-282.3	26.2	3.00	2.12	0.88	0.88	393.0	0	149	546	FRACTURE	AX,S	8.9
8-10	11-215	60020	75	0.02	0.3750	28.6	0.3750	0.1104	0.500	26.8	3.00	275.0	-295.7	98	541.7	276.1	-265.6	26.2	3.00	2.07	0.93	0.92	393.0	0	149	639	FRACTURE	IX,S,.17	10.4

6/16/2007

Sample ID: 741-85143.mss
Specimen Number: 1

Sample Information:

Name	Value
Specimen ID	16-11
Temperature	70
Test No:	T-167008

Load (lbf)
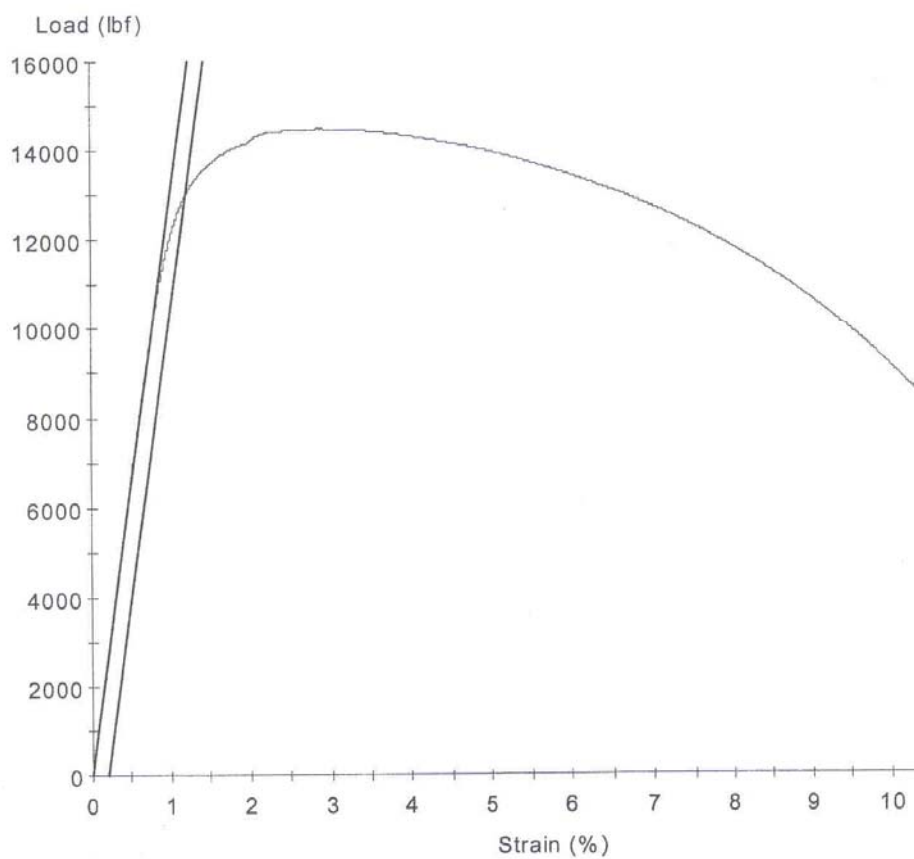
Strain (%)

6/16/2007

Sample ID: 741-85143.mss
Specimen Number: 2

Sample Information:

Name	Value
Specimen ID	21-4
Temperature	70
Test No:	T-167009

Load (lbf)
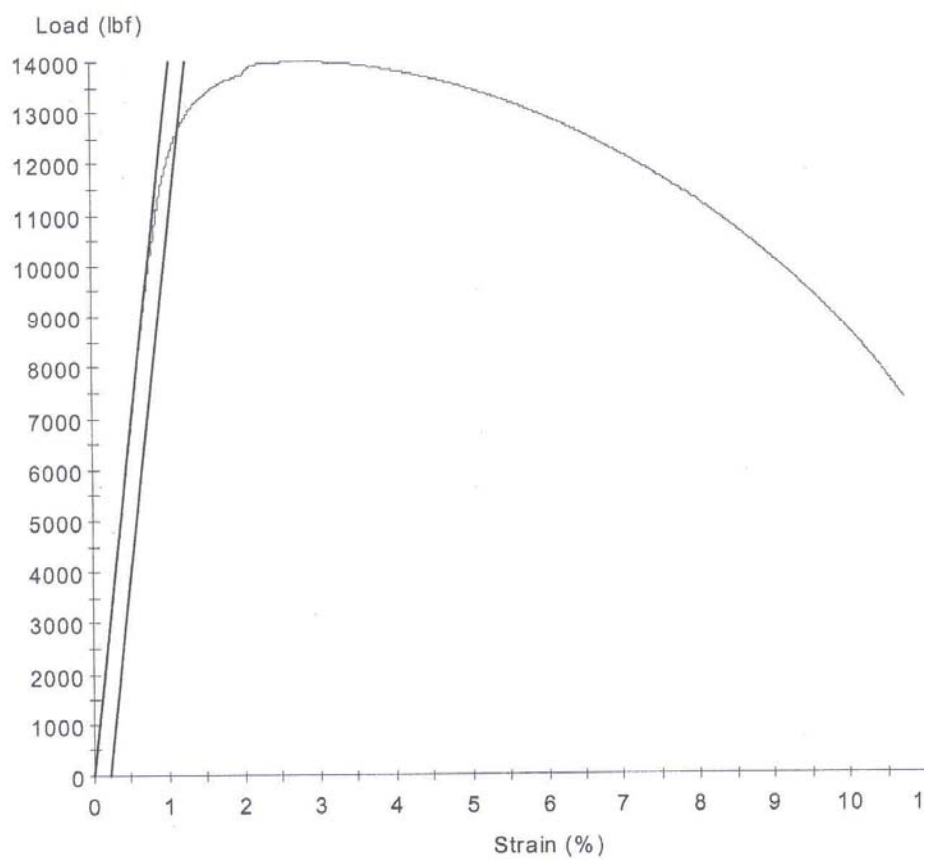
Strain (%)

6/16/2007

Sample ID: 741-85143.mss
Specimen Number: 3

Sample Information:

Name	Value
Specimen ID	23-7
Temperature	70
Test No:	T-167010
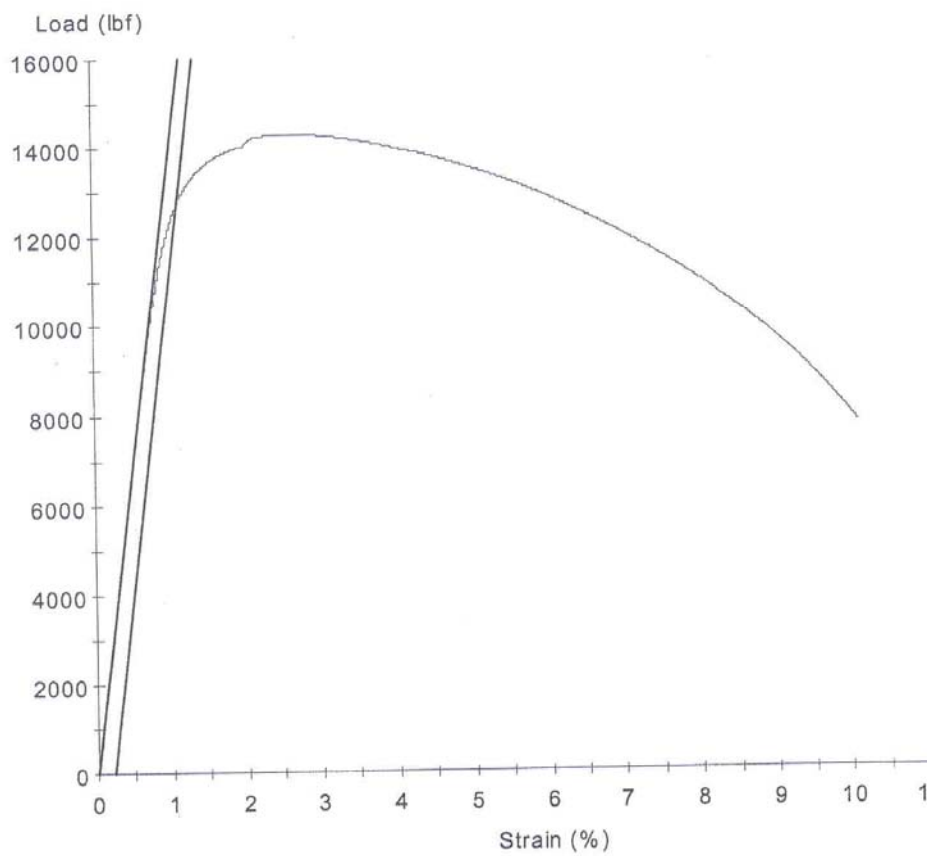
Appendix F
Procedures for Low-Stress Grinding

The goals to be achieved by hand polishing these fatigue specimens are as follows:

- Remove any machining markings and large anomalies that are transversely oriented to the loading direction from the specimens' gage and radii sections, which might influence the test results.

- Keep the surface residual stresses low by minimizing pressure and heat generation during the final surface preparation. Our goal is to keep the residual stresses in the range called out by low stress, specimen preparation specifications we are following.

- Achieve the appropriate surface finish called out by the low stress specimen preparation specifications we are following without creating a mirror finish.

General Procedures –

(1) Follow the Low Stress metallic test specimen preparation procedures

    a. We used 180, 240, 320, and 400 grit SiC paper whereas the procedures call out for 240, 400, and 600 grit Al2O3 paper. This is to be decided.

(2) Do's and Don'ts

    a. Wipe the specimen with ethanol using a Kimwipe

    b. Find a flat surface to work and make sure your work surface is clean before you begin.

    c. Secure your specimen down gently using a quick grip or other clamp such that you can work on the desired surface. Make sure the specimen is flat to the work surface and does not flex.

    d. Use a piece of wood with a sharp corner to back your SiC or Al2O3 paper – cut a piece of paper to wrap around the wood block that is wider than the surface you are going to work on.

    e. Start pushing the blocked paper longitudinally across the specimen away from you – start at the start of the tab and end at the start of the opposite tab. When starting and stopping, use a quick and smooth motion.

    f. <u>Only go in one direction (longitudinally) – away from you</u>.

g. Use very little pressure – enough to feel a slight amount of resistance, especially with the largest grit paper. The specimen should not flex, especially in the thinner gage section. If you press too hard you will impart residual stresses in the surface which is what we are trying to avoid.

h. Clean the specimen off with a clean Kim Wipe often, after every few strokes.

i. Polish with each finer grit paper until all longitudinal marks caused by the previous grit size paper are removed.

j. Between grit sizes, clean area entirely, wipe specimen with alcohol, and clean hands.

k. Do not grip block and paper too tightly – this will cause you discomfort. Do not press too hard – not good for you or your specimens. Take breaks often to rest.

Procedures for C-F Specimens:

1) Number the 4 surfaces of the specimen in the tab area with a Sharpie marker. Put your label on the tab end that has the hole in it. Label the flat surfaces 1 & 2 and the edge surfaces 3 & 4.

3 → 1̊   ← 4   1 → 4 ← 2

(Tab)

← radius →

The region to be polished is that between the tabs – including the radii and gage sections

← Gage section →

← radius →

(Tab)
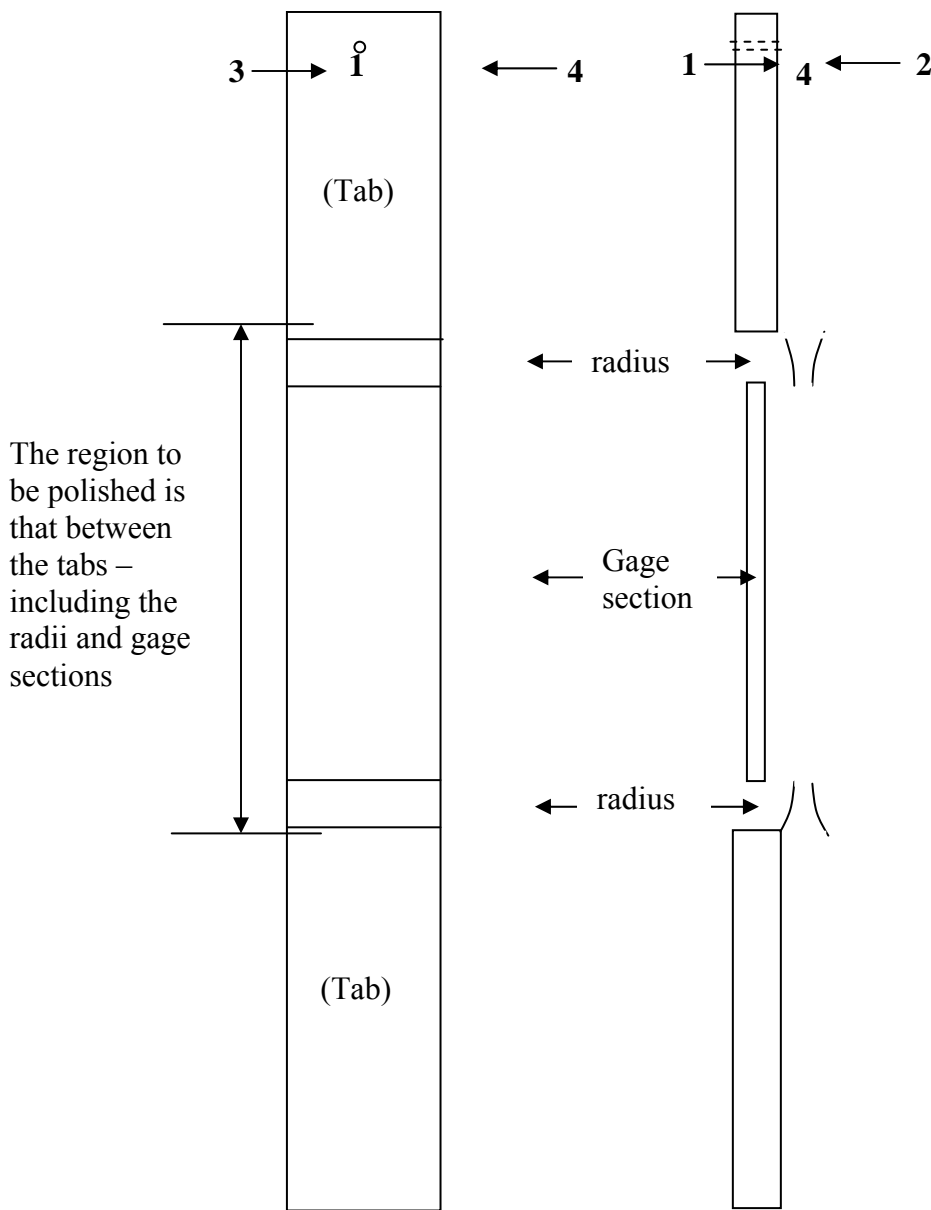
2) Inspect your specimen on all surfaces at 50x (5x objective) to get an idea of what the damage on the surface looks like. Take note of scratches or other anomalies that are perpendicular to the long axis of the specimen. Pay particular attention to damage at the corners. These need to be removed along with deep features.

3) Start with 180 grit – We tended to work on the edges first (sides 3 and 4) and then worked on the big flat surfaces (sides 1 and 2). Sometimes one can slip when working on 3 and 4, which puts scratches on 1 and 2. So we would do 1 and 2 last for each grit.

a. Start on surface 3. Set up specimen such that the end with the number #3 you wrote on the specimen is away from you.

    i. With your finger or the block backing the paper, start polishing the corners, with longitudinal strokes going away from you. Only go in the direction away from you.

    ii. Start with the left corner and continue for 5 minutes using longitudinal strokes going away from you.

    iii. Wipe the specimen often between strokes during that 5 minutes.

    iv. You should probably average about 30 strokes per minute (?)

    v. Next polish the right corner and continue for 5 minutes using longitudinal strokes going away from you.

    vi. Clean specimen with alcohol.

    vii. With light pressure, start polishing surface #3 using longitudinal strokes going away from you for a total of 5 minutes.

    viii. Wipe the specimen often between strokes during that 5 minutes.

    ix. You should probably average about 30 strokes per minute (?)

    x. After 5 minutes, unclamp specimen, wipe it and your area if necessary and rotate specimen such that the number #3 is closest to you.

    xi. Repeat procedure such that each corner and the surface gets a total of 30 minutes.

    xii. Clean specimen with alcohol and check surface #3 and both corners (left and right) under the microscope and see if there are any marks that are not parallel to the long axis within the gage section.

    xiii. If there are, then repeat the entire process in the corners and on the edge labeled side 3. Repeat as necessary until all large anomalies and transverse marks are gone. Do not move on to another grit until all of the transverse marks are gone.

    xiv. If all transverse marks and large anomalies are gone, then stop using 180 on surface #3. Clean the specimen with alcohol.

b. Start on surface 4. Set up specimen such that the end with the number #4 you wrote on the specimen is away from you.

    i. With your finger or the block backing the paper, start polishing the corners, with longitudinal strokes going away from you. Only go in the direction away from you.

    ii. Start with the left corner and continue for 5 minutes using longitudinal strokes going away from you.

    iii. Wipe the specimen often between strokes during that 5 minutes.

    iv. You should probably average about 30 strokes per minute (?)

    v. Next polish the right corner and continue for 5 minutes using longitudinal strokes going away from you.

    vi. Clean specimen with alcohol.

    vii. With light pressure, start polishing surface #4 using longitudinal strokes going away from you for a total of 5 minutes.

    viii. Wipe the specimen often between strokes during that 5 minutes.

    ix. You should probably average about 30 strokes per minute (?)

    x. After 5 minutes, unclamp specimen, wipe it and your area if necessary and rotate specimen such that the number #4 is closest to you.

    xi. Repeat procedure such that each corner and the surface gets a total of 30 minutes.

    xii. Clean specimen with alcohol and check surface #4 and both corners (left and right) under the microscope and see if there are any marks that are not parallel to the long axis within the gage section.

    xiii. If there are, then repeat the entire process in the corners and on the edge labeled side 4. Repeat as necessary until all large anomalies and transverse marks are gone. Do not move on to another grit until all of the transverse marks are gone.

    xiv. If all transverse marks and large anomalies are gone, then stop using 180 on surface #4. Clean the specimen with alcohol.

c. Start on surface 1. Set up specimen such that the tab end with the number #1 you wrote on the specimen is away from you.

    i. With light pressure, start polishing using longitudinal strokes going in the direction away from you only for a total of 5 minutes.

    ii. Wipe the specimen often between strokes during that 5 minutes.

    iii. You should probably average about 30 strokes per minute (?)

    iv. After 5 minutes, unclamp specimen, wipe it and your area if necessary and rotate specimen such that the number #1 is closest to you.

    v. Repeat this process rotating the specimen every 5 minutes until you have a total time on the specimen of 20 minutes.

    vi. Clean specimen with alcohol and check surface #1 under the microscope and see if there are any marks that are not parallel to the long axis within the gage section.

    vii. If there are, then continue process for 20 more minutes and recheck. If still there are non-parallel marks, then continue for 20 more minutes, and repeat as necessary until all large anomalies and transverse marks are gone. Do not move on to another grit until all of the transverse marks are gone.

    viii. If all transverse marks and large anomalies are gone, then stop using 180 on surface #1. Clean the specimen with alcohol.

d. Start on surface 2. Set up specimen such that the end with the number #2 you wrote on the specimen is away from you.

    i. With light pressure, start polishing using longitudinal strokes going in the direction away from you only for a total of 5 minutes.

    ii. Wipe the specimen often between strokes during that 5 minutes.

    iii. You should probably average about 30 strokes per minute (?)

    iv. After 5 minutes, unclamp specimen, wipe it and your area if necessary and rotate specimen such that the number #2 is closest to you.

    v. Repeat this process rotating the specimen every 5 minutes until you have a total time on the specimen of 20 minutes.

vi. Clean specimen with alcohol and check surface #2 under the microscope and see if there are any marks that are not parallel to the long axis within the gage section.

vii. If there are, then continue process for 20 more minutes and recheck. If still there are non-parallel marks, then continue for 20 more minutes, and repeat as necessary until all large anomalies and transverse marks are gone. Do not move on to another grit until all of the transverse marks are gone.

viii. If all transverse marks and large anomalies are gone, then stop using 180 on surface #2. Clean the specimen with alcohol.

REPEAT PROCEDURES USING PROGRESSIVELY SMALLER GRIT SIZES WITH THE 5 MINUTE ROTATIONS TO ACHIEVE THE MAXIMUM TIMES IN THE CHART BELOW:

Name:			Specimen:			Date:			
SiC Paper	LC3	S3	RC3	LC4	S4	RC4	S1	S2	
(grit)	(10 min)	(10 min)	(10 min)	(10 min)	(10 min)	(10 min)	(20 min)	(20 min)	
180	5↑ 5↓	5↑ 5↓	5↑ 5↓	5↑ 5↓	5↑ 5↓	5↑ 5↓	5↑ 5↓ 5↑ 5↓	5↑ 5↓ 5↑ 5↓	1 hr + 40 min
240	5↑ 5↓	5↑ 5↓	5↑ 5↓	5↑ 5↓	5↑ 5↓	5↑ 5↓	5↑ 5↓ 5↑ 5↓	5↑ 5↓ 5↑ 5↓	1 hr + 40 min
320	5↑ 5↓	5↑ 5↓	5↑ 5↓	5↑ 5↓	5↑ 5↓	5↑ 5↓	5↑ 5↓ 5↑ 5↓	5↑ 5↓ 5↑ 5↓	1 hr + 40 min
400	5↑ 5↓	5↑ 5↓	5↑ 5↓	5↑ 5↓	5↑ 5↓	5↑ 5↓	5↑ 5↓ 5↑ 5↓	5↑ 5↓ 5↑ 5↓	1 hr + 40 min
								total	6 hr + 40 min

LC3 = left corner side 3
S3 = the small flat of side 3
RC3 = right corner side 3

LC4 = left corner side 4
S4 = the small flat of side 4
RC4 = right corner side 4

S1 = big flat surface – side 1
S2 = big flat surface – side